Universiteit Leiden
The Netherlands

Assessing T cell differentiation at the single-cell level

Gerlach, C.

Citation
Gerlach, C. (2012, January 17). *Assessing T cell differentiation at the single-cell level*. Retrieved from https://hdl.handle.net/1887/18361

Version:	Corrected Publisher's Version
License:	Licence agreement concerning inclusion of doctoral thesis in the Institutional Repository of the University of Leiden
Downloaded from:	https://hdl.handle.net/1887/18361

Note: To cite this publication please use the final published version (if applicable).

Assessing T cell differentiation at the single-cell level

Carmen Gerlach

The research described in this thesis was performed at the Division of Immunology of the Netherlands Cancer Institute – Antoni van Leeuwenhoek Hospital (NKI-AvL), Amsterdam, the Netherlands.

The printing of this thesis was financially supported by the NKI-AvL.

Layout and printing by Off Page, Amsterdam

Copyright © 2011 by Carmen Gerlach

Assessing T cell differentiation at the single-cell level

Proefschrift
ter verkrijging van
de graad van Doctor aan de Universiteit Leiden,
op gezag van Rector Magnificus prof.mr. P.F. van der Heijden,
volgens besluit van het College voor Promoties
te verdedigen op dinsdag 17 januari 2012
klokke 15:00 uur

door **Carmen Gerlach**
geboren te Hamburg, Duitsland
in 1980

Promotiecommissie

Promotor:	Prof. Dr. T.N.M. Schumacher
Overige leden:	Prof. Dr. J.J. Neefjes
	Prof. Dr. C.J.M. Melief
	Prof. Dr. S.H. van der Burg
	Prof. Dr. R.E. Mebius (Vrije Universiteit Amsterdam)
	Prof. Dr. R.J. de Boer (Universiteit Utrecht)
	Prof. Dr. J. Borst (Universiteit van Amsterdam)

Voor mijn ouders en Sytze

CONTENTS

Chapter 1	General introduction	9
Chapter 2	Mapping the life histories of T cells *Nat Rev Immunol 10: 621-631 (2010)*	19
Chapter 3	The descent of memory T cells *Ann N Y Acad Sci. 1217: 139-53 (2011)*	45
Chapter 4	Dissecting T cell lineage relationships by cellular barcoding *J Exp Med. 205: 2309-18 (2008)*	69
Chapter 5	One naïve T cell, multiple fates in CD8+ T cell differentiation *J Exp Med. 207: 1235-46 (2010)*	95
Chapter 6	Effector and memory lineage decision occurs after naïve T cell priming *Unpublished*	123
Chapter 7	Recruitment of antigen-specific CD8+ T cells in response to infection is markedly efficient *Science. 325:1265-9 (2009)*	139
Chapter 8	The CD8+ T cell response to infection is dominated by the progeny of a few naïve T cells *Unpublished*	159
Chapter 9	Summary and general discussion	187
Appendix	Nederlandse Samenvatting	199
	Curriculum Vitae	207
	List of publications	209

1

GENERAL INTRODUCTION

Thanks to our immune system we only rarely suffer from infectious diseases, although we are continuously exposed to pathogens. Many pathogens are prevented from accessing our body by the physical barriers of our skin and inner epithelia, but when a pathogen succeeds in crossing these barriers, it is attacked by the immune system from multiple angles.

The first signs of 'danger' (infection and tissue damage) are sensed by the innate immune system. Macrophages, neutrophils, dendritic cells (DCs), natural killer (NK) cells, mast cells and eosinophils are classified as cells of the innate immune system. They express intracellular and extracellular innate immune receptors that are also called pattern recognition receptors (PRR), which allow them to recognize molecular patterns that are indicative of infection (pathogen-associated molecular patterns; PAMPs) or tissue injury (damage-associated molecular patterns; DAMPs)[1-7]. Interestingly, these mechanisms of innate immune recognition are shared between vertebrate animals, invertebrates and even plants[8-10]. The ability to recognize PAMPs and DAMPs allows the innate immune system to identify pathogens and infected, damaged, and in some cases cancerous host cells. Bacteria are recognized by their lipopolysaccharide or teichoic acid structures, which are essential cell wall components of gram-negative or gram-positive bacteria, respectively[1,2,11]. Infected host cells can be identified by the presence of DNA containing unmethylated CpG motifs, which is characteristic of bacterial DNA, or by the presence of double-stranded RNA, which is indicative of viral infection[1,2,11]. Also cells lacking the expression of molecules that are normally present on the cell surface, such as major histocompatibility complex (MHC) class I and sialylated glycoproteins and glycolipids can be identified as infected or cancerous[2]. Conditions of cellular stress and injury are sensed if endogenous factors that are normally shielded from recognition by the immune system are released or exposed upon cell death[3-7,12]. Examples of such DAMPs are heat shock proteins, uric acid and mitochondrial DNA[3,7,12].

Both PAMP and DAMP detection activates the innate immune cells to commence pathogen clearance, the inflammatory response and the adaptive immune response. Pathogen clearance is initiated by locally resident macrophages and maintained by neutrophils, macrophages, DCs and NK cells that are recruited to the site of infection or injury in response to inflammatory signals. The phagocytes engulf pathogens, abnormal cells and cell debris and subsequently destroy it. NK cells actively lyse infected or otherwise abnormal host cells through the release of cytotoxic molecules. The inflammatory response is initiated when tissue resident macrophages release cytokines and chemokines upon PAMP or DAMP binding. Inflammation functions as an alarm signal sent out to further parts of the body to recruit other innate and adaptive immune cells to the site of infection, where many of these join in the production of inflammatory mediators. As all innate immune cells of the same cell type express the same set of PRRs, virtually all cells of that particular cell type can aid in the response. The high numbers of readily available innate immune cells provide

immediate action. However, complete resolution of infection often requires additional actions of the adaptive immune system, which is activated when DCs and to minor extent macrophages that had been recruited to the site of infection migrate further to lymphoid organs where they activate B and T lymphocytes.

B and T lymphocytes (also termed B and T cells) are the cells of the adaptive immune system. These cells are predominantly activated by mature DCs and only when the DCs display pathogen-derived peptide fragments on their cell surface. In contrast to innate immune cells, lymphocytes do not recognize general patterns associated with infection or injury, but specific pathogen-derived peptide sequences. This specificity is provided by the B cell receptor (BCR) or T cell receptor (TCR) molecules[13-17]. The exact BCR and TCR sequence – and thereby lymphocyte specificity - is generated through random gene rearrangements within the BCR and TCR loci occurring during lymphocyte development. This process generates a large diversity of lymphocyte specificities which ensures that the adaptive immune system can identify also those pathogens that have evolved strategies to evade their recognition by innate receptors. As a downside to the large diversity in lymphocyte specificities, each pathogen is recognized by not more than a minor subset of B and T cells that needs to be expanded by extensive proliferation in order to generate sufficient cell numbers to clear the infection – a process that takes time. Adaptive immunity is therefore slow, but highly pathogen-specific. Furthermore, adaptive immune cells are capable of providing long-lasting protection to previously encountered infections, which is termed 'memory'[18-20] and forms the basis of most prophylactic vaccines[18,21]. Immune memory provides the host with large numbers of pathogen-specific B and T cells that are rapidly reactivated upon renewed infection with the same pathogen.

The major difference between B and T cell responses to infection is the mechanism by which the cells exert their function. B lymphocytes act through the secretion of antibodies, which are soluble proteins that can directly bind extracellular pathogens and thereby tag them for destruction by the innate immune system. T lymphocytes in contrast secrete cytokines and cytotoxic proteins. Depending on their mode of antigen recognition and particular functions, T lymphocytes are subdivided into $CD4^+$ and $CD8^+$ subsets. $CD8^+$ T lymphocytes recognize antigen presented by MHC class I molecules (and thus mainly derived from intracellular pathogens) and can directly kill infected host cells through mechanisms similar to NK cells. $CD4^+$ T cells on the contrary recognize antigen derived from phagocytosed particles, presented on MHC class II complexes. These cells mainly act through the secretion of inflammatory or suppressive cytokines and play a role in enhancing B cell and $CD8^+$ T cell responses, or alternatively, in dampening the actions of $CD8^+$ T cells to prevent excessive responses.

This thesis focuses on $CD8^+$ T cell responses to infection, which will therefore be described in more detail here. $CD8^+$ T cell responses are initiated when naïve, antigen-specific $CD8^+$ T cells encounter mature DCs that display pathogen-derived peptides bound to MHC class I molecules on their cell surface. This leads to activation of the

antigen-specific T cells, resulting in their proliferation and differentiation. Already early during the response, the pool of activated CD8$^+$ T cells displays a remarkable heterogeneity, with lymph node homing molecules (CD62L)[22,23], cytokines (IL-2)[24], cytokine receptors (CD25, CD127)[22,24-27] and other molecules (KLRG-1)[24,28-30] being differentially expressed. Nevertheless, most activated T cells acquire effector functions, which allow them to specifically lyse infected host cells. After pathogen clearance, the majority of activated T cells die by apoptosis, but a small fraction (~10%) remains alive and forms a stable pool of long-lived memory cells[19].

In this thesis I wished to investigate I) how different antigen-specific CD8$^+$ T cell clones contribute to the heterogeneity within the CD8$^+$ T cell respons, II) at what point during *in vivo* CD8$^+$ T cell differentiation fate decisions take place and III) to what extent the clonal expansion of individual antigen-specific CD8$^+$ T cells shapes the overall response magnitude. To address these issues, it is crucial to follow individual T cells over time rather than tracking the behavior of a cell population, as not necessarily all cells within a population follow the same path of differentiation.

Over the past years, several *in vitro* and *in vivo* technologies have been developed with the aim to track individual cells. **Chapter 2** describes these technologies and discusses their potential and limitations, and how informative lineage tracing experiments should be set up. This chapter also describes the 'cellular barcoding' technology that we have developed in chapter 4.

Since long, immunologists have been fascinated by the question why some antigen-specific T cells are able to persist long-term as memory cells, while others die by apoptosis when the infection has been eradicated. What determines whether a T cell adopts a short-lived or a long-lived fate and when is this fate decision taken? **Chapter 3** of this thesis discusses the current knowledge regarding the generation of memory T cells. The main focus lies on different models that have been proposed to explain when CD8$^+$ T cells commit to a short- or long-lived fate.

Most single-cell tracking methodologies are limited by the number of individual cells that can be followed over time. To address this issue, we have developed a technology termed 'cellular barcoding' that enables fate mapping of hundreds of individual T cells during infection *in vivo*. With this technology, individual T cells are provided with unique DNA sequences (barcodes) that are transferred to all progeny of the labeled T cell during cell division. In this way, all T cells that share a common precursor are marked with the same genetic tag. To determine which barcodes are present in a particular cell population, the DNA content of the cells is isolated, barcode sequences are amplified and subsequently hybridized onto a barcode-microarray for sequence identification. In **chapter 4** we describe this novel technology and apply it to determine whether T cells that have been activated in a particular lymph node preferentially migrate towards the organ that was drained by the lymph node in which the T cells were activated, or whether T cells also migrate to distant tissue sites, irrespective of their site of priming.

As discussed in chapter 3, a longstanding question in immunology is at what point during an immune response CD8$^+$ T cells commit to a short- or long-lived fate. One of the proposed models predicts that this fate is imprinted in the antigen-specific T cells as early as during T cell activation and thus before the first cell division[31]. In this model, the factor that determines T cell fate is the strength of T cell activation, as imposed by the priming dendritic cell and its surroundings. In particular at early and late times after infection, the levels of costimulatory molecules and antigenic peptides on the surface of the dendritic cells, as well as the inflammatory environments are likely to differ to such an extent that T cell activation strengths could be considerably dissimilar. In **chapter 5**, we directly tested by cellular barcoding if short- and long-lived T cell fates are *in vivo* imprinted into activated T cells before their first cell division. To achieve this, it was crucial to obtain naïve T cells that are uniquely labeled by a barcode, so that we could study if these naïve T cells developed into either short-lived effector cells or long-lived memory cells or both. Therefore, I first developed a new technology that allows the generation of naïve, barcode-labeled T cells. This technology relies on the transduction of thymocytes with the barcode sequences and is described in detail in this chapter.

An alternative model has been put forward that poses that fate commitment does not occur before, but during the first cell division through a process called asymmetric cell division[32,33]. Specifically, Reiner and colleagues have proposed that through the asymmetric partitioning of cell fate determining factors into the first two daughter cells, the daughter cell that is formed proximal to the priming dendritic cell will commit to a short-lived effector fate, while the distal daughter cell adopts a memory fate. In **chapter 6** we test this hypothesis by providing daughter cells of the 1st to 3rd generation with our unique barcode sequences and subsequent monitoring if these early daughter cells were already committed to either fate.

In addition to the functional heterogeneity that exists within the responding T cell population, CD8$^+$ T cell responses to different infections are highly variable in their overall size. The magnitude of the total response depends on the pathogen type, dose of infection and route of pathogen entry. In general, more severe infections lead to larger T cell response sizes. In **chapter 7**, we address the question how the magnitude of the overall CD8$^+$ T cell response is regulated. Principally, this could be achieved either through regulating the number of antigen-specific naïve T cells that are recruited into the response, or through controlling the expansion (a combination of proliferation and cell death) of the recruited T cell clones. As the overall magnitude of the response is the product of naïve T cell recruitment and clonal expansion, measuring two of these parameters allows calculation of the third. The cellular barcoding technology enables us to quantify naïve T cell recruitment by counting the amount of different barcodes that are found in the response. This is a direct reflection of the number of recruited naïve T cells. The overall magnitude of the response can be easily determined by flow-cytometry based counting of how many barcode-labeled

T cells are present during the response. Using these two measurements we determined to what extent changes in naïve T cell recruitment and clonal expansion regulate the overall CD8$^+$ T cell response size.

Even before CD8$^+$ T cells acquire effector functions, they start to proliferate. This expansion of the antigen-specific T cell pool ensures that high numbers of pathogen-reactive T cells are available to prevent spread of the infection and to ultimately eliminate the pathogen. While the importance of this expansion is well recognized, it remains unclear to what extent individual antigen-specific naïve T cells contribute to the overall response. Do all clones produce an equal amount of progeny, or are immune responses numerically dominated by the progeny of only a few naïve T cells? Answering these questions requires on one hand the ability to distinguish between the progeny of different naïve T cells (i.e. between different T cell families) and on the other hand the quantification of T cell family sizes. The former can be achieved by cellular barcoding, but the latter was not possible using the microarray-based barcode readout system we had originally developed, as this system only provides semi-quantitative data on barcode prevalence. In **chapter 8** we therefore first set up a new and quantitative readout system for barcode analysis, which involves deep sequencing of barcodes. Using this new method, we then quantified the size of different responding T cell families during various infection conditions.

REFERENCES

1. Medzhitov, R. & Janeway, C. A., Jr. Innate immunity: impact on the adaptive immune response. *Curr. Opin. Immunol.* 9, 4-9 (1997).
2. Medzhitov, R. & Janeway, C. A., Jr. Decoding the patterns of self and nonself by the innate immune system. *Science* 296, 298-300 (2002).
3. Chen, G. Y. & Nunez, G. Sterile inflammation: sensing and reacting to damage. *Nat. Rev. Immunol.* 10, 826-837 (2010).
4. Matzinger, P. An innate sense of danger. *Ann. N Y Acad. Sci.* 961, 341-342 (2002).
5. Matzinger, P. The danger model: a renewed sense of self. *Science* 296, 301-305 (2002).
6. Seong, S. Y. & Matzinger, P. Hydrophobicity: an ancient damage-associated molecular pattern that initiates innate immune responses. *Nat. Rev. Immunol.* 4, 469-478 (2004).
7. Rock, K. L., Latz, E., Ontiveros, F. & Kono, H. The sterile inflammatory response. *Annu. Rev. Immunol.* 28, 321-342 (2010).
8. Hoffmann, J. A., Kafatos, F. C., Janeway, C. A. & Ezekowitz, R. A. Phylogenetic perspectives in innate immunity. *Science* 284, 1313-1318 (1999).
9. Jones, J. D. & Dangl, J. L. The plant immune system. *Nature* 444, 323-329 (2006).
10. Ausubel, F. M. Are innate immune signaling pathways in plants and animals conserved? *Nat. Immunol.* 6, 973-979 (2005).
11. Janeway, C. A., Jr. & Medzhitov, R. Innate immune recognition. *Annu. Rev. Immunol.* 20, 197-216 (2002).
12. Krysko, D. V. *et al.* Emerging role of damage-associated molecular patterns derived from mitochondria in inflammation. *Trends Immunol.* 32, 157-164 (2011).
13. Krogsgaard, M. & Davis, M. M. How T cells 'see' antigen. *Nat. Immunol.* 6, 239-245 (2005).
14. Smith-Garvin, J. E., Koretzky, G. A. & Jordan, M. S. T cell activation. *Annu. Rev. Immunol.* 27, 591-619 (2009).
15. Reth, M. & Wienands, J. Initiation and processing of signals from the B cell antigen receptor. *Annu. Rev. Immunol.* 15, 453-479 (1997).
16. Davis, M. M. *et al.* Ligand recognition by alpha beta T cell receptors. *Annu. Rev. Immunol.* 16, 523-544 (1998).

17. Williams, A. F. & Barclay, A. N. The immunoglobulin superfamily--domains for cell surface recognition. *Annu. Rev. Immunol.* 6, 381-405 (1988).
18. Ahmed, R. & Gray, D. Immunological memory and protective immunity: understanding their relation. *Science* 272, 54-60 (1996).
19. Williams, M. A. & Bevan, M. J. Effector and memory CTL differentiation. *Annu. Rev. Immunol.* 25, 171-192 (2007).
20. Yoshida, T. *et al.* Memory B and memory plasma cells. *Immunol. Rev.* 237, 117-139 (2010).
21. Sallusto, F., Lanzavecchia, A., Araki, K. & Ahmed, R. From vaccines to memory and back. *Immunity* 33, 451-463 (2010).
22. Huster, K. M. *et al.* Selective expression of IL-7 receptor on memory T cells identifies early CD40L-dependent generation of distinct CD8+ memory T cell subsets. *Proc. Natl. Acad. Sci. U S A* 101, 5610-5615 (2004).
23. Obar, J. J. & Lefrancois, L. Early signals during CD8 T cell priming regulate the generation of central memory cells. *J. Immunol.* 185, 263-272 (2010).
24. Sarkar, S. *et al.* Functional and genomic profiling of effector CD8 T cell subsets with distinct memory fates. *J. Exp. Med.* 205, 625-640 (2008).
25. Schluns, K. S., Kieper, W. C., Jameson, S. C. & Lefrancois, L. Interleukin-7 mediates the homeostasis of naive and memory CD8 T cells in vivo. *Nat. Immunol.* 1, 426-432 (2000).
26. Kalia, V. *et al.* Prolonged interleukin-2Ralpha expression on virus-specific CD8+ T cells favors terminal-effector differentiation in vivo. *Immunity* 32, 91-103 (2010).
27. Kaech, S. M. *et al.* Selective expression of the interleukin 7 receptor identifies effector CD8 T cells that give rise to long-lived memory cells. *Nat. Immunol.* 4, 1191-1198 (2003).
28. Voehringer, D. *et al.* Viral infections induce abundant numbers of senescent CD8 T cells. *J. Immunol.* 167, 4838-4843 (2001).
29. Joshi, N. S. *et al.* Inflammation directs memory precursor and short-lived effector CD8(+) T cell fates via the graded expression of T-bet transcription factor. *Immunity* 27, 281-295 (2007).
30. McMahon, C. W. *et al.* Viral and bacterial infections induce expression of multiple NK cell receptors in responding CD8(+) T cells. *J. Immunol.* 169, 1444-1452 (2002).
31. Farber, D. L. Differential TCR signaling and the generation of memory T cells. *J. Immunol.* 160, 535-539 (1998).
32. Chang, J. T. *et al.* Asymmetric T lymphocyte division in the initiation of adaptive immune responses. *Science* 315, 1687-1691 (2007).
33. Chang, J. T. *et al.* Asymmetric Proteasome Segregation as a Mechanism for Unequal Partitioning of the Transcription Factor T-bet during T Lymphocyte Division. *Immunity* 34, 492-504 (2011).

2

MAPPING THE LIFE HISTORIES OF T CELLS

Ton N. M. Schumacher[1], Carmen Gerlach[1] and Jeroen W. J. van Heijst[1]

[1]Division of Immunology, The Netherlands Cancer Institute, Amsterdam, the Netherlands

Nat Rev Immunol 10: 621-631 (2010)

The behaviour of T cells is not fixed in the germ line, but is highly adaptable depending on experiences encountered during a T cell's life. To understand how different T cell subsets arise and how prior signalling input regulates subsequent T cell behaviour, approaches are required that couple a given T cell state to signals received by the cell, or by one of its ancestors, at earlier times. Here we describe recently developed technologies that have been used to determine the kinship of different T cell subsets and their prior functional characteristics. Furthermore, we discuss the potential value of new technologies that would allow assessment of T cell migration patterns and prior signalling events.

2

INTRODUCTION

In the naive T cell repertoire, antigen-specific T cells are exceedingly rare. Prior to antigen encounter, the frequency of antigen-specific T cells is estimated to be 1 in 10^5 cells, which is ~200 T cells in the total lymphoid system of a mouse[1, 2, 3]. Following activation these rare antigen-specific T cells expand rapidly, dividing once every 4–6 hours[4, 5, 6, 7]. The extent of this T cell expansion depends on the pathogen type and the severity of infection, but it can in some cases yield more than 10^4 progeny per activated T cell[8, 9, 10, 11]. The fate of the resulting T cell pool is not uniform. First, following antigen clearance, ~90% of activated T cells die. Second, those cells that do survive can reside either in the lymphoid compartment or in peripheral organs and may, for example, differ in their capacity for renewed proliferation[12, 13, 14, 15]. The development of different memory T cell populations is just one example of the range of phenotypes and functions that T cells can adopt. To understand how these different T cell subsets arise and how prior signalling affects subsequent cellular function, we need to be able to link a current T cell state to the prior input that the cell has received. This is not a straightforward task. First, the functional activity of T cells can be influenced by signals received months or perhaps even years earlier. Second, T cells are highly migratory, making it challenging to couple the input that a given cell receives to the fate or functional activity of its progeny at later time points and at different locations. To this end, a series of technologies have been developed over the past few years that allow the fate and history of individual cells to be monitored. Here we discuss the strengths and limitations of these technologies in the analysis of both kinship and prior functional activity of different T cell subsets, as well as of other immune cell types. Furthermore, we describe the potential value of new technologies that could aid the visualization of T cell migration patterns and prior signalling input.

UNDERSTANDING FAMILY TIES

Kinship analysis at the population level. Depending on the nature of encountered signals, naive T cells can give rise to several distinct subsets that differ greatly in phenotypical and functional properties[15, 16, 17, 18, 19]. How can the origin of these different T cell subsets be determined? A relatively straightforward way to determine the fate of T cells at the population level is to adoptively transfer donor cells that can be distinguished from recipient cells by the expression of a congenic[20, 21, 22] or fluorescent[23, 24] marker (Table 1). Such markers allow multiple T cell populations to be monitored simultaneously in the same host. For example, the transfer of both recently generated and long-term memory $CD8^+$ T cells isolated from different congenic strains of mice has been used to show that memory T cell recall capacity increases progressively over time[25]. As a variation on this theme, the kinetics with which immune cell populations equilibrate across different immunological sites has been determined using congenic markers in parabiotic mice[26, 27, 28].

Table 1: Strategies for monitoring family ties of T cell subsets.

Strategy	Level of resolution	Advantages	Limitations
Adoptive transfer using congenic markers	Bulk	Straightforward to perform	No data on potential of individual cells
TCR sequencing	Oligoclonal	Tracks endogenous repertoire	TCR sharing by different cells
Intravital imaging	Single cell	Real-time analysis at physiological sites	Temporally and spatially restricted
Adoptive transfer of single cells	Single cell	Unambiguous read-out of developmental potential	Difficult to demonstrate rare alternative fates
Cellular barcoding	Single cell	High-throughput identification of cell fate	Invasive method of tag detection
Brainbow	Single cell	Direct visualization of descent	Stable inheritance of different colours by progeny has not been established

TCR, T cell receptor.

Although the use of congenic or fluorescent markers provides a valuable tool to examine the behaviour of a bulk population of cells that have been transferred into a different host, there is one crucial limitation to the conclusions that can be drawn from this experimental approach. Specifically, it is impossible to distinguish whether all of the transferred cells have a particular behaviour or whether some of the cells differentiate into cell type A, whereas others differentiate into cell type B (Fig. 1a). As a simple example, following the adoptive transfer of a population of haematopoietic progenitor cells that yield both T cells and granulocytes, it is impossible to determine whether the transferred cells consisted of multipotent progenitors or a mixture of lymphoid and myeloid precursor cells. To address such fundamental questions regarding cell differentiation, methods are required that enable the fate of individual cells rather than a bulk population of cells to be traced. Over the past few years, three different experimental strategies have been developed that can be used to follow cell fate at the single-cell level. The benefits and limitations of each of these strategies are discussed below.

Monitoring cell fate by continuous observation. Traditionally, microscopy techniques have been used to gain insights into the static distribution of haematopoietic cells[29]. However, with the advent of dynamic imaging techniques, such as intravital multiphoton microscopy, it has become possible to study the interactions of individual cells during the development of immune responses in a physiological setting as well as over time[30,

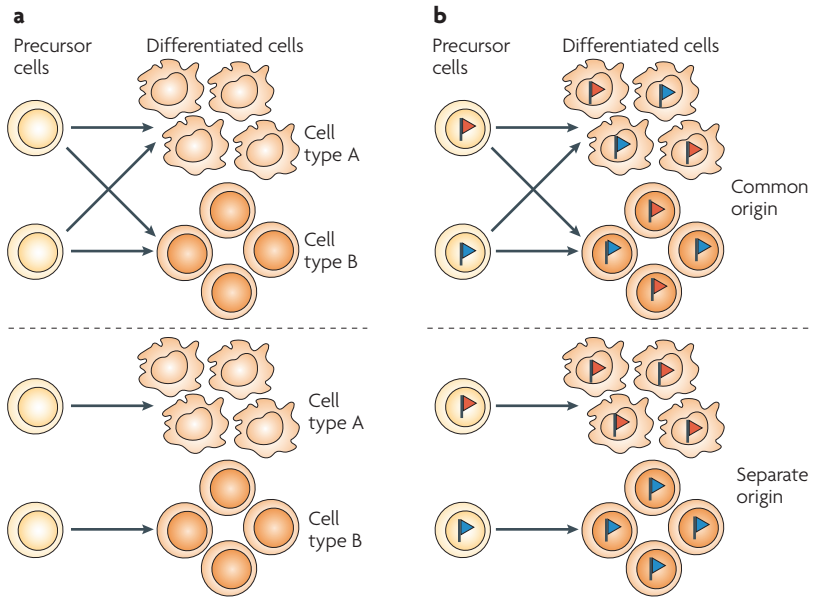

Figure 1: Identifying kinship by comparing barcodes. a | The two cell types depicted here could be derived from either common (top panel) or separate (bottom panel) precursors. Analysis of cell fate at the population level (for example, by the use of congenic markers) cannot distinguish between these two scenarios. **b** | When each precursor cell is labelled with a unique genetic tag that is passed on to all progeny (shown as a red or blue flag) the origin of the two cell populations can be revealed. If the two cell populations have a common origin, genetic tags present in these populations will be overlapping (top panel, both red and blue flags are found in both populations). If the two cell populations have a separate origin, genetic tags present in these populations will be distinct (bottom panel, only one type of flag is found in each population). Note that in those cases in which individual precursor cells have a bias to produce a certain type of progeny, the tags carried by these precursor cells will show a proportional enrichment in the descendant population of daughter cells.

[31, 32, 33, 34, 35]. Intravital microscopy has allowed the interaction between single naive T cells and antigen-presenting dendritic cells (DCs) in lymph nodes to be visualized[36, 37, 38, 39] and quantified[40, 41, 42]. These studies revealed that naive T cell priming occurs in distinct phases, with initial transient interactions between T cells and DCs followed by stable contacts that eventually lead to T cell division.

An important benefit of intravital microscopy is that it allows cells to be visualized in their physiological environment. However, the information obtained by using this technology is mostly restricted to cell behaviour over a period of a few hours, as photodamage induced by the excitation source can affect cell viability during prolonged imaging. As a second and more fundamental limitation, T cells that leave a particular site (such as the lymph node) are invariably lost from analysis. As a result, intravital microscopy is currently used mainly for short-term monitoring of T cell activation and

function at a given site. One powerful alternative is provided by the recent development of methodology for the long-term imaging of cell differentiation in vitro[43, 44]. This type of bio-imaging set-up can allow the continuous monitoring of single cells and their progeny for periods of up to one week. By tracing the fate of individually plated mouse embryonic stem cell-derived mesoderm cells, Schroeder and colleagues recently showed that adherent endothelial cells can directly give rise to non-adherent haematopoietic cells[45], suggesting that during embryonic development the first haematopoietic stem cells (HSCs) may be derived from endothelial cell precursors[46, 47]. Using a similar approach to image the differentiation of individual HSCs in conditioned culture medium, the same group showed that cytokines can instruct haematopoietic lineage selection[48].

The use of long-term in vitro imaging to monitor the fate of lymphocytes has so far been restricted to B cells stimulated by CpG-containing DNA[49]. An intriguing study by Hodgkin and colleagues showed that all progeny of single founder B cells underwent a similar number of cell divisions, whereas the number of divisions of progeny from different founder cells varied greatly. This observation has led the authors to propose that the proliferative potential of B cells is a (transiently) heritable property. In addition, this study found a strong correlation between the size of the founder B cell at the time of its first division and the number of divisions that its progeny underwent. One hypothesis to explain these results is that cell-cycle promoting factors that are produced by the founder cell before the first cell division are subsequently diluted in all progeny during consecutive divisions[49].

The fact that individual founder cells in this system have a distinct behaviour in an essentially homogeneous environment provides indirect evidence for the possibility that lymphocyte fate may, in some cases, be controlled stochastically. In line with a role for stochastic processes in the regulation of cell fate, naturally occurring fluctuations in the levels of apoptosis regulators have been shown to account for cell-to-cell variability in the timing and probability of receptor-mediated death[50]. Interestingly, such fluctuations in protein levels can be transmitted from mother to daughter, resulting in a transient inheritance of cell state, and the rate at which this correlation in protein levels between mother and daughter is lost varies among different proteins[51]. Together, these results highlight the possibility that, in concert with the very large number of well-defined external triggers that mediate lymphocyte activation and differentiation, stochastic processes may contribute to the generation of distinct lymphocyte subsets, and this is an area that deserves greater attention[52, 53].

Monitoring cell fate by single-cell transfer. As mentioned above, approaches that aim to track cell fate in vivo by continuous observation are restricted to relatively short periods of time and are complicated by cell migration. An alternative strategy for monitoring the fate of individual cells in vivo is to adoptively transfer a single donor cell that can be distinguished from all host cells by a congenic marker. This strategy allows one to unambiguously assess the developmental potential of this single cell in its physiological environment. In a pioneering study by Nakauchi and colleagues,

transfer of a single CD34$^-$KIT$^+$SCA1$^+$lineage$^-$ cell was shown to provide long-term reconstitution of the haematopoietic system in 20% of recipient mice, indicating that this cell population was highly enriched for HSCs[54]. A more recent study has identified expression of the signalling lymphocytic activation molecule (SLAM) family member CD150 as an additional marker for distinguishing self-renewing HSCs, and use of this marker allowed long-term multilineage reconstitution by 50% of cells following single-cell transfer[55]. An important caveat to these studies is the fact that adoptive transfer was carried out in irradiated recipients, and the altered cytokine and cellular environment in these mice could influence cell fate. More generally, lineage-tracing studies in which cell differentiation is studied in an altered host environment provide valuable insights into the potential of a cell, but do not necessarily inform us of physiological cell fate.

More recently, the concept of single-cell transfer was applied to the analysis of T cell differentiation by Busch and colleagues[56]. By transferring a single congenically marked antigen-specific CD8$^+$ T cell into recipient mice that were subsequently infected with Listeria monocytogenes, it was shown that one naive T cell can give rise to diverse effector and memory T cell subsets. More recent work from the same group suggests that the descendants of one naive CD8$^+$ T cell can, after vaccination, provide protection against an otherwise lethal bacterial challenge (D. Busch, personal communication). These results suggest that all CD8$^+$ T cell types required for effective immunity can, in theory, be provided by a single activated antigen-specific T cell.

As a limitation to single-cell adoptive transfers, the successful engraftment of viable single cells can be difficult for more 'fragile' cell populations (such as activated T cells). Furthermore, although single-cell transfer studies can readily reveal common cell fates, the fact that each experiment tests the fate of only a single cell makes it difficult to exclude (or demonstrate) rarer alternative fates.

Monitoring cell fate by unique labelling of many cells. The limitations of single-cell adoptive transfer raise the question of how in vivo cell tracking can be extended to high-throughput analysis. Ideally, one would like to study the behaviour of the progeny of a population of cells while still being able to determine which ancestor gave rise to which daughter cells. In such an experimental set-up, each ancestor would have to bear a unique and heritable marker to allow the progeny of different ancestors to be distinguished. Three such approaches have been developed so far with the aim of achieving this goal.

One strategy for fate analysis of endogenous T cell populations makes use of the natural sequence variation that occurs in rearranged T cell receptor (TCR) and B cell receptor (BCR) genes[57]. TCR sequence analysis has been used to monitor the evolution of TCR repertoires during antigen-driven responses[2, 58, 59, 60, 61, 62, 63, 64, 65, 66, 67], to analyse the kinship of different memory T cell subsets[68, 69, 70, 71, 72] and to examine the conversion of conventional CD4$^+$ T cells into forkhead box P3 (FOXP3)-expressing regulatory T cells[73]. BCR sequence analysis has been used to study the clonal origin of early antibody producing and germinal centre B cells[74].

A major drawback of TCR sequencing-based approaches for the monitoring of cell fate is that in the naive T cell pool multiple T cells can — and in most cases will — share a given TCR sequence, making it difficult to unambiguously determine the fate of individual naive T cells. This problem is particularly evident when analysing TCR β-chain sequences, as thymocytes undergo a strong proliferative burst following β-selection. In addition, a given TCR sequence can occur multiple times when formed by a frequent recombination event or because of homeostatic proliferation. To what extent does the presence of multiple T cells with the same TCR limit the conclusions that can be drawn from clonal analyses? In cases in which multiple founder T cells in the naive T cell pool share the same TCR sequence, a difference in TCR sequence between two cell populations of interest is still informative and indicates a separate ancestry. By contrast, the sharing of TCR sequences no longer provides evidence for a shared population of founder cells. Given that developing B cells also undergo a strong proliferative burst after BCR heavy chain rearrangement, similar concerns apply to the interpretation of BCR sequencing data. On a more general note, in all cases in which a given tag used for lineage tracing (such as a TCR sequence or a designed genetic tag, see later) occurs multiple times within a precursor population, the kinship of two cell populations can only be convincingly demonstrated when a correction is made for the overlap in tags that occurs by chance (Box 1).

To allow lineage tracing without the limitations of TCR- or BCR-based analyses and to allow kinship studies beyond the lymphocyte lineage, strategies have been developed that are based on the experimental introduction of unique markers. In early work in this field, irradiation-induced damage and retroviral insertion sites have been used to mark cells in an essentially random manner (Table 2). More recently, two different approaches have been developed that allow unique labelling of many individual cells. One approach is based on the introduction of a highly diverse collection of DNA sequences and the second is based on the induction of a diverse set of fluorescent labels.

In the first approach, a retroviral library containing thousands of unique DNA sequences (termed barcodes) was developed and coupled to a microarray-based detection platform[75]. The labelling of founder populations of interest with a unique heritable barcode was then achieved by infection with this retroviral library. In the case of T cells, this labelling can either be performed at the peripheral T cell stage or at the T cell precursor (thymocyte) stage, the latter to circumvent the need for T cell activation[76]. After transfer of a pool of labelled cells into recipient mice, analysis of the barcode content in cell populations that emerge in vivo can be used to dissect the fate of many individual cells in a single experiment. Such cellular barcoding technology can be used to address two types of biological question regarding T cell responses. First, the technology can be used to determine whether cell populations that differ in location or functional activity arise from common or from separate precursors (Fig. 1). Second, the technology can be used to determine the number of precursors that produce a given cell population (Fig. 2).

BOX 1

In studies that use genetic tags (such as T cell receptor (TCR) sequences, barcodes or fluorescent colour codes) to analyse kinship of cell populations, two essential controls have to be carried out before meaningful conclusions can be drawn about the relatedness of the cell populations under investigation. The first control is a tag sampling control (see the figure, part **a**), which tests how well the entire repertoire of genetic tags that is present in the populations of interest is recovered. Only when the reproducibility of tag recovery from a labelled cell population has been assessed does it become meaningful to compare these tags to a different cell population. To assess the efficiency of tag detection, each sample is split into two equal halves before analysis (sample A and sample B). Overlap in tags recovered from these A and B samples, which are by definition related, will indicate the maximum tag overlap that can be obtained in any biological comparison (for example, effector and memory T cells). If no sampling controls are carried out, one cannot distinguish whether two cell populations are unrelated or whether tag recovery from both populations was inefficient (part **a**).

The second control is a tag distribution control (part b), which tests to what extent individual precursor cells share similar tags by chance (rather than by kinship). For example, this can occur when different T cells share the same TCR sequence or when multiple T cells are labelled with the same genetic tag. To assess background tag overlap between cell populations, tags recovered from two samples that are by definition unrelated (for example, labelled cells present in different mice) can be compared. When samples from two different mice share the same tags, an overlap in tags between samples from the same mouse must take this background overlap into account. If no tag distribution controls are performed, one cannot distinguish whether two cell populations are related or whether they share tags based on chance (part b). Together, these two controls set the experimental window in which kinship of different cell populations can be measured.

Table 2: Early studies using genetic tagging for lineage tracking.

Strategy	Detection system	Conceptual advance	Refs
Radiation-induced chromosome aberrations	Karyotype analysis	First to demonstrate multi-lineage potential of single precursors	109-111
Retroviral integration site analysis	Southern blotting	Stable introduction of unique clonal markers	112-114
Retroviral oligonucleotide marking	PCR and sequencing	Tag libraries of high complexity	115, 116

TCR, T cell receptor.

BOX 1 FIGURE

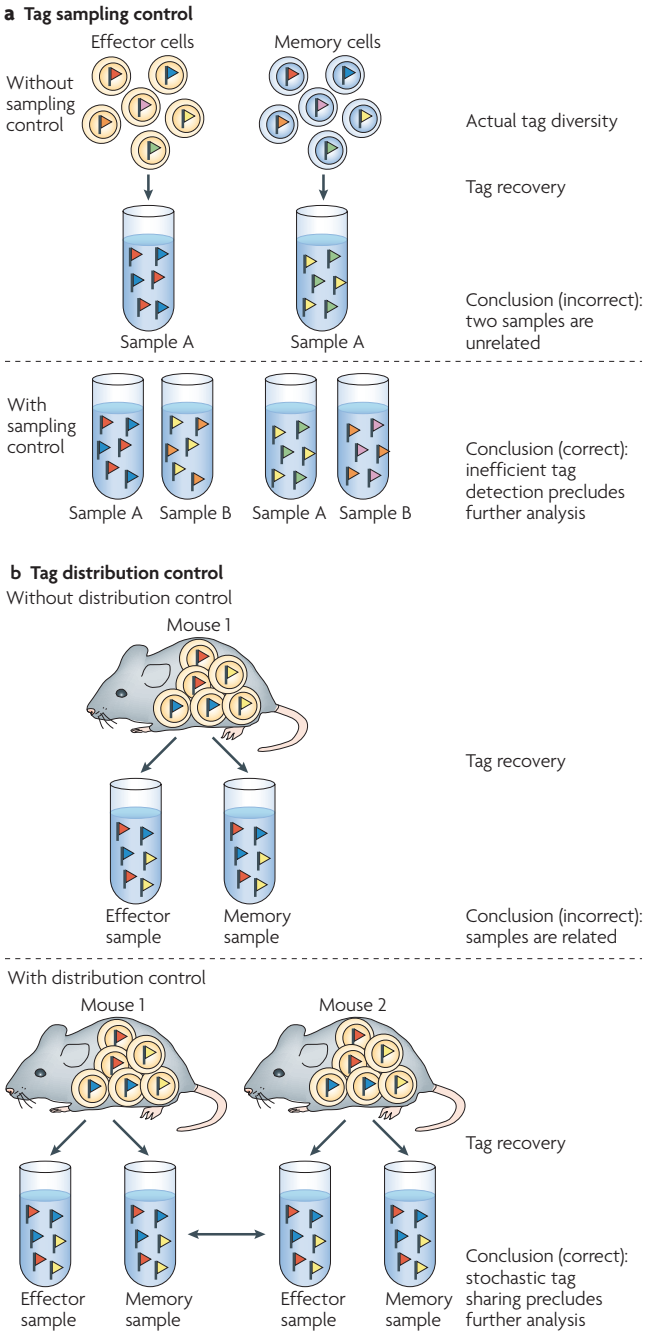
a Tag sampling control
Effector cells
Memory cells
Without sampling control
Actual tag diversity
Tag recovery
Sample A
Sample A
Conclusion (incorrect): two samples are unrelated
With sampling control
Sample A
Sample B
Sample A
Sample B
Conclusion (correct): inefficient tag detection precludes further analysis
b Tag distribution control
Without distribution control
Mouse 1
Tag recovery
Effector sample
Memory sample
Conclusion (incorrect): samples are related
With distribution control
Mouse 1
Mouse 2
Tag recovery
Effector sample
Memory sample
Effector sample
Memory sample
Conclusion (correct): stochastic tag sharing precludes further analysis

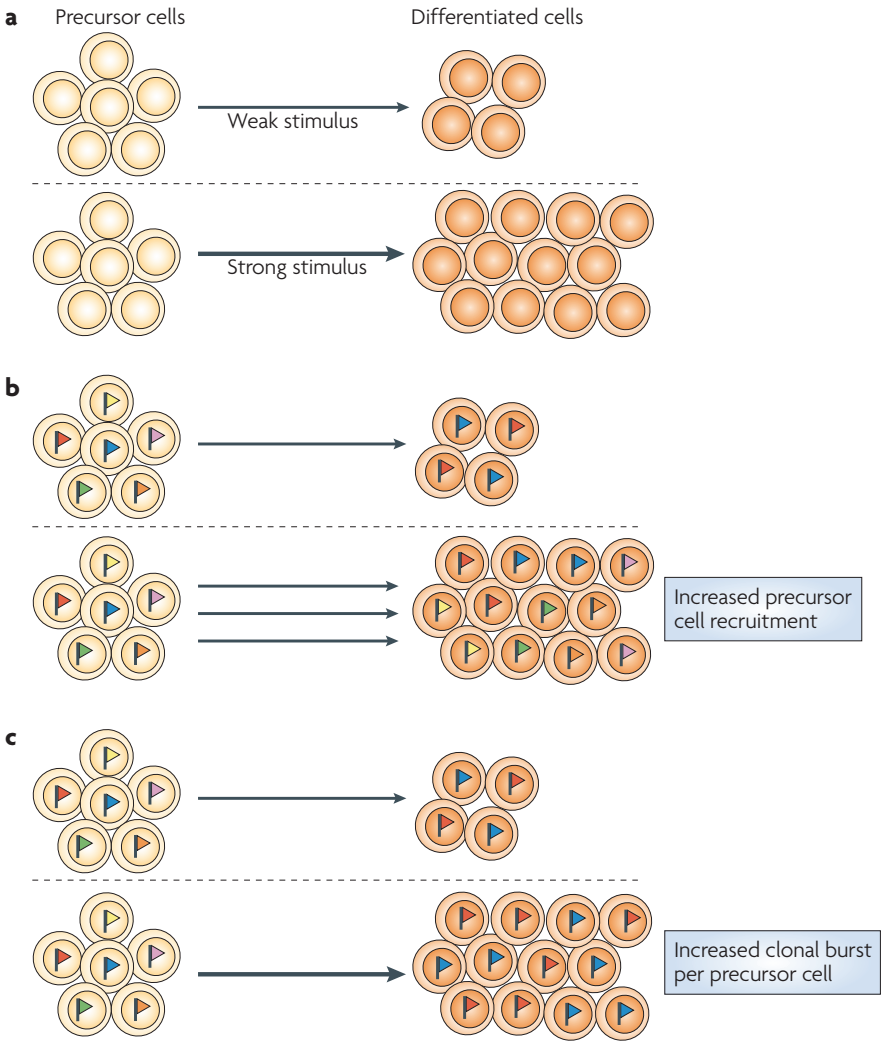

Figure 2: Measuring clonal diversity by counting barcodes. a | In this example, varying stimulation of precursor cells (for example, naive T cells, haematopoietic stem cells or natural killer cells) gives rise to either a small (top panel) or a large (bottom panel) population of differentiated cells. Analysis at the cell population level cannot reveal whether the increased population size following stronger stimulation is the result of increased precursor cell recruitment or an increased clonal burst per precursor cell. **b** | When each precursor cell is labelled with a unique genetic tag that is passed on to all progeny (shown as coloured flags) the clonal diversity of the two cell populations can be revealed. If the population increase following stronger stimulation is the result of increased precursor cell recruitment, the number of different genetic tags present in the differentiated cells will increase proportionally with response magnitude (all six flags are found). **c** | If the population increase following stronger stimulation is the result of an increased clonal burst per precursor cell, the number of different genetic tags present in the differentiated cells will remain constant (only red and blue flags are found).

With respect to the first application, cellular barcoding has been used to monitor T cell migration patterns to multiple inflammatory sites. In an experimental set-up in which the same mouse simultaneously received two localized antigenic challenges, it was found that although distinct T cell families were present in both draining lymph nodes shortly after priming, following lymph node exit their progeny had the capacity to migrate to both effector sites[75]. These data suggest that, independent of the site of priming, individual T cell clones retain the capacity to migrate to multiple tissues[77, 78]. In a different study, cellular barcoding was used to determine whether effector and memory $CD8^+$ T cells are progeny of the same or of different naive T cells[76]. Under conditions of either local or systemic infection, it was found that each naive T cell gives rise to both effector and memory T cells, indicating that the progeny of a single naive T cell can take on multiple fates. Furthermore, this shared ancestry of effector and memory T cells was observed for both low- and high-affinity T cells.

How quantitative are the data that can be obtained using this genetic tagging technology? The analyses carried out so far have used microarrays to read out barcode abundance and should therefore be considered semi-quantitative. However, with the advent of second-generation sequencing approaches, it should now be possible to quantify the contribution of individual precursors with high precision. Importantly, for such quantitative analyses to be meaningful it will be essential that the relative abundance of different tags following recovery and amplification faithfully represents their distribution in the cell population of interest; an issue that can be evaluated by a straightforward sampling control (Box 1). In particular, the development of a quantitative technology for high-throughput fate mapping should be valuable for analysing situations in which individual cells are neither fully committed nor completely bipotent but have a bias towards producing cell type A or B.

A second biological question that can be addressed by cellular barcoding (or other genetic tagging strategies) concerns the clonal diversity of cell populations (Fig. 2). Because each precursor contains a unique marker, the number of different barcodes present in a marked cell population directly correlates with the number of founder cells that yielded this population. Based on this concept, cellular barcoding has been used to test whether the magnitude of antigen-specific T cell responses is determined by the number of naive T cells that are recruited into the response or by the clonal burst (that is, the number of progeny) of each recruited cell[79]. Under different conditions of infection, with various pathogens and doses, it was found that recruitment of naive antigen-specific T cells is markedly constant and is in fact close to complete. These findings indicate that recruitment of rare antigen-specific T cells is highly efficient for T cell responses of varying magnitude, and from these data it can be concluded that the overall magnitude of T cell responses is mainly regulated by clonal burst size.

Although cellular barcoding provides a powerful technology for the analysis of T cell fate, the unique identifiers that labelled cells carry can only be revealed by DNA isolation. Consequently, it is impossible to determine the identity of a cell and to follow its fate afterwards. A potential solution to this issue might be in the use of

cellular tags that can be analysed in a non-invasive manner. In an impressive study, Lichtman and co-workers developed and used a mouse strain (termed Brainbow) in which a Cre–lox approach is used to drive stochastic expression of three fluorescent proteins[80]. By using multiple tandem integrations of the Brainbow construct and limiting expression to the developing brain, the authors showed that individual neurons could be distinguished by expression of 1 of almost 100 different colour variations. So far, the Brainbow system has not been used to determine precursor–progeny relationships either in neuronal tissue or in other tissues. To allow such tracking of cell populations, the 'hue' of cells will have to remain stable over time and across cell generations, and to our knowledge this has not been established to date. Furthermore, for many types of research questions it will be important to develop technology to distinguish different hues by flow cytometry rather than microscopy. If both of these hurdles can be overcome, the potential of this approach is considerable.

REVEALING PRIOR FUNCTIONAL STATES

Following antigen encounter, activated T cells undergo dramatic changes in their gene expression programme, resulting in the acquisition of novel functional characteristics[81, 82, 83]. Furthermore, following clearance of antigen (and also when antigen becomes persistent), T cell populations can emerge that lack some of the functions present in effector T cells and that have a different set of properties[84, 85]. How do prior functional states influence subsequent T cell fate? For instance, do T cells that express granzymes or perforin during an ongoing immune response preferentially die or gain a memory phenotype after antigen clearance, or is this specific functional characteristic irrelevant for long-term survival? Likewise, is the ability of differentiated T helper cells to express a particular profile of effector cytokines stably maintained over long periods or can their phenotype be reset[86]?

The key requirement for answering these questions is that (transient) expression of a specific functional property is translated into a stable and heritable marker that can be measured at a later point in time. To this end, several research groups have generated reporter mice in which expression of a gene of interest is coupled to expression of a fluorescent label. One way to generate these reporter mice is by insertion of a bicistronic fluorescent reporter cassette into the locus of the gene of interest[87, 88]. In such knock-in mice, reporter expression is transient, as the fluorescent mark is only produced as long as the gene of interest is expressed and, consequently, these systems are unlikely to allow longitudinal fate mapping of T cell populations. Several strategies have therefore been developed to provide differentiating cells with a more stable mark. One way to prolong marker expression is to stabilize reporter transcripts by inclusion of exogenous untranslated regulatory sequences. Stabilization of an interferon-γ (IFNγ)-Thy1.1 reporter by inclusion of a 3' untranslated SV40 intron/polyadenylation sequence has allowed the identification of Thy1.1-positive T cells for a prolonged period following termination of IFNγ protein expression (and for more

than 40 days post-infection)[89]. The finding that expression of the Thy1.1 marker proved to be so stable in this system may indicate that regulation of IFNγ expression in memory T cells primarily occurs at the post-transcriptional stage. More importantly, the fact that reporter-positive $CD4^+$ and $CD8^+$ T cells could give rise to functional memory cells indicates that T cells that express IFNγ during the effector phase can survive the contraction phase of the immune response.

The detection of stabilized reporter constructs depends on the half-life of the measured transcript. As the half-life of most mRNAs is in the order of hours, these systems are expected to be restricted to the monitoring of prior gene expression for periods of days at most. Allowing gene expression to induce an irreversible genetic mark circumvents this limitation. By using Cre expression, driven by a truncated human granzyme B promoter to activate a placental alkaline phosphatase (PLAP) reporter by recombination, it was shown that $CD8^+$ T cells that expressed granzyme B during primary lymphocytic choriomeningitis virus (LCMV) infection also had the capacity to develop into long-lived memory T cells[90]. In a more recent study by Fearon and colleagues, a bacterial artificial chromosome (BAC) transgenic mouse line was generated, in which a conditional Cre cassette was inserted into the gene encoding granzyme B. Subsequently, this BAC transgenic was crossed with a yellow fluorescent protein (YFP) reporter strain[91]. In this experimental set-up, which has the distinct advantage that it measures granzyme B expression using the natural promoter and surrounding sequences, it was also found that $CD8^+$ T cells that expressed granzyme B during primary influenza virus infection gave rise to functional memory T cells.

Although these results convincingly show that effector T cells (as defined by specific promoter activity) can be precursors of memory T cells, it is important to realize what is and what is not measured in these types of experiment that use reporters of prior functional states (here discussed in the context of effector and memory T cells, but the underlying principles are generally applicable). First, these reporter constructs measure transcriptional activity of the gene of interest and not expression or activity of the protein itself. Thus, it cannot be definitively concluded that reporter-positive cells are functional effector T cells, as there are additional layers of regulation that can prevent protein expression until later stages of cell differentiation[92]. Second, the current reporter systems do not have a 100% tagging efficiency and typically mark only a fraction of gene-expressing cells. As a result, it is difficult to determine whether memory T cells only come from effector T cells that expressed the gene of interest or whether memory T cells can also come from T cells that did not express that gene (Fig. 3a). Third, although reporter constructs can indicate that at least some T cells with an effector property can give rise to memory T cells, they cannot provide information on whether the effector population is homogeneous in this respect. Specifically, the ability to form memory T cells could be determined by an unknown marker that is displayed by only a portion of the effector T cell population and which is not being measured (Fig. 3b). In such cases the most accurate conclusion would not be that effector T cells form memory T cells but that effector T cells contain a subset of cells that form the precursors of memory T cells.

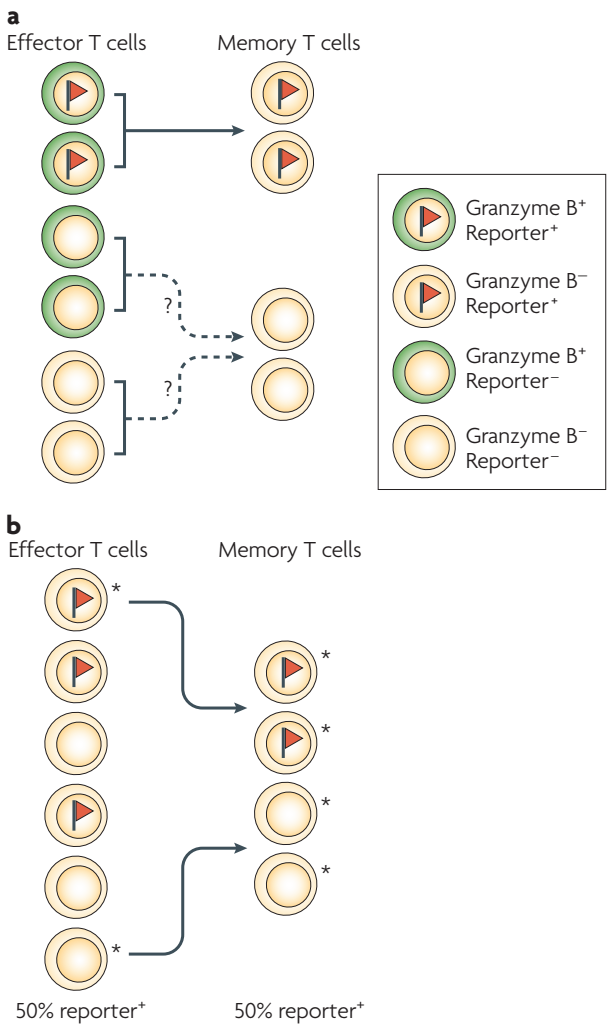

Figure 3: Pitfalls of gene expression reporters in kinship analysis. **a** | In this example, a reporter for gene expression associated with effector function (for example, granzyme B or perforin expression) is used to assess kinship of effector and memory T cells. Because of suboptimal tagging efficiency, only half of all effector T cells that express the gene of interest also express the reporter. Although the origin of the reporter-positive memory cells (top two memory T cells) can be traced back to effector T cells that expressed the gene of interest, the origin of the reporter-negative memory T cells (bottom two memory T cells) remains unclear, as these cells can be the progeny of cells that did or did not express the gene of interest. **b** | Similarity in the fraction of reporter-positive effector and memory T cells does not show that the effector T cell population is homogeneous and that all reporter-positive effector T cells can give rise to memory T cells. Specifically, the ability to form memory T cells could be determined by an unknown feature (*) that is displayed by only a portion of the effector T cells. Thus, although the presence of reporter-positive memory T cells indicates that at least some cells with an effector phenotype can give rise to memory T cells, it does not show that all effector T cells are equipotent in this respect.

MAPPING MIGRATION AND PRIOR SIGNALLING

T cells travel through highly dynamic environments and interact with many other haematopoietic as well as non-haematopoietic cells. During an immune response, many of these interactions have the potential to affect T cell proliferation, differentiation and survival[93, 94]. Measuring the cellular interactions that T cells encounter during an immune response and analysing how these affect subsequent cell behaviour are important goals to further our understanding of T cell function. In the final part of this Review, we discuss how new technologies can aid in the visualization of T cell migration patterns and reveal the diverse signalling input received by T cells at different sites.

Tracking T cell migration. Although it is well established that antigen-specific T cell responses are initiated in secondary lymphoid organs, it remains largely unclear where activated T cells migrate to after these priming sites are abandoned. For example, did bone marrow-resident memory T cells at one point reside at the site of infection[95, 96, 97]? Similarly, do T cells that are present at an effector site yield further progeny when leaving that site through the afferent lymph vessels? Part of this obscurity stems from the technical difficulty in tracking migrating T cell populations. Any experimental system that aims to follow T cell migration patterns in vivo is therefore likely to depend on the ability to induce stable markers at the moment T cells are present at a given site and to record the same markers at later time points and at different locations (Fig. 4).

A promising approach for the monitoring of T cell migration builds on the use of light to induce conformational changes in photoreceptive proteins. One group of studies used the protein Kaede, which fluoresces green after synthesis but can be photoconverted to red fluorescence by exposure to violet light[98]. In transgenic mice expressing Kaede, photoconversion at a specific site allows the subsequent migration patterns of these cells to be followed. By photoconverting inguinal lymph node cells and tracking their migration, it has been shown that 1 day after exposure to violet light, the photoconverted cells had disseminated to the spleen and to other lymph nodes, indicating that in the steady-state, lymph node cells are highly migratory[99].

As photoconverted Kaede is rapidly diluted by cell proliferation, this system is less suitable for longitudinal monitoring of cell migration patterns and, ideally, strategies based on light-induced switching would give rise to the irreversible genetic marking of cells present at a defined site. Conceptually, this strategy resembles the reporter systems that are used to reveal prior T cell function, but with the important difference that the signal that drives cell marking uses a synthetic, rather than an endogenous, signalling pathway. The emerging field of synthetic biology has already yielded customized signalling pathways that form interesting entry points for the generation of such cell migration reporters[100]. Many signal transduction proteins consist of two types of domain: one that displays catalytic activity and one that links the protein to upstream regulators and downstream targets. Because these domains are often structurally autonomous, they can carry out their function in a context-independent

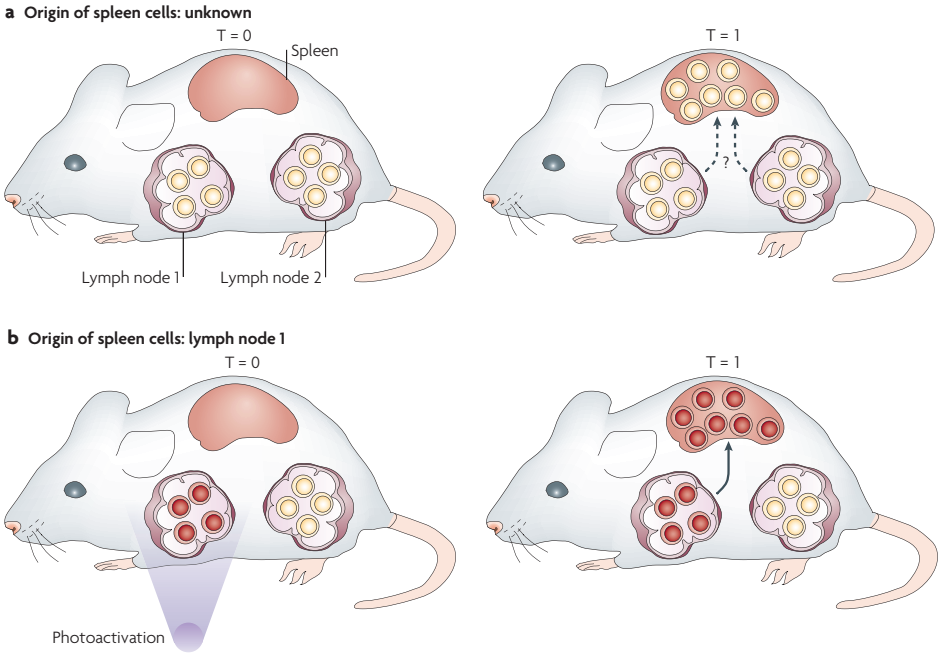

Figure 4: Tracking T cell migration by light-activated markers. a | At baseline (T = 0) both lymph nodes contain a phenotypically identical T cell population (for example, recently primed antigen-specific T cells). At T = 1, some of these T cells have migrated to the spleen. In this scenario, it is impossible to determine whether the splenic T cells are derived from lymph node 1, 2 or both. **b** | In this case, photoactivation of cells in lymph node 1 is used to specifically mark these cells with a unique label (for example, a red fluorescent protein induced by light-activated transcription). At T = 1 all splenic T cells harbour the red fluorescent marker, and because of this the origin of these T cells can be traced back to cells originating from lymph node 1.

manner. As an example, coupling of a light-sensitive input module to a DNA-binding output module might yield a light-activated transcription factor. In fact, by fusing the photoactive LOV2 domain of Avena sativa phototropin 1 to the Escherichia coli trp repressor, Sosnick and colleagues showed the feasibility of designing transcription factors for which DNA binding is made responsive to blue light excitation[101]. Although at this point there are no studies available that used light to induce stable cell marking, the fact that many LOV domains respond to photoexcitation with a conformational change suggests that it may be possible to design (sets of) photoactive switches that use a synthetic light reporter to enable stable fluorescent cell marking.

Revealing prior cell signalling events. As activated T cells migrate throughout the body, they can receive a multitude of signals from many different cell types, each of which can potentially direct subsequent T cell function. Mapping these diverse signals will require experimental strategies that can couple a given signalling event to the

expression of detectable markers. Triggering of a given cell surface receptor may be monitored either upstream or downstream of the endogenous signalling cascade (Fig. 5). The monitoring of downstream targets of signalling cascades (for example, activation of a cytokine promoter) is now relatively well established and can be achieved by placing a fluorescent protein or Cre recombinase under the control of this promoter (as described above)[102, 103]. However, in many cases a given cell surface receptor (for example, a T cell co-stimulatory receptor) does not have unique downstream targets, making downstream signalling reporters unsuitable for selectively reporting on the triggering of that specific receptor. In such cases, receptor triggering will have to be measured upstream in the signalling cascade, and this will require the use of synthetic signal transduction pathways. In such pathways, receptor signalling input is coupled to a new signalling output aimed at inducing marker expression, such that a cell will, for example, express a fluorescent protein after a defined cell surface receptor has been triggered.

What kinds of strategies could be pursued to build such synthetic signalling pathways aimed at monitoring signalling input? As an initial strategy, Lim and colleagues generated a system in which Rho guanine-nucleotide exchange factor (Rho–GEF) activity is controlled by flanking the Rho–GEF with a PSD95, DLGA and ZO1 homology (PDZ) domain (a peptide-binding motif) at one end and its cognate

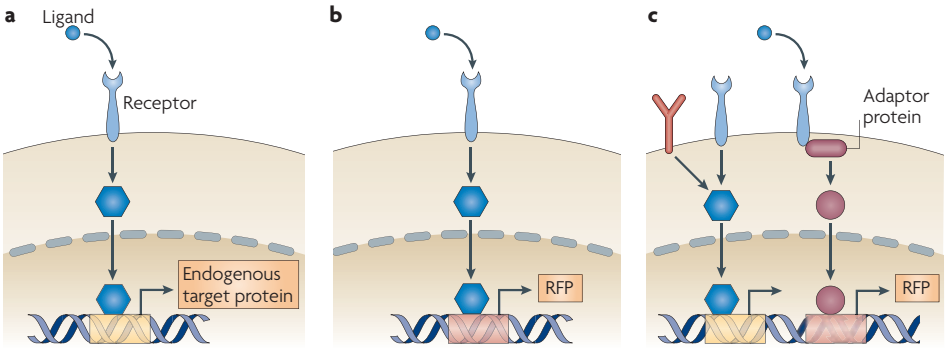

Figure 5: Strategies for revealing prior cell signalling. a | Triggering of a cell surface receptor initiates an intracellular signalling cascade, eventually leading to transcription of a target gene. To detect such a signalling event at a later point in time, the use of a reporter that converts this transient signal into a permanent mark is required. **b** | If a given cell surface receptor has a unique downstream target, receptor triggering can be monitored by placing a recombinase gene under the control of the activated promoter (not shown). Recombinase activity will lead to permanent expression of a fluorescent protein. **c** | If a given cell surface receptor does not have a unique downstream target, receptor triggering should be monitored upstream in the signalling cascade; this is likely to require the use of synthetic signal transduction pathways. Here, the cell surface receptor has been coupled to a hybrid adaptor protein, which following signal transduction will give rise to a transient burst of recombinase expression and permanent expression of a fluorescent protein. For the sake of simplicity, the recombination step in b and c is not depicted. RFP, red fluorescent protein.

target peptide at the other[104]. The resulting intramolecular PDZ–peptide interaction inhibited the intervening Rho–GEF activity. As the peptide was modified to contain a protein kinase A (PKA) target sequence, signalling through PKA could disrupt the PDZ–peptide binding, hence making this modified GEF a reporter of PKA activity[104]. Given that PDZ–peptide interactions have also been used to inhibit the function of other proteins[105], it may be worthwhile to pursue the generation of novel autoinhibition constructs, with which specific protein kinase activity can be monitored by the activation of reporter proteins.

A second group of strategies that measure receptor triggering are based on the action of hybrid receptors or hybrid adaptor proteins. An early study that aimed to directly monitor receptor activation made use of the fact that activation of Notch family receptors triggers the release of their cytoplasmic tail. When this cytoplasmic tail was replaced by a heterologous transcription factor, a new transcriptional programme could be initiated by Notch signalling[106]. Using a similar strategy, it might be feasible to visualize Notch signalling in T cells during antigen-specific responses by linking its signalling to expression of a detectable marker[107]. As a second example, one study artificially connected the epidermal growth factor (EGF) receptor pathway to the FAS (also known as CD95)-mediated cell death receptor pathway by constructing a hybrid adaptor protein[108]. As a result, mitogenic EGF receptor signalling led to caspase activation and cell death. Although inducing cells to die will clearly not be a very efficient strategy to track cells that underwent receptor triggering, the general concept used here can also be applied to induce more innocuous tags. Together, these studies highlight how in the coming years synthetic signalling pathways might be used to link the multitude of signals received by activated T cells during the course of an immune response to the expression of detectable markers.

CONCLUDING REMARKS

The T cell-based immune system is arguably one of the most complex organ systems. Rather than being confined to one specific location, T cells migrate around the body and receive many receptor-mediated signals at different locations and points in time that affect subsequent cell behaviour. Currently, we are just beginning to understand the total 'package' of signals that T cells encounter during antigen-induced responses and how these different signals influence the functional states both of that cell and of its downstream progeny. In this Review, we have focused on existing technologies and discussed some potential strategies that allow us to 'look back in time' and examine the cellular origins and past cellular experiences of different T cell subsets. Technologies such as single-cell and genetic tracking have already proven to be valuable for furthering our understanding of how cell-fate heterogeneity can arise. However, as neither of these technologies can directly reveal the signals that cells have received, new strategies will be required to help to explain how the sum of the signalling input dictates eventual T cell function and destiny. Ultimately, by connecting

a T cell's past experience to its current function, we should be better able to predict T cell behaviour in disease as well as therapeutic settings.

ACKNOWLEDGEMENTS

The authors thank S. Naik and G. Bendle for valuable input during conception of this manuscript and members of the Schumacher laboratory for stimulating discussions.

COMPETING INTERESTS STATEMENT

The authors declare no competing financial interests.

REFERENCES

1. Blattman, J. N. *et al*. Estimating the precursor frequency of naive antigen-specific CD8 T cells. J. Exp. Med. 195, 657–664 (2002).
2. Moon, J. J. *et al*. Naive CD4$^+$ T cell frequency varies for different epitopes and predicts repertoire diversity and response magnitude. Immunity 27, 203–213 (2007).
3. Obar, J. J., Khanna, K. M. & Lefrancois, L. Endogenous naive CD8$^+$ T cell precursor frequency regulates primary and memory responses to infection. Immunity 28, 859–869 (2008).
4. Butz, E. A. & Bevan, M. J. Massive expansion of antigen-specific CD8$^+$ T cells during an acute virus infection. Immunity 8, 167–175 (1998).
5. Murali-Krishna, K. *et al*. Counting antigen-specific CD8 T cells: a reevaluation of bystander activation during viral infection. Immunity 8, 177–187 (1998).
6. Busch, D. H., Pilip, I. M., Vijh, S. & Pamer, E. G. Coordinate regulation of complex T cell populations responding to bacterial infection. Immunity 8, 353–362 (1998).
7. van Stipdonk, M. J., Lemmens, E. E. & Schoenberger, S. P. Naive CTLs require a single brief period of antigenic stimulation for clonal expansion and differentiation. Nature Immunol. 2, 423–429 (2001).
8. Wherry, E. J., Puorro, K. A., Porgador, A. & Eisenlohr, L. C. The induction of virus-specific CTL as a function of increasing epitope expression: responses rise steadily until excessively high levels of epitope are attained. J. Immunol. 163, 3735–3745 (1999).
9. Badovinac, V. P., Porter, B. B. & Harty, J. T. Programmed contraction of CD8$^+$ T cells after infection. Nature Immunol. 3, 619–626 (2002).
10. Prlic, M., Hernandez-Hoyos, G. & Bevan, M. J. Duration of the initial TCR stimulus controls the magnitude but not functionality of the CD8$^+$ T cell response. J. Exp. Med. 203, 2135–2143 (2006).
11. Harty, J. T. & Badovinac, V. P. Shaping and reshaping CD8$^+$ T-cell memory. Nature Rev. Immunol. 8, 107–119 (2008).
12. Williams, M. A. & Bevan, M. J. Effector and memory CTL differentiation. Annu. Rev. Immunol. 25, 171–192 (2007).
13. Reiner, S. L., Sallusto, F. & Lanzavecchia, A. Division of labor with a workforce of one: challenges in specifying effector and memory T cell fate. Science 317, 622–625 (2007).
14. Ahmed, R., Bevan, M. J., Reiner, S. L. & Fearon, D. T. The precursors of memory: models and controversies. Nature Rev. Immunol. 9, 662–668 (2009).
15. Jameson, S. C. & Masopust, D. Diversity in T cell memory: an embarrassment of riches. Immunity 31, 859–871 (2009).
16. Zhou, L., Chong, M. M. & Littman, D. R. Plasticity of CD4$^+$ T cell lineage differentiation. Immunity 30, 646–655 (2009).
17. Locksley, R. M. Nine lives: plasticity among T helper cell subsets. J. Exp. Med. 206, 1643–1646 (2009).
18. King, C. New insights into the differentiation and function of T follicular helper cells. Nature Rev. Immunol. 9, 757–766 (2009).
19. Weaver, C. T. & Hatton, R. D. Interplay between the T_H17 and T_{Reg} cell lineages: a (co-)evolutionary perspective. Nature Rev. Immunol. 9, 883–889 (2009).
20. Greenberg, P. D. & Cheever, M. A. Treatment of disseminated leukemia with cy-

clophosphamide and immune cells: tumor immunity reflects long-term persistence of tumor-specific donor T cells. J. Immunol. 133, 3401–3407 (1984).

21. Shen, F. W. *et al*. Cloning of Ly-5 cDNA. Proc. Natl Acad. Sci. USA 82, 7360–7363 (1985).
22. Kearney, E. R., Pape, K. A., Loh, D. Y. & Jenkins, M. K. Visualization of peptide-specific T cell immunity and peripheral tolerance induction *in vivo*. Immunity 1, 327–339 (1994).
23. Okabe, M., Ikawa, M., Kominami, K., Nakanishi, T. & Nishimune, Y. 'Green mice' as a source of ubiquitous green cells. FEBS Lett. 407, 313–319 (1997).
24. Parish, C. R. Fluorescent dyes for lymphocyte migration and proliferation studies. Immunol. Cell Biol. 77, 499–508 (1999).
25. Roberts, A. D., Ely, K. H. & Woodland, D. L. Differential contributions of central and effector memory T cells to recall responses. J. Exp. Med. 202, 123–133 (2005).
26. Wright, D. E., Wagers, A. J., Gulati, A. P., Johnson, F. L. & Weissman, I. L. Physiological migration of hematopoietic stem and progenitor cells. Science 294, 1933–1936 (2001).
27. Klonowski, K. D. *et al*. Dynamics of blood-borne CD8 memory T cell migration *in vivo*. Immunity 20, 551–562 (2004).
28. Merad, M. *et al*. Langerhans cells renew in the skin throughout life under steady-state conditions. Nature Immunol. 3, 1135–1141 (2002).
29. von Andrian, U. H. & Mempel, T. R. Homing and cellular traffic in lymph nodes. Nature Rev. Immunol. 3, 867–878 (2003).
30. Miller, M. J., Wei, S. H., Parker, I. & Cahalan, M. D. Two-photon imaging of lymphocyte motility and antigen response in intact lymph node. Science 296, 1869–1873 (2002).
31. Stoll, S., Delon, J., Brotz, T. M. & Germain, R. N. Dynamic imaging of T cell-dendritic cell interactions in lymph nodes. Science 296, 1873–1876 (2002).
32. Bousso, P., Bhakta, N. R., Lewis, R. S. & Robey, E. Dynamics of thymocyte-stromal cell interactions visualized by two-photon microscopy. Science 296, 1876–1880 (2002).
33. Germain, R. N., Miller, M. J., Dustin, M. L. & Nussenzweig, M. C. Dynamic imaging of the immune system: progress, pitfalls and promise. Nature Rev. Immunol. 6, 497–507 (2006).
34. Cahalan, M. D. & Parker, I. Choreography of cell motility and interaction dynamics imaged by two-photon microscopy in lymphoid organs. Annu. Rev. Immunol. 26, 585–626 (2008).
35. Bousso, P. T-cell activation by dendritic cells in the lymph node: lessons from the movies. Nature Rev. Immunol. 8, 675–684 (2008).
36. Mempel, T. R., Henrickson, S. E. & von Andrian, U. H. T-cell priming by dendritic cells in lymph nodes occurs in three distinct phases. Nature 427, 154–159 (2004).
37. Miller, M. J., Safrina, O., Parker, I. & Cahalan, M. D. Imaging the single cell dynamics of $CD4^+$ T cell activation by dendritic cells in lymph nodes. J. Exp. Med. 200, 847–856 (2004).
38. Hugues, S. *et al*. Distinct T cell dynamics in lymph nodes during the induction of tolerance and immunity. Nature Immunol. 5, 1235–1242 (2004).
39. Henrickson, S. E. *et al*. T cell sensing of antigen dose governs interactive behavior with dendritic cells and sets a threshold for T cell activation. Nature Immunol. 9, 282–291 (2008).
40. Bousso, P. & Robey, E. Dynamics of $CD8^+$ T cell priming by dendritic cells in intact lymph nodes. Nature Immunol. 4, 579–585 (2003).
41. Miller, M. J., Hejazi, A. S., Wei, S. H., Cahalan, M. D. & Parker, I. T cell repertoire scanning is promoted by dynamic dendritic cell behavior and random T cell motility in the lymph node. Proc. Natl Acad. Sci. USA 101, 998–1003 (2004).
42. Beltman, J. B., Maree, A. F., Lynch, J. N., Miller, M. J. & de Boer, R. J. Lymph node topology dictates T cell migration behavior. J. Exp. Med. 204, 771–780 (2007).
43. Wu, M. *et al*. Imaging hematopoietic precursor division in real time. Cell Stem Cell 1, 541–554 (2007).
44. Schroeder, T. Imaging stem-cell-driven regeneration in mammals. Nature 453, 345–351 (2008).
45. Eilken, H. M., Nishikawa, S. & Schroeder, T. Continuous single-cell imaging of blood generation from haemogenic endothelium. Nature 457, 896–900 (2009).
This study uses long-term *in vitro* time-lapse microscopy to show that adherent endothelial cells can directly give rise to non-adherent haematopoietic cells.
46. Zovein, A. C. *et al*. Fate tracing reveals the endothelial origin of hematopoietic stem cells. Cell Stem Cell 3, 625–636 (2008).

47. Boisset, J. C. *et al*. *In vivo* imaging of haematopoietic cells emerging from the mouse aortic endothelium. Nature 464, 116–120 (2010).
48. Rieger, M. A., Hoppe, P. S., Smejkal, B. M., Eitelhuber, A. C. & Schroeder, T. Hematopoietic cytokines can instruct lineage choice. Science 325, 217–218 (2009).
49. Hawkins, E. D., Markham, J. F., McGuinness, L. P. & Hodgkin, P. D. A single-cell pedigree analysis of alternative stochastic lymphocyte fates. Proc. Natl Acad. Sci. USA 106, 13457–13462 (2009).
This study uses long-term *in vitro* imaging to reveal that progeny of single founder B cells have markedly synchronized division properties.
50. Spencer, S. L., Gaudet, S., Albeck, J. G., Burke, J. M. & Sorger, P. K. Non-genetic origins of cell-to-cell variability in TRAIL-induced apoptosis. Nature 459, 428–432 (2009).
51. Sigal, A. *et al*. Variability and memory of protein levels in human cells. Nature 444, 643–646 (2006).
52. Chang, H. H., Hemberg, M., Barahona, M., Ingber, D. E. & Huang, S. Transcriptome-wide noise controls lineage choice in mammalian progenitor cells. Nature 453, 544–547 (2008).
53. Feinerman, O., Veiga, J., Dorfman, J. R., Germain, R. N. & Altan-Bonnet, G. Variability and robustness in T cell activation from regulated heterogeneity in protein levels. Science 321, 1081–1084 (2008).
54. Osawa, M., Hanada, K., Hamada, H. & Nakauchi, H. Long-term lymphohematopoietic reconstitution by a single CD34-low/negative hematopoietic stem cell. Science 273, 242–245 (1996).
55. Kiel, M. J. *et al*. SLAM family receptors distinguish hematopoietic stem and progenitor cells and reveal endothelial niches for stem cells. Cell 121, 1109–1121 (2005).
56. Stemberger, C. *et al*. A single naive $CD8^+$ T cell precursor can develop into diverse effector and memory subsets. Immunity 27, 985–997 (2007).
This study analyses *in vivo* T cell fate by performing single cell transfer and shows that one naive $CD8^+$ T cell can yield diverse effector and memory T cell subsets.
57. Kedzierska, K., La Gruta, N. L., Stambas, J., Turner, S. J. & Doherty, P. C. Tracking phenotypically and functionally distinct T cell subsets via T cell repertoire diversity. Mol. Immunol. 45, 607–618 (2008).
58. Maryanski, J. L., Jongeneel, C. V., Bucher, P., Casanova, J. L. & Walker, P. R. Single-cell PCR analysis of TCR repertoires selected by antigen *in vivo*: a high magnitude CD8 response is comprised of very few clones. Immunity 4, 47–55 (1996).
59. Busch, D. H., Pilip, I. & Pamer, E. G. Evolution of a complex T cell receptor repertoire during primary and recall bacterial infection. J. Exp. Med. 188, 61–70 (1998).
60. Sourdive, D. J. *et al*. Conserved T cell receptor repertoire in primary and memory CD8 T cell responses to an acute viral infection. J. Exp. Med. 188, 71–82 (1998).
61. Lin, M. Y. & Welsh, R. M. Stability and diversity of T cell receptor repertoire usage during lymphocytic choriomeningitis virus infection of mice. J. Exp. Med. 188, 1993–2005 (1998).
62. McHeyzer-Williams, L. J., Panus, J. F., Mikszta, J. A. & McHeyzer-Williams, M. G. Evolution of antigen-specific T cell receptors *in vivo*: preimmune and antigen-driven selection of preferred complementarity-determining region 3 (CDR3) motifs. J. Exp. Med. 189, 1823–1838 (1999).
63. Blattman, J. N., Sourdive, D. J., Murali-Krishna, K., Ahmed, R. & Altman, J. D. Evolution of the T cell repertoire during primary, memory, and recall responses to viral infection. J. Immunol. 165, 6081–6090 (2000).
64. Fasso, M. *et al*. T cell receptor (TCR)-mediated repertoire selection and loss of TCR Vβ diversity during the initiation of a $CD4^+$ T cell response *in vivo*. J. Exp. Med. 192, 1719–1730 (2000).
65. Turner, S. J., Diaz, G., Cross, R. & Doherty, P. C. Analysis of clonotype distribution and persistence for an influenza virus-specific $CD8^+$ T cell response. Immunity 18, 549–559 (2003).
66. Kedzierska, K., Turner, S. J. & Doherty, P. C. Conserved T cell receptor usage in primary and recall responses to an immunodominant influenza virus nucleoprotein epitope. Proc. Natl Acad. Sci. USA 101, 4942–4947 (2004).
67. Malherbe, L., Hausl, C., Teyton, L. & McHeyzer-Williams, M. G. Clonal selection of helper T cells is determined by an affinity threshold with no further skewing of TCR binding properties. Immunity 21, 669–679 (2004).
68. Sallusto, F., Lenig, D., Forster, R., Lipp, M. & Lanzavecchia, A. Two subsets of memory T lymphocytes with distinct homing potentials and effector functions. Nature 401, 708–712 (1999).

69. Masopust, D., Vezys, V., Marzo, A. L. & Lefrancois, L. Preferential localization of effector memory cells in nonlymphoid tissue. Science 291, 2413–2417 (2001).
70. Baron, V. *et al*. The repertoires of circulating human CD8$^+$ central and effector memory T cell subsets are largely distinct. Immunity 18, 193–204 (2003).
71. Bouneaud, C., Garcia, Z., Kourilsky, P. & Pannetier, C. Lineage relationships, homeostasis, and recall capacities of central- and effector-memory CD8 T cells *in vivo*. J. Exp. Med. 201, 579–590 (2005).
72. Kedzierska, K. *et al*. Early establishment of diverse T cell receptor profiles for influenza-specific CD8$^+$CD62L^{hi} memory T cells. Proc. Natl Acad. Sci. USA 103, 9184–9189 (2006).
73. Wong, J., Mathis, D. & Benoist, C. TCR-based lineage tracing: no evidence for conversion of conventional into regulatory T cells in response to a natural self-antigen in pancreatic islets. J. Exp. Med. 204, 2039–2045 (2007).
74. Jacob, J. & Kelsoe, G. *In situ* studies of the primary immune response to (4-hydroxy-3-nitrophenyl)acetyl. II. A common clonal origin for periarteriolar lymphoid sheath-associated foci and germinal centers. J. Exp. Med. 176, 679–687 (1992).
75. Schepers, K. *et al*. Dissecting T cell lineage relationships by cellular barcoding. J. Exp. Med. 205, 2309–2318 (2008).
76. Gerlach, C. *et al*. One naive T cell, multiple fates in CD8$^+$ T cell differentiation. J. Exp. Med. 207, 1235–1246 (2010).
This study develops barcode tagging of thymocytes and uses it to show that the progeny of single naive CD8$^+$ T cells can take on multiple fates under various infectious challenges.
77. Masopust, D. *et al*. Activated and memory CD8 T cells migrate to nonlymphoid tissues regardless of site activation or tissue of origin. J. Immunol. 172, 4875–4882 (2004).
78. Masopust, D. *et al*. Dynamic T cell migration program provides resident memory within intestinal epithelium. J. Exp. Med. 207, 553–564 (2010).
79. van Heijst, J. W. *et al*. Recruitment of antigen-specific CD8$^+$ T cells in response to infection is markedly efficient. Science 325, 1265–1269 (2009).
This paper uses cellular barcoding to show that the magnitude of CD8$^+$ T cell responses is primarily determined by clonal burst size.
80. Livet, J. *et al*. Transgenic strategies for combinatorial expression of fluorescent proteins in the nervous system. Nature 450, 56–62 (2007).
In this paper, a Cre–lox-based approach is described that leads to the stochastic expression of multiple fluorescent proteins, allowing the identity of individual neurons to be distinguished by expression of 1 out of almost 100 different colour variations.
81. Hodgkin, P. D., Lee, J. H. & Lyons, A. B. B cell differentiation and isotype switching is related to division cycle number. J. Exp. Med. 184, 277–281 (1996).
82. Gett, A. V. & Hodgkin, P. D. Cell division regulates the T cell cytokine repertoire, revealing a mechanism underlying immune class regulation. Proc. Natl Acad. Sci. USA 95, 9488–9493 (1998).
83. Bird, J. J. *et al*. Helper T cell differentiation is controlled by the cell cycle. Immunity 9, 229–237 (1998).
84. Kaech, S. M., Hemby, S., Kersh, E. & Ahmed, R. Molecular and functional profiling of memory CD8 T cell differentiation. Cell 111, 837–851 (2002).
85. Shin, H. & Wherry, E. J. CD8 T cell dysfunction during chronic viral infection. Curr. Opin. Immunol. 19, 408–415 (2007).
86. O'Shea, J. J. & Paul, W. E. Mechanisms underlying lineage commitment and plasticity of helper CD4$^+$ T cells. Science 327, 1098–1102 (2010).
87. Mohrs, M., Shinkai, K., Mohrs, K. & Locksley, R. M. Analysis of type 2 immunity *in vivo* with a bicistronic IL-4 reporter. Immunity 15, 303–311 (2001).
88. Stetson, D. B. *et al*. Constitutive cytokine mRNAs mark natural killer (NK) and NK T cells poised for rapid effector function. J. Exp. Med. 198, 1069–1076 (2003).
89. Harrington, L. E., Janowski, K. M., Oliver, J. R., Zajac, A. J. & Weaver, C. T. Memory CD4 T cells emerge from effector T-cell progenitors. Nature 452, 356–360 (2008).
90. Jacob, J. & Baltimore, D. Modelling T-cell memory by genetic marking of memory T cells *in vivo*. Nature 399, 593–597 (1999).
91. Bannard, O., Kraman, M. & Fearon, D. T. Secondary replicative function of CD8$^+$ T cells that had developed an effector phenotype. Science 323, 505–509 (2009).
This paper uses a conditional granzyme B–YFP reporter mouse to show that granzyme B-expressing effector T cells can give rise to functional memory T cells.

92. O'Connell, R. M., Rao, D. S., Chaudhuri, A. A. & Baltimore, D. Physiological and pathological roles for microRNAs in the immune system. Nature Rev. Immunol. 10, 111–122 (2010).

93. Gett, A. V. & Hodgkin, P. D. A cellular calculus for signal integration by T cells. Nature Immunol. 1, 239–244 (2000).

94. Hawkins, E. D., Turner, M. L., Dowling, M. R., van Gend, C. & Hodgkin, P. D. A model of immune regulation as a consequence of randomized lymphocyte division and death times. Proc. Natl Acad. Sci. USA 104, 5032–5037 (2007).

95. Becker, T. C., Coley, S. M., Wherry, E. J. & Ahmed, R. Bone marrow is a preferred site for homeostatic proliferation of memory CD8 T cells. J. Immunol. 174, 1269–1273 (2005).

96. Mazo, I. B. *et al*. Bone marrow is a major reservoir and site of recruitment for central memory $CD8^+$ T cells. Immunity 22, 259–270 (2005).

97. Tokoyoda, K. *et al*. Professional memory $CD4^+$ T lymphocytes preferentially reside and rest in the bone marrow. Immunity 30, 721–730 (2009).

98. Hatta, K., Tsujii, H. & Omura, T. Cell tracking using a photoconvertible fluorescent protein. Nature Protoc. 1, 960–967 (2006).

99. Tomura, M. *et al*. Monitoring cellular movement *in vivo* with photoconvertible fluorescence protein 'Kaede' transgenic mice. Proc. Natl Acad. Sci. USA 105, 10871–10876 (2008).
In this paper, the Kaede transgenic mouse model is described, in which photoconversion of a fluorescent protein can be used to track cell migration.

100. Pryciak, P. M. Designing new cellular signaling pathways. Chem. Biol. 16, 249–254 (2009).

101. Strickland, D., Moffat, K. & Sosnick, T. R. Light-activated DNA binding in a designed allosteric protein. Proc. Natl Acad. Sci. USA 105, 10709–10714 (2008).
This paper provides proof-of-concept for a light-activated transcription factor by fusing a photoactive LOV domain to the *E. coli* trp repressor and inducing DNA binding by blue light excitation.

102. Croxford, A. L., Kurschus, F. C. & Waisman, A. Cutting edge: an IL-17F-CreEYFP reporter mouse allows fate mapping of Th17 cells. J. Immunol. 182, 1237–1241 (2009).

103. Schlenner, S. M. *et al*. Fate mapping reveals separate origins of T cells and myeloid lineages in the thymus. Immunity 32, 426–436 (2010).

104. Yeh, B. J., Rutigliano, R. J., Deb, A., Bar-Sagi, D. & Lim, W. A. Rewiring cellular morphology pathways with synthetic guanine nucleotide exchange factors. Nature 447, 596–600 (2007).
This study provides proof-of-concept for a reporter of kinase activity that is based on the combination of a PDZ–peptide autoinhibition moiety and a Rho–GEF reporter domain.

105. Dueber, J. E., Yeh, B. J., Chak, K. & Lim, W. A. Reprogramming control of an allosteric signaling switch through modular recombination. Science 301, 1904–1908 (2003).

106. Struhl, G. & Adachi, A. Nuclear access and action of notch *in vivo*. Cell 93, 649–660 (1998).

107. Radtke, F., Fasnacht, N. & Robson MacDonald, H. R. Notch signaling in the immune system. Immunity 32, 14–27 (2010).

108. Howard, P. L., Chia, M. C., Del Rizzo, S., Liu, F. F. & Pawson, T. Redirecting tyrosine kinase signaling to an apoptotic caspase pathway through chimeric adaptor proteins. Proc. Natl Acad. Sci. USA 100, 11267–11272 (2003).

109. Wu, A. M., Till, J. E., Siminovitch, L. & McCulloch, E. A. A cytological study of the capacity for differentiation of normal hemopoietic colony-forming cells. J. Cell. Physiol. 69, 177–184 (1967).

110. Wu, A. M., Till, J. E., Siminovitch, L. & McCulloch, E. A. Cytological evidence for a relationship between normal hemotopoietic colony-forming cells and cells of the lymphoid system. J. Exp. Med. 127, 455–464 (1968).

111. Abramson, S., Miller, R. G. & Phillips, R. A. The identification in adult bone marrow of pluripotent and restricted stem cells of the myeloid and lymphoid systems. J. Exp. Med. 145, 1567–1579 (1977).

112. Dick, J. E., Magli, M. C., Huszar, D., Phillips, R. A. & Bernstein, A. Introduction of a selectable gene into primitive stem cells capable of long-term reconstitution of the hemopoietic system of W/Wv mice. Cell 42, 71–79 (1985).

113. Keller, G., Paige, C., Gilboa, E. & Wagner, E. F. Expression of a foreign gene in myeloid and lymphoid cells derived from multipotent haematopoietic precursors. Nature 318, 149–154 (1985).

114. Lemischka, I. R., Raulet, D. H. & Mulligan, R. C. Developmental potential and dynam-

ic behavior of hematopoietic stem cells. Cell 45, 917–927 (1986).

115. Walsh, C. & Cepko, C. L. Widespread dispersion of neuronal clones across functional regions of the cerebral cortex. Science 255, 434–440 (1992).

116. Golden, J. A., Fields-Berry, S. C. & Cepko, C. L. Construction and characterization of a highly complex retroviral library for lineage analysis. Proc. Natl Acad. Sci. USA 92, 5704–5708 (1995).

3

THE DESCENT OF MEMORY T CELLS

Carmen Gerlach[1], Jeroen W.J van Heijst[1] and Ton N.M. Schumacher[1]

[1]Division of Immunology, The Netherlands Cancer Institute, Amsterdam, the Netherlands

Ann N Y Acad Sci. 1217: 139-53 (2011)

Our T cell repertoire is shaped by antigen encounter. From a naive T cell pool that contains millions of different T cells with unknown specificities, pathogen infection leads to selection of those T cells that can detect pathogen-derived antigens. Following clearance of infection, a population of memory T cells remains and protects the individual from severe reinfection. A central question in the field has been how the generation of long-lived memory T cells, versus short-lived ("terminally differentiated") T cells, is controlled. In this review we discuss the models that have been put forward to explain the generation of memory T cells after infection and the experimental evidence supporting these hypotheses. Based on the available data we propose a new model that stipulates that during immune responses T cells do not acquire different *fates* that determine their subsequent long-term survival but rather T cells assume different *states* that simply reflect the likelihood of future survival, states that can still be modulated by external signals.

INTRODUCTION

The formation of T cell memory has been an area of intense research, both because it concerns a fundamental aspect of adaptive immunity and because the induction of robust T cell memory is a goal of vaccination strategies. Kinetically, T cell responses can be subdivided into three distinct phases. During the initial expansion phase, naive antigen-specific T cells get activated and respond by extensive proliferation, leading to a massive (up to 10^4–10^5-fold) increase in antigen-specific T cell numbers. After antigen clearance, this population of antigen-specific T cells goes down in size (in immunological slang "contracts") due to apoptosis. When this contraction phase has ended, a small but stable pool of memory T cells remains behind. Enumeration of antigen-specific T cells at different times after infection by MHC multimer staining easily identifies the onset of this memory phase (i.e., the time point at which antigen-specific T cell numbers stay constant). However, it does not provide a clue on which individual T cells commit to longevity and at what point in their development these cells—or their ancestors—made this commitment. With the aim to establish this "descent of memory T cells," a multitude of studies have been performed over the past decades that followed T cell populations at the bulk level, and these studies have resulted in the proposition of a variety of models. Furthermore, in recent years, novel technologies that follow T cell history at the single cell level have been developed and used, thereby providing much better insight into memory T cell descent.

Below, we will discuss the different models for memory T cell generation and the predictions they make with respect to three central questions in the field:

1. Can long-lived memory T cells arise from effector T cells?
2. Which factors determine whether an individual T cell survives long-term?
3. When does an individual T cell commit to long-term persistence?

It is important to point out that these should be considered three entirely separate questions and—contrary to what has been done occasionally—data on one of these provide very little insight into the others. To provide some examples, models that predict that T cells commit to long-term persistence before the first cell division do not provide any insight into the question whether the daughter cells might transiently acquire certain effector properties prior to forming long-term memory. Similarly, models that invoke signal strength as a determining factor in the control of T cell fate do not inform us when exactly after T cell activation such signals act.

DEFINITIONS

Before discussing these different models, it is important to clarify some key terminology.

» Strictly speaking, effector T cells are those T cells that are responsible for pathogen removal, and depending on the type of pathogen, this could either involve functionalities such as cytokine secretion or direct lysis of infected cells. However, as it

would be impractical to use a definition of effector T cells that varies between infections, a pragmatic solution is to identify any T cell capable of producing cytokines such as IFN-γ, capable of producing molecules involved in target cell lysis such as granzyme B or perforin, or capable of killing infected cells as an effector cell.

- Terminally differentiated cells are by definition cells that can no longer differentiate further to adopt another identity. There is no *a priori* reason that a terminally differentiated cell should be short-lived. However, for terminally differentiated effector T cells this is the general assumption. The terms "effector" cell and "terminally differentiated" cell are not synonymous: the fact that a T cell displays effector cell properties does not imply that it is terminally differentiated.
- Memory T cells are those cells that survive beyond the contraction phase and persist long-term in the absence of pathogen.[1] Memory T cells can be subdivided, for instance based on their localization to lymphoid or peripheral tissues.[2,3] However, for the sake of simplicity we will here treat them as a single entity, characterized by the ability to survive long-term.
- Cell state is the phenotypic and functional state of a cell, which can be transient or permanent.
- Cell fate is a permanent and heritable cell state. In other words, a T cell that would commit to a memory T cell fate would only produce progeny that can survive in the absence of antigen. From the moment a T cell adopts a particular fate it is considered "committed," its future and that of its progeny is "programmed."
- T cell priming is the event of T cell activation, leading to its first cell division.

CAN LONG-LIVED MEMORY CELLS ARISE FROM EFFECTOR T CELLS?

Fifteen years ago, little more was known about the generation of memory T cells than that these cells survived beyond the contraction phase and persisted at relatively stable numbers in the absence of antigen. From this, it was assumed that a fraction of effector T cells resisted apoptosis and differentiated further into long-lived memory T cells. Thus, in this linear differentiation model (Fig. 1A), memory T cells arise directly from effector T cells. Only relatively recent it was realized that it is impossible to deduce a precursor–product relationship between effector and memory T cells from the overall response kinetics. Specifically, it is possible that all effector T cells would be terminally differentiated (i.e., unable to convert to memory T cells) and thus die during contraction phase, whereas a dedicated subset of memory precursor cells that lack effector function would survive. To dissect whether long-lived memory T cells can directly arise from effector cells, several approaches have been taken, in particular the cell-tracing experiments performed in recent years have been informative.

In early experiments, proliferating antigen-specific T cell receptor transgenic (TCRtg) $CD4^+$ or $CD8^+$ T cell populations generated through *in vitro* peptide stimulation[4,5] or *in vivo* lymphocytic choriomeningitis virus (LCMV) infection[6] were adoptively transferred

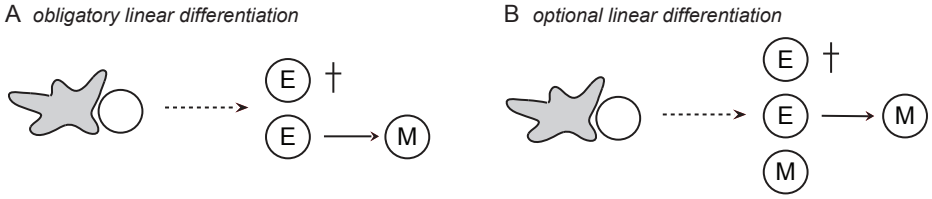

Figure 1: Linear differentiation model. According to the linear differentiation model, some effector T cells die after antigen clearance, while others give rise to memory T cells. (**A**) Linear differentiation might be obligatory in the sense that all memory T cells are direct descendants of effector cells. (**B**) Linear differentiation might also be optional in the sense that memory T cells can arise from effector cells, but can also arise independently of effector function.

into mice, and the potential of the transferred population to form persisting memory cells was monitored. As memory cells did develop in these experiments, the data were used as evidence for linear effector to memory differentiation. However, in all these early studies a heterogeneous population of dividing cells was transferred, of which the functional characteristics remained undefined, and the possibility remained that the memory cells arose from a subset of transferred cells that were not effector cells. Subsequent work demonstrated that the transfer of an essentially pure population of cells showing expression of perforin[7] or granzyme B[8] also resulted in the formation of T cell memory. To exclude the formal possibility that the memory T cells that developed in these experiments arose from a few contaminating non-effector T cells, several groups have subsequently used technologies that specifically tag effector T cells. Specifically, a number of reporter mouse strains have been created in which IFN-γ or granzyme B promoter activity leads to the long-term expression of a fluorescent or cell surface marker.[9–11] Using these mouse models, the groups of Baltimore, Weaver, and Fearon demonstrated that upon LCMV and influenza A infection long-lived $CD4^+$ and $CD8^+$ memory T cells can arise from T cells that have previously transcribed IFN-γ or granzyme B genes. It may be argued that the activity of the truncated human granzyme B reporter in an early study in this field[9] would not necessarily reflect the function of the endogenous murine promoter. However, as the same result was obtained in subsequent studies using reporter systems that are based on murine control elements,[10,11] these concerns are alleviated. Thus, the data obtained to date provide strong evidence that memory T cells can be formed from cells that previously transcribed genes associated with effector T cell function.

Two important questions remain, however. First, does the activity of the IFN-γ or granzyme B promoter reflect the actual production and secretion of these proteins? In other words, did the cells that are marked in these studies actually function as an effector cell? Second, do all memory T cells during natural infection arise from cells with effector properties (Fig. 1A), or can memory T cells also develop independently of effector function (Fig. 1B)? *In vitro* data in which peptide-stimulated TCRtg $CD8^+$

T cells were cultured in different cytokine environments have been used as evidence that memory T cells do not necessarily need to pass through an effector stage.[12] This conclusion was based on the observation that a $CD8^+$ T cell population cultured in high doses of IL-2 was able to lyse target cells more efficiently than a T cell population cultured in IL-15 and low doses of IL-2, while both populations were able to form memory. These data suggest that the capacity to kill infected cells may not be a necessary prerequisite to becoming memory cells. It should be noted though that cells grown under either condition produced IFN-γ, indicating that this particular effector function was possessed by both cell populations. Furthermore, the data do not address whether memory T cell formation without the transient acquisition of cytolytic capacity forms a physiological route for memory T cell production. Indirect evidence against the model that memory T cells are also formed *in vivo* without the transient acquisition of effector properties has been obtained in the reporter mouse studies. The tagging efficiency in these reporter mice is not absolute and consequently only a fraction of the cells transcribing the IFN-γ or granzyme B genes is marked by the reporter. However, the percentage of reporter-positive cells was similar in the effector phase as in the memory phase.[11] Thereby, these data suggest that a large fraction of memory T cells pass through an effector T cell stage. The possibility that a fraction (or specific subset) of memory T cells never displayed effector cell properties remains a possibility though,[13] and deserves further study.

WHICH FACTORS DETERMINE LONG-TERM T CELL SURVIVAL?

The above data indicate that at least part of the memory T cells are derived from the pool of T cells that display effector cell properties. Is there heterogeneity within the effector population that explains why some effector cells continue to develop into memory cells, while others die during contraction?

In an attempt to explain why some activated T cells would survive beyond the contraction phase and others not, Ahmed and Gray proposed the decreasing potential hypothesis, in which the level of antigenic stimulation was seen as the crucial factor dictating whether a cell would commit to a long-lived memory fate (weak stimulus) or undergo apoptosis after terminal differentiation (strong stimulus)[14] (Fig. 2A). Such variation in the strength of signals received by individual antigen-specific T cells was thought to be the result of exposure to different amounts of antigen or inflammatory environments, for example, due to difference in tissue localization, or asynchronous recruitment of naive T cells into the response (with early recruits receiving distinct signals from T cells activated later during infection). Also, Lanzavecchia and Sallusto argued that the strength of stimulation—the combination of TCR triggering, engagement of costimulatory molecules, and the duration of stimulation—that a T cell receives is fate determining. Their progressive differentiation model (Fig. 2B) proposes that T cells undergo progressive degrees of differentiation by accumulating increasing amounts of activation signals.[15,16] Weakly stimulated cells would initiate some proliferation but

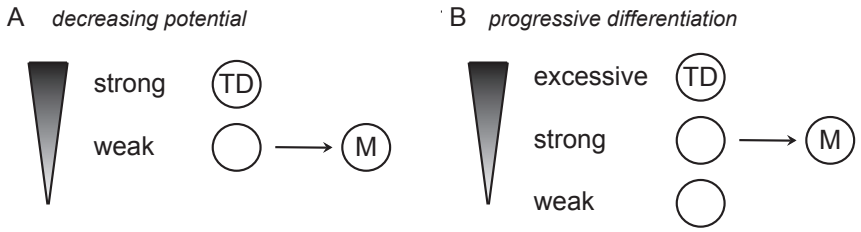

Figure 2: Comparison of decreasing potential and progressive differentiation models. (**A**) The decreasing potential model suggests that weakly stimulated T cells commit to a memory fate (cell marked M), while a strong stimulus leads to the fate of terminal differentiation (cell marked TD). (**B**) Also, the progressive differentiation model predicts that the most strongly (excessively) stimulated T cells undergo terminal differentiation. An intermediate stimulus leads to a memory fate, while weakly stimulated cells remain uncommitted (unmarked cell).

eventually die by neglect after antigen withdrawal, and without further differentiation into effector or memory cells. Cells that receive a strong signal would have the capacity to develop into memory cells, while excessively stimulated T cells were thought to undergo activation-induced cell death after terminal differentiation. For reasons that are unclear, the progressive differentiation model has sometimes been interpreted as opposing the decreasing potential hypothesis. It does not. To draw an analogy with T cell selection within the thymus, the decreasing potential model from Gray and Ahmed focuses on how the difference between a medium- and a high-strength signal can mean the difference between survival and negative selection, whereas the progressive differentiation model from Lanzavecchia and Sallusto also takes into account how the difference between a weak signal and a medium-strength signal can mean the difference between neglect and positive selection. Thus, both the progressive differentiation model and the decreasing potential model suggest that T cells that receive an intermediate activation signal can survive into the memory phase, whereas T cells that receive a stronger signal will die during contraction.

What is the experimental evidence supporting the hypothesis that high signal strength leads to the preferential development of terminally differentiated T cells? Most evidence comes from experiments in which the ratio between memory T cells and terminally differentiated cells (or the total number of antigen-specific T cells present at the peak of the response, which primarily consists of terminally differentiated cells) was monitored under diverse inflammatory conditions, or in situations of altered antigen availability. With one exception,[17] the diminished inflammation and antigen presentation that occurs upon treatment of bacterially infected animals with antibiotics has been shown to lead to a reduced magnitude of the peak T cell response.[8,18–20] In contrast, the absolute number of memory T cells that developed[19] or the number of KLRG1$^{lo/int}$CD127^{hi} cells[8]—presumed precursors of memory T cells[8,21]—was hardly affected. These data demonstrate that antigen-derived and/or inflammatory signals can influence the relative size of the memory population. In these studies,

the effects of antigen availability and inflammatory signals have also been investigated independently, and both reduced antigenic stimulation and limited inflammation were shown to result in an increase in the proportion of KLRG1$^{lo/int}$CD127^{hi} cells.[8,21] On the contrary, a strong inflammatory stimulus through the administration of exogenous IL-12 led to an increased percentage of antigen-specific T cells that expressed CD25, a phenotypic property linked to terminal differentiation.[22] In line with this, mice lacking functional IL-12 generated larger memory populations after *Listeria monocytogenes* infection than did wild-type mice.[23] Furthermore, exposure to the inflammatory cytokines IL-12 and IL-4 has been shown to induce expression of the transcription factors T-bet and Blimp-1,[8,24,25] which in turn induce the expression of KLRG-1 and CD25, molecules that are associated with terminal differentiation.[8,21,22,26] Thus, these studies suggest that both antigen and inflammation can form signals that lead to terminal T cell differentiation.

Nevertheless, not all studies support the hypothesis that increased signal strength promotes terminal differentiation. Specifically, the ratio between terminally differentiated and memory T cells was not affected when the duration of antigen availability was shortened through specific depletion of antigen presenting cells at different times after infection.[27] Similarly, recent work by Bevan and colleagues indicates that differences in TCR affinity for antigen do not alter the ratio between the number of effector phase and memory phase T cells.[28]

Taken together, a majority of studies suggest that at least some types of prolonged or increased stimulation favor the formation of terminally differentiated cells, while weak stimulation is sufficient for the generation of long-lived memory cells. Intuitively this makes sense, as it provides the system with the flexibility to alter output depending on the magnitude or duration of infection. However, our knowledge of the exact molecular interactions that do and do not determine "signal strength"—and thereby the ratio of terminally differentiated to memory cells—is at present still sketchy.

WHEN DOES AN INDIVIDUAL T CELL COMMIT TO LONG-TERM PERSISTENCE?

While there is now substantial evidence that the strength of at least some signals received by T cells can influence the balance between the number of terminally differentiated and memory T cells, this does not inform us at what point in development an individual T cell commits to either terminal differentiation or to long-term persistence as a memory T cell.

A number of studies have demonstrated that already early after infection the responding antigen-specific T cell population shows remarkable heterogeneity in terms of surface molecule expression as well as cytokine secretion. This raises the question whether this heterogeneity can serve as a reliable marker for T cell survival into the memory phase. If so, this would also indicate that the commitment to form memory or to undergo terminal differentiation occurred prior to the moment of first marker expression.

One of the molecules that are differentially expressed in responding $CD8^+$ T cells is killer cell lectin-like receptor G1 (KLRG1), which appears on the surface of a subset of antigen-specific T cells 4–5 days after LCMV infection[8,21,29] and is induced through the transcription factor T-bet.[8] Furthermore, heterogeneity has also been observed with respect to IL-2 production[21] and expression of CD62L[30,31] and the IL-7Rα (CD127)[21,26,31–33] and IL-2Rα (CD25) chains.[26] Specifically, IL-2, CD62L and CD127 were primarily produced by/expressed on the KLRG-$1^{lo/int}$ population,[8,21,30] while CD25 was predominantly expressed on KLRG-1^{hi} cells.[26] To determine whether these molecules could serve as markers of T cell fate, two different approaches have been taken. First, the percentage of cells expressing a certain marker has been followed during the course of an immune response. These experiments have led to the suggestion that T cells expressing CD62L or CD127 and low levels of KLRG-1 early during the response were precursors of memory T cells, as the percentage of cells within the antigen-specific population that displayed this phenotype was increased during the memory phase.[8,30,31,33] The evidence obtained by this type of analysis is obviously highly indirect: as marker expression can change over time it is uncertain whether a T cell expressing such a marker late during the response is the (progeny of a) cell that expressed this molecule earlier during the response. In a second—more informative—approach that has also been followed in most of the studies, T cell populations have been sorted based on marker expression and have subsequently been transferred into different hosts. Provided that cell isolation affects survival to an equal extent for both populations, this approach allows one to directly compare the capacity of the two sorted populations to persist as memory T cells.

In early experiments, $CD127^{hi}$ and $CD127^{lo}$ populations were sorted during the contraction phase and their potential to survive long-term was evaluated after transfer into naive recipients.[31,33] $CD127^{hi}$ cells were shown to preferentially survive, but it was not addressed to what extent survival would differ when transferred into an infectious environment. More recently, transfer of KLRG-1^{hi} and KLRG-$1^{lo/int}$ TCRtg $CD8^+$ T cells 4 or 8 days after LCMV infection into timed recipients has revealed that KLRG-$1^{lo/int}$ cells were ~5–12 times more efficient in surviving for several months after transfer,[8,21,33] suggesting that low KLRG-1 expression is associated with persistence into the memory phase. Similarly, it has been observed that the extent of IL-2 signaling, a property that is directly linked to CD25 expression, influenced expression of effector molecules and surface markers associated with terminal differentiation.[22,26,34] Specifically, analysis of $CD25^{hi}$ and $CD25^{lo}$ cells 3.5 days after LCMV infection revealed preferential expression of CD127, CD62L, and IL-2 in the $CD25^{lo}$ population.[26] Transfer of sorted $CD25^{hi}$ or $CD25^{lo}$ cells, as well as of cells previously activated in high or low IL-2 concentrations, demonstrated that limited IL-2 signaling through CD25 favored long-term persistence, presumably through higher resistance to apoptosis.[26] One of the transcriptional regulators involved in this process is B lymphocyte-induced maturation protein-1 (Blimp-1), which is induced in $CD4^+$ and $CD8^+$ T cells after IL-2 signaling. Blimp-1 activity induces CD25[24,35] and T-bet expression,[36] and in line with this Blimp-1

has been shown to promote terminal differentiation and T cell exhaustion.[36–39] Taken together, the above data indicate that terminal differentiation is associated with the expression of KLRG-1 and CD25 at 3–4 days after infection.

What does this early heterogeneity tell us about the moment of fate commitment? Does it suggest that T cells commit to longevity or terminal differentiation early during the response, and, if so, can this be linked to a defined event of cell division? Thus far, several models have been proposed that aim to explain at which point in development an individual cell commits to persistence or to death after antigen clearance. These models can be categorized into models that predict fate determination before the first cell division (D0), during the first cell division (D1), or after the first cell division (D1+) (Fig. 3). The evidence for each of these models will be discussed in relation to the strengths and weaknesses associated with the technologies used for the tracking of T cell fate.

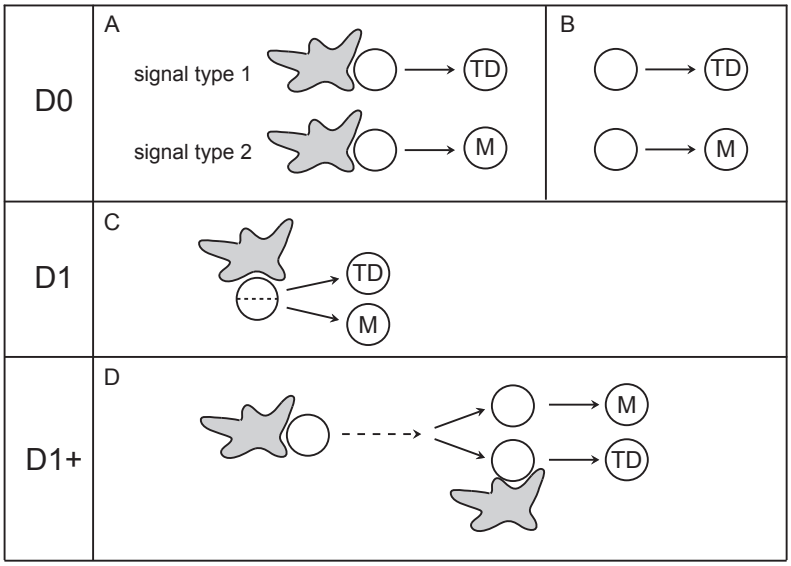

Figure 3: Models predicting the moment of fate commitment. (**A, B**) T cells commit to the fates of terminal differentiation (TD) and memory (M) before the first cell division (at division 0, D0). (**A**) Signal type 1 given to the naive T cell upon priming leads to terminal differentiation of itself and essentially all its progeny, whereas signal type 2 in turn programs a memory fate. (**B**) Naive T cells are intrinsically different and thus already committed even before activation. (**C**) Fate commitment occurs during the first cell division (D1) through asymmetry of the division. The daughter cell located proximal to the priming DC commits to terminal differentiation and the daughter cell distal to the DC commits to a memory fate. (**D**) Fate commitment as a late event in T cell proliferative bursts (D1+). Daughter T cells receiving additional stimuli after priming commit to terminal differentiation. Daughter cells that do not acquire additional stimuli or only receive weak stimuli adopt a memory fate. Uncommitted cells are depicted as empty.

Models predicting fate determination at the D0 stage

When the progressive differentiation and decreasing potential models from Lanzavecchia/Sallusto and Gray/Ahmed were first brought forward, the prevailing view was that proliferation of activated T cells required their continuous stimulation by antigen. However, subsequent work by the groups of Pamer, Schoenberger, and Ahmed demonstrated that a brief encounter with antigen is sufficient to induce naive T cells to undergo several rounds of division.[40–43] Furthermore, the progeny of T cells that were activated by such a brief stimulus acquired effector functions and could survive as memory T cells.[40–42,44] These results opened the interesting possibility that T cell fate (i.e., terminal differentiation or long-term persistence) may already be programmed at the level of the naive T cell (Fig. 3A), as suggested previously by Farber.[45] T cells could for instance acquire heterogeneous fate determining signals before the first cell division by interacting with multiple antigen presenting cells of potentially variable maturation states before they form the stable contacts that lead to initial cell division.[46,47] Furthermore, the time after infection at which an individual T cell would be primed could affect the signals (the amount of antigen or the nature and amount of inflammatory signals) that different T cells receive during initial activation. As an alternative possibility for T cell commitment at the D0 stage and that does not invoke differential signals during T cell priming, it may also be postulated that individual naive T cells are intrinsically different, and that this heterogeneity would influence the fate of its daughters (Fig. 3B).

Indirect evidence. Some evidence for models predicting fate determination at the D0 stage comes from studies in which the formation of long-lived memory cells was assessed after manipulation of antigen availability during priming. One study demonstrated that limiting the available amount of antigen through injection of antibody specific for peptide-MHC complexes before vesicular stomatitis virus (VSV) infection reduced the formation of antigen-specific $CD4^+$ memory T cells, compared to mice injected with control antibody, while the height of the peak T cell response was unaltered.[48] A similar reduction in the formation of persisting $CD8^+$ memory T cells was observed when *Listeria monocytogenes*-infected mice were treated with ampicillin 24 h after infection.[17] These studies suggest that the development of long-lived memory cells occurs more efficiently after a strong stimulus early during the T cell response. However, it is difficult to judge whether the manipulations used in these studies only affected the strength of signals received by T cells during priming (i.e., before the first cell division), or—perhaps more likely—during the course of T cell proliferation. Furthermore, such a reduction in the formation of T cell memory relative to the peak T cell response was not observed when antigen availability was altered through depletion of antigen presenting DCs via stimulation of the diphtheria toxin receptor selectively present on transferred antigen-loaded DCs as early as 1 h after DC transfer.[27] Furthermore, an opposite result, in which a strong stimulus during priming increased the magnitude of the peak T cell response rather than memory T cell

frequencies, was obtained in *in vitro* T cell priming experiments in which the duration of antigenic stimulation was tightly controlled and restricted to the time before the first cell division. In these experiments, memory T cell development *in vivo* was equally efficient for a population of briefly (4 h) and longer (20 h) stimulated T cells, while the magnitude of the peak T cell response was reduced after short antigen exposure.[49]

Indirect support for fate commitment at the D0 stage has also been provided by the finding that CD25 is already differentially expressed on *in vitro* activated but still undivided T cells.[22] As CD25 preferentially marks T cells with limited memory potential,[22,26] these data suggest the possibility that the capacity to persist long-term is programmed before the first cell division. However, since IL-2 signaling at later stages after activation, and thus after the first cell division, can further regulate CD25 expression, it remains possible that signals received after priming can modulate the potential for long-term persistence. Sorting of undivided $CD25^{hi}$ and $CD25^{lo}$ cells, followed by transfer into infected recipients, would allow one to assess whether different fates have already been programmed in these subsets before the first cell division.

Finally, a recent report assessed the role of TCR signaling on the formation of memory cells by generating T cells expressing a TCR harboring a point mutation in the β transmembrane domain.[50] These T cells failed to persist as memory cells, whereas their differentiation into functional effector cells was not impaired. These data suggest that different signaling events are required for terminal differentiation and for long-term persistence. At present, it is unclear whether any physiological stimuli exist that convey a TCR signal similar to the signal transmitted by this mutant TCR, and that could therefore control memory and effector T cell fate. Furthermore, although these data have been taken as support for the model that fate determination occurs during T cell priming,[50] it is unknown at which point in development T cells expressing the mutant TCR fail to receive a signal required for long-term survival. As a consequence, the experiments do not appear informative with respect to the question at which point in development commitment to long-term persistence occurs.

Taken together, a number of studies are consistent with fate commitment at the D0 stage. However, not all data can be reconciled with this model and—most importantly—in these studies it has not been directly assessed at what point in development the signal that influenced long-term survival was received by the T cells; consequently the evidence remains indirect.

Direct evidence. To directly assess at what stage a T cell commits to either long-term persistence or to terminal differentiation, it is valuable to follow individual T cells rather than T cell populations through time. Specifically, by tracing individual T cells and their progeny, one can reveal whether this cell still has the potential to yield both terminally differentiated offspring and memory T cells, or whether the cell can only generate one type of output and is therefore committed. Over the past years, several techniques have been developed to allow cell tracing at the single cell level and the general concept and available technology are discussed in a recent review.[13]

As a first approach, the sequencing of TCR genes has been used by a number of groups to dissect the development of antigen-specific T cell responses. TCR sequencing offers the substantial advantage that it allows one to follow the endogenous T cell response, rather than that of transferred TCRtg T cells. Sequence analysis of the CDR3 region of TCRβ-chains has revealed that close to half of the identified sequences were shared between primary expansion, resting memory phase, and recall responses within the same mouse.[51,52] However, sequences that appeared unique for the effector phase T cell pool or the memory phase T cell pool were also observed. At first glance, these data appear to indicate that some naive T cell clones contribute to the formation of long-lived, as well as short-lived, cells, while other clones only had the potential to produce progeny with either only long-term or only short-term survival potential. However, the interpretation of these data is complicated by two factors. First, TCRβ-chains are shared by multiple naive T cell clones.[53] Consequently, if the same TCRβ sequence is observed in both terminally differentiated and in long-lived memory T cells this does not indicate that this involved the progeny of the same naive T cell.[13] Second, in at least some studies that have used TCRβ-chain analysis to track the developmental potential of naive T cells, it was not assessed whether the repertoire present in a given sample was representative of that population (something that can readily be determined by multiple sampling). In the absence of such a control, any statements on the lack of kinship between cell populations are precluded.[13]

An elegant study that was able to monitor the developmental potential of naive T cells truly at the individual T cell level has been performed by the group of Busch. In this study, single naive TCRtg $CD8^+$ T cells were obtained by micromanipulation, and each individual cell was injected into a separate mouse that was subsequently infected with *Listeria monocytogenes*.[54] The progeny of this single naive T cell had the capacity to develop into a heterogeneous effector population, and the progeny of a single transferred T cell was capable of responding to secondary infection. These experiments suggest that individual naive T cells can yield both effector and memory T cell progeny. However, as the throughput of this experimental system is limited (the potential of only one antigen-specific T cell can be studied per mouse), the experiments do not address whether all naive antigen-specific T cells primed during infection can produce effector and memory cell progeny.

To enable cell tracking of large numbers of individual naive T cells at the single-cell level, we have recently developed a cellular barcoding technology. In this technology, individual naive T cells are provided with unique genetic tags (barcodes) that are transmitted to all progeny.[18,55,56] These barcodes may be introduced into peripheral T cells by standard retroviral infection. However, to avoid the potential effect of *in vitro* T cell activation on subsequent fate, one can also perform retroviral transduction of TCRtg thymocytes. The resulting barcode-labeled thymocytes are subsequently injected into the thymus of unmanipulated recipient mice, and this allows their differentiation into mature barcode-labeled naive T cells.[56] Provided the essential controls are performed to assess the boundaries in which kinship mapping can be

performed,[13] this technology allows one to distinguish whether any cell populations of interest are derived from common or from distinct progenitors.[18,55,56]

To test whether the progeny of individual naive T cells would be able to develop into both short-lived and long-lived T cells, or only one of these subsets, naive OT-I $CD8^+$ T cells, each harboring a unique genetic barcode, were transferred into recipient mice and challenged by recombinant *Listeria monocytogenes* or influenza infection.[56] Subsequent barcode analysis of T cells participating in the primary response and those persisting long-term revealed that the same barcodes were present in both populations and at roughly similar frequencies. Also KLRG-$1^{hi}$$CD127^{lo}$ and KLRG-$1^{lo}$$CD127^{hi}$ populations isolated at the peak of the primary T cell response harbored largely the same barcodes. These data indicate that both during systemic and local infections, memory and effector phase $CD8^+$ T cells are progeny of the same individual naive T cells. As it can be assumed that not all barcode-labeled naive T cells were primed simultaneously but rather over a physiological range of time, these data also demonstrate that T cells primed at distinct time points during infection produce a similar ratio of terminally differentiated and long-term persisting progeny. Furthermore, within the range tested, the affinity of TCR-pMHC interactions did not influence the capacity of individual T cells to yield both short- and long-lived progeny.[56]

What are the limitations of the types of analysis performed in the single-cell transfer and cellular barcoding studies? A first limitation that could be noted is that cell tracking was performed on monoclonal T cells. This argument is actually not particularly compelling; when analyzing T cell responses at the single cell level, one, by definition, examines T cell reactivity at the clonal level. A second argument that could be made is that the response of the adoptively transferred T cells is not representative of endogenous T cell responses. However, as very low numbers of adoptively transferred cells were used in these studies (in the case of Busch at n= 1 per mouse) and as these cells responded amidst polyclonal endogenous antigen-specific cells, this concern does not seem significant.

While the single-cell transfer and barcoding studies demonstrate that under physiological conditions of infection, individual naive T cells yield functionally diverse progeny, this does not necessarily imply that all recently primed T cells are identical. Interestingly, recent multi-photon microscopy experiments suggests that heterogeneity in at least some functional properties can be acquired during priming and can be passed on to early daughter populations under conditions in which further antigenic and inflammatory stimuli are absent.[57] This finding may potentially be reconciled with the *in vivo* lineage tracing studies discussed above by assuming that the cumulative signals that T cells receive during further *in vivo* differentiation cancel out the early heterogeneity observed by Bousso and colleagues.

In summary, there is now strong evidence from both single-cell transfer and barcoding studies that single naive T cells yield heterogeneous progeny: fate is not fix at the D0 stage.

Models predicting fate determination at the D1 stage

At which point in development could commitment to terminal differentiation or to long-term persistence occur if naive T cells are still bipotent? Recently, it has been proposed that these different T cell fates may be programmed during the first cell division through asymmetry of this division[58] (Fig. 3C). Asymmetric cell division has so far mainly been associated with the ability of stem cells to simultaneously self-renew, while also producing progeny that commits to differentiation.[59–61] Generally speaking, unequal daughter fates (as must take place in any self-renewing system that generates differentiated progeny) can be generated through symmetric or through asymmetric divisions (Fig. 4). In the first case, initially equal daughter cells adopt different fates through subsequent encounter of different fate-determining signals.[62] In the second case, acquisition of unequal daughter fates is achieved during division through defined cell intrinsic or niche-controlled mechanisms that have been described in detail in invertebrate model systems.[59,60,62,63] Cell intrinsic mechanisms rely on the establishment of a polarity axis that enables unequal distribution of intrinsic cell fate determinants over the two daughter cells during mitosis, which directs the daughters into different fates. Alternatively, originally equipotent daughter cells can acquire unequal fates if niche-derived signals are required to maintain self-renewal capacity and if one of the daughter cells is forced to lose contact with the niche during mitosis.

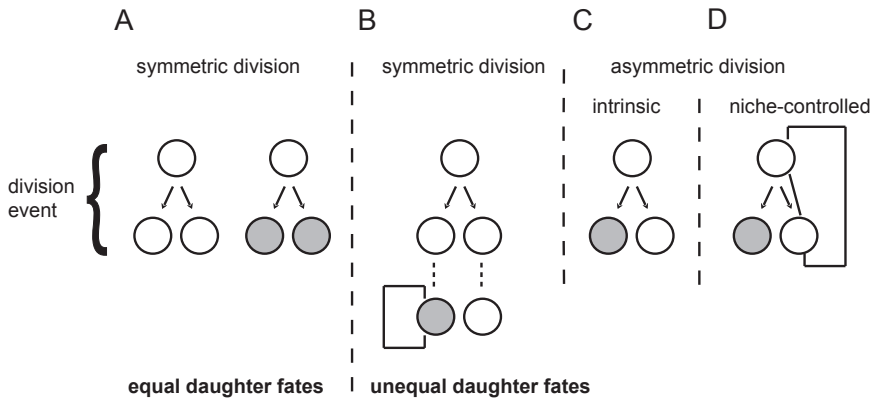

Figure 4: Mechanisms leading to equal or unequal daughter fates. (**A**) Equal daughter fates are by definition generated through symmetric cell division. During this division, either two uncommitted (white) or two committed (gray) cells can be formed. Unequal daughter fates can be the result of either symmetric or asymmetric division. (**B**) Cell division produces two initially equal daughters, of which one remains uncommitted, while the other initiates commitment through encounter of particular environmental factors. (**C**) Unequal distribution of cell fate determinants over the two daughter cells during the mitotic event results in unequal daughter fates. (**D**) Following mitosis, one of the two daughter cells loses contact with a niche that is required for maintaining an uncommitted state, and this results in a niche-controlled asymmetric cell fate. Note that in B, commitment to differentiation is random, whereas in C and D commitment invariably occurs for one of the two daughter cells.

Many of the proteins involved in asymmetric cell division in invertebrates are conserved in mammals. In line with this, intrinsic asymmetric division has been shown to occur in the mammalian brain,[60] and for long it has been postulated that also hematopoietic stem cells could generate diverse progeny through asymmetric division. However, evidence that diverse progeny may result from intrinsic asymmetric divisions of hematopoietic stem cells has only been provided recently. Specifically, using a time lapse microscopy setup in which GFP is expressed after Notch signaling,[64] it was demonstrated that GFP-expressing hematopoietic stem cells can give rise to two GFP^+ daughters, two GFP^- daughters, or to one GFP^- and one GFP^+ daughter.[65] Notch signaling has previously been shown to be fate determining,[64] and the loss of GFP expression correlated with acquisition of lineage markers and differentiation on a population level.[64,65] In combination with the finding that Numb, an inhibitor of Notch signaling, was asymmetrically localized during mitosis, these experiments suggest that murine hematopoietic stem cells can undergo both symmetric divisions and intrinsic asymmetric divisions.[62]

Strikingly, Reiner and colleagues have suggested that not only hematopoietic stem cells but also naive $CD8^+$ and $CD4^+$ T cells may divide asymmetrically after activation, and that this asymmetry would determine the fate of subsequent progeny.[58,66,67] In a first set of experiments, adoptively transferred $CD4^+$ or $CD8^+$ TCRtg T cells, primed *in vivo* by infection with *Leishmania* or recombinant *Listeria monocytogenes*, were isolated before their first cell division.[58] In more recent experiments, $CD8^+$ T cells were activated *in vitro*, using peptide-pulsed DCs.[67] Confocal microscopy of cells obtained in both systems revealed polarized expression of several molecules, but with remarkable differences between the two systems. After *in vivo* priming, ~60% of cells showed polarized expression or unequal inheritance of molecules that have been associated with the immunological synapse (CD8, LFA-1, IFN-γ receptor (IFN-γR)), molecules involved in establishing cell polarity (PKCζ, Scribble) and polarized expression of the cell fate determinant Numb.[58] With the exception of PKCζ, all of these molecules were localized at the same side of the cell as the microtubule organizing center (MTOC), and thus assumed to have been facing the immunological synapse. Also *in vitro* priming of T cells induced polarized expression and asymmetric inheritance of the polarity proteins Par3, Scribble, and atypical PKC, but no polarization of CD8 was observed in this system.[67] Furthermore, in this case the cell fate determinant Numb was observed to be enriched in the DC-distal daughter cell rather than the (putative) DC-proximal daughter. To test whether the unequal inheritance of molecules had an effect on the fate of the two initial daughters, *in vivo* primed TCRtg $CD8^+$ T cells that had divided once were sorted into $CD8^{hi}$ and $CD8^{lo}$ populations and transferred into recipient mice. Subsequently, the potential of the two cell populations to reduce bacterial burden was assessed by bacterial challenge either shortly after infusion or at a late time point after transfer. Both $CD8^{hi}$ and $CD8^{lo}$ populations were able to convey protection against infection at early and late time points. However, the bacterial load after late infection was reduced to a larger extent in mice that had received $CD8^{lo}$ cells. Based on the

critical assumption that CD8^{hi} and CD8^{lo} cells represent the DC-proximal and DC-distal daughters respectively, this experiment suggests that DC-distal daughters are superior in their capacity to protect against reinfection.

However, as the CD8^{hi} (i.e., the putative DC-proximal) cell population displayed a potential to control infection at a late time point, these experiments suggest that the two cell populations used do not display an absolute difference in fate but rather are either composed of a mixture of cells with different fates, or—as will be discussed more extensively below—represent subsets that differ in their propensity to persist long-term. Experiments in which single cell tracing is performed on cells that have undergone their first division will be helpful to directly reveal to what extent asymmetry during the first division results in an asymmetry in fate. Conceptually this should be feasible, using either single cell transfer or cellular barcoding. However, the technological hurdle is significant.

Models predicting fate determination later than D1

Models for early determination of T cell fate can be intuitive if one assumes that T cell priming initiates a fixed program of differentiation. However, the finding that a short period of antigen exposure is sufficient for survival, proliferation, and the formation of effector and memory T cells[40–42,68] does not imply that primed T cells can no longer integrate signals that influence the capacity of this cell and its progeny to persist as a memory T cell.

Direct evidence for the hypothesis that T cells can still integrate signals acquired after priming is provided by experiments in which T cells were isolated 3–5 days after infection, a time point at which most T cells have already divided as based on CFSE dilution. Transfer of these cells into hosts that were either pathogen-free or infected with pathogens that did or did not express cognate antigen showed that both further proliferation and the phenotype of the transferred T cells can be influenced by late-acting signals.[18,21] It should be noted though that these experiments have thus far not addressed whether such late-acting signals are (partially) responsible for the commitment to either terminal differentiation or long-term persistence.

T CELL HETEROGENEITY AS AN INDICATOR FOR CELL STATE RATHER THAN CELL FATE?

Heterogeneity within the responding T cell population has been interpreted as evidence for the adoption of divergent fates early during the response, but do the available data indeed allow the conclusion that T cells expressing defined molecules are already committed to a particular fate? Whenever the memory potential of T cell populations, sorted on the basis of a distinct marker profile, was evaluated after transfer, the populations only showed a gradual difference in their ability to survive long-term.[21,26,58] Thus, the marker expression profiles used were unable to distinguish cells with an absolute difference in fate. Ignoring the "dull" and unlikely explanation

of an impure sort for now, we see two possible explanations. First, T cells are already truly committed at this stage, but the expression levels of CD25, KLRG-1, or CD8 after the first cell division are simply not sufficient to unambiguously separate the two committed T cell populations. At the moment, a new marker (not necessarily a cell surface marker; it may, for instance, involve histone modifications) or a combination of several molecules would be identified that unmistakably identify committed cells, the pure isolation of terminally differentiated or long-term persisting clones would become feasible. Second, the fact that current markers only partially separate long-term and short-term persisting cells might simply mean that T cells do not commit to a particular fate early during the response, or perhaps do not commit at all. Rather than signifying cell fate, marker expression could signify the current cell state and thereby the probability that an individual cell will either survive long-term, or will die during the contraction phase (Fig. 5). To draw a simple analogy, a high cholesterol level increases the likelihood of a heart attack. However, at no point in time is there a "fate decision" that segregates individuals into two groups (the equivalent of T cell fates), one that will and one that will not die from heart disease. Instead, the phenotype (cholesterol level) at a given point in time reports on the current state, but subsequent signals (a low cholesterol diet) may still influence future state and thereby the probability of heart disease.

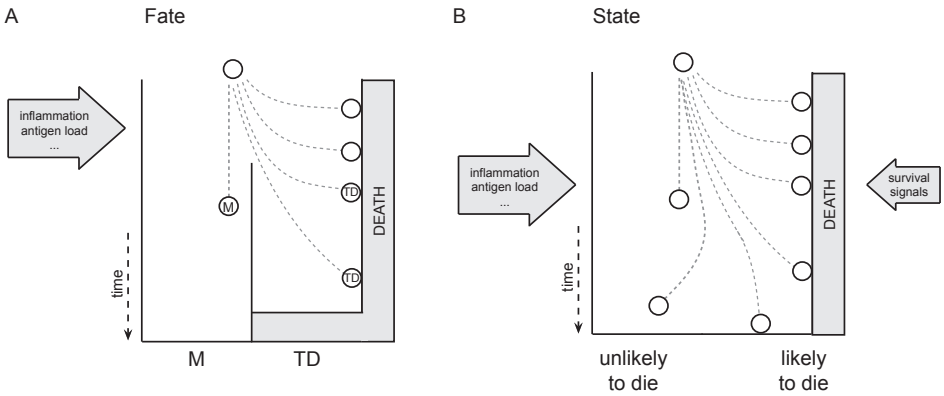

Figure 5: Cell fate versus cell state. (**A**) Activated T cells commit to the fates of terminal differentiation (TD) or memory (M). Before commitment takes place (committed cells are marked by "TD" or "M"), T cells can integrate external signals (inflammation, antigen load), and the extent of this stimulation determines the fate that is adopted by the cell. Once a cell is committed (i.e., ends up to the right or to the left of the line separating TD and M), external signals can no longer influence whether a cell will die after pathogen clearance or will survive as a memory cell. (**B**) Activated T cells do not commit to a particular fate. The cells integrate external signals that influence their likelihood to die, but commitment never takes place. At any point in time—before the cell initiates apoptosis—external signals can act to modulate the cell state, and thereby the likelihood to die.

How could such a regulation of T cell state be envisioned? At the superficial level, a given T cell state would reflect the balance between intracellular mediators that favor survival and those that predispose to death, and this balance could be modulated after additional antigenic or inflammatory signals. What would this mean molecularly? It is evident that the balance between anti-apoptotic and pro-apoptotic molecules forms a likely candidate as the principal indicator of T cell state. Interesting in this respect is the observation that TCRtg $CD8^+$ T cells lacking the pro-apoptotic molecule Bim form a stable pool of memory T cells, while hardly undergoing contraction.[69] With the caution in mind that this study was not performed at a single cell level, these experiments suggest that all cells taking part in the primary response, including KLRG-$1^{hi}$$CD127^{lo}$ cells, can form memory cells if they are simply prevented from dying.

CONCLUSION

To date, there is strong evidence that memory T cells can be direct progeny of cells that display effector gene expression, but it is still uncertain whether effector function is a prerequisite for memory development. Less clear is the exact timing at which individual T cells commit to terminal differentiation or memory, and whether such commitment actually takes place at all. Studies in which the developmental potential of individual naive T cells was examined at the single-cell level clearly demonstrate that fate commitment does not take place before the first cell division. This rules out the possibility that naive T cells are predisposed toward memory or terminal differentiation, or that fate is dictated through differential priming by APCs. The scenarios in which T cell fate is either determined through asymmetric division or through cumulative signals acquired after priming remain distinct possibilities. However, as the heterogeneity observed thus far within T cell populations has not led to the identification of T cell populations with a full commitment to terminal differentiation or to long-term persistence, it also seems possible that T cells do not make a fate decision that determines whether they will survive or die. Instead, T cells might assume a continuum of cell states that indicate the likelihood by which an individual cell will either die during contraction or will persist. In this model, signals in the form of antigen or inflammation acquired early during the response or at later points in time influence cell state and, thereby, the likelihood of survival or death, but do not induce commitment. At present, evidence for this "no-fate-but-state" model of T cell differentiation is still limited. However, the flexibility it allows appears attractive from an evolutionary point of view.

CONFLICTS OF INTEREST

The authors declare no conflicts of interest.

REFERENCES

1. Murali-Krishna, K. *et al.* Persistence of memory CD8 T cells in MHC class I-deficient mice. *Science* 286, 1377-1381 (1999).
2. Sallusto, F., Lenig, D., Forster, R., Lipp, M. & Lanzavecchia, A. Two subsets of memory T lymphocytes with distinct homing potentials and effector functions. *Nature* 401, 708-712 (1999).
3. Masopust, D., Vezys, V., Marzo, A. L. & Lefrancois, L. Preferential localization of effector memory cells in nonlymphoid tissue. *Science* 291, 2413-2417 (2001).
4. Swain, S. L., Hu, H. & Huston, G. Class II-independent generation of CD4 memory T cells from effectors. *Science* 286, 1381-1383 (1999).
5. Hu, H. *et al.* CD4(+) T cell effectors can become memory cells with high efficiency and without further division. *Nat. Immunol.* 2, 705-710 (2001).
6. Kaech, S. M., Hemby, S., Kersh, E. & Ahmed, R. Molecular and functional profiling of memory CD8 T cell differentiation. *Cell* 111, 837-851 (2002).
7. Opferman, J. T., Ober, B. T. & Ashton-Rickardt, P. G. Linear differentiation of cytotoxic effectors into memory T lymphocytes. *Science* 283, 1745-1748 (1999).
8. Joshi, N. S. *et al.* Inflammation directs memory precursor and short-lived effector CD8(+) T cell fates via the graded expression of T-bet transcription factor. *Immunity* 27, 281-295 (2007).
9. Jacob, J. & Baltimore, D. Modelling T-cell memory by genetic marking of memory T cells in vivo. *Nature* 399, 593-597 (1999).
10. Harrington, L. E., Janowski, K. M., Oliver, J. R., Zajac, A. J. & Weaver, C. T. Memory CD4 T cells emerge from effector T-cell progenitors. *Nature* 452, 356-360 (2008).
11. Bannard, O., Kraman, M. & Fearon, D. T. Secondary replicative function of CD8+ T cells that had developed an effector phenotype. *Science* 323, 505-509 (2009).
12. Manjunath, N. *et al.* Effector differentiation is not prerequisite for generation of memory cytotoxic T lymphocytes. *J. Clin. Invest.* 108, 871-878 (2001).
13. Schumacher, T. N. M., Gerlach, C. & van Heijst, J. W. Mapping the life histories of T cells. In press. Nature Reviews Immunology.
14. Ahmed, R. & Gray, D. Immunological memory and protective immunity: understanding their relation. *Science* 272, 54-60 (1996).
15. Lanzavecchia, A. & Sallusto, F. Dynamics of T lymphocyte responses: intermediates, effectors, and memory cells. *Science* 290, 92-97 (2000).
16. Lanzavecchia, A. & Sallusto, F. Progressive differentiation and selection of the fittest in the immune response. *Nat Rev Immunol* 2, 982-987 (2002).
17. Williams, M. A. & Bevan, M. J. Shortening the infectious period does not alter expansion of CD8 T cells but diminishes their capacity to differentiate into memory cells. *J. Immunol.* 173, 6694-6702 (2004).
18. van Heijst, J. W. *et al.* Recruitment of antigen-specific CD8+ T cells in response to infection is markedly efficient. *Science* 325, 1265-1269 (2009).
19. Badovinac, V. P., Porter, B. B. & Harty, J. T. CD8+ T cell contraction is controlled by early inflammation. *Nat. Immunol.* 5, 809-817 (2004).
20. Badovinac, V. P., Porter, B. B. & Harty, J. T. Programmed contraction of CD8(+) T cells after infection. *Nat. Immunol.* 3, 619-626 (2002).
21. Sarkar, S. *et al.* Functional and genomic profiling of effector CD8 T cell subsets with distinct memory fates. *J. Exp Med* 205, 625-640 (2008).
22. Pipkin, M. E. *et al.* Interleukin-2 and inflammation induce distinct transcriptional programs that promote the differentiation of effector cytolytic T cells. *Immunity* 32, 79-90 (2010).
23. Pearce, E. L. & Shen, H. Generation of CD8 T cell memory is regulated by IL-12. *J. Immunol.* 179, 2074-2081 (2007).
24. Gong, D. & Malek, T. R. Cytokine-dependent Blimp-1 expression in activated T cells inhibits IL-2 production. *J. Immunol.* 178, 242-252 (2007).
25. Takemoto, N., Intlekofer, A. M., Northrup, J. T., Wherry, E. J. & Reiner, S. L. Cutting Edge: IL-12 inversely regulates T-bet and eomesodermin expression during pathogen-induced CD8+ T cell differentiation. *J. Immunol.* 177, 7515-7519 (2006).
26. Kalia, V. *et al.* Prolonged interleukin-2Ralpha expression on virus-specific CD8+ T cells favors terminal-effector differentiation in vivo. *Immunity* 32, 91-103 (2010).
27. Prlic, M., Hernandez-Hoyos, G. & Bevan, M. J. Duration of the initial TCR stimulus controls the magnitude but not functionality of the CD8+ T cell response. *J. Exp. Med.* 203, 2135-2143 (2006).

28. Zehn, D., Lee, S. Y. & Bevan, M. J. Complete but curtailed T-cell response to very low-affinity antigen. *Nature* 458, 211-214 (2009).
29. McMahon, C. W. *et al*. Viral and bacterial infections induce expression of multiple NK cell receptors in responding CD8(+) T cells. *J. Immunol*. 169, 1444-1452 (2002).
30. Obar, J. J. & Lefrancois, L. Early signals during CD8(+) T cell priming regulate the generation of central memory cells. *J. Immunol*. 185, 263-272 (2010).
31. Huster, K. M. *et al*. Selective expression of IL-7 receptor on memory T cells identifies early CD40L-dependent generation of distinct CD8+ memory T cell subsets. *Proc. Natl. Acad. Sci. U S A* 101, 5610-5615 (2004).
32. Schluns, K. S., Kieper, W. C., Jameson, S. C. & Lefrancois, L. Interleukin-7 mediates the homeostasis of naive and memory CD8 T cells in vivo. *Nat. Immunol*. 1, 426-432 (2000).
33. Kaech, S. M. *et al*. Selective expression of the interleukin 7 receptor identifies effector CD8 T cells that give rise to long-lived memory cells. *Nat Immunol* 4, 1191-1198 (2003).
34. Belz, G. T. & Masson, F. Interleukin-2 tickles T cell memory. *Immunity* 32, 7-9 (2010).
35. Martins, G. A., Cimmino, L., Liao, J., Magnusdottir, E. & Calame, K. Blimp-1 directly represses Il2 and the Il2 activator Fos, attenuating T cell proliferation and survival. *J. Exp. Med*. 205, 1959-1965 (2008).
36. Rutishauser, R. L. *et al*. Transcriptional repressor Blimp-1 promotes CD8(+) T cell terminal differentiation and represses the acquisition of central memory T cell properties. *Immunity* 31, 296-308 (2009).
37. Kallies, A., Xin, A., Belz, G. T. & Nutt, S. L. Blimp-1 transcription factor is required for the differentiation of effector CD8(+) T cells and memory responses. *Immunity* 31, 283-295 (2009).
38. Shin, H. *et al*. A role for the transcriptional repressor Blimp-1 in CD8(+) T cell exhaustion during chronic viral infection. *Immunity* 31, 309-320 (2009).
39. Welsh, R. M. Blimp hovers over T cell immunity. *Immunity* 31, 178-180 (2009).
40. Mercado, R. *et al*. Early programming of T cell populations responding to bacterial infection. *J Immunol* 165, 6833-6839 (2000).
41. van Stipdonk, M. J., Lemmens, E. E. & Schoenberger, S. P. Naive CTLs require a single brief period of antigenic stimulation for clonal expansion and differentiation. *Nat. Immunol*. 2, 423-429 (2001).
42. Bevan, M. J. & Fink, P. J. The CD8 response on autopilot. *Nat. Immunol*. 2, 381-382 (2001).
43. Kaech, S. M. & Ahmed, R. Memory CD8+ T cell differentiation: initial antigen encounter triggers a developmental program in naive cells. *Nat. Immunol*. 2, 415-422 (2001).
44. Kaech, S. M. & Ahmed, R. Memory CD8+ T cell differentiation: initial antigen encounter triggers a developmental program in naive cells. *Nat. Immunol*. 2, 415-422 (2001).
45. Farber, D. L. Differential TCR signaling and the generation of memory T cells. *J. Immunol*. 160, 535-539 (1998).
46. Bousso, P. & Robey, E. Dynamics of CD8+ T cell priming by dendritic cells in intact lymph nodes. *Nat. Immunol*. 4, 579-585 (2003).
47. Mempel, T. R., Henrickson, S. E. & von Andrian, U. H. T-cell priming by dendritic cells in lymph nodes occurs in three distinct phases. *Nature* 427, 154-159 (2004).
48. Blair, D. A. & Lefrancois, L. Increased competition for antigen during priming negatively impacts the generation of memory CD4 T cells. *Proc. Natl. Acad. Sci. U S A* 104, 15045-15050 (2007).
49. van Stipdonk, M. J., Sluijter, M., Han, W. G. & Offringa, R. Development of CTL memory despite arrested clonal expansion. *Eur. J. Immunol*. 38, 1839-1846 (2008).
50. Teixeiro, E. *et al*. Different T cell receptor signals determine CD8+ memory versus effector development. *Science* 323, 502-505 (2009).
51. Turner, S. J., Diaz, G., Cross, R. & Doherty, P. C. Analysis of clonotype distribution and persistence for an influenza virus-specific CD8+ T cell response. *Immunity* 18, 549-559 (2003).
52. Kedzierska, K., Turner, S. J. & Doherty, P. C. Conserved T cell receptor usage in primary and recall responses to an immunodominant influenza virus nucleoprotein epitope. *Proc Natl Acad Sci U S A* 101, 4942-4947 (2004).
53. La Gruta, N. L. *et al*. Primary CTL response magnitude in mice is determined by the extent of naive T cell recruitment and subsequent clonal expansion. *J. Clin. Invest*. 120, 1885-1894 (2010).
54. Stemberger, C. *et al*. A single naive CD8+ T cell precursor can develop into diverse

effector and memory subsets. *Immunity* 27, 985-997 (2007).

55. Schepers, K. *et al*. Dissecting T cell lineage relationships by cellular barcoding. *J Exp Med* 205, 2309-2318 (2008).
56. Gerlach, C. *et al*. One naive T cell, multiple fates in CD8+ T cell differentiation. *J. Exp. Med*. 207, 1235-1246 (2010).
57. Beuneu, H. *et al*. Visualizing the functional diversification of CD8+ T cell responses in lymph nodes. *Immunity* 33, 412-423 (2010).
58. Chang, J. T. *et al*. Asymmetric T lymphocyte division in the initiation of adaptive immune responses. *Science* 315, 1687-1691 (2007).
59. Betschinger, J. & Knoblich, J. A. Dare to be different: asymmetric cell division in Drosophila, C. elegans and vertebrates. *Curr. Biol*. 14, R674-R685 (2004).
60. Knoblich, J. A. Mechanisms of asymmetric stem cell division. *Cell* 132, 583-597 (2008).
61. Morrison, S. J. & Kimble, J. Asymmetric and symmetric stem-cell divisions in development and cancer. *Nature* 441, 1068-1074 (2006).
62. Schroeder, T. Asymmetric Cell Division in Normal and Malignant Hematopoietic Precursor Cells. *Cell Stem Cell* 1, 479-481 (2007).
63. Horvitz, H. R. & Herskowitz, I. Mechanisms of asymmetric cell division: two Bs or not two Bs, that is the question. *Cell* 68, 237-255 (1992).
64. Duncan, A. W. *et al*. Integration of Notch and Wnt signaling in hematopoietic stem cell maintenance. *Nat. Immunol*. 6, 314-322 (2005).
65. Wu, M. *et al*. Imaging hematopoietic precursor division in real time. *Cell Stem Cell* 1, 541-554 (2007).
66. Littman, D. R. & Singh, H. Immunology. Asymmetry and immune memory. *Science* 315, 1673-1674 (2007).
67. Oliaro, J. *et al*. Asymmetric Cell Division of T Cells upon Antigen Presentation Uses Multiple Conserved Mechanisms. *J. Immunol*. (2010).
68. Kaech, S. M. & Ahmed, R. Memory CD8+ T cell differentiation: initial antigen encounter triggers a developmental program in naive cells. *Nat. Immunol*. 2, 415-422 (2001).
69. Prlic, M. & Bevan, M. J. Exploring regulatory mechanisms of CD8+ T cell contraction. *Proc. Natl. Acad. Sci. U S A* 105, 16689-16694 (2008).

4

DISSECTING T CELL LINEAGE RELATIONSHIPS BY CELLULAR BARCODING

Koen Schepers[1], Erwin Swart[1], Jeroen W.J. van Heijst[1], Carmen Gerlach[1], Maria Castrucci[3], Daoud Sie[2], Mike Heimerikx[2], Arno Velds[2], Ron M. Kerkhoven[2], Ramon Arens[1] and Ton N.M. Schumacher[1]

[1]Division of Immunology and [2]Central Microarray Facility, The Netherlands Cancer Institute, Amsterdam, the Netherlands; [3]Istituto Superiore di Sanità, Roma, Italy

J Exp Med. 205: 2309-18 (2008)

T cells, as well as other cell types, are composed of phenotypically and functionally distinct subsets. However, for many of these populations it is unclear whether they develop from common or separate progenitors. To address such issues, we developed a novel approach, termed cellular barcoding, that allows the dissection of lineage relationships. We demonstrate that the labeling of cells with unique identifiers coupled to a microarray-based detection system can be used to analyze family relationships between the progeny of such cells. To exemplify the potential of this technique, we studied migration patterns of families of antigen-specific $CD8^+$ T cells in vivo. We demonstrate that progeny of individual T cells rapidly seed independent lymph nodes and that antigen-specific $CD8^+$ T cells present at different effector sites are largely derived from a common pool of precursors. These data show how locally primed T cells disperse and provide a technology for kinship analysis with wider utility.

INTRODUCTION

To ascertain whether different cell types have a common or separate ancestor has generally been difficult. Historically, differentiation assays have been used to study lineage relationships. In most of these assays, the in vitro or in vivo developmental potential of progenitors with a homogeneous phenotype is studied under different conditions. However, the finding that a phenotypically homogeneous cell population can give rise to two types of cellular output does not necessarily imply that individual cells within the population are multipotent. This problem can be remedied by the use of clonal assay systems in which the cellular output of a single (injected) cell is studied, but the difficulties of single cell experiments preclude its use in many settings. An appealing strategy to address this issue is the use of larger pools of progenitor cells in which each individual cell carries a mark that allows one to distinguish its offspring from the offspring of other cells. In previous studies, the site of random retroviral integration has been used as a marker to identify the progeny of individual hematopoietic cells by Southern blot analysis or PCR[1-3]. Furthermore, Golden et al.[4] have previously used a sequencing-based detection technique to study lineage relationships between different cell populations in the developing brain by retroviral tagging. In this paper, we extend this general concept to a high-throughput approach in which individual progenitor cells are tagged with a molecular barcode that can be analyzed by microarray hybridization. This technique allows a high-throughput analysis of differentiation and migration patterns of families of cells. We demonstrate the utility of this technology by dissecting the kinship of antigen-specific T cells that accumulate at priming and effector sites during local antigen-driven T cell responses. This technology will be of value in addressing lineage relationships and progenitor potential of T cell subsets and other subsets of hematopoietic cells.

RESULTS

Dissecting lineage relationships by cellular barcoding: general strategy and proof of principle

To uniquely tag individual cells with molecular barcodes, we generated a retroviral plasmid library, consisting of ~5,000 different plasmids. Each plasmid contains GFP as a marker gene and a so-called barcode, formed by a semirandom stretch of 98 bp of noncoding DNA. To allow for rapid analysis of barcodes present within a given cell population, each barcode present in this library was also amplified individually by PCR and spotted on microarray slides, resulting in a barcode microarray. In a typical experiment, cells are labeled by retroviral transduction with the barcode library and reintroduced into mice. After in vivo expansion and differentiation of the barcode-labeled cells, barcodes present in different subsets of cells are recovered by PCR, fluorescently labeled, and hybridized on the barcode microarray. Determining the overlap of barcodes between different subsets by cellular barcoding (Fig. 1A) should then allow one to determine the kinship between these cell populations. In addition

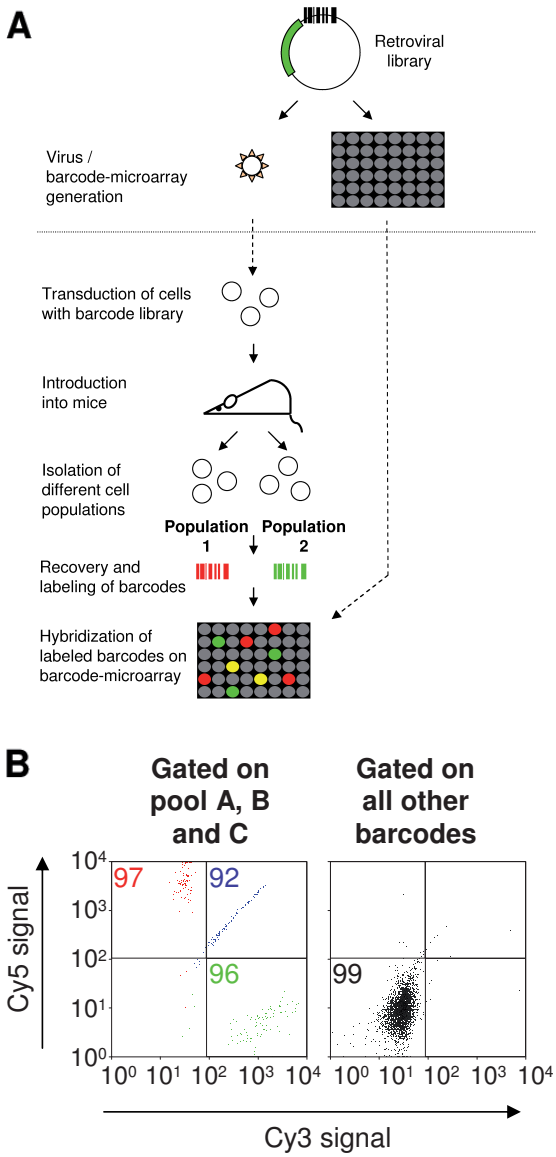

Figure 1. Cellular barcoding strategy. (**A**) To allow the analysis of lineage relationships between cell populations, a retroviral plasmid library was constructed containing a GFP marker gene and a semirandom stretch of 98 bp of noncoding DNA (the barcode). The barcodes that are present in this library were amplified by PCR and individually spotted on microarray slides. In addition, from this plasmid library, a retroviral library was generated that is used to transduce T cells or other cells. Barcode-labeled cells are introduced into mice to allow proliferation and differentiation, and at different time points after infusion, populations of cells can be isolated for kinship analysis by comparing the barcodes present within the different cell populations. Barcode analysis is performed by hybridization on microarray slides containing the individual barcodes. (**B**) Analysis of a hybridization with PCR products of 273 individual *E. coli* clones of the master library. The PCR products were pooled into three pools (A, B, and C), each containing PCR products of 91 clones. The x-axes show nonnormalized fluorescence intensities of a Cy3-labeled sample that contains PCR products of pools A and B, and the y-axes show nonnormalized fluorescence intensities of a Cy5-labeled sample that contains PCR products of pools B and C. Barcodes that are present in pools A, B, and C are plotted on the left and are labeled green, blue, and red, respectively. Barcodes that are not present in pools A, B or C are plotted on the right. Colored numbers indicate the percentage of barcodes present in the respective gates (black rectangles) as a percentage of the total number of barcodes that is present in the corresponding pool.

to the retroviral barcode library used here, a lentiviral barcode library was prepared to allow tagging of quiescent cell types that are refractory to retroviral infection (unpublished data).

Before assessing the feasibility of kinship analysis, we first established whether the barcode microarray shows any crosshybridization between different barcodes present in the barcode library. When the barcode microarray was hybridized with PCR products of 273 individual *Escherichia coli* clones of the master library that were labeled with Cyanine-3 (Cy3), with Cy5, or with both Cy3 and Cy5 dyes, no detectable crosshybridization between different barcodes was observed (Fig. 1B). Second, as the effective size of the barcode library will decrease proportionally with the number of barcodes that is introduced per cell, we also established retroviral transduction conditions under which the mean number of barcodes per cell is close to one (Fig. S1).

As a first test of the barcoding technology, we assessed whether cellular barcoding can be used to analyze kinship between cell populations that are either kin or nonkin. For this purpose, OVA-specific MHC class I–restricted T cell receptor transgenic OT-I T cells were transduced with the barcode library. Subsequently, sorted barcode-labeled OT-I T cells were i.v. injected into mice that were then challenged with antigen (i.v. challenge with *Listeria monocytogenes* encoding OVA [LM-OVA]). At day 7 after challenge, the OT-I T cell pool present in the spleen was split into two samples (which are evidently derived from the same pool of precursors), hereafter referred to as half-samples. From the genomic DNA of these half-samples, barcodes were recovered by PCR, labeled with Cy3 and Cy5 dyes, and cohybridized on the barcode microarray. Resulting data are presented in two-dimensional plots, depicting the Cy3 and Cy5 signals of each individual spot on the barcode microarray. In these plots, each dot represents a clone (or family) of cells that are the progeny of a precursor containing a specific barcode. The presence or absence of a barcode within a cell population is then determined by calculation of the distribution of background signals from averaged Cy3 and Cy5 signals, as described in Materials and methods. When two half-samples from the same spleen are compared for the presence of barcodes, >85% of the barcodes that show detectable signal in one of the spleen samples is also detected in the other half-sample (Fig. 2A, left and middle). In contrast, when barcodes recovered from spleen samples of two different mice (representing two cell pools that are nonkin) are compared, the barcodes that are detected are largely unique to either one of the spleen samples (Fig. 2A, right). The small percentage of the barcodes that is shared between the T cell populations in the two mice is close to the overlap that is expected based on chance (i.e., the introduction and activation of T cells that by chance have the same barcode in the different mice; Fig. 2A, legend). Together these data indicate that cellular barcoding can distinguish between cells that are kin or nonkin and establish the patterns of barcode overlap that may be expected under conditions of full kinship or lack thereof.

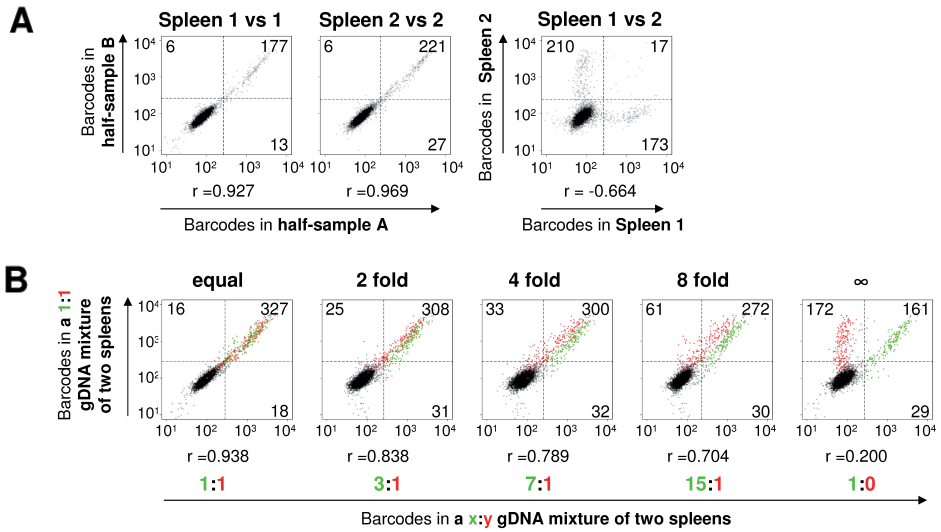

Figure 2. Proof of principle and sensitivity of kinship analysis by cellular barcoding. (**A**) Barcode analysis of indicated samples (at day 7 after challenge) from mice that received 1,000 barcode-labeled OT-I T cells and that were subsequently challenged by i.v. LM-OVA infection. Plots represent the fluorescence intensities of the barcode microarray spots. Left and middle: Dot plots of barcode analysis of T cells isolated from two half-samples from the same spleen for two individual mice. Right: Dot plot of barcode analysis of T cells isolated from spleens of two different mice. Numbers indicate the number of barcodes present in each quadrant (black rectangles; cutoff used, $P < 0.0005$). With the assumption that ~3,300 of the 4,743 barcodes can effectively be used for lineage analysis (supplemental Materials and methods) and that each barcode has the same probability to participate in the T cell response, the expected overlap between barcodes present in the two unrelated cell populations in A is 200/3,300 × 200 = 12 (in which 200 is the approximate number of barcodes within a half-sample of a spleen), which is close to the observed overlap between the two unrelated samples (i.e., 17 barcodes). (**B**) Barcode analysis of genomic DNA mixtures of the two spleen samples shown in A. Plots represent the fluorescence intensities of the barcode microarray spots. The y-axes show fluorescence intensities of a sample that contains a 1:1 mixture of genomic DNA of spleen 1 and 2. The x-axes show fluorescence intensities of samples that contain a 1:1, 3:1, 7:1, 15:1, or 1:0 mixture of genomic DNA of spleen 1 and 2, respectively. Barcodes uniquely present in spleen 1 and spleen 2 are labeled green and red, respectively. Numbers above each plot indicate the level at which the cells of spleen 2 are overrepresented in the sample on the y-axis as compared with the sample on the x-axis. R values represent the correlation between hybridization signals of all barcodes present in either spleen 1 or 2.

Subsequently, we determined whether cellular barcoding can also detect more subtle differences in kinship, reflecting situations where only part of the T cells in two effector T cell pools has a common ancestor in the naive T cell compartment or where the progeny of a given naive T cell is enriched but not unique to a certain T cell population. For this purpose, we performed microarray hybridizations of barcodes isolated from genomic DNA of two spleen samples that were mixed at different ratios

(1:1, 3:1, 7:1, 15:1, and 1:0). In the most extreme situation, where part of the barcodes is unique to one of the samples and the remainder is shared (i.e., the 1:1 versus 1:0 comparison; Fig. 2B, right), those barcodes that are common or private (represented by green and red dots, respectively) are readily distinguished. Furthermore, in situations where part of the barcodes is overrepresented 2–8-fold in one of the samples, these barcodes (Fig. 2B, red dots) become progressively separated from the other barcodes. In the analysis shown in Fig. 2B, relatedness of cell populations is revealed by grouping barcodes as either shared or private (i.e., present in either the top right quadrant or the bottom right/top left quadrant). As an alternative measure of relatedness, the correlation between the Cy3 and Cy5 hybridization signals for each barcode can be used. Analysis of the data in Fig. 2B by such correlation analysis demonstrates that an increasing difference in the frequency of half of the barcodes in two samples leads to a progressive loss in correlation (Fig. 2B, r values). These data indicate that cellular barcoding can be used to reveal cellular progeny that are enriched in a certain cell population and demonstrate that the fluorescence intensity of barcode microarray signals correlates with the frequency at which a specific barcode is present within a certain sample.

Dissecting kinship between antigen-specific T cells at distinct priming and effector sites

Having established the feasibility of lineage analysis by cellular barcoding, we assessed whether T cell families that accumulate at distinct priming and effector sites share common ancestors in the naive T cell pool. It has previously been shown that T cell subsets can be distinguished on the basis of differential expression of chemokine receptors and adhesion molecules, and such differential expression is thought to guide the migration of these subsets to distinct sites in the body[5-9]. For instance, it has been shown that T cells that are activated in vitro by dendritic cells from gut draining LN (DLN) or skin DLN preferentially migrate to the corresponding effector site[10-12] upon reintroduction. To determine whether selective migration of T cells also occurs upon antigen encounter in vivo in a case where there is a choice between two antigen-positive effector sites, we analyzed the kinship between antigen-specific T cells in a dual challenge model. For this purpose, mice were challenged by s.c. inoculation of EL4-OVA tumor cells and parallel intranasal infection with WSN-OVA influenza virus to generate two local independent effector sites. We considered the possibility that a potential effect of imprinting could be masked or reduced when T cell activation in the two sets of DLN would not occur simultaneously as, in this case, the progeny of T cells activated within the first set of DLN could seed the other LN bed (Fig. 3)[13] and thereby dominate the T cell response at that site. In particular, in view of recent data that suggest that programming of T cell functions may not be fixed[10,12], such a situation could lead to an underestimate of the potential of imprinting. To avoid this issue, we first determined the kinetics of T cell priming at the two different LN sites. Analysis of CFSE dilution of labeled OT-I T cells in tumor and lung DLN of mice that

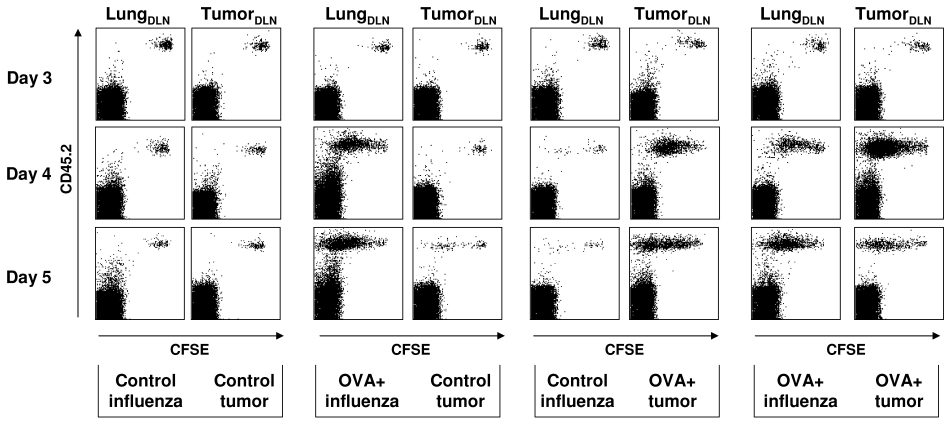

Figure 3. Simultaneous priming of OT-I T cells in tumor DLN and lung DLN. Four groups of B6 Ly5.1$^+$ mice that received 3 × 10^6 CFSE-labeled mock-transduced OT-I T cells (Ly5.2$^+$) on day 0 were challenged intranasally with the indicated influenza virus on day 0 and challenged s.c. with the indicated tumor cells on day 1. Plots show representative flow cytometric analyses of tumor-draining axillary/inguinal LNs (TDLN) and lung-draining mediastinal LNs (LDLN) at different time points after initial challenge. In each plot the same amount of living CD8$^+$ lymphocytes is depicted. Plots are representative for three to four mice per experiment, out of two experiments.

received an s.c. inoculation of EL4-OVA tumor cells or intranasal WSN-OVA influenza infection revealed that detectable T cell proliferation is first observed at days 3 and 4 after antigenic challenge, respectively (unpublished data). To allow simultaneous priming of T cells in the two LN beds, mice were therefore challenged with EL4-OVA tumor inoculation 1 d after intranasal WSN-OVA influenza inoculation in all subsequent experiments (Fig. 3).

The kinship of antigen-specific T cells that accumulate at the two priming and two effector sites was subsequently monitored by barcode analysis. When barcodes are recovered from tumor DLN at day 5 or later time points, the percentage of barcodes recovered from two half-samples of a tumor DLN that is found in both half-samples is markedly higher than the random overlap observed between tumor DLN samples obtained from different mice (Fig. 4). Likewise, when barcodes are recovered from lung DLN, the percentage of barcodes recovered from two half-samples of a lung DLN that is found in both half-samples is markedly higher than the background overlap observed between lung DLN samples from different mice (Fig. 4). Together, these data indicate that barcode analysis of LN-resident T cell populations is feasible, even early after the induction of T cell proliferation.

To reveal whether draining LNs of tumor and lung contain the same sets of T cell families, barcodes obtained from tumor DLN and lung DLN were subsequently compared. Early after antigenic challenge (day 5), the overlap in barcodes present in tumor and lung DLN obtained from the same mouse (Fig. 4, A [right, top two rows]

Figure 4. Redistribution of T cell families over LN beds through time. Barcode analysis of T cell populations isolated from draining LNs in mice that received 10,000 barcode-labeled OT-I T cells and that were subsequently challenged intranasally with WSN-OVA influenza virus (day 0) and s.c. with EL4-OVA cells (day 1). At indicated days after challenge, TDLN and LDLN were each split into two half-samples that were separately cultured for 4 d and used for barcode analysis. The results represent data from two to three mice analyzed separately within one experiment. (**A** and **B**) Representative dot plots of the fluorescence intensities of the barcode microarray spots at days 5 (A) and 10 (B). Left and middle, top two rows: dot plots of barcode analysis of two pools of T cells isolated from the same tissue for two individual mice. Right, top two rows: dot plots of barcode analysis of T cells isolated from the TDLN versus T cells isolated from the LDLN for two individual mice. Bottom row: evaluation of background overlap by comparison of samples from mouse 1 with samples from mouse 2. Numbers indicate the barcodes that are present within each quadrant (black rectangles; cutoff used, $P < 0.005$). (**C**) Percentage of barcode overlap between different tissue samples. Each sample was compared with a second sample generated from the same tissue (TDLN or LDLN) or from a different tissue (TDLN vs LDLN), either of the same mouse (intra) or of a different mouse (inter). The percentages indicate the number of barcodes that is present within the top right quadrant as a fraction of the total number of barcodes present in the top left, top right, and bottom right quadrant (as indicated in A and B). By normalizing for background and maximal overlap, data can be converted to percentage identity between T cell families at both sites (numbers in text). Percentage identity of T cell families in the control comparisons (TDLN-X vs. LDLN-Y) was 1, 0, −1, and 0% on days 5, 6, 8, and 10, respectively.

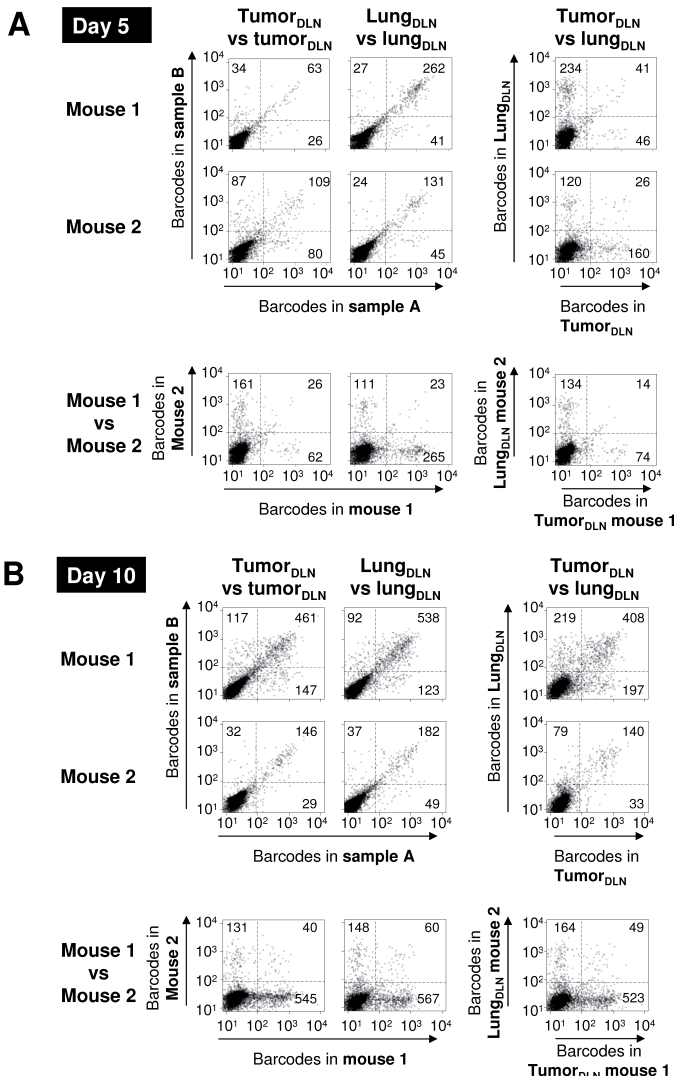

and C) is small and only slightly higher than the overlap between barcodes obtained from tumor and lung DLN from different mice (Fig. 4, A [right, bottom row] and C). This indicates that early after antigen-induced activation, T cell families mostly remain confined to the original site of priming. Interestingly, from days 6 to 8 after challenge, a marked shift occurs, in which a large fraction of barcodes becomes shared between T cells isolated from tumor and lung DLN, suggesting that within days after priming, the offspring of T cells intermingles within different DLN.

To provide a more quantitative assessment of the similarity of T cell families present at the two sites, data were converted into percentage identity, in which the percentage of shared barcodes, as shown in Fig. 4C, is corrected for maximal and background overlap (analogous to the correction of data for background and maximal lysis in CTL assays, see Materials and methods for details). Based on this analysis, T cell families within tumor and lung DLN share 8 and 16% identity on days 5 and 6. This abruptly changes to 78 and 75% identity on days 8 and 10. Also, when the data are analyzed by correlation analysis, T cell families at the two sites are clearly distinct early after antigenic challenge but become close to identical from day 8 (Fig. S2). To test whether the increase in barcode overlap between tumor and lung DLN over time is indeed caused by T cell migration, we treated mice with FTY720, a compound which blocks LN egress of T lymphocytes[14,15]. Importantly, when LN egress is blocked during the course of antigenic challenge, the relatedness of T cells that are present in tumor and lung DLN remains low even late during infection (day 8, 29% identity; Fig. S3). These data show that the time-dependent increase in relatedness of T cell families isolated from lung and tumor DLN is a result of T cell migration.

To test whether barcode analysis of effector site–resident T cells was feasible, barcodes were obtained from tumor and lung tissue at various time points after antigenic challenge. When T cells are isolated from the tumor and lung effector sites during the OVA-specific T cell response, barcodes can be recovered reliably from these samples (Fig. 5, A [left and middle, top two rows] and B). Importantly, of the barcodes that are present at one effector site, the majority is also found at the other effector site within the same mouse (Fig. 5, A [right, top two rows] and B), whereas samples derived from different mice do not show such a shared set of barcodes (Fig. 5, A [bottom row] and B). Furthermore, this high overlap is observed both at day 8, when substantial T cell accumulation at both sites has just begun (Fig. 5), and at the peak of the antigen-specific T cell response (day 10 after challenge; not depicted). Thus, although the T cell populations that develop within tumor and lung DLN initially consist of distinct families, the progeny that accumulates at the lung and tumor effector sites are highly related (81% identity at day 8; Fig. S4A) Together, these data show that, in this model, the progeny of $CD8^+$ T cells disperses, essentially indiscriminately, over two effector sites.

To investigate whether this pattern also applies to a third effector site, we analyzed the kinship of T cells migrating to inflamed gut and s.c. tumor effector sites. To this purpose, mice were challenged by oral infection with LM-OVA and s.c. inoculation of EL-4 OVA tumor cells. Again, challenges were timed such that priming occurred

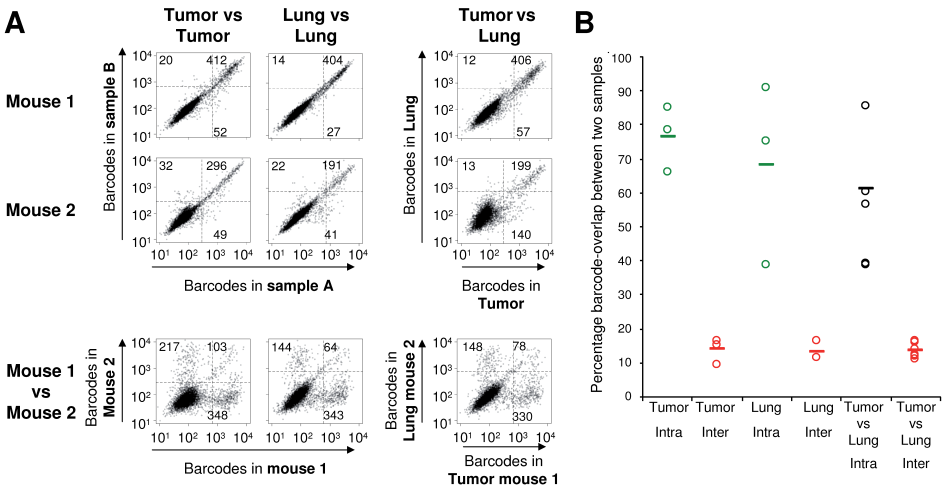

Figure 5. T cells present at lung and tumor effector sites are derived from the same precursors. Barcode analysis of T cell populations from effector sites in mice that received 10,000 barcode-labeled OT-I T cells and that were subsequently challenged intranasally with WSN-OVA influenza virus (day 0) and s.c. with EL4-OVA cells (day 1). At day 8 after challenge, T cells were isolated from tumor and lung tissue for barcode analysis. Results are representative of two independent experiments in which seven mice were analyzed separately in total. (**A**) Representative dot plots of the fluorescence intensities of the barcode microarray spots. Left and middle, top two rows: dot plots of barcode analysis of two pools of T cells isolated from the same tissue for two individual mice. Right, top two rows: dot plots of barcode analysis of T cells isolated from tumor versus T cells isolated from lung for two individual mice. Bottom row: evaluation of background overlap by comparison of samples from mouse 1 with samples from mouse 2. Numbers indicate the barcodes that are present within each quadrant (black rectangles; cutoff used, $P < 0.00005$). (**B**) Percentage of barcode overlap between different tissue samples. Each sample was compared with a second sample generated from the same tissue (tumor or lung) or from a different tissue (tumor vs. lung), either of the same mouse (intra) or of a different mouse (inter). The percentages indicate the number of barcodes that is present within the top right quadrant as a fraction of the total number of barcodes present in the top left, top right, and bottom right quadrant (as indicated in A). By normalizing for background and maximal overlap, data can be converted to percentage identity between T cell families at both sites (numbers in text). Percentage identity of T cell families in the control comparison (tumor-X vs. lung-Y) was 0%.

simultaneously in gut and TDLNs (unpublished data). Furthermore, by comparing barcodes isolated from different half-samples around the peak of the OVA-specific T cell response, it was established that barcodes from gut tissue can also be recovered reliably (Fig. 6). When barcodes present in T cells that accumulated in the gut and the tumor of the same mouse were compared, no evidence was found for selective migration of T cell families toward the tumor site (Fig. 6, A [right, top two rows] and B; and Fig. S4B). In some mice, a small fraction of barcodes was enriched in gut tissue, suggesting that selective migration toward the gut may occur to some degree.

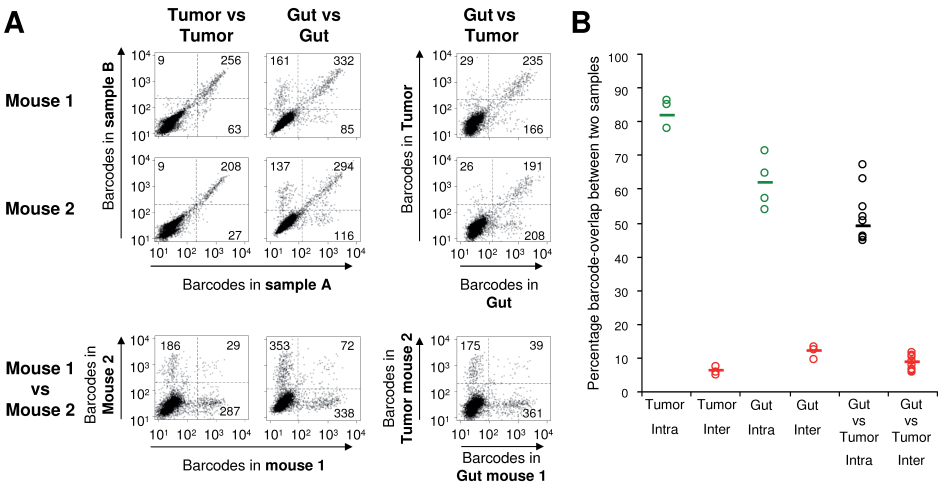

Figure 6. T cells present at gut and tumor effector sites are derived from the same precursors. Barcode analysis of T cell populations in mice that received 10,000 barcode-labeled OT-I T cells and that were subsequently challenged orally with LM-OVA and s.c. with EL4-OVA cells (both on the same day). At day 7 after challenge, T cells were isolated from tumor and gut tissue for barcode analysis. Before analysis, T cells isolated from gut tissue from each mouse were split into two half-samples that were subsequently cultured for 4 d. Results represent data from four mice analyzed separately within one experiment. (**A**) Representative dot plots of the fluorescence intensities of the barcode-microarray spots. Left and middle, top two rows: dot plots of barcode analysis of two pools of T cells isolated from the same tissue for two individual mice. Right, top two rows: dot plots of barcode analysis of T cells isolated from the gut versus T cells isolated from tumor for two individual mice. Bottom row: evaluation of background overlap by comparison of samples from mouse 1 with samples from mouse 2. Numbers indicate the barcodes that are present within each quadrant (black rectangles; cutoff used, $P < 0.0005$. (**B**) Percentage of barcode overlap between different tissue samples. Each sample was compared with a second sample generated from the same tissue (gut or tumor) or from a different tissue (gut vs. tumor), either of the same mouse (intra) or of a different mouse (inter). The percentages indicate the number of barcodes that is present within the top right quadrant as a fraction of the total number of barcodes present in the top left, top right, and bottom right quadrant (as indicated in A). By normalizing for background and maximal overlap, data can be converted to percentage identity between T cell families at both sites (numbers in text). Percentage identity of T cell families in the control comparison (tumor-X vs. gut-Y) was −2%.

However, the majority of T cell families also appeared to be equally represented at these two effector sites (translating into an identity of 64% between T cell families in gut and tumor of the same mouse). As expected, tissue samples derived from different mice did not show such a shared set of barcodes (Fig. 6, A and B, bottom rows). Together, these data indicate that also in this comparison, the majority of T cell families that locally develop accumulate at both effector sites.

Finally, a possible limitation of the experiments described in the previous paragraphs is that the 3-d in vitro culture used to introduce the Moloney-based retroviral barcode

library may conceivably influence T cell migration properties. To address this issue, we have developed a strategy in which naive barcode-labeled T cells are obtained via the transduction of OT-I thymocytes (see Materials and methods for details). Also, when naive barcode-labeled OT-I T cells were used, a high degree of overlap between barcodes present in T cells that accumulated in the lung and the tumor of the same mouse was observed (Fig. S5, A [right, top two rows] and B).

DISCUSSION

In this paper, we developed a novel approach, termed cellular barcoding, to dissect lineage relationships between different cell populations. In this approach, retroviral or lentiviral tagging of individual cells with molecular barcodes is coupled to a microarray-based detection system to allow kinship analysis of the progeny of such cell populations. By analyzing family relationships between different barcode-labeled T cell populations, we demonstrate that cellular barcoding can be used to distinguish cells that are kin or nonkin. In essence, this technology provides an in vivo system for high throughput parallel clonal assays.

To exemplify the potential of cellular barcoding, we analyzed the kinship of $CD8^+$ T cells that accumulate at different DLN and effector sites. A picture that has emerged from recent studies is that T cells primed within a specific LN, or by antigen-presenting cells obtained from LNs draining a specific tissue site, acquire a phenotype that is consistent with preferential migration[10-13,16,17]. Furthermore, cells that are induced to display such a phenotype in vitro also show selective homing upon injection[11,12]. Interestingly, one study showed that the in vivo expression of markers that could result in preferential migration is transient, possibly through the action of signals encountered in other LN beds[13]. In addition, this reprogramming has also been observed in vitro[10,12].

In the current paper, we have used cellular barcoding to study the kinship between T cells that accumulate at different effector sites in situations where antigen is available at multiple locations. Data obtained in this analysis demonstrate that from the first time point at which substantial amounts of T cells accumulate at the tumor and lung effector sites, the T cell families at both sites are largely identical, even though unique T cell families are found in the LNs draining these tissues shortly after antigen challenge. In addition, a high identity was also observed when comparing T cell families that accumulate in inflamed gut and s.c. tumor tissue. In this case, a small set of barcodes appears enriched in gut tissue in at least some animals. Although these data suggest that a minority of T cell families might display the capacity to selectively migrate to this site, based on signal intensity, the contribution of this set of clones to the total T cell pool in gut is not expected to be large. Collectively, these data indicate that after a brief period of local accumulation, the dominant pattern of T cell accumulation at effector sites is aselective. We speculate that selective T cell migration may only play a significant role at very early time points during infection[13] and perhaps in situations where the effector sites generate limited inflammatory signals. In contrast, we suggest

that aselective migration forms the dominant process at the moment two effector sites produce sufficient proinflammatory signals, and aselective migration, in fact, seems a preferred strategy to combat spreading infections.

Interestingly, a strong time-dependent increase in the relatedness of T cell families isolated from lung DLN and tumor DLN of the same mouse was observed. Furthermore, this increase was found to be dependent on lymphocyte egress from the LN, as it was blocked in the presence of FTY720. The mingling of T cell families at two LN sites is consistent with the LN recycling of recently activated T cells observed by Liu et al.[13] but also with the recent description of effector T cell entry into reactive LNs via high endothelial venules[18]. As a result of such T cell redistribution over tumor and lung DLN, an indiscriminate accumulation of T cell families at the two effector sites may occur as a secondary effect (Fig. 7A). As an alternative model, accumulation of effector T cells at both sites could occur independently of LN cross-seeding (Fig. 7B), and equilibration of LN T cell populations could then occur as a secondary

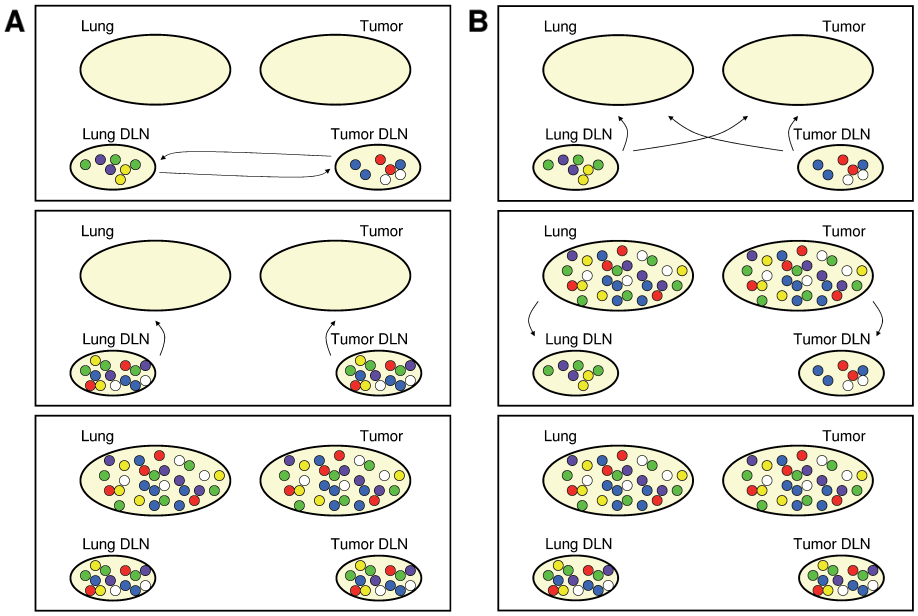

Figure 7. Pathways for intermingling of T cell families. (**A**) After priming, two local and genetically distinct populations of antigen-specific T cells develop. Upon LN exit, these T cell families accumulate at both effector sites, and mixing of T cell families within the DLN occurs as a secondary phenomenon upon migration or passive transport of T cells via afferent lymph. (**B**) After priming, two local and genetically distinct populations of antigen-specific T cells develop. Upon LN exit, these T cell families redistribute over the reactive LNs (in which the possibility of reprogramming of migration patterns may exist[11], and both effector sites are subsequently seeded by T cells from all families, regardless of the site of original priming. As evidence for both pathways of effector T cell entry into LNs exists[12,13], it is possible that both processes operate in parallel.

effect, through T cell recycling from effector sites via the afferent lymph[19]. In view of the rapid equilibration of T cell families in lung and tumor DLN between days 6 and 8, a time point at which T cell numbers at effector sites are still low, we favor the former possibility, but formal evidence is lacking.

Together, the current data demonstrate that cellular barcoding can be used to dissect the migration patterns of T cell families in vivo and show that the majority of T cells that are activated during a T cell response acquire the capacity to accumulate at multiple tissue sites. In addition to the potential value of the barcoding technology for the analysis of cellular differentiation and migration within the lymphoid system, we consider it likely that this technology can also be used to examine stem cell, cancer stem cell, and differentiation issues for other hematopoietic and transplantable cell types.

MATERIALS AND METHODS

Mice. C57BL/6 (B6), B6 Ly5.1$^+$ and C57BL/6.OT-I mice (OT-I)[20] were obtained from the animal department of the Netherlands Cancer Institute. All animal experiments were performed in accordance with institutional and national guidelines and were approved by the Experimental Animal Committee (DEC) of the Netherlands Cancer Institute.

Barcode library and microarray generation. The semirandom stretch $((N)_8\text{-}(SW)_5)_5\text{-}N_8$ was inserted 3' of the GFP ORF in the pLentilox3.4 vector (Supplemental Materials and methods). Subsequently, 4,743 individual *E. coli* cell clones containing this vector were picked and grown in 96-well plates. This master library was used to generate a barcode microarray and a Moloney-based retroviral library (supplemental Materials and methods). To generate the barcode microarray, PCR products were generated from the individual *E. coli* cell clones of the master library and were spotted in duplicate onto poly-L-lysine–coated glass slides using the MicroGrid II arrayer (Isogen Life Science). PCR products of 93 additional *E. coli* cell clones that are not present in the master library were spotted in hexaplicate to function as internal controls for the labeling and hybridization procedure (supplemental Materials and methods).

Retroviral transduction procedure. Retroviral supernatants were generated using Phoenix-E packaging cells, as described previously[21], and stored at −80°C. Total OT-I splenocytes were isolated and mixed with CD4-enriched B6 splenocytes at a 10:1 ratio. CD4-enriched B6 splenocytes were obtained by staining B6 splenocytes with PE- or APC-conjugated anti-CD4 mAbs (BD Biosciences), labeling with anti-PE or anti-APC Microbeads (Miltenyi Biotec), followed by Midi-MACS enrichment (Miltenyi Biotec). Enrichment was ≥90%. Cells were activated in IMDM (Invitrogen) supplemented with 8% heat-inactivated FCS, 100 U/ml penicillin, 100 μg/ml streptomycin (Boehringer Ingelheim), and 0.5×10^{-5} M β-mercaptoethanol (culture medium) in the presence of ConA and IL-7 and transduced with diluted retroviral supernatants by spin infection as previously described[21]. Retroviral supernatants were used at dilutions resulting in transduction efficiencies of ~1–2%. At this transduction efficiency, the mean number

of barcodes per cell is close to one (Fig. S1). 24 h after retroviral transduction, transduced T cells were purified using Ficoll Paque PLUS (GE Healthcare), stained with PE-conjugated anti-Vα2 and APC-conjugated anti-CD8α, and sorted on a FACSAria (BD Biosciences) for GFP^+ $V\alpha2^+$ $CD8\alpha^+$ cells. Subsequently, the cells were washed once in culture medium and twice in HBSS (Invitrogen), resuspended in HBSS, and injected i.v. (1,000–10,000 GFP^+ cells per mouse). To obtain naive barcode-labeled T cells, OT-I thymocytes were transduced with the barcode library in culture medium supplemented with 10 ng/ml IL-7. The next day, transduced cells were sorted for GFP expression and injected in the thymi of B6 recipient mice (~10^6 cells/mouse). 3 wk after intrathymic injection, $CD8^+$ T cells containing barcode-labeled OT-I cells were isolated from spleen and LNs. Barcode-modified OT-I T cells generated in this manner are phenotypically naive and respond to antigen encounter with identical kinetics as unmanipulated OT-I T cells (unpublished data).

Influenza A virus, *L. monocytogenes*, and tumor challenge. The recombinant influenza A strain WSN-OVA that expresses the H-$2K^b$–restricted $OVA_{257-264}$ epitope (SIINFEKL) has been previously described[22]. A recombinant influenza A virus that expresses epitope IV of the SV40 large T antigen was generated as previously described[22]. Influenza A strains were grown in and titered on MDCK (Madin Darby canine kidney) cells. Mice were infected with 500 PFU of the influenza A variants by intranasal application. EL4-OVA tumor cells were produced by retroviral transduction of EL4 thymoma cells with a pMX vector that encodes a GFP-$OVA_{257-264}$ fusion protein[23], and EL4-NP cells have been previously described[24]. For tumor challenge, tumor cells were washed three times with HBSS, resuspended in HBSS, and injected s.c. into mice (10^7 cells per mouse). The LM-OVA recombinant *L. monocytogenes* strain that expresses OVA[25] was provided by D. Busch (Technical University Munich, Munich, Germany). Mice were infected by gavage with ±10^8 CFU LM-OVA or i.v. with ±2.5 × 10^4 CFU LM-OVA.

Isolation of barcode-labeled T cells, in vitro culture, and flow cytometric analysis. Cell suspensions of spleen, LN, lung, and tumor tissue were generated as previously described[26]. Cell suspensions of gut tissue were generated according to a previously published procedure[24]. In brief, the small intestine was flushed with 50 ml HBSS containing 2% FCS. Peyers patches were excised and intestine was cut into small pieces longitudinally and laterally. After washing, the tissue was transferred to a 50-ml tube containing 20 ml HBSS/5% FCS/0.1mM EDTA and stirred for 20 min at 37°C. The supernatant was harvested, EDTA treatment was repeated twice, and all supernatants were pooled. Subsequently, the material was digested in 20 ml IMDM containing 200 U/ml collagenase (type VIII; Sigma-Aldrich) and stirred for 1 h at 37°C. The supernatant was harvested and collagenase treatment was repeated once. Supernatants were pooled and the thus-obtained cell suspension was used for subsequent enrichment of OT-I cells. To enrich OT-I cells from tissue samples, cells were stained with PE-conjugated anti-Vα2 mAbs (BD Biosciences), labeled with anti-PE

Microbeads (Miltenyi Biotec), followed by autoMACS (Miltenyi Biotec) enrichment. For analysis of barcodes from T cells present in LNs, LN cells were first expanded for 4 d in culture medium supplemented with 20 U/ml of recombinant human IL-2 (Chiron) and 12 ng/ml of recombinant mouse IL-7 (PeproTech). Half-samples were cultured separately to avoid bias introduction during in vitro culture. The mAbs used for flow cytometric analysis were APC-conjugated anti-CD8α (BD Biosciences) and PE-conjugated anti-Ly5.2 (eBioscience). Before analysis, 1 μg/ml propidium iodide (Sigma-Aldrich) was added to enable selection for propidium iodide–negative (living) cells.

Barcode recovery, microarray hybridizations, and data analysis. Genomic DNA was isolated using a DNeasy tissue kit (QIAGEN) and barcodes were amplified by nested PCR (supplemental Materials and methods). PCR products were purified, concentrated, labeled with Cy3 or Cy5 fluorescent groups, and hybridized to the barcode microarray (supplemental Materials and methods). Fluorescence intensities, as quantified using Imagene 6.0 (BioDiscovery, Inc.), were corrected for background noise and normalized according to Yang et al.[27].

After averaging of duplicates, barcodes present above background were selected based on the probability that a signal differed from an artificial background distribution. In barcode microarray hybridizations, the majority of signals reflects a negative biological signal and, consequently, the mode of the signal distribution can be taken as an approximation of the mean of the background distribution. As signals below the mode are the least contaminated by positive signals, an artificial background distribution was constructed from the signals lower than the mode and an extrapolation/mirroring of these signals to the positive side of the slope. For each sample, this artificial background was determined based on the distribution of the averaged Cy3 and Cy5 signals of the hybridization in which two half-samples of the same tissue were hybridized (the cutoffs used [p-values given in the figure legends] are indicated by the horizontal and vertical dividers in the dot plots). The two dimensional plots depict Cy3 and Cy5 signals for all 4,743 barcodes that were present in the master library. For comparison of barcodes in samples analyzed in different hybridizations, we performed in silico hybridizations in which the Cy3 and Cy5 signals of the two samples were plotted against each other. Percentage identity was calculated as: $(A\text{-}B^{EXP})\text{-}(\sqrt{A\text{-}A^{INTER}} x \sqrt{B\text{-}B^{INTER}})/(\sqrt{A\text{-}A^{INTRA}} x \sqrt{B\text{-}B^{INTRA}})\text{-}(\sqrt{A\text{-}A^{INTER}} x \sqrt{B\text{-}B^{INTER}})x100\%$, in which A−B is the experimental comparison (EXP) and A−A and B−B comparisons of two samples from a given site, in which the samples are either from the same mouse (INTRA) or from two different mice (INTER). All numbers refer to the fraction of shared barcodes of the total number of detected barcodes in both samples. Conceptually, this calculation is analogous to the calculation of percentage of specific lysis in CTL assays, with the one distinction that the maximal and minimal signals are now defined by the efficiency of barcode recovery from two sites ($A–A^{INTRA}$ + $B–B^{INTRA}$ and $A–A^{INTER}$ + $B–B^{INTER}$, respectively), assuming that the percentage of shared barcodes within a sample is the product of two samples that have an equal efficiency of barcode recovery.

For each barcode comparison, the Pearson Correlation between Cy3 and Cy5 signals was calculated. To avoid dominance of signals from barcodes not present within a given sample in the correlation analysis, a small fraction of barcodes present in the bottom left quadrant (1/3 of the number of barcodes present in the top left, top right and bottom quadrants) was randomly drawn and incorporated in the correlation analysis. To minimize variations in correlation values introduced by the random drawing of a subset of barcodes from the bottom left, all correlation values were averaged from 100 calculations, based on 100 random drawings from the bottom left.

Supplemental material. Fig. S1 presents additional data showing that under the conditions used, the majority of transduced cells contain a single transgene. Fig. S2 shows the redistribution of T cell families over LN beds through time as analyzed by correlation analysis. Fig. S3 shows that the redistribution of T cell families over LN beds is dependent on LN egress. Fig. S4 shows the kinship of T cells present at different effector sites as determined by correlation analysis. Fig. S5 shows the kinship of T cells present at lung and tumor effector sites when naive barcode-labeled T cells are used. A detailed description of barcode library generation, microarray generation, barcode recovery, and microarray hybridization is available as supplemental Materials and methods.

ACKNOWLEDGMENTS

The authors thank Drs. J. Borst, H. Jacobs, and S.H. Naik for discussions and critical reading of the manuscript, Dr. N.J. Armstrong for advice on data analysis, Dr. D. Busch for the kind provision of LM-OVA, W. Brugman for microarray production, and A. Pfauth and F. van Diepen for cell sorting. R.A. is supported by a grant from the Netherlands Organization for Scientific Research (NWO-Veni 916.56.155).

REFERENCE LIST

1. Williams, D. A., Lemischka, I. R., Nathan, D. G. & Mulligan, R. C. Introduction of new genetic material into pluripotent haematopoietic stem cells of the mouse. *Nature* 310, 476-480 (1984).
2. Dick, J. E., Magli, M. C., Huszar, D., Phillips, R. A. & Bernstein, A. Introduction of a selectable gene into primitive stem cells capable of long-term reconstitution of the hemopoietic system of W/Wv mice. *Cell* 42, 71-79 (1985).
3. Lemischka, I. R., Raulet, D. H. & Mulligan, R. C. Developmental potential and dynamic behavior of hematopoietic stem cells. *Cell* 45, 917-927 (1986).
4. Golden, J. A., Fields-Berry, S. C. & Cepko, C. L. Construction and characterization of a highly complex retroviral library for lineage analysis. *Proc. Natl. Acad. Sci. U S A* 92, 5704-5708 (1995).
5. Hamann, A., Andrew, D. P., Jablonski-Westrich, D., Holzmann, B. & Butcher, E. C. Role of alpha 4-integrins in lymphocyte homing to mucosal tissues in vivo. *J Immunol* 152, 3282-3293 (1994).
6. Johansson-Lindbom, B. *et al.* Selective generation of gut tropic T cells in gut-associated lymphoid tissue (GALT): requirement for GALT dendritic cells and adjuvant. *J Exp Med* 198, 963-969 (2003).
7. Picker, L. J., Kishimoto, T. K., Smith, C. W., Warnock, R. A. & Butcher, E. C. ELAM-1 is an adhesion molecule for skin-homing T cells. *Nature* 349, 796-799 (1991).
8. Svensson, M. *et al.* CCL25 mediates the localization of recently activated CD8alpha-beta(+) lymphocytes to the small-intesti-

nal mucosa. *J Clin Invest* 110, 1113-1121 (2002).

9. Tietz, W. *et al.* CD4+ T cells migrate into inflamed skin only if they express ligands for E- and P-selectin. *J Immunol* 161, 963-970 (1998).
10. Dudda, J. C. *et al.* Dendritic cells govern induction and reprogramming of polarized tissue-selective homing receptor patterns of T cells: important roles for soluble factors and tissue microenvironments. *Eur. J. Immunol.* 35, 1056-1065 (2005).
11. Mora, J. R. *et al.* Selective imprinting of gut-homing T cells by Peyer's patch dendritic cells. *Nature* 424, 88-93 (2003).
12. Mora, J. R. *et al.* Reciprocal and dynamic control of CD8 T cell homing by dendritic cells from skin- and gut-associated lymphoid tissues. *J Exp Med* 201, 303-316 (2005).
13. Liu, L., Fuhlbrigge, R. C., Karibian, K., Tian, T. & Kupper, T. S. Dynamic programming of CD8+ T cell trafficking after live viral immunization. *Immunity* 25, 511-520 (2006).
14. Cyster, J. G. Chemokines, sphingosine-1-phosphate, and cell migration in secondary lymphoid organs. *Annu Rev Immunol* 23, 127-159 (2005).
15. Rosen, H., Sanna, M. G., Cahalan, S. M. & Gonzalez-Cabrera, P. J. Tipping the gatekeeper: S1P regulation of endothelial barrier function. *Trends Immunol* 28, 102-107 (2007).
16. Calzascia, T. *et al.* Homing phenotypes of tumor-specific CD8 T cells are predetermined at the tumor site by crosspresenting APCs. *Immunity* 22, 175-184 (2005).
17. Dudda, J. C., Simon, J. C. & Martin, S. Dendritic cell immunization route determines CD8+ T cell trafficking to inflamed skin: role for tissue microenvironment and dendritic cells in establishment of T cell-homing subsets. *J Immunol* 172, 857-863 (2004).
18. Guarda, G. *et al.* L-selectin-negative CCR7-effector and memory CD8+ T cells enter reactive lymph nodes and kill dendritic cells. *Nat. Immunol.* 8, 743-752 (2007).
19. Mackay, C. R., Marston, W. L. & Dudler, L. Naive and memory T cells show distinct pathways of lymphocyte recirculation. *J Exp Med* 171, 801-817 (1990).
20. Hogquist, K. A. *et al.* T cell receptor antagonist peptides induce positive selection. *Cell* 76, 17-27 (1994).
21. Kessels, H. W., Wolkers, M. C., van den Boom, M. D., van der Valk, M. A. & Schumacher, T. N. Immunotherapy through TCR gene transfer. *Nat. Immunol.* 2, 957-961 (2001).
22. Topham, D. J., Castrucci, M. R., Wingo, F. S., Belz, G. T. & Doherty, P. C. The role of antigen in the localization of naive, acutely activated, and memory CD8(+) T cells to the lung during influenza pneumonia. *J Immunol* 167, 6983-6990 (2001).
23. Kessels, H. W., Schepers, K., van den Boom, M. D., Topham, D. J. & Schumacher, T. N. Generation of T cell help through a MHC class I-restricted TCR. *J Immunol* 177, 976-982 (2006).
24. Wolkers, M. C., Stoetter, G., Vyth-Dreese, F. A. & Schumacher, T. N. Redundancy of direct priming and cross-priming in tumor-specific CD8+ T cell responses. *J Immunol* 167, 3577-3584 (2001).
25. Pope, C. *et al.* Organ-specific regulation of the CD8 T cell response to Listeria monocytogenes infection. *J. Immunol.* 166, 3402-3409 (2001).
26. Arens, R. *et al.* Tumor rejection induced by CD70-mediated quantitative and qualitative effects on effector CD8+ T cell formation. *J Exp Med* 199, 1595-1605 (2004).
27. Yang, Y. H. *et al.* Normalization for cDNA microarray data: a robust composite method addressing single and multiple slide systematic variation. *Nucleic Acids Res* 30, e15 (2002).

SUPPLEMENTAL MATERIALS AND METHODS

Barcode library and microarray generation. Using the primers top, 5′-GGGAAAGTC-GACTAAGCCACCATGGTGAGCAAGGGCGAG -3′; and bottom, 5′-CCCGAAT-TCGATCTCGAATCAGGCGCTTAGGATCCTCCCCTTCCCTCGAGTGTTCTAGTT-GACGGCAGCATTACTTGTACAGCTCGTCCATG-3′ and the enhanced GFP gene as template, a PCR product containing GFP and unique cloning sites for library insertion was created and cloned into the XhoI and EcoRI sites of the retroviral vector pLentiLox3.4 (gift from L. van Parijs), to obtain pLentiLox3.4-GFP2. A semirandom stretch of DNA was subsequently cloned 3′ of the GFP ORF in the pLentilox3.4-GFP2 vector. For this purpose the oligo 5′-TGCTGCCGTCAACTAGAACACTCGAG-((N)8-(SW)5)5-N8-GGATCCTAAGCGCCT GATTCGAGATC-3′ (in which N = A, C, T, or G, S = C or G, and W = A or T) was amplified using the following primers: top-LIB primer, 5′-TGCTGCCGTCAACTAGAACA-3′; and bottom-LIB primer, 5′-GATCTCGAATCAG-GCGCTTA-3′. The resulting library was digested and ligated into the XhoI and BamHI sites of pLentiLox3.4-GFP2. Ligation products were introduced into electroporation-competent *E. coli* cells (electro Ten-blue; Stratagene) by electroporation and plated on 10-cm Ampicillin-containing LB plates. For the generation of the Moloney-based pMX-GFP-bc library, DNA was isolated from the pooled *E. coli* cell clones of the master library and subcloned into a variant of the pMX retroviral vector (Kitamura, T. 1998. *Int J. Hematol.* 67:351–359) that contains a PacI cloning site, using the restriction enzymes PacI and EcoRI. To determine which barcodes can effectively be used for lineage analysis, barcodes recovered in at least one experiment were plotted as a function of the number of experiments performed. In a first set of seven experiments, 3,029 different barcodes were observed, and extrapolation of this curve suggests that the number of informative barcodes is ~3,300. The lack of detection for the remainder is likely due to loss of barcodes during the different procedures of generating the library for retrovirus production and the generation of the microarray.

Barcode recovery and microarray hybridizations. Barcodes were amplified by nested PCR in a DNA Engine PTC-200 PCR machine (Bio-Rad Laboratories) using the primers top, 5′- GTCCTGCTGGAGTTCGTGAC -3′; and bottom 5′- GACCAACTGG-TAATGGTAGCGAC -3′ in the first round, and the top-LIB and bottom-LIB primers in the second round. The first round consisted of a linear PCR of 50 cycles (5′′ 94°C, 5′′ 55°C, and 5′′ 72°C), in which only the top primer was present followed by another 30 cycles (5′′ 94°C, 5′′ 55°C, and 5′′ 72°C) of exponential amplification in the presence of both primers. The second round consisted of 30 cycles (5′′ 94°C, 5′′ 57.2°C, and 5′′ 72°C). Starting with a linear amplification rather than an exponential amplification decreases the probability that the amplification reaction changes the relative composition of a barcode pool due to founder effects, in particular for samples that initially contain barcodes in low copy numbers. In all barcode PCRs, reagent controls were performed in parallel to exclude the presence of contaminating barcode sequences. PCR products were purified and concentrated with a MinElute PCR Purification Kit (QIAGEN),

digested with BamHI and XhoI, concentrated, and purified again using a MinElute PCR Purification Kit. After adding ~2.6 ng of purified digested PCR products of the 93 control barcodes per 200 ng of PCR product of the sample, PCR products were labeled with Cy3 or Cy5 fluorescent groups using the Universal Linkage System (ULS; Kreatech Biotechnology) and purified over a KREApure spin column (Kreatech Biotechnology). To reduce background signals, samples containing 25–100 ng of labeled PCR product were supplemented with 0.25–1 μg of each of the following unlabeled oligos: oligo 1, 5′-TCGAGTGTTCTAGTTGACGGCAGCA-3′; oligo 2, 5′-TGCTGCCGTCAACTAGAACAC-3′; oligo 3, 5′-GATCCTAAGCGCCTGATTCGAGATC-3′; and oligo 4, 5′-GATCTCGAATCAGGCGCTTAG-3′, which all correspond to the primer binding sites of the barcode PCR products present on the array. Subsequently, samples were concentrated, heated to 95 °C for 1 min, snap cooled, diluted in 30 μl of 32.7% formamide, 53 SSC, 0.85% SDS, and 2.6% DMSO (final concentrations) and applied to the array. Samples were hybridized overnight at 42 °C, washed, and scanned using a DNA Microarray scanner (Agilent Technologies). As the normalization procedure requires that the average Cy3/Cy5 ratio is 1, all experiments were performed by cohybridization of two half-samples of one tissue.

SUPPLEMENTAL FIGURES

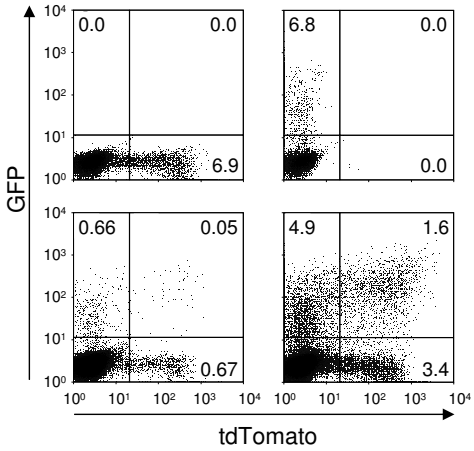

Figure S1. The majority of transduced cells contains a single transgene. Flow cytometric analysis of total splenocytes 1 d after transduction with a retroviral vector encoding tdTomato (top left), a retroviral vector encoding GFP (top right panel), or both vectors (bottom two panels). Plots show living lymphocytes after exclusion of cell doublets by pulse-width analysis. Numbers indicate the percentages of cells in each quadrant. In the bottom left panel, where low virus concentrations were used, of the 1.38% (0.66 + 0.05 + 0.67) transduced cells, 0.05/1.38 × 100 = 3.6% express both GFP and tdTomato, indicating that under this condition 100 – (2 × 3.6) = 92.8% of the transduced cells contains a single transgene. Under these conditions, the number of barcodes present within a given cell population is therefore approximately equivalent to the number of progenitors that yielded this population. In the bottom right panel, where ~10-fold higher virus concentrations were used, 67.7% of the transduced cells contains a single transgene.

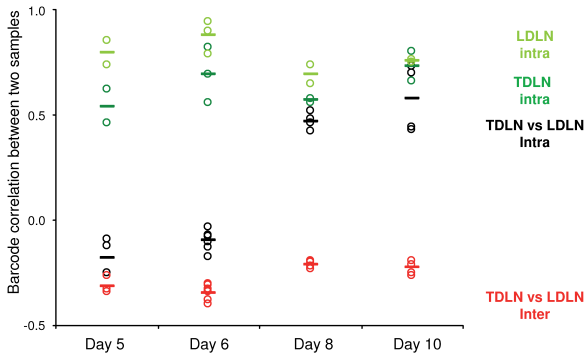

Figure S2. Redistribution of T cell families over lymph node beds through time examined by correlation analysis. Pearson's correlation coefficients of the comparisons of different tissue samples as shown in Fig. 4 C. R values represent the correlation between hybridization signals of all barcodes present in either the Cy3- or Cy5-labeled sample.

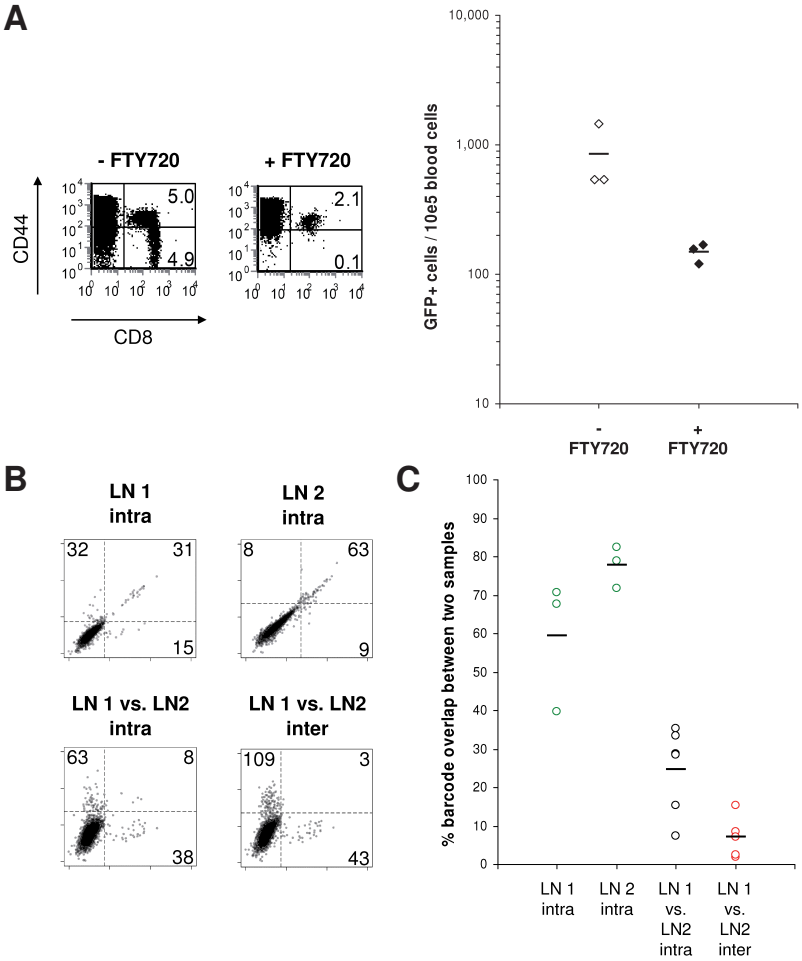

Figure S3. Redistribution of T cell families over lymph node beds is dependent on lymph node egress. Mice received 10,000 conA-activated barcode-labeled OT-I T cells and were subsequently challenged intranasally with WSN-OVA influenza virus (day 0) and s.c. with EL4-OVA tumor cells (day 1). Starting at day 0, mice were injected every 2 d with 1 mg/kg FTY720 (+FTY720; Cayman chemical) or left untreated (−FTY720). At day 8 after challenge, peripheral blood, as well as TDLN and LDLN were isolated. Results represent data from three mice, analyzed separately within one experiment. (**A**) Blood cells were stained for CD8 and CD44 (left) and the number of GFP^+ cells per 10^5 blood cells was enumerated (right). (**B**) TDLN and LDLN from the FTY720-treated mice were each split into two half-samples, independently amplified by PCR, and used for barcode analysis. Top row: self–self comparisons of barcodes isolated from TDLN (left) or LDLN (right). Bottom row: comparison of barcodes isolated from TDLN and LDLN from the same mouse (left) or from different mice (right). Numbers indicate the barcodes of barcodes detected above background for each quadrant (black rectangles; cutoff used, $P < 0.0005$). (**C**) Cumulative data of three mice showing the percentage of barcode overlap for the indicated samples. Percentage of barcode overlap indicates the number of barcodes present in the top right quadrant as a fraction of the total number of barcodes present in the top left, top right and bottom right quadrants.

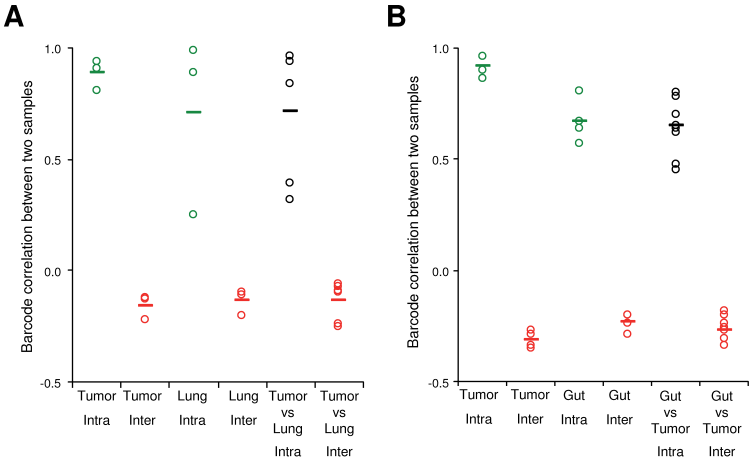

Figure S4. Kinship of T cells present at different effector sites examined by correlation analysis. Pearson's correlation coefficients of the comparisons of different tissue samples as shown in Fig. 5 B (A) and Fig. 6 B (B). R values represent the correlation between hybridization signals of all barcodes present in either the Cy3- or Cy5-labeled sample.

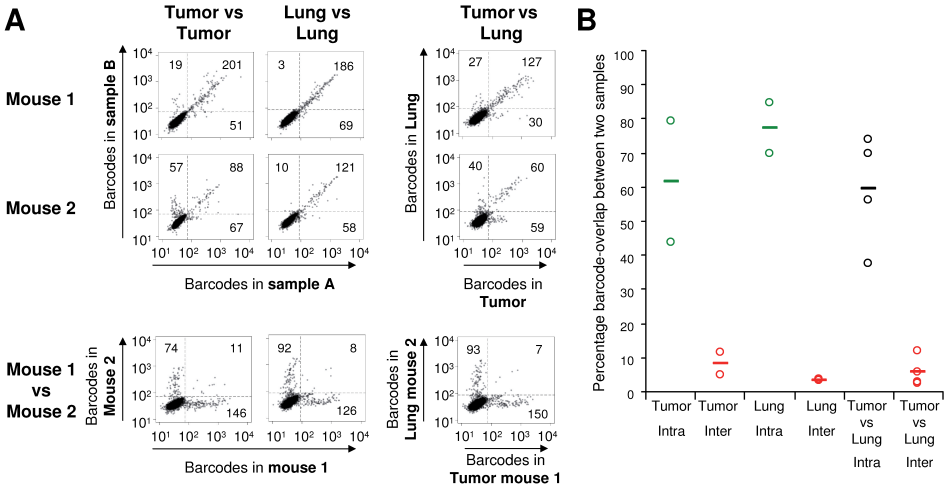

Figure S5. T cells present at lung and tumor effector sites are largely derived from the same naive T cell precursors. Barcode analysis of T cell populations from effector sites of mice that received ±1,000 naive barcode-labeled OT-I T cells and that were subsequently challenged intranasally with WSN-OVA influenza virus (day 0) and s.c. with EL4-OVA cells (day 1). At day 8 after challenge, T cells were isolated from tumor and lung tissue for barcode analysis. Naive barcode-labeled T cells were generated by retroviral transduction of thymocytes with the barcode library and subsequent development into mature T cells upon intrathymic injection in B6 mice (unpublished data). Results represent data from two mice analyzed separately within one experiment. (**A**) Representative dot plots of the fluorescence intensities of the barcode microarray spots. Left and middle, top two rows: dot plots of barcode analysis of two pools of T cells isolated from the same tissue for two individual mice. Right, top two rows: dot plots of barcode analysis of T cells isolated from tumor versus T cells isolated from lung for two individual mice. Bottom row: evaluation of background overlap by comparison of samples from mouse 1 with samples from mouse 2. Numbers indicate the barcodes that are present within each quadrant (black rectangles) as a percentage of the total number of barcodes present in the top left, top right, and bottom right quadrants. (**B**) Percentage of barcode overlap between different tissue samples. Each sample was compared with a second sample generated from the same tissue (tumor or lung) or from a different tissue (tumor vs. lung), either of the same mouse (intra) or of a different mouse (inter). The percentages indicate the number of barcodes that is present within the top right quadrant as a fraction of the total number of barcodes present in the top left, top right, and bottom right quadrant (as indicated in A).

5

ONE NAÏVE T CELL - MULTIPLE FATES IN CD8$^+$ T CELL DIFFERENTIATION

Carmen Gerlach[1], Jeroen W.J. van Heijst[1], Erwin Swart[1], Daoud Sie[2], Nicola Armstrong[3], Ron M. Kerkhoven[2], Dietmar Zehn[4], Michael J. Bevan[5], Koen Schepers[1] and Ton N.M. Schumacher[1,8]

[1]Division of Immunology, [2]Central Microarray Facility and [3]Bioinformatics and Statistics Group, Division of Molecular Biology, The Netherlands Cancer Institute, Amsterdam, The Netherlands; [4]Swiss Vaccine Research Institute, Lausanne, Switzerland; [5]Howard Hughes Medical Institute, University of Washington, Seattle, USA

J Exp Med. 207: 1235-46 (2010)

The mechanism by which the immune system produces effector and memory T cells is largely unclear. To allow a large-scale assessment of the development of single naive T cells into different subsets, we have developed a technology that introduces unique genetic tags (barcodes) into naive T cells. By comparing the barcodes present in antigen-specific effector and memory T cell populations in systemic and local infection models, at different anatomical sites, and for TCR–pMHC interactions of different avidities, we demonstrate that under all conditions tested, individual naive T cells yield both effector and memory $CD8^+$ T cell progeny. This indicates that effector and memory fate decisions are not determined by the nature of the priming antigen-presenting cell or the time of T cell priming. Instead, for both low and high avidity T cells, individual naive T cells have multiple fates and can differentiate into effector and memory T cell subsets.

5

INTRODUCTION

Activation of naïve antigen-specific T cells is characterized by a vigorous proliferative burst, resulting in the formation of a large pool of effector T cells. Following pathogen clearance, ~95% of activated T cells die, leaving behind a stable pool of long-lived memory cells [1]. Two fundamentally different mechanisms could give rise to the production of effector and memory T cells during an immune response. First, single naïve T cells may be destined to produce either effector T cells or memory T cells, but not both (one naïve cell - one fate). As an alternative, effector and memory T cells could derive from the same clonal precursors within the naïve T cell pool (one naïve cell - multiple fates). As the fate decisions that control T cell differentiation could either be taken during initial T cell priming (i.e. before the first cell division) or at later stages, at least four conceptually different models describing effector and memory T cell differentiation can be formulated (Fig. S1).

A first model predicts a separate origin of effector and memory T cells as a result of differential T cell priming by APCs. In this scenario, fate decisions would be taken before the first cell division and even though cells destined to become memory cells may transiently display traits associated with effector T cells (e.g. expression of Granzyme B or IFN-γ; see below), their ability for long-term survival would be predetermined. In line with this model, several studies have provided evidence that the fate of $CD8^+$ T cells may, to some extent, be programmed during initial activation [1-5].

A second model, which relies on recent data from Chang *et al.* [6], likewise suggests that the priming APC plays the crucial role in determining effector or memory T cell fate, but by a strikingly different mechanism and with an opposite prediction concerning the lineage relationship of effector and memory T cells. Specifically, analysis of T cell – APC conjugates has shown that the first division of activated T cells can be asymmetric, with the daughter T cell that is formed proximal to the APC being more likely to contribute to the effector T cell subset and the distal daughter T cell being more likely to generate memory T cells [6]. Assuming that all primary daughter cells survive and yield further progeny, these data would predict that single naïve T cells contribute to both the effector and the memory subset.

In contrast to these two models that are based on a determining role of the priming APC, two other models predict that T cell fate is determined by the cumulative effect of signals that not only naïve T cells but also their descendants receive. The first of these models, termed the 'decreasing potential model', argues that T cell progeny that receive additional stimulation after priming undergo terminal differentiation towards the effector subset, whereas descendants that do not encounter these signals may transiently display certain effector functions, but will ultimately become memory T cells [7]. In support of this model, it has been demonstrated that continued inflammatory signals [8,9] and prolonged antigenic stimulation [10] can lead descendant $CD8^+$ T cells to preferentially develop into effector cells.

If the descendants of all individual naïve T cell have an equal chance of receiving signals for terminal differentiation, the standard decreasing potential model predicts that memory and effector T cells will be derived from the same population of naïve T cells. There is however evidence that the environmental factors that promote either terminal differentiation or memory T cell development may alter over the course of infection [10]. A fourth model therefore argues that the progeny of T cells that are activated early or late during infection will receive distinct signals, and hence assume (partially) different fates [11-14].

A large number of studies in which cell differentiation was analyzed at the population level have been informative in revealing which effector properties can be displayed by T cells that subsequently differentiate into memory T cells (reviewed in [15]). In particular, two recent studies using IFN-γ or granzyme B reporter mice have shown that memory T cells can arise from cells that have previously transcribed IFN-γ or granzyme B genes [5,16]. It is however important to realize that these studies reveal little with regard to the developmental potential of individual naïve T cells. Specifically, the fact that T cells that have a particular effector capacity can become memory T cells does not indicate that all naïve T cells yield such effector cells, nor does it indicate that all memory T cells have gone through an effector phase.

To determine the developmental potential of naïve T cells, it is essential to develop technologies in which T cell responses can be analyzed at the single naïve T cell level. In early work that aimed to follow T cell responses at the clonal level, TCR repertoire analysis has been used to assess the kinship of T cell populations [17,18]. However, as several naïve T cell clones can share the same TCR, it has been argued that such analyses do not necessarily monitor T cell fate at the single T cell level [19,20]. Recently, Stemberger *et al.* have reported on a more elegant approach to address naïve T cell potency [14]. Using the transfer of single naïve $CD8^+$ T cells into mice, this study provides direct evidence that a single naïve $CD8^+$ T cell can form both effector and memory cell subsets. However, the statistical power of single cell transfer studies obviously has limitations. In addition, if homeostatic proliferation would occur prior to antigen-driven proliferation in this system, this would limit the conclusions that can be drawn with regard to the pluripotency of a single naïve T cell.

In this study, we have developed a technology that allows the generation of naïve T cells that carry unique genetic tags (barcodes), and we describe how this technology can be utilized for the large-scale assessment of the developmental potential of single naïve T cells. Using physiological frequencies of barcode-labeled naïve $CD8^+$ T cells of different functional avidities, we demonstrate that in both systemic and local infection models, effector and memory $CD8^+$ T cell subsets share the same precursors in the naïve T cell pool. These data demonstrate that under all conditions analyzed, single naïve T cells do not selectively yield effector or memory T cells. Rather, T cell differentiation into effector and memory T cell subsets occurs by a one naïve cell - multiple fates principle.

RESULTS

Generation of a barcode-labeled naïve T cell pool

To study the lineage relationship between effector and memory $CD8^+$ T cells, we aimed to follow the progeny of individual naïve $CD8^+$ T cells during the course of infection. Recently, we have developed a genetic tagging technology that allows lineage analysis in a high-throughput fashion [21]. In this technology, unique DNA barcodes are introduced into cell populations of interest. As these barcodes are transmitted to all progeny, microarray-based analysis of barcodes present in different cell populations can be used to reveal their common or separate ancestry.

A potential concern in using this technology for fate mapping within the T cell lineage is that the retroviral transduction procedure that is used to introduce barcode sequences requires T cell activation, which could influence subsequent T cell fate (note that lentiviral transduction strategies to modify quiescent murine T cells have not been developed). To permit T cell fate mapping without a confounding effect of the barcoding procedure itself, we set out to develop a technology that allows the generation of 'untouched' naïve barcode-labeled T cells (Fig. 1A). To this purpose, total thymocytes from young OT-I TCR-transgenic mice were transduced using a retroviral library containing approximately 3,500 unique genetic tags plus a GFP marker gene (the barcode-library). One day after transduction, approximately 10% of thymocytes showed GFP expression (Fig. 1B), and the large majority (89%) of GFP-positive thymocytes was $CD4^+CD8^+$ (double-positive; DP) (Fig. 1B). Based on the kinetics of thymocyte maturation, it is likely that both proliferating double-negative (DN) and DP thymocytes contributed to the generation of these barcode-labeled cells [22], "unpublished data").

To investigate whether barcode-labeled thymocytes could be utilized to generate barcode-labeled naïve T cells, GFP-expressing OT-I thymocytes were sorted and injected intra-thymically into unmanipulated primary recipient mice. Three weeks after intra-thymic injection, primary recipients contained a clear population of peripheral $CD8^+$ T cells that were GFP-positive (barcode-labeled) and donor-derived ($CD45.1^+$) (Fig. 1C). Importantly, these barcode-labeled $CD8^+$ T cells showed a naïve phenotype, as evidenced by the expression profiles of CD62L and CD44 (Fig. 1D).

To test whether barcode-labeled OT-I cells behave similarly to unmanipulated OT-I cells upon activation, both were co-transferred into secondary recipients. Recipient mice were then infected with a *Listeria monocytogenes* strain expressing ovalbumin (LM-OVA). Absolute peak heights of T cell responses cannot be compared because of the difficulty in determining the exact number of transferred barcode-labeled cells (see Materials and Methods). However, the kinetics of expansion, contraction and survival into the memory phase were comparable between barcode-labeled and unmanipulated OT-I cells (Fig. 2A). Furthermore, both types of OT-I cells displayed a similar activated phenotype ($CD44^{hi}$, $CD62L^{lo}$, $CD43^{hi}$, $CD127^{lo}$, mostly $KLRG\text{-}1^{hi}$) (Fig. 2B + Fig. S2).

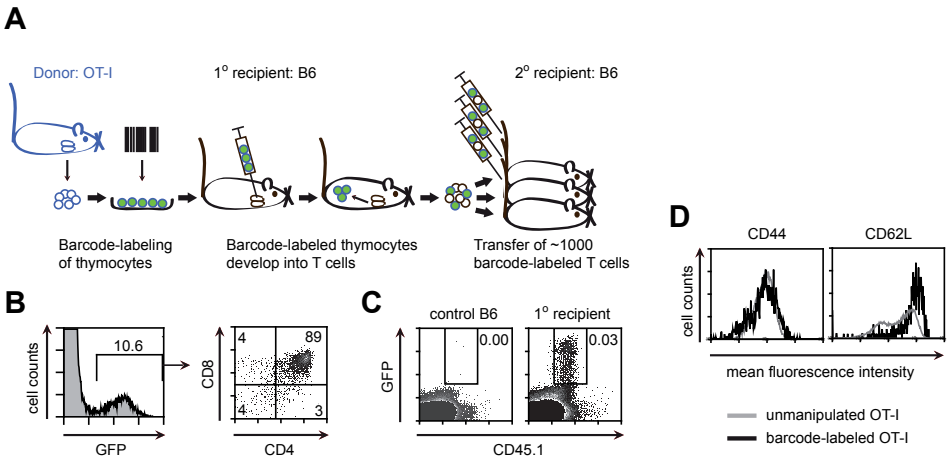

Figure 1. Genetic tagging of naïve T cells. (A) Experimental set-up for the generation and use of naïve, barcode-labeled T cells. Donor thymocytes are transduced with a barcode library. Transduced cells are sorted and injected intra-thymically into primary (1°) recipient mice. 3 weeks later, mature T cells are isolated from 1° recipients, pooled and transferred into 2° recipients. **(B)** Total CD45.1$^+$ OT-I thymocytes were transduced with the retroviral barcode library. One day after transduction, cells were stained and analyzed by flow cytometry. CD4 and CD8 expression is shown for the GFP$^+$ (barcode-labeled) population. Numbers indicate percentages. Data are representative of two independent experiments. **(C and D)** Sorted GFP$^+$ CD45.1$^+$ OT-I thymocytes were injected into the thymi of CD45.2$^+$ B6 1° recipient mice (n=3). 3 weeks later, spleen and LN cells were isolated, pooled, enriched for CD8$^+$ cells, stained for the indicated surface markers and analyzed by flow cytometry. Data are representative of two independent experiments. **(C)** Expression of CD45.1 and GFP on gated CD8$^+$ cells from unmanipulated (control) B6 or 1° recipient mice. Numbers indicate percentages. **(D)** Expression of CD44 and CD62L on unmanipulated (CD45.1$^+$) and barcode-labeled (GFP$^+$ CD45.1$^+$) CD8$^+$ T cells.

Having established a strategy to generate naïve barcode-labeled T cells, we investigated the potential of these cells for lineage tracking. Any effective lineage tracking strategy must meet two criteria. First, it must be able to reveal a high degree of relatedness between two cell populations known to be derived from a common progenitor. Second, it must demonstrate the absence of relatedness when assessing two populations known to be derived from separate progenitors. To create an experimental setting in which related and unrelated cell populations co-exist within a single mouse, secondary recipient mice received naïve barcode-labeled OT-I cells and were challenged with both an $OVA_{(257-264)}$-expressing influenza strain (WSN-OVA) and $OVA_{(257-264)}$-expressing tumor cells (EL-4-OVA). In this setting, priming of naïve T cells occurs independently and simultaneously in the lymph nodes that drain the two separate sites of antigenic challenge [21]. Five days after infection, when activated T cells are still largely confined to the site of priming, lymph node cells were isolated and divided into 2 pools (sample A and B) per lymph node. These lymph node

half-samples were independently expanded *in vitro* to boost T cell numbers prior to barcode analysis. As expected, the same barcodes were found in both half-samples of the same lymph node (Fig. 2C, upper left and middle plot). This indicates that cellular barcoding using naïve barcode-labeled T cells is able to establish that these two T cell populations are progeny of the same naïve T cell pool. In contrast, T cells isolated from two separate lymph nodes of the same mouse harbored a different set of barcodes (Fig. 2C, upper right plot), indicating that the technology can also correctly identify two T cell populations as being unrelated (i.e. derived from two different naïve T cell pools). As a further control, barcode content was compared between T cell populations recovered from different mice. These 'between-mice' comparisons are of use to reveal the background overlap that could, for instance, arise in case of clonal dominance of a small number of thymocytes during reconstitution of primary recipients. Notably, the overlap in barcode content between such evidently unrelated samples was low (Fig. 2C, lower plot).

To quantify the degree of relatedness between different samples, the correlation between barcode signals was calculated (see Materials and Methods). Analysis of lymph node samples from 3 mice revealed a consistently high positive correlation between barcode signals from two cell populations known to be related (sample A and B of the same LN) (Fig. 2D). In contrast, negative correlation values were obtained in all cases where two cell populations known to be unrelated were compared (Fig. 2D). In conclusion, these data show that the introduction of genetic tags in thymocytes can be used to generate naïve T cell populations suited for lineage tracking.

In all subsequent experiments intra-population comparisons were included as a barcode 'sampling control' to determine the reliability of barcode analysis for a given population, and 'between-mice' comparisons were included to reveal the background overlap seen in a particular experiment. These two control comparisons of cells that are by definition related or unrelated set the boundaries for all biological analyses.

$CD8^+$ T cells that are present during effector and resting memory phase are derived from the same naïve T cells

Traditionally, memory T cells are defined on the basis of their long-term persistence after antigen clearance. More recently, it has been suggested that precursors of memory cells can already be identified around the peak of the response, by the expression of high CD127 and low KLRG-1 levels [9,23]. As a first test of the lineage relationship of effector and memory T cells, we therefore performed a preliminary experiment to examine whether $CD127^{hi}KLRG\text{-}1^{lo}$ and $CD127^{lo}KLRG\text{-}1^{hi}$ $CD8^+$ T cells are derived from the same or distinct naïve T cells.

To this end, naïve barcode-labeled OT-I T cells were injected into secondary recipient mice that were subsequently infected with LM-OVA. Ten days after infection, $CD127^{hi}KLRG\text{-}1^{lo}$ and $CD127^{lo}KLRG\text{-}1^{hi}$ $CD8^+$ T cells were sorted from spleen and lymph nodes and each subset was divided into two half-samples (sample A and B) (Fig. S3A). As pilot experiments had shown that barcode copy numbers were too

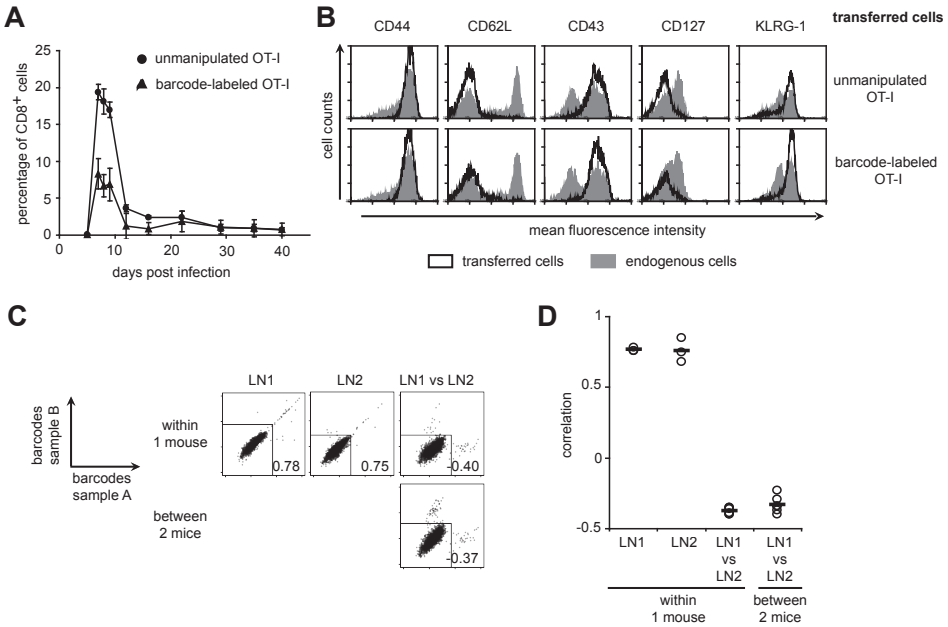

Figure 2. Barcode-labeled T cells can be utilized for lineage relationship analysis. **(A)** CD45.1$^+$ B6 2° recipient mice (n=5) received unmanipulated CD8$^+$CD45.2$^+$ OT-I cells plus naïve barcode-labeled CD8$^+$CD45.1$^+$ OT-I cells and subsequent i.v. LM-OVA infection. Average responses of transferred OT-I cells are depicted; error bars indicate standard deviations. **(B)** Naïve, barcode-labeled or unmanipulated CD8$^+$CD45.1$^+$ OT-I cells were injected i.v. into CD45.2$^+$ B6 2° recipient mice (n=7 and n=2, respectively). Mice were subsequently infected i.v. with LM-OVA. At day 7 post-infection, blood cells were stained for the indicated surface markers and analyzed by flow cytometry. Filled gray histograms represent total endogenous CD45.1$^-$CD8$^+$ T cells; black lines represent transferred CD45.1$^+$ OT-I cells. One representative mouse per group is shown. Data are representative of 2 independent experiments. **(C and D)** Naïve, barcode-labeled CD8$^+$CD45.1$^+$ OT-I cells were injected into CD45.2$^+$ B6 2° recipient mice. Mice were subsequently challenged with WSN-OVA (intra-nasal) and EL-4 OVA tumor cells (s.c.) the next day. At day 5 post-infection, lung-draining and tumor-draining lymph node cells were isolated, and each lymph node sample was split into two half-samples (sample A and B). Each half-sample was cultured separately for 3-4 days *in vitro* in the presence of 10μg/ml IL-7 and 20U/ml IL-2. Barcode analysis was performed independently on sample A and B of both lymph nodes (LN1 and LN2). Barcodes with a P-value of <0.001 were considered to be present above background. Rectangular dividers indicate which barcodes are present above background. Note that rather than fixing the absolute position of dividers in terms of intensity, it is the statistical probability of barcode presence that is kept constant for all samples in a given experiment. Data are representative of two independent experiments. **(C)** Representative 2-D plots of barcode analyses. Numbers indicate the correlation between signals from sample A and B. **(D)** Correlation analysis of barcodes present in T cells from the same or from distinct LN. Data are shown for 3 mice from 2 independent experiments. Mice of which barcodes in one of the 2 draining lymph nodes could not be sampled reliably were excluded from further analysis.

low for representative recovery from CD127^{hi}KLRG-1^{lo} cells, both half-samples of this subset were expanded separately *in vitro* to boost cell numbers prior to barcode analysis.

For all mice analyzed, barcodes were recovered representatively from the CD127^{lo}KLRG-1^{hi} subset (Fig. S3B, upper left plot + Fig. S3C), as indicated by the high correlation between barcode signals from sample A and B. Barcode signals from CD127^{hi}KLRG-1^{lo} half-samples were also well correlated, although some barcodes were only recovered from one of the two half-samples (Fig. S3B, upper middle plot + Fig. S3C). Furthermore, all 'between-mice' comparisons showed the expected inverse correlation (Fig. S3B, lower plots + Fig. S3C triangles).

Importantly, comparison of barcodes detected within the CD127^{lo}KLRG-1^{hi} and the CD127^{hi}KLRG-1^{lo} subset showed a strong correlation of barcode signals (Fig. S3B, upper right plot + Fig. S3C), demonstrating a high relatedness of both subsets. A small fraction of barcodes was only detected in one of the two subsets. However, this fraction of outliers was similar to that detected within intra-CD127^{hi}KLRG-1^{lo} comparisons. In line with this, the correlation of CD127^{lo}KLRG-1^{hi} versus CD127^{hi}KLRG-1^{lo} barcode comparisons was similar to that of intra-CD127^{hi}KLRG-1^{lo} comparisons (Fig. S3C). Note that when two related populations are compared of which one is sampled sub-optimally, the inter-sample correlation approximates the lowest of the two intra-sample correlations (Fig. S4A and B). To further test the potential significance of the observed difference between CD127^{hi}KLRG-1^{lo} and CD127^{lo}KLRG-1^{hi} subsets, data were reanalyzed after exclusion of outliers present within the intra-subset comparison, a strategy that can be utilized to facilitate the detection of small differences (Fig. S4C and D). Also after this filtering, no clear population of either CD127^{lo}KLRG-1^{hi} or CD127^{hi}KLRG-1^{lo}-specific barcodes was observed (Fig. S4E). Together, these preliminary data indicate that CD127^{lo}KLRG-1^{hi} and CD127^{hi}KLRG-1^{lo} by and large share the same set of progenitors.

To address the kinship of effector and memory phase CD8^{+} T cells in a direct manner, we analyzed the barcode content of antigen-specific T cells that are present within the same mouse at different time points following infection. To this purpose, secondary recipient mice were infected with LM-OVA and blood was drawn for barcode analysis at the peak of the effector response. Animals were then kept until the resting memory phase, when both blood and spleen samples were obtained for barcode analysis. Analysis of sampling controls indicated that barcodes could be identified reliably during the memory phase and also in a small sample of peripheral blood obtained during the effector phase (Fig. 3A, upper plots). 'Between-mice' comparisons demonstrated that these unrelated cell populations were also correctly identified as such (Fig. 3A and B, lower plots + Fig. 3C, triangles).

Importantly, when the barcode repertoire present in effector and memory phase samples was compared, it was apparent that the two were highly correlated, independent of whether the memory sample was drawn from blood (Fig. 3B, upper left plot + Fig. 3C) or spleen (Fig. 3B, upper right plot + Fig. 3C). Furthermore, few

Figure 3. CD8⁺ T cells that are present during effector and resting memory phase are derived from the same naïve T cells. CD45.2⁺ B6 2° recipient mice (n=4) were injected with naïve, barcode-labeled CD8⁺CD45.1⁺ OT-I cells and subsequently infected i.v. with LM-OVA. Barcode analysis was performed on a 250-300µl blood sample drawn at day 8 post-infection (effector phase), and on a blood sample as well as on spleen isolated at day 28 post-infection (memory phase) from the same mice. Blood and spleen samples were divided into two halves (sample A and B) that were independently analyzed for barcode content. Barcodes with a P-value <0.005 were considered to be present above background. On average, 150 barcodes were detected per mouse. Data are representative of two independent experiments. **(A and B)** Representative 2-D plots of barcode comparisons. Numbers indicate the correlation between signals from sample A and B. **(C)** Correlation analysis of barcodes present in sample A and B from effector phase blood and memory phase blood (left plot) or effector phase blood and memory phase spleen (right plot). Data from 4 mice are depicted.

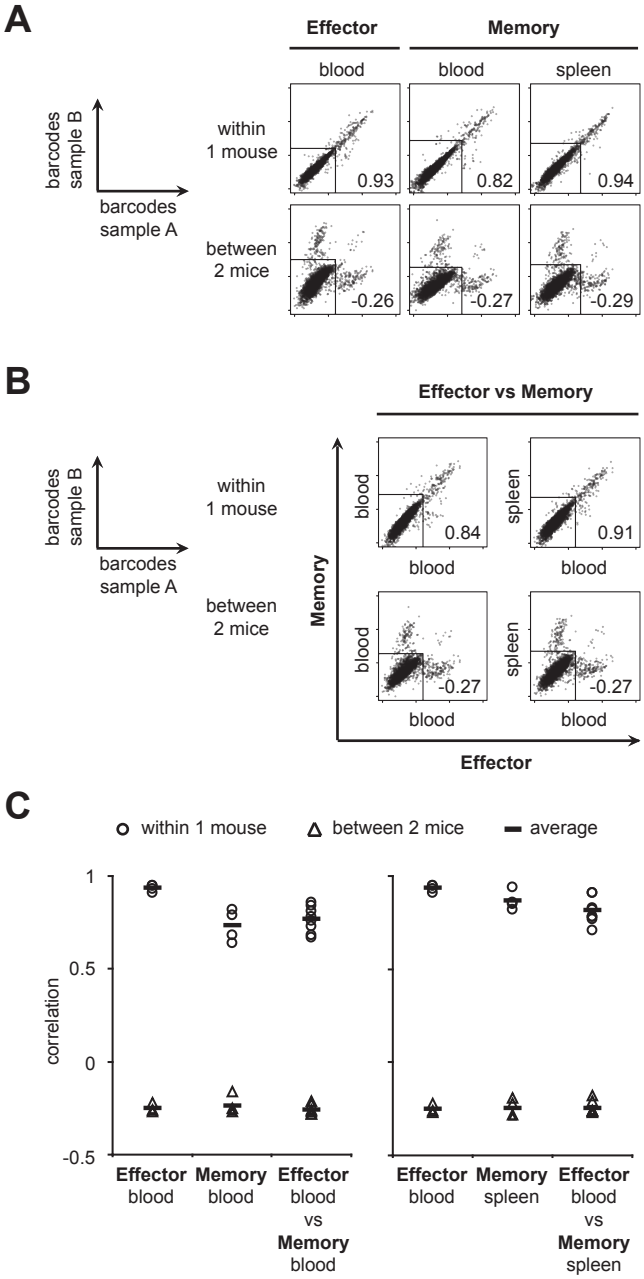

if any barcodes were identified that were selectively present in either the effector phase or the memory phase T cell population. These data demonstrate that CD8$^+$ T cells participating in the effector response and those present during memory phase in blood and spleen are derived from the same naïve CD8$^+$ T cells.

CD8$^+$ T cells that are present in different lymphoid organs are derived from the same naïve T cells

Prior work has suggested that the bone marrow can serve as a site of T cell priming [24]. In addition, there is evidence to suggest that the bone marrow may contain a specialized memory T cell compartment [25]. Based on these data it could be postulated that while effector and memory phase T cells in blood and spleen are derived from the same naïve T cells, bone-marrow resident T cells may form a separate pool.

To investigate the lineage relationship of CD8$^+$ T cells that are found in different organs during the effector and memory phase, naïve barcode-labeled OT-I T cells were transferred into secondary recipient mice. Mice were then infected with LM-OVA and barcode analysis was performed on cells isolated from blood, spleen, bone marrow and lymph nodes at the peak of the effector response or during the memory phase. Barcodes were recovered efficiently from all four organs during the effector phase, albeit with a somewhat lower efficiency for lymph nodes and bone marrow (Fig. 4A and Fig. 4B, circles), consistent with the lower number of barcode-labeled T cells isolated from these organs.

To assess whether T cells present at these distinct sites share common progenitors within the naïve T cell pool, barcode content of the different T cell populations was compared. In all these comparisons, barcode content of T cells from the different anatomical sites was highly correlated and similar to the poorest sampled intra-organ comparison (Fig. 4A and Fig. 4B, circles). This demonstrates that the progeny of naïve T cells activated within an antigen-specific T cell response seeds all secondary lymphoid organs, including the bone marrow. Note that this analysis also validates the use of blood samples for lineage analysis during the effector phase (Fig. 3), as barcodes found in a 300µl blood sample are representative of barcodes found in all other lymphoid organs at the peak of the effector response.

Barcode analysis was subsequently performed on cells isolated from blood, spleen, lymph node and bone marrow samples at a late time point post-infection (day 28) (Fig. S5A and B). Efficiency of barcode recovery was again high for spleen and blood, but lower for bone marrow and lymph nodes, consistent with the lower number of GFP$^+$ cells in these organs. Nevertheless, in all possible comparisons the inter-organ correlation was similar to the correlation of the least efficiently sampled intra-organ comparison. Together, these data indicate that CD8$^+$ T cells that are present in different lymphoid organs are largely, if not fully derived from the same set of antigen-specific precursors within the naïve T cell repertoire.

Shared T cell families in resting memory and secondary T cell responses

To investigate whether all naïve T cell clones of which the progeny persisted into

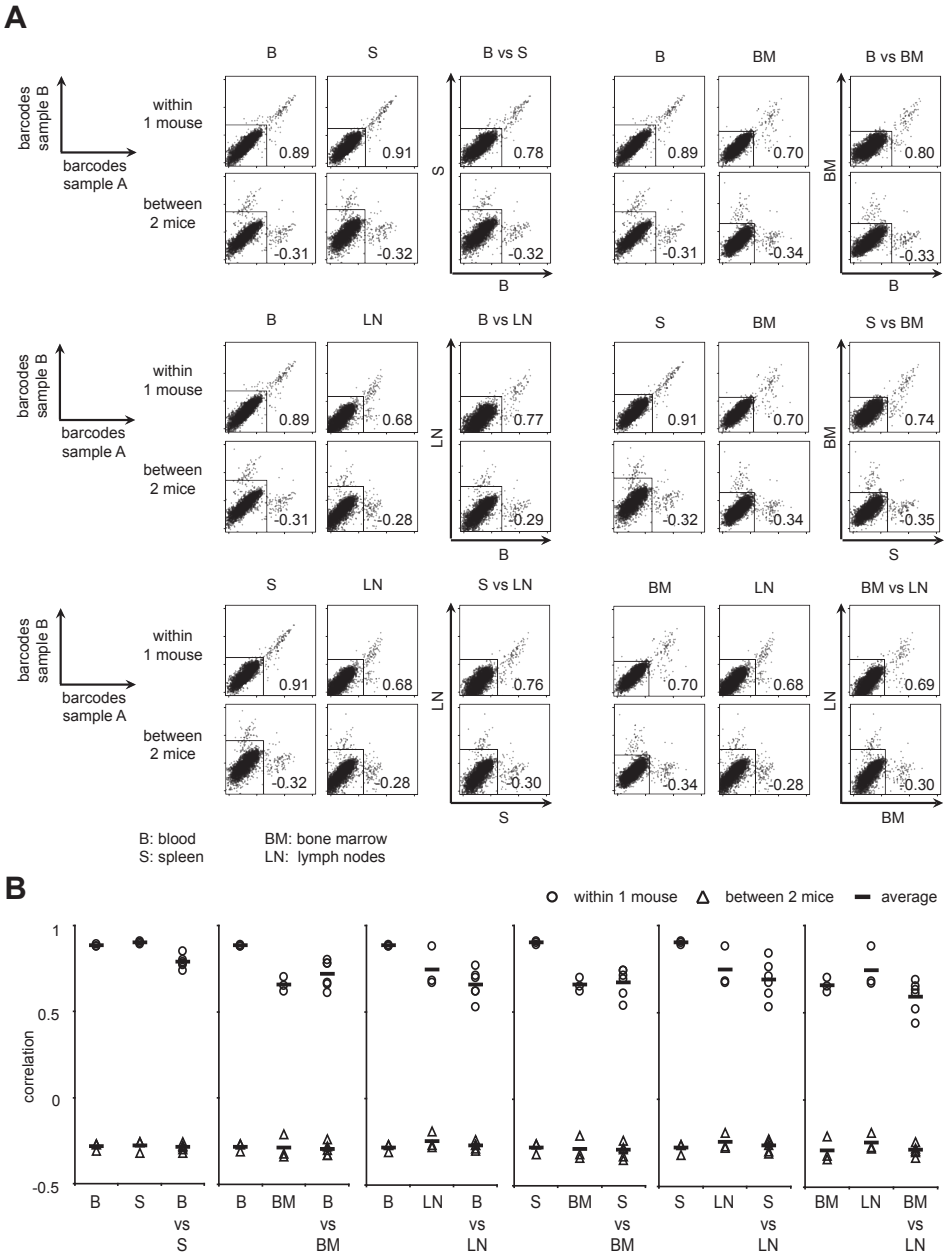

Figure 4. Effector phase CD8⁺ T cells present in blood, spleen, bone marrow and lymph nodes are derived from the same naïve T cells. CD45.2⁺ B6 2° recipient mice (n=3) were injected with naïve, barcode-labeled CD8⁺CD45.1⁺ OT-I cells and subsequently infected i.v. with LM-OVA. Barcode analysis was performed at day 8 post-infection on cells recovered from blood (B), spleen (S), bone-marrow (BM) and lymph nodes (LN). All samples were divided into two halves (sample A and B) that were ▷

resting memory phase also had descendants that were able to respond to secondary infection, naïve barcode-labeled OT-I T cells were transferred into secondary recipients that were subsequently infected with LM-OVA. At the resting memory phase, cells from blood, spleen, lymph nodes and bone marrow were isolated and pooled. Two parts were then used for independent barcode analysis and a third part was transferred into a tertiary recipient mouse that was thereafter infected with LM-OVA. At the peak of the secondary response, spleen samples were isolated for barcode analysis.

Analysis of the resting memory and secondary expansion sampling controls showed that barcodes could be reliably identified at both time points (Fig 5A, upper left and middle plot + Fig 5B). As expected, 'between-mice' comparisons were poorly correlated, although higher than in previous experiments due to the larger number of participating barcodes in this experiment (Fig 5A, lower plots + Fig 5B, triangles).

Subsequent comparison of the barcode repertoire present in resting memory and secondary expansion samples showed that at both time points, essentially the same barcode pool was present (Fig 5A, upper right plot + Fig 5B). Thus, these data show that all naïve T cell clones that contribute to the resting memory population also have progeny that respond to secondary antigen encounter. This indicates that the kinship of effector and memory T cells applies not only to resting memory T cells, but also to memory T cells as defined by their ability to respond to secondary antigen encounter.

Kinship of effector and memory phase $CD8^+$ T cells upon local infection

To establish whether the observed kinship of effector and memory subsets is restricted to systemic infection models, we determined the lineage relationship of these subsets in a local influenza A infection model. As pilot experiments had shown that the number of barcode-labeled cells in a blood sample drawn at the peak of the influenza-specific T cell response was too low for reliable barcode sampling, barcodes were read from a spleen sample obtained by partial splenectomy at the peak of the effector response. Mice were then kept until the resting memory phase, when the remainder of the spleen was analyzed for barcode content.

Sampling control comparisons demonstrated that both during effector and memory phase, barcodes could be read reliably (Fig 6A, upper left and middle plot + Fig 6B). 'Between-mice' controls showed the expected low correlation, although the number of shared barcodes was relatively high, due to the higher amount of barcodes participating in this experiment (Fig 6A, lower plots + Fig 6B, triangles). Importantly,

▷ independently analyzed for barcode content. Barcodes with a P-value <0.02 were considered to be present above background. On average, 150 barcodes were detected per mouse. S vs. B comparisons are representative of two independent experiments, LN and BM barcodes were analyzed in one experiment. **(A)** Representative 2-D plots of barcode comparisons. Numbers indicate the correlation between signals from sample A and B. **(B)** Correlation analysis of barcodes present in sample A and B. Data from 3 mice are depicted.

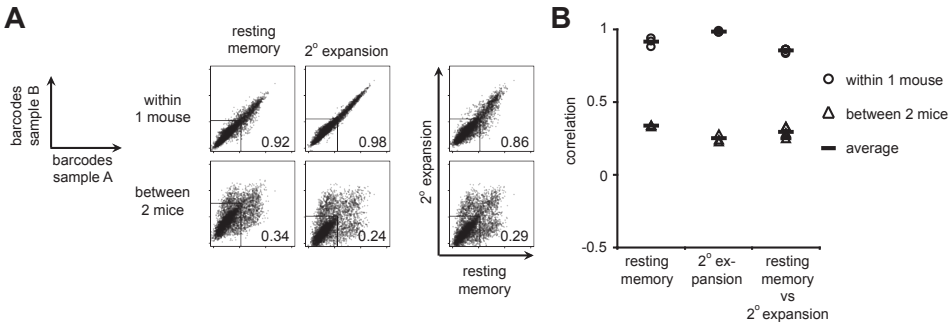

Figure 5. Naïve T cell clones that contribute to the resting memory population, also have progeny that respond to secondary antigen encounter. B6 2° recipient mice (n=3) were injected with naïve, barcode-labeled CD8$^+$ OT-I cells and subsequently infected i.v. with LM-OVA. 28 days post-infection, blood, spleen, LN and BM cells were isolated, pooled per mouse and divided into 3 parts. 2 parts were used for barcode analysis (sample A and B, resting memory phase) and the third was transferred into a B6 3° recipient mouse that was then infected with LM-OVA. 5 days later, barcodes were analyzed from spleen half-samples (2° expansion). Barcodes with a P-value <0.01 were considered to be present above background. On average, 1080 barcodes were detected per mouse. **(A and B)** Representative 2-D plots of barcode comparisons. Numbers indicate the correlation between signals from sample A and B. **(C)** Correlation analysis of barcodes present in sample A and B. Data are derived from 3 2° recipient and 3 3° recipient mice analyzed within one experiment. These data confirm results obtained in an independent pilot experiment in which 1° expansion (effector phase) and 2° expansion memory populations could be compared for one mouse.

when barcode signals were compared between effector and memory phase samples, it was apparent that also during WSN-OVA infection, barcode content was highly correlated at both time points (Fig 6A, upper right plot + Fig 6B). This demonstrates that also in a local infection model, effector and memory phase T cells are progeny of the same naïve T cells.

Relatedness of effector and memory T cells is independent of TCR avidity

As the naïve T cell repertoire consists of a variety of clones that recognize the same antigen but with different avidities, we performed two experiments to address whether the lineage relationship of effector and memory subsets is dependent on the strength of the TCR - pMHC interaction.

To assess the lineage relationship of effector and memory CD8$^+$ T cells in an oligoclonal antigen-specific T cell population we made use of 'Limited' (Ltd) mice that express the OT-I TCRβ chain together with a Vα2 TCRα chain minilocus, which can recombine to form a 'limited' repertoire of TCRs [26]. This focused repertoire of TCRs expressed by Ltd T cells recognizes the OVA epitope with a range of avidities, as measured by K^b-OVA tetramer binding [27]. Presumably due to the fact that only a single V segment is available for recombination, thymic selection of Ltd thymocytes is inefficient. Because of this low efficiency, it was technically not feasible to generate

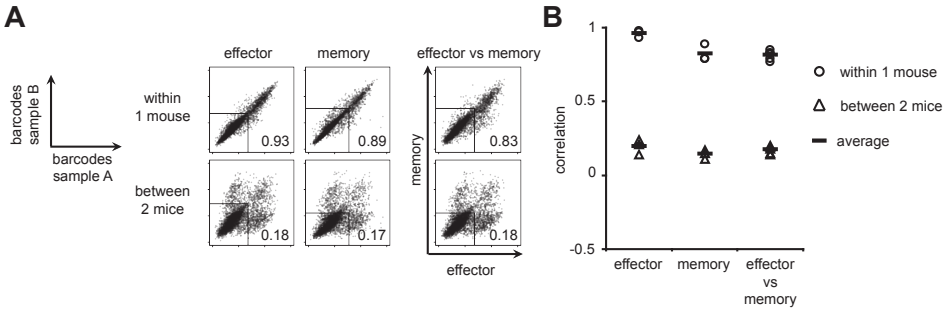

Figure 6. Kinship of effector and memory phase CD8⁺ T cells upon local infection. B6 2° recipient mice (n=4) were injected with naïve, barcode-labeled CD8⁺ OT-I cells and subsequently infected i.n. with WSN-OVA. Barcode analysis was performed on a ¼ spleen sample obtained by partial splenectomy at day 9 post-infection (effector phase), and on a spleen sample isolated at day 25 post-infection (memory phase) from the same mice. Effector and memory phase samples were divided into two halves (sample A and B) that were independently analyzed for barcode content. Barcodes with a P-value <0.001 were considered to be present above background. On average, 800 barcodes were detected per mouse. **(A and B)** Representative 2-D plots of barcode comparisons. Numbers indicate the correlation between signals from sample A and B. **(C)** Correlation analysis of barcodes present in sample A and B. Data from 4 mice are depicted. These data confirm results obtained in an independent pilot experiment in which effector and memory phase populations could be compared for one mouse.

naïve barcode-labeled Ltd cells by intra-thymic injection of transduced thymocytes. Therefore, barcode labeling was performed on *in vitro* activated peripheral Ltd T cells. Following transfer into recipient mice and LM-OVA infection, barcode content of effector and memory T cells was compared. Barcode sampling of the effector phase was less efficient in this preliminary experiment, possibly due to a reduced clonal burst size of *in vitro* activated T cells. Nevertheless, comparisons of effector and memory samples showed that barcodes in effector phase and secondary expansion phase T cells were largely shared (Fig. S6).

To study the kinship of effector and memory T cells in relation to T cell avidity in a system that does allow the use of naïve barcode-labeled T cells, we made use of a recombinant Listeria strain (LM-Q4-OVA) that expresses a variant of the $OVA_{257-264}$ epitope. Functional recognition of this Q4 variant by OT-I T cells requires approximately 18-fold more ligand than recognition of the parental epitope [28]. In line with the notion that Q4 forms a low avidity ligand, OT-I responses induced by LM-Q4-OVA have a reduced magnitude and earlier contraction [28].

Barcode-labeled naïve OT-I T cells were transferred into recipient mice that were challenged with LM-Q4-OVA at day 0 and re-challenged at day 27. At the peak of the effector response, barcodes were read from a spleen sample obtained by partial splenectomy and memory barcodes were read from the remainder of the spleen at the peak of the secondary response. Control comparisons showed that both during the effector and the secondary expansion phase, barcodes could be identified reliably

(Fig 7A, upper left and middle plot + Fig 7B), and that barcodes present in different mice were largely distinct (Fig 7A, lower plots + Fig 7B, triangles). In contrast, the barcode content of T cells present during effector and secondary expansion phase was highly correlated (Fig 7A, upper right plot + Fig 7B). This demonstrates that also for a lower avidity T cell response, effector and memory cells are derived from the same naïve T cells.

DISCUSSION

To date, our understanding of the process by which activation of naïve T cells leads to formation of effector and memory T cells remains incomplete with some studies favoring a principle of 'one naïve cell - one fate' and others of 'one naïve cell - multiple fates' [29]. The aim of this study was to determine which of these two principles applies to *in vivo* CD8$^+$ T cell differentiation.

Previous fate mapping studies were, with the exception of a study by Stemberger et al. [14], performed on the T cell population level, which precludes conclusions on the developmental potential of single naïve T cells. To allow large-scale fate mapping of naïve T cells at the single cell level, we have developed a technology in which naturally cycling thymocytes are provided with unique genetic tags (barcodes) by

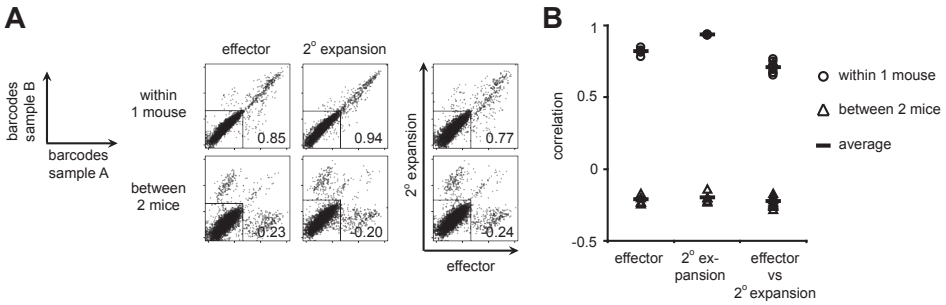

Figure 7. Relatedness of effector and memory T cells is independent of TCR avidity. B6 2° recipient mice (n=5) were injected with naïve, barcode-labeled CD8$^+$ OT-I cells and subsequently infected i.v. with LM-Q4-OVA. 27 days later, mice were re-challenged with LM-Q4-OVA. Barcode analysis was performed on a ¼ spleen sample obtained by partial splenectomy at day 7 post-infection (effector phase), and on a spleen sample isolated at day 5 after re-challenge (2° expansion) from the same mice. Effector and 2° expansion samples were divided into two halves (sample A and B) that were independently analyzed for barcode content. Barcodes with a P-value <0.005 were considered to be present above background. On average, 250 barcodes were detected per mouse. **(A and B)** Representative 2-D plots of barcode comparisons. Numbers indicate the correlation between signals from sample A and B. **(C)** Correlation analysis of barcodes present in sample A and B. Data from 5 mice analyzed within one experiment are depicted. Data were confirmed in a second experiment (5 mice) performed with LM-A2-OVA, a Listeria strain containing another lower functional avidity variant of the OVA epitope (SAINFEKL).

retroviral transduction. Intra-thymic injection of these genetically labeled thymocytes into unmanipulated recipient mice is then used to create a pool of naïve barcode-labeled T cells. This strategy allows the use of genetic tagging for the analysis of T cell fate without any potential confounding effect of the *in vitro* T cell activation that is used for standard T cell gene modification. By following the progeny of physiological numbers of these naïve barcode-labeled OT-I T cells during systemic or local infection, the lineage relationship of different T cell subsets could be assessed at the single cell level.

The current large-scale analysis of naïve $CD8^+$ T cell fate complements and extends the finding of Stemberger *et al.*, who utilized single cell transfer to assess the formation of $CD8^+$ T cell subsets [14]. While the Stemberger study stands out as the first example of *in vivo* analysis of T cell fate at the single naïve T cell level, a number of issues remained. First, in single cell transfer studies it is difficult to exclude homeostatic proliferation as a confounding factor. Second, the possibility remained that selective differentiation into either effector or memory subsets would not occur during systemic T cell responses -in which inflammatory signals are omnipresent- but would take place upon local infection. Most importantly, the fact that a single naïve T cell can form both effector and memory cells does not necessarily imply that all antigen-specific naïve T cells, including T cells activated by a low avidity stimulus, follow this pathway of differentiation.

Here we provide strong evidence that effector and memory T cells present under different conditions of infection and at different anatomical sites are in all cases derived from the same single naïve T cells. Furthermore, this shared ancestry of effector and memory cells applies both to T cells that are activated by a low avidity and by a high avidity stimulus.

An important technical advance of the current approach for fate mapping is that it allows one to demonstrate that in case two unrelated T cell populations are present within an animal, such populations can readily be distinguished, something that is impossible in single cell transfer systems. Specifically, the lack of kinship of T cells present in two different lymph nodes early after priming (Fig. 8, LN1 vs LN2) forms a crucial control to remove any concerns on homeostatic proliferation of T cells prior to antigen-driven activation, something that would obviously limit the ability to visualize a difference in ancestry of different T cell subsets.

The difference in ancestry of T cell populations residing in different lymph nodes early after infection forms a very strong contrast to the shared ancestry of all other T cell populations examined (Fig. 8). Specifically, 1) Effector and memory T cells are progeny of the same naïve T cells, both when memory is defined by long-term persistence and when defined by capacity for secondary expansion; 2) Effector and memory T cells are progeny of the same naïve T cells, both in systemic and local infection models, and independent of the anatomical site in which they reside and 3)

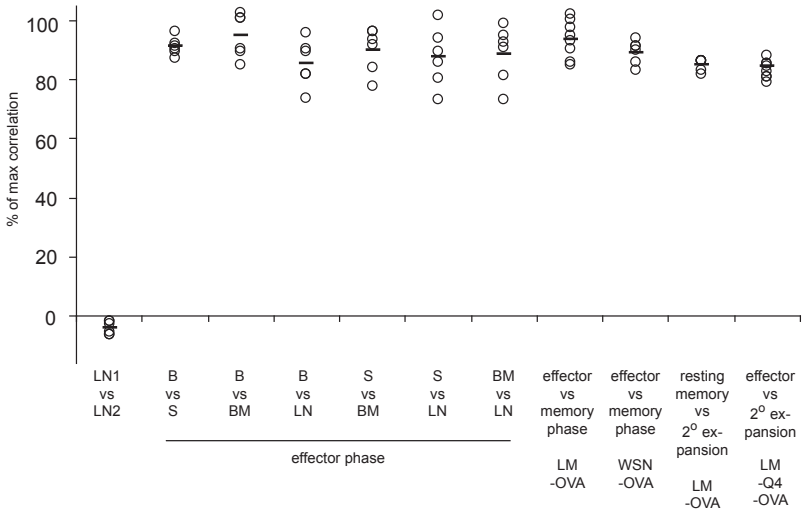

Figure 8. Relatedness of different T cell subsets. Results from barcoding experiments in Fig. 2-7 depicted as the percentage of maximal attainable correlation. 100% reflects the mean correlation of all intra-sample correlations for each individual experiment. 0% reflects the mean correlation of all 'between mice' comparisons for each individual experiment. (Note that the average correlation of two sampling controls forms a reasonable estimate and possibly a slight overestimate of the maximal attainable correlation in case the two cell populations would be fully related, Figure S4B). From the effector vs memory phase comparison during LM-OVA infection, only the effector blood vs memory blood comparison is depicted. Circles represent correlations within individual mice, bars indicate group averages. B=blood; S=spleen; BM=bone marrow; LN=lymph nodes.

Effector and memory T cells are progeny of the same naïve T cells in T cell responses of different functional avidities (Fig. 8).

These data argue against a model in which effector or memory fate is imprinted by distinct APC-derived signals delivered during initial priming. Likewise, a model assuming disparate fates for naïve T cells that are primed early or late during infection is not supported by the data. Instead, the current data indicate that under a variety of conditions the dominant pathway of $CD8^+$ T cell differentiation is 'one naïve cell - multiple fates'.

MATERIALS AND METHODS

Mice. $CD45.1^+$ and $CD45.2^+$ C57BL/6 (B6), as well as $CD45.1^+$ and $CD45.2^+$ TCR-transgenic OT-I and Limited (Ltd) mice were bred and housed in the animal department of the Netherlands Cancer Institute (NKI). All animal experiments were approved by the Experimental Animal Committee of the NKI.

Retroviral transductions. Total thymocytes isolated from 4-8 weeks old $CD45.1^+$ OT-I donor mice were transduced by spin-infection (90min. 2000rpm) in the presence

of 10ng/ml recombinant murine IL-7 (Peprotech) and retroviral supernatant that had been incubated with 10µg/ml DOTAP (Roche). Retroviral supernatants containing the barcode-library [21] were generated as described [30] and diluted prior to use to reach a transduction efficiency of approximately 10%. 4h after transduction, thymocytes were washed and cultured o/n in culture medium (IMDM/ 8%FCS/ 100U/ml penicillin/ 100µg/ml streptomycin/ $5x10^{-6}$ M 2-ME) supplemented with 10ng/ml IL-7. Ltd cells were isolated from spleen and lymph nodes, activated for 2 days in culture medium containing 2 µg/ml Concanavalin A (Calbiochem) and 1 ng/ml IL-7, and subsequently transduced by spin infection in the presence of 10ng/ml recombinant murine IL-7 and retroviral supernatant. Transduced Ltd cells were sorted on the basis of GFP expression and absence of staining with anti-B220 and anti-CD4 mAb.

Intra-thymic injection of transduced thymocytes. One day after transduction, thymocytes were purified using Lympholite (Cedarlane) and GFP^+ cells were sorted by FACS. Sorted cells were injected intra-thymically into 4-6 weeks old primary (1°) recipient B6 mice. 1° recipients were sedated i.p. with azepromazine (1µg/g body weight, Ceva Sante Animale) and anesthesized i.p. with a mixture of midazolam (7.5µg/g body weight; Roche), fentanyl citrate (0.47µg/g body weight; VetaPharma) and fluanisone (15µg/g body weight; VetaPharma). For pain relief, carprofen (5µg/g body weight; Pfizer) was given s.c. The fur overlying the thymus was disinfected with iodine and a small (max 1cm) longitudinal incision was made in the skin along the sternum. The salivary gland was pushed aside and each thymic lobe was injected with 25µl cell suspension. Thereafter, the skin was closed with 2-3 stitches. Each mouse received $0.5\text{-}1x10^6$ sorted, GFP^+ thymocytes.

Isolation, purification and transfer of naïve OT-I T cells. Barcode-labeled OT-I cells were isolated ~3 weeks after intra-thymic injections from spleen and LNs (cervical, axillary, brachial, mesenteric, inguinal, lumbar) of 1° recipient mice. $CD8^+$ cells were enriched by negative selection (Mouse CD8 T Lymphocyte Enrichment Set; BD Biosciences). Enriched $CD8^+$ cells were pooled from several 1° recipients, and then analyzed by flow cytometry and/or transferred i.v. into several 8-10 weeks old B6 2° recipients (~1000 barcode-labeled cells / 2° recipient). This pooling and distribution approach guarantees that each 2° recipient receives an equal number of barcode-labeled T cells. In addition, it serves as an important control to ensure that the technology allows the detection of differences in kinship (see: 'between mice' controls). In all experiments, the number of transferred barcode-labeled cells as indicated in the legends is based on the analysis of very low percentages (~0.01%) of GFP^+ T cells and therefore an approximation. On average, $\sim 2x10^3$ barcode-labeled $CD8^+$ T cells were isolated per 1° recipient. Non-barcode-labeled OT-I cells were isolated from spleen and LNs of OT-I mice.

Listeria and influenza A infections and tumor challenge. 2° recipient mice were infected i.v. with $2.5x10^4$ (1° infection) or $2.5x10^5$ CFU (2° infection) of a *Listeria monocytogenes* strain expressing ovalbumin (LM-OVA) [31]. Infection with

LM-Q4-OVA, a *Listeria monocytogenes* strain expressing the SIIQFEKL sequence [28] occurred at $2.5x10^3$ (1° infection) or $2.5x10^5$ CFU (2° infection) i.v. Alternatively, mice were anesthesized with ether and infected intra-nasally (i.n.) with 10^3 PFU of the recombinant influenza A/WSN/33 strain (WSN-OVA) that expresses the H-$2K^b$-restricted $OVA_{257-264}$ epitope [32], followed by s.c. injection of 10^7 EL4-OVA thymoma cells the next day [30].

Recovery and *in vitro* expansion of transferred cells. Transferred OT-I or Ltd cells were recovered from spleen, BM (femur, tibia, iliac crest), LN (cervical, axillary, brachial, mesenteric, inguinal, lumbar) and blood. Blood was either drawn from the tail vein, cheek (~300µl; in experiments in which mice were kept for longitudinal analysis), or heart (~800µl; after sacrificing the mice). To recover barcode-labeled spleen cells from living mice, partial splenectomy was performed. Recovered cells were either used for flow cytometry or for barcode analysis. To allow for efficient barcode recovery, spleen, LN and BM samples were enriched for $V\alpha2^+$ cells by MACS (Miltenyi Biotec; anti-PE Microbeads). Where indicated, cells were expanded *in vitro* for 3-4 days prior to Vα2 enrichment. All samples were divided into two equal parts (sample A and B) from which barcodes were recovered independently. This division was performed after Vα2 enrichment or, in case *in vitro* expansion was performed, prior to *in vitro* expansion.

Partial splenectomy. Mice were anesthesized with isoflurane and the skin overlying the spleen was shaved and disinfected. A <1cm incision was made in the skin and peritoneum. ¼ of the spleen was resected and the wound on the spleen was closed with Histoacryl ® Topical Skin Adhesive (TissueSeal). Thereafter, peritoneum and skin were closed with ~3 stitches and buprenorphine (0.1µg/g body weight; Schering-Plough) was given as pain relief.

Flow cytometry. Cell surface stainings were performed with the following reagents: Vα2-PE (B20.1), CD62L-PE (MEL-14), CD45.1-PE (A20), CD43-PE (1B11), SA-PE-Cy7, CD4-APC (L3T4), CD8α-APC-Cy7 (53-6.7), KLRG-1-biotin (2F1), CD4-APC (RM4-5), B220-APC (RA3-6B2) (BD Biosciences), CD45.1-APC (A20; Southern Biotech), CD127-PE (A7R34), CD44-Pe-Cy7 (IM7), CD127-APC (A7R34) and CD45.2-APC (104) (eBiosciences). Dead cells were excluded by DAPI staining. Analyses were performed on a $CyAn_{ADP}$ (Summit v4.3; Beckman Coulter). Cell sorting was carried out on a FACSAria Cell Sorter (Diva 5.0.1; BD Biosciences) or MoFlo Highspeed Sorter (Summit v3.1; Beckman Coulter).

Barcode recovery, microarray hybridizations and data analysis. Genomic DNA was isolated and barcode sequences were amplified by nested PCR as described [21]. PCR products were purified, labeled with Cyanine-3 or Cyanine-5 and co-hybridized to the barcode microarray. Fluorescence signals were quantified and normalized, and duplicates were averaged. Barcodes present above background were defined for each sample, based on the probability a signal differed from a calculated background distribution [21]. The rectangular divider in 2-D barcode plots indicates which barcodes are present above background, based on the indicated probability (see legends). Note that rather than fixing the absolute position of dividers in terms of intensity, it is

the statistical probability of barcode presence that is kept constant for all samples in a given experiment. The Pearson correlation between fluorescent signals of barcodes present within two samples was calculated. Calculations included a randomly drawn fraction of barcodes that were not present in a given sample (reference population), as described previously [21]. Note that the use of such a reference population within the calculations restricts correlation values to a range of 1 (full kinship) to approximately -0.5 (lack of kinship).

Online supplemental material. Fig. S1 depicts different models for the formation of effector and memory T cell subsets. Fig. S2 shows that activated barcode-labeled and unmanipulated OT-I T cells have a similar phenotype. Fig. S3 depicts the relatedness of CD127^{lo}, KLRG-1^{hi} and CD127^{hi}, KLRG-1^{lo} CD8^{+} T cells. Fig. S4 shows how barcode analysis is interpreted when barcode sampling is suboptimal. Fig. S5 indicates that resting memory T cells present in different lymphoid organs are largely derived from the same naïve T cells. Fig. S6 shows that effector and memory T cells in an oligoclonal antigen-specific T cell response are related.

Abbreviations used. 2-D, two dimensional; Ltd, Limited.

ACKNOWLEDGMENTS

We would like to thank Anita Pfauth and Frank van Diepen for cell sorting, Wim Brugman for microarray production, Dirk Busch (Munich, Germany) for providing LM-OVA and Claudio Nunes-Alves and Margarida Correia-Neves (Braga, Portugal) for Ltd mice. We thank Loes Rijswijk and Ton Schrauwers for demonstrating the intra-thymic injection and partial splenectomy, and Sjaak Greven, Maaike Voetêl and Henk Grimminck for animal care and cheek bleedings. We also thank Gavin Bendle, Andrew Kaiser and Shalin Naik for critically reading the manuscript. M.B. was supported by grant U54 AI081680. The authors have no conflicting financial interests.

REFERENCES

1. Williams, M. A. & Bevan, M. J. Effector and memory CTL differentiation. *Annu Rev Immunol* 25, 171-192 (2007).
2. Kaech, S. M. & Ahmed, R. Memory CD8+ T cell differentiation: initial antigen encounter triggers a developmental program in naive cells. *Nat. Immunol.* 2, 415-422 (2001).
3. van Stipdonk, M. J. *et al.* Dynamic programming of CD8+ T lymphocyte responses. *Nat Immunol* 4, 361-365 (2003).
4. Masopust, D., Kaech, S. M., Wherry, E. J. & Ahmed, R. The role of programming in memory T-cell development. *Curr. Opin Immunol* 16, 217-225 (2004).
5. Bannard, O., Kraman, M. & Fearon, D. T. Secondary replicative function of CD8+ T cells that had developed an effector phenotype. *Science* 323, 505-509 (2009).
6. Chang, J. T. *et al.* Asymmetric T lymphocyte division in the initiation of adaptive immune responses. *Science* 315, 1687-1691 (2007).
7. Ahmed, R. & Gray, D. Immunological memory and protective immunity: understanding their relation. *Science* 272, 54-60 (1996).
8. Badovinac, V. P., Porter, B. B. & Harty, J. T. CD8+ T cell contraction is controlled by early inflammation. *Nat. Immunol.* 5, 809-817 (2004).
9. Joshi, N. S. *et al.* Inflammation directs memory precursor and short-lived effector CD8(+) T cell fates via the graded expres-

sion of T-bet transcription factor. *Immunity* 27, 281-295 (2007).

10. Sarkar, S. *et al.* Functional and genomic profiling of effector CD8 T cell subsets with distinct memory fates. *J. Exp Med* 205, 625-640 (2008).
11. van Faassen, H. *et al.* Reducing the stimulation of CD8+ T cells during infection with intracellular bacteria promotes differentiation primarily into a central (CD62LhighCD44high) subset. *J. Immunol.* 174, 5341-5350 (2005).
12. D'Souza, W. N. & Hedrick, S. M. Cutting edge: latecomer CD8 T cells are imprinted with a unique differentiation program. *J. Immunol* 177, 777-781 (2006).
13. Quigley, M., Huang, X. & Yang, Y. Extent of stimulation controls the formation of memory CD8 T cells. *J. Immunol* 179, 5768-5777 (2007).
14. Stemberger, C. *et al.* A single naive CD8+ T cell precursor can develop into diverse effector and memory subsets. *Immunity* 27, 985-997 (2007).
15. Jameson, S. C. & Masopust, D. Diversity in T cell memory: an embarrassment of riches. *Immunity* 31, 859-871 (2009).
16. Harrington, L. E., Janowski, K. M., Oliver, J. R., Zajac, A. J. & Weaver, C. T. Memory CD4 T cells emerge from effector T-cell progenitors. *Nature* 452, 356-360 (2008).
17. Kedzierska, K., Turner, S. J. & Doherty, P. C. Conserved T cell receptor usage in primary and recall responses to an immunodominant influenza virus nucleoprotein epitope. *Proc Natl Acad Sci U S A* 101, 4942-4947 (2004).
18. Maryanski, J. L., Jongeneel, C. V., Bucher, P., Casanova, J. L. & Walker, P. R. Single-cell PCR analysis of TCR repertoires selected by antigen in vivo: a high magnitude CD8 response is comprised of very few clones. *Immunity* 4, 47-55 (1996).
19. Obar, J. J., Khanna, K. M. & Lefrancois, L. Endogenous naive CD8+ T cell precursor frequency regulates primary and memory responses to infection. *Immunity* 28, 859-869 (2008).
20. Stemberger, C., Neuenhahn, M., Buchholz, V. R. & Busch, D. H. Origin of CD8+ effector and memory T cell subsets. *Cell Mol. Immunol.* 4, 399-405 (2007).
21. Schepers, K. *et al.* Dissecting T cell lineage relationships by cellular barcoding. *J Exp Med* 205, 2309-2318 (2008).
22. Egerton, M., Scollay, R. & Shortman, K. Kinetics of mature T-cell development in the thymus. *Proc Natl Acad Sci U S A* 87, 2579-2582 (1990).
23. Kaech, S. M. *et al.* Selective expression of the interleukin 7 receptor identifies effector CD8 T cells that give rise to long-lived memory cells. *Nat Immunol* 4, 1191-1198 (2003).
24. Feuerer, M. *et al.* Bone marrow as a priming site for T-cell responses to blood-borne antigen. *Nat. Med.* 9, 1151-1157 (2003).
25. Palendira, U. *et al.* Selective accumulation of virus-specific CD8+ T cells with unique homing phenotype within the human bone marrow. *Blood* 112, 3293-3302 (2008).
26. Correia-Neves, M., Waltzinger, C., Mathis, D. & Benoist, C. The shaping of the T cell repertoire. *Immunity* 14, 21-32 (2001).
27. van Heijst, J. W. *et al.* Recruitment of antigen-specific CD8+ T cells in response to infection is markedly efficient. *Science* 325, 1265-1269 (2009).
28. Zehn, D., Lee, S. Y. & Bevan, M. J. Complete but curtailed T-cell response to very low-affinity antigen. *Nature* 458, 211-214 (2009).
29. Reiner, S. L., Sallusto, F. & Lanzavecchia, A. Division of labor with a workforce of one: challenges in specifying effector and memory T cell fate. *Science* 317, 622-625 (2007).
30. Kessels, H. W., Wolkers, M. C., van den Boom, M. D., van der Valk, M. A. & Schumacher, T. N. Immunotherapy through TCR gene transfer. *Nat Immunol* 2, 957-961 (2001).
31. Pope, C. *et al.* Organ-specific regulation of the CD8 T cell response to Listeria monocytogenes infection. *J. Immunol* 166, 3402-3409 (2001).
32. Topham, D. J., Castrucci, M. R., Wingo, F. S., Belz, G. T. & Doherty, P. C. The role of antigen in the localization of naive, acutely activated, and memory CD8(+) T cells to the lung during influenza pneumonia. *J. Immunol* 167, 6983-6990 (2001).

SUPPLEMENTARY FIGURES

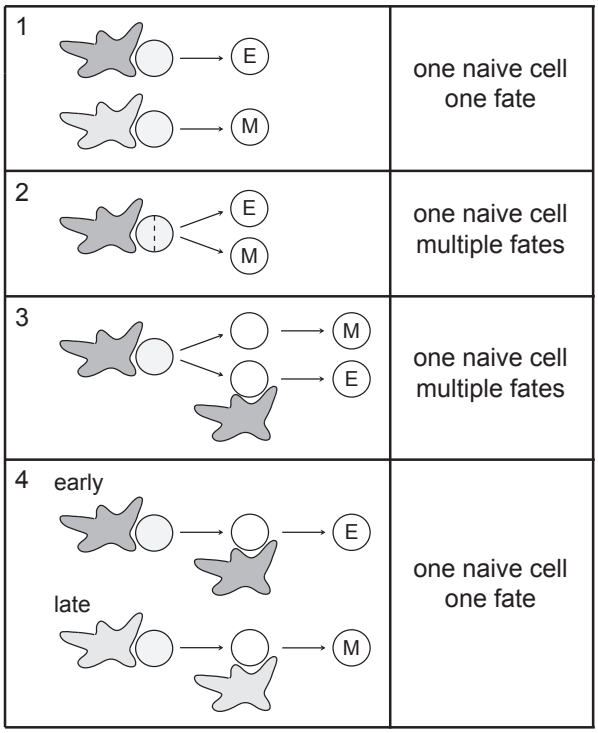

Figure S1. Models predicting effector and memory T cell lineage relationship. Schematic representation of four of the proposed models describing the lineage relationship of effector (E) and memory (M) T cells. Dendritic cells with different stimulating capacities are depicted in light and dark blue. Naïve T cells are drawn in pink. Note that other (variations on these) models have been proposed, but the fundamental distinguishing feature of the different models for the current study is whether they predict that single naïve T cells produce single or multiple subsets.

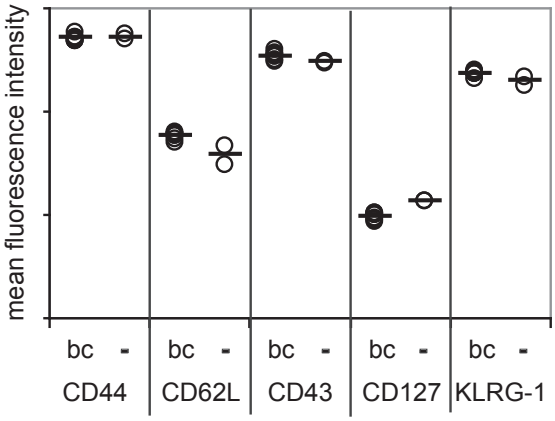

Figure S2. Phenotypic characterization of barcode-labeled and unlabeled OT-I T cells after LM-OVA infection. CD45.2$^+$ B6 2° recipient mice were injected with naïve, barcode-labeled (bc) CD8$^+$CD45.1$^+$ OT-I cells or unmanipulated (-) CD8$^+$CD45.1$^+$ OT-I cells (n=7 and n=2 respectively). Mice were subsequently infected i.v. with LM-OVA. At day 7 post-infection, blood cells were stained for the indicated surface markers and analyzed by flow cytometry. Circles represent individual mice, bars indicate group averages. Data are representative of two independent experiments.

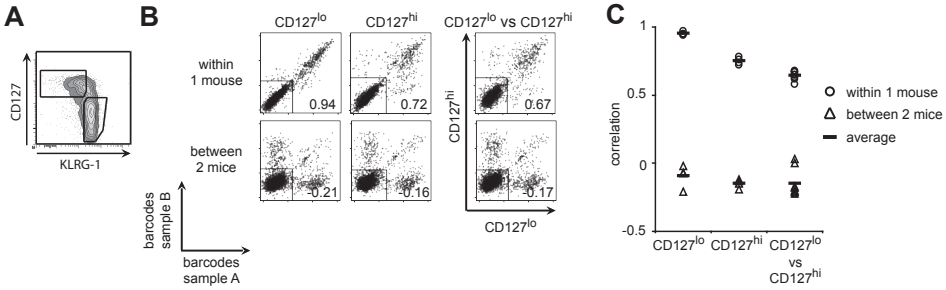

Figure S3. CD127^{lo}KLRG-1^{hi} and CD127^{hi}KLRG-1^{lo} are related. CD45.2$^+$ B6 2° recipient mice (n=4) were injected with naïve, barcode-labeled CD8$^+$CD45.1$^+$ OT-I cells and subsequently infected i.v. with LM-OVA. 10 days after infection, spleen and lymph node cells were isolated, enriched for CD8$^+$ cells and sorted into CD8$^+$, CD45.1$^+$, CD127^{lo}KLRG-1^{hi} and CD8$^+$, CD45.1$^+$, CD127^{hi}KLRG-1^{lo} cells. Data are derived from 4 mice, analyzed within one experiment. **(A)** Flow cytometric sorting plot, gated on CD8$^+$CD45.1$^+$GFP$^+$ cells; sorting gates are indicated. **(B and C)** Both sorted populations, abbreviated as CD127^{lo} and CD127^{hi} were divided into two halves (sample A and B) that were independently analyzed for barcode content. CD127^{hi} half-samples were separately expanded for 3 days *in vitro* in the presence of OVA$_{(257-264)}$-loaded splenic DCs at a T:DC ratio of 10:1 prior to barcode analysis. Barcodes with a P-value <0.0001 were considered to be present above background. On average, 430 different barcodes were detected per mouse. **(B)** Representative 2-D plots of barcode comparisons. Numbers indicate the correlation between signals from sample A and B. **(C)** Correlation analysis of barcodes present in sample A and B. Data from 4 mice analyzed within one experiment are depicted.

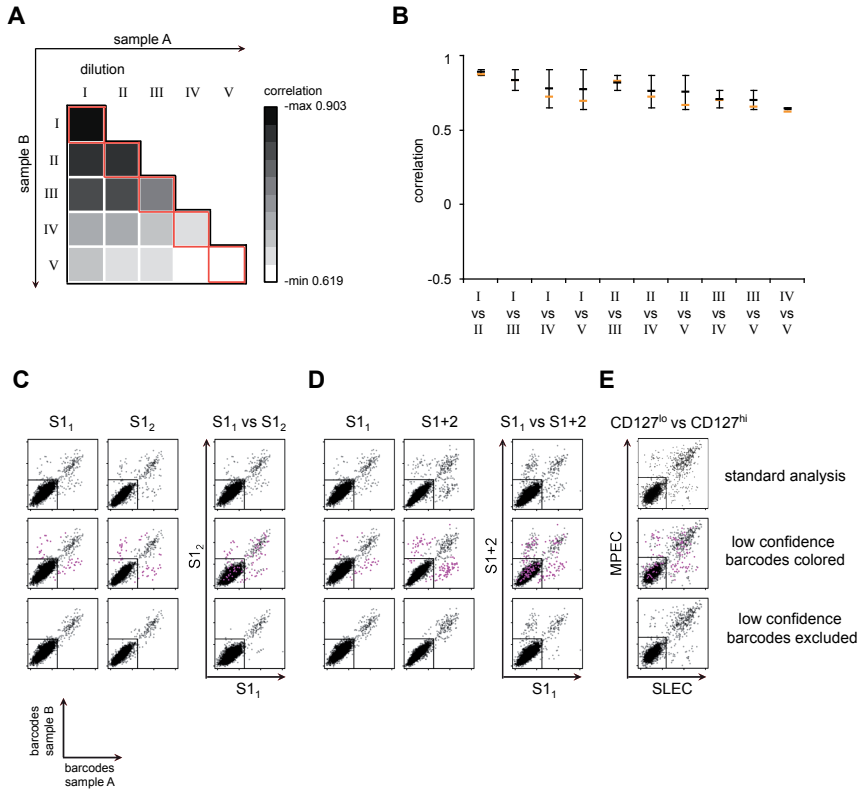

Figure S4. Barcode data analysis in case of suboptimal sampling. CD45.2$^+$ B6 2° recipient mice were injected with naïve, barcode-labeled CD8$^+$CD45.1$^+$ OT-I cells and subsequently received an i.v. infection with LM-OVA at day 0 and day 30. Five days later, genomic DNA was isolated from the spleen of two 2° recipient mice. **(A and B)** To determine how suboptimal sampling would affect correlation analyses on cell populations of which one is sampled less efficiently than the other, 1.5% of the spleen 1 DNA was diluted in 4 steps of 2-fold dilutions (dilutions I-V with I being the highest and V the lowest concentration). For each dilution, 2 samples were independently analyzed for barcode content. Barcodes with a P-value of <0.0001 were considered to be present above background. **(A)** The correlation of intra-dilution (red squares) and inter-dilution comparisons is depicted in a heat-map. **(B)** The correlation of different inter-dilution comparisons (orange horizontal bars) is depicted in relation to the correlation of the two corresponding intra-dilution comparisons and their mean correlation (highest, lowest and middle black horizontal bar respectively). Note that when correlation analyses are performed for two samples that have substantially different intra-sample correlation values (e.g. I vs IV, I vs V, II vs V), this value approximates that of the poorest intra-sample comparison. **(C and D)** To test whether the exclusion of barcodes detected with low confidence would facilitate the detection of barcodes that are differentially present, part of DNA of spleen 1 was divided in two samples ($S1_1$ and $S1_2$) and part of spleen 1 DNA was mixed with part of spleen 2 DNA (S1+2). All three samples were diluted and split in 2 halves (sample A + B) for independent barcode analysis. Standard barcode analysis is shown in the first row. To statistically determine which barcodes are likely to be outliers (i.e. detected with low confidence), a linear model was fitted through the barcode signals from the intra-sample comparisons and the studentized residuals were calculated per barcode. Barcodes with residuals ≥3 (97.5% chance of being an outlier) in the intra-sample comparisons were either colored (second row) or excluded (third row). Barcodes with a P-value of <0.0005 were considered to be present above background. **(C)** Barcode comparison between two related samples ($S1_1$ vs $S1_2$) in relation to the corresponding intra-sample comparisons. **(D)** Barcode comparison between two partially unrelated samples ($S1_1$ vs S1+2) in relation to the corresponding intra-sample comparisons. **(E)** Barcode comparison between CD127^{lo}KLRG-1^{hi} (CD127^{lo}) and CD127^{hi}KLRG-1^{lo} (CD127^{hi}) from the experiment shown in Fig. S3. Standard barcode analysis is shown in the first row. Barcodes with residuals ≥3 in the intra-sample comparisons were either colored (second row) or excluded (third row) as described for C and D.

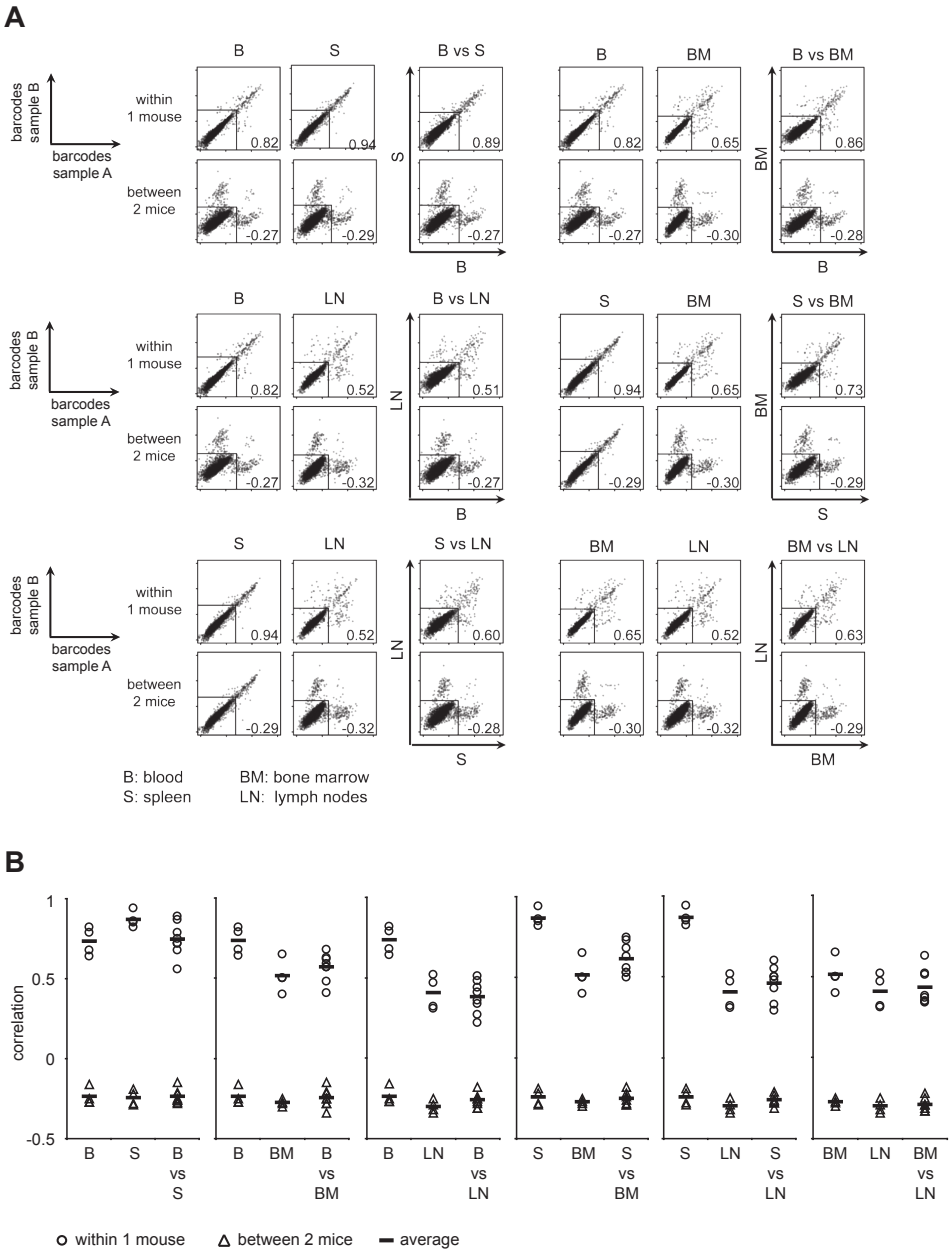

Figure S5. Memory CD8⁺ T cells present in different organs harbor the same set of barcodes. CD45.2⁺ B6 2° recipient mice (n=4) were injected with naïve, barcode-labeled CD8⁺CD45.1⁺ OT-I cells and subsequently received an i.v. infection with LM-OVA. Barcode analysis was performed on blood, spleen, BM and LN cells isolated at day 28 post-infection. All samples were divided into two halves (sample A and B) that were independently analyzed for barcode content. Barcode comparisons are made between sample A and B taken from the same mouse ('within 1 mouse') or ▷

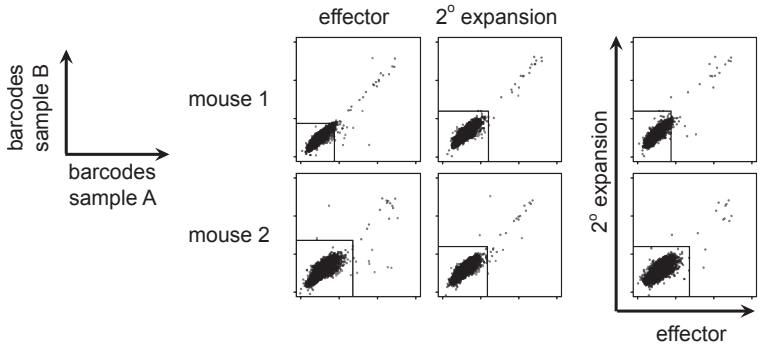

Figure S6. Relatedness of effector and memory T cells in an oligoclonal antigen-specific T cell response. B6 2° recipient mice were injected with barcode-labeled Ltd cells and subsequently infected i.v. with LM-OVA. 27 days later, mice were re-challenged with LM-OVA. Barcode analysis was performed on a 250-300µl blood sample drawn at day 8 post-infection (effector phase), and on spleen isolated at day 5 after re-challenge (2° expansion) from the same mice. Blood and spleen samples were divided into two halves (sample A and B) that were independently analyzed for barcode content. Barcodes with a P-value $<1x10^{-8}$ were considered to be present above background. On average, 25 barcodes were detected per mouse. 2-D plots of barcode comparisons are shown for 2 mice within one experiment. All barcodes present in more than 1 mouse were excluded. To limit analysis to barcodes detected with high reliability, barcodes with residuals ≥3 (97.5% chance of being an outlier) in the intra-sample comparisons (depicted in purple in the intra-sample comparisons) were excluded in the inter-sample comparisons, as described for Fig. S3 C and D. Note that this filtering procedure precludes the calculation of correlation values. Data from one experiment are depicted.

▷ from two different mice ('between 2 mice'). Barcodes with a P-value <0.005 were considered to be present above background. **(A)** Representative 2-D plots of barcode comparisons. Numbers indicate the correlation between signals from sample A and B. **(B)** Correlation analysis of barcodes present in sample A and B isolated from blood (B), spleen (S), bone marrow (BM) and lymph nodes (LN). Data from 4 mice analyzed within one experiment are depicted.

6

EFFECTOR AND MEMORY LINEAGE DECISION OCCURS AFTER NAÏVE T CELL PRIMING

Jeroen W.J. van Heijst[1], Carmen Gerlach[1], Silvia Ariotti[1]
and Ton N.M. Schumacher[1]

[1]Division of Immunology, The Netherlands Cancer Institute, Amsterdam, the Netherlands

unpublished

Following pathogen encounter, naïve CD8 T cells give rise to both short-lived effector and long-lived memory cells. At which point during an immune response the progeny of activated T cells commit to either of these lineages remains poorly understood. Here we assessed the developmental potential of recently activated T cells, by labeling the first four daughter cell generations (D1-D4) after infection with unique genetic tags and analyzing their fate in infection-matched recipients. These experiments reveal that the vast majority of D1-D4 cells are still multipotent and give rise to both effector and memory progeny. These data indicate that signals received by downstream progeny are required for commitment to short- or long-lived fate. Lineage commitment is therefore a relatively late event in antigen-specific T cell responses.

6

INTRODUCTION

When a pathogen enters a host, the adaptive immune system is faced with two important tasks. The first task is to recruit as many naïve T cells as possible that have the potential to recognize the invading pathogen[1]. As activation of naïve antigen-specific T cells results in vigorous proliferation[2-4], this warrants the generation of sufficient effector cells to combat the infection. The second task is to ensure that any naïve T cell that was able to recognize the foreign invader, and therefore is of high value to the host, is clonally preserved as memory cell for potential future encounters with the same infectious agent[5]. Thus, the simultaneous generation of both effector and memory cells is required to maintain optimal fitness. At population level, ~90% of expanded antigen-specific T cells die following pathogen clearance, whereas ~10% survive and are maintained long-term. During an immune response, the progeny of activated T cells can therefore adopt two distinct fates, namely they can become short-lived effector cells or long-lived memory cells. Exactly how cells of different longevity are generated during a response is a matter of long-standing debate[6-11].

Over the years, a number of models have been proposed that aim to explain how T cell commitment to either the effector or the memory lineage is regulated. A straightforward explanation would be that different naïve T cells give rise to either effector or memory progeny. In this model, fate could either be predetermined in the naïve T cell, or be determined by the nature of the antigen-presenting cell (APC) or the time of naïve T cell priming[12-15]. However, a study by Stemberger and colleagues in which the fate of single adoptively-transferred CD8 T cells was followed, has demonstrated that a single naïve T cell can give rise to both effector and memory progeny[16]. Furthermore, by monitoring a population of naïve CD8 T cells separated by individual genetic markers, we have recently shown that under a variety of conditions, individual naïve T cells yield both lineages[17]. Thus, naïve T cells (N cells) are not committed, and commitment to effector or memory fate must therefore occur within the daughter cell generations (D cells).

Currently, there are two models describing CD8 T cell differentiation that are compatible with one naïve T cell yielding both effector and memory progeny. However, these models differ greatly in the proposed mechanism controlling fate divergence. The first model suggests that lineage commitment is an early event following antigen encounter. This model proposes that asymmetry during the first T cell division can give rise to two daughter cells with skewed differentiation potential, resulting in the proximal daughter cell giving rise to effector progeny and the distal daughter cell yielding memory progeny (bifurcative differentiation model)[8,18]. The deterministic nature of this model suggests that signals delivered by the priming APC could suffice to allow the simultaneous development of effector and memory cells, which at its most extreme implies that already the first few daughter cell generations would be lineage committed. Alternatively, a second model suggests that lineage commitment is a relatively late event following antigen encounter. This model proposes that

activated T cells differentiate in a stepwise manner, where progression towards short-lived effector fate is controlled by successive stimulation of downstream progeny by antigen or inflammatory signals (decreasing potential model)[19,20]. Despite being stochastic in nature, this model assumes memory fate as a less differentiated (and thus earlier reached) state after activation, and therefore to some extent warrants the generation of memory cells out of each activated naïve T cell. Thus, while it is clear that naïve T cells are uncommitted, it is currently not understood whether lineage commitment during a response occurs early in the first few daughter cell generations or relatively late in more downstream progeny.

In this study, we sought to determine at which point during an immune response the progeny of activated T cells commit to either short- or long-lived fate. To assess whether lineage commitment could be an early event, we labeled the first four daughter cell generations (D1-D4) after infection with unique genetic tags (barcodes)[21], and transferred these labeled D1-D4 cells into infection-matched recipient mice to analyze their fate. Barcode distributions between effector and memory populations revealed that the vast majority of these early daughter cells still displayed uniform potential to yield both short- and long-lived progeny. These data indicate that signals received by downstream progeny are required for commitment to the effector or memory lineage and lineage commitment is therefore a relatively late event in antigen-specific T cell responses.

RESULTS

Monitoring the developmental potential of early daughter cells

To assess lineage commitment of the first few daughter cell generations that arise after naïve CD8 T cell activation, we made use of the property that retroviruses only integrate into actively dividing cells[22]. In theory, by infecting a bulk population of recently activated T cells with a retroviral barcode library at a time point when T cells have undergone a maximum of four divisions, one would expect that only the cycling daughter cells become marked with these barcode sequences. The fact that each virion contains two RNA genomes raises the possibility that both daughter cells of an activated naïve T cell inherit the same barcode. However, both RNA templates appear to be required for the integration of a single DNA provirus[23,24]. In addition, a study in fibroblasts has shown that retroviruses integrate post chromosomal DNA replication, resulting in only one of the two daughters on an infected cell inheriting the provirus[25]. These studies suggest that even if the first daughter T cell generation (D1) would be lineage committed[18], our labeling strategy should reflect this by the integration of different barcode sequences. Therefore, this retroviral barcoding strategy allows the fate of the first four daughter cell generations (D1-D4) to be monitored at the single-cell level.

To study the fate of early daughter cells by retroviral barcoding we adopted an experimental setup that has previously shown fate divergence in the first daughter cell

generation (D1)[18]. To allow barcode labeling, naïve OT-I T cells were initially primed by infection of C57Bl/6 mice with *Listeria monocytogenes* expressing ovalbumin (LM-OVA, Fig. 1A). Then, after 48 hours, activated daughter cells were isolated from spleen and labeled with barcodes in vitro. Four hours later, these labeled cells were transferred into infection-matched recipient mice to allow further effector and memory cell development in vivo. Following isolation of effector and memory populations, microarray analysis of barcodes was used to determine their ancestry.

Analysis of CFSE dilution revealed that 48 hours after LM-OVA infection, OT-I T cells isolated from spleen had either not divided or had divided 1-4 times (Fig. 1B). No T cell division was detected after 24 hours (not shown); indicating that 2 days post infection is the earliest time point at which the developmental potential of early daughter cells can be assessed. Importantly, in vivo T cell activation prior to retroviral transduction at day 2 is essential for barcode-labeling, as only OT-I T cells primed by LM-OVA but not wild-type LM efficiently integrated the barcode retroviruses (Fig. 1C). These data indicate that the use of retroviruses allows the selective marking of the first four daughter cell generations (D1-D4) generated after pathogen infection *in vivo*.

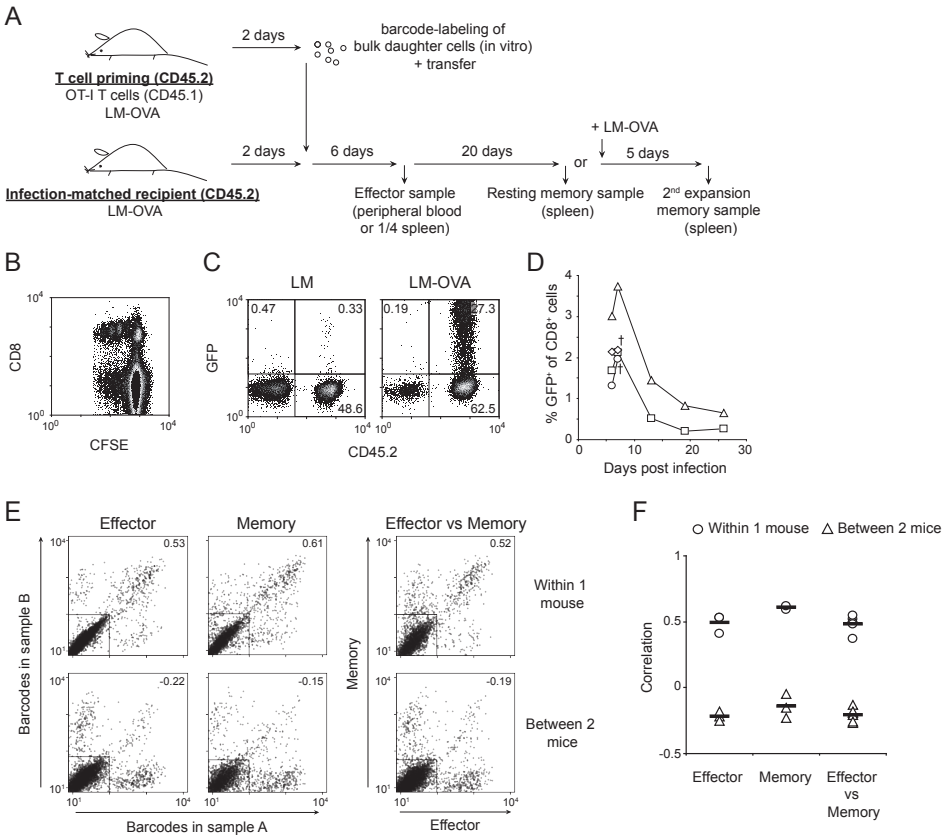

Figure 1. Developmental potential of early daughter cells. (**A**) General set-up of the adoptive transfer experiments. CD45.2 mice received 10^6 CD45.1$^+$ OT-I T cells and were infected with LM-OVA (T cell priming group). Concomitantly, CD45.2 mice were infected with LM-OVA, however without receiving any OT-I T cells (infection-matched recipient group). At day 2 post infection, spleen cells from T cell priming mice were isolated, enriched for CD8$^+$ cells, labeled with barcode retrovirus, and transferred into infection-matched recipient mice. At day 8 and 28, blood and spleen samples were obtained for barcode analysis of effector and memory populations. (**B**) CD45.2 recipients received 10^6 CFSE-labeled CD45.1 OT-I cells and were infected with LM-OVA. Flow cytometry plot, derived from spleen cells at day 2 post infection, is gated on live CD45.1$^+$ cells. (**C**) CD45.1 recipients received 10^6 CD45.2 OT-I T cells and were infected with either wild-type LM or LM-OVA. At day 2 post infection, CD8 enriched spleen cells were infected with barcode retrovirus expressing GFP and cultured for two days. Flow cytometry plots are gated on live Vα2$^+$ CD8$^+$ cells. (**D**) Following transfer of barcode-labeled daughters into infection-matched recipient mice, peripheral blood responses were tracked in time. Plot depicts the responses of four mice, of which two were sacrificed at day 7. (**E**) From infection-matched recipients, a large (~300 µl) blood sample was collected at day 8 to determine barcodes present in the effector population. From the same mice, a spleen sample was obtained at day 28 to determine barcode content of the resting memory population. Effector and memory samples were split into two halves (A and B), on which independent barcode analysis was performed. Representative barcode dot plots are shown. In these plots, each dot represents the fluorescent intensity of one barcode of the library. Rectangular dividers indicate which barcodes are present above background. Values indicate the correlation between barcode signals of sample A and B. (**F**) Correlation analysis of barcodes present in effector and memory cells of either the same or different mice.

Following transduction, CD8-purified splenocytes were transferred into infection-matched recipients and blood responses of barcode-labeled daughters were followed in time. As indicated in Fig. 1D, these responses displayed typical kinetics following acute infection; i.e. the labeled cells expanded and peaked in numbers around day 8, after which the short-lived effector cells died and the long-lived memory cells reached stable numbers around day 28. These data established that, at population level, the barcode-labeled daughters gave rise to both short-lived effector and long-lived memory cells.

To determine the kinship of these early daughter-derived effector and memory cells, a new experiment was conducted during which a large blood sample was collected at day 8 and a spleen sample was obtained at day 28, in order to analyze the barcode content of the short- and long-lived population. Each blood and spleen sample was split into two equal halves (A and B) from which barcodes were independently amplified and compared to each other. This comparison of barcodes recovered from two by definition related samples indicates how well the barcode repertoire is sampled; thereby establishing the maximum correlation that barcodes in any biologically relevant comparison can have (such as barcodes present in effector and memory populations). Likewise, barcode comparisons between two samples obtained from different mice, which are by definition unrelated, indicate the minimum correlation that barcodes from any two biologically relevant samples can have. As indicated by the barcode dot plots in Fig. 1E, barcodes present in sample A and B of the effector and memory populations were recovered reasonably well, having a mean correlation of 0.49 and 0.61 on a scale that ranges from -0.5 (completely unrelated barcodes) to 1 (completely related barcodes, Fig. 1F). Furthermore, barcodes recovered from samples of two different mice had a very low correlation (around -0.2). Interestingly, comparison of effector and memory samples revealed that most barcodes were shared, having a mean correlation of 0.48 (Fig. 1E and F). This suggests that the vast majority of D1-D4 cells is still multipotent and gives rise to both short-lived effector and long-lived memory progeny.

Kinship of primary effector and secondary expanding memory cells

Despite the fact that most barcodes between the effector and memory populations were overlapping, there were also some barcodes that were only present in either the effector or the memory sample. Although this might suggest the presence of early daughters that only gave rise to effector or memory progeny, it is difficult to firmly draw this conclusion, given that the recovery of barcodes present in the effector and memory populations was not complete. As a result, barcodes that appear unique in the effector or memory population could have been truly absent from the other population or, alternatively, could have been present but not detected.

To improve barcode recovery from effector and memory cells, we performed an experiment in which the effector sample was obtained from the spleen by partial splenectomy and the memory sample was obtained after secondary expansion,

a hallmark of memory cells. To this end, recipients of barcode-labeled OT-I daughters underwent surgery at day 8 to remove ¼ of the spleen. Subsequently, at day 28 these mice were rechallenged with LM-OVA and the remaining ¾ of the spleen was isolated 5 days later (see also Fig. 1A). Barcode analysis indicated that both effector and memory populations were efficiently sampled, with mean barcode correlations of 0.77 and 0.91, respectively (Fig. 2C and D). Importantly, barcode comparison between the well-sampled effector and memory populations showed that the majority of barcodes was overlapping, which was reflected by a mean correlation of 0.68 (Fig. 2D). Interestingly, this correlation was slightly lower than the self-self correlative values of the effector and memory comparisons, suggesting that although most effector and memory cells are progeny of the same early daughters, there might be a few clones that are already lineage committed at this early time point. Especially given the near-perfect barcode recovery of the memory population (Fig. 2C), the appearance of effector-unique barcodes, which constitute on average 23% of all recovered barcodes, might suggest that at the time of labeling some daughter cells had already lost memory potential and were destined for terminal effector differentiation.

Developmental potential of early daughter cells defined by CFSE dilution

Although a previous study in fibroblasts has shown that only half of the progeny of an infected cell inherits the proviral integration[25], the presence of two RNA genomes in each virion potentially allows both daughter cells of an activated naïve T cell to inherit the same barcode. Assuming lineage commitment in the first daughter cell generation (D1)[18], this potential double labeling could lead to false-positive kinship

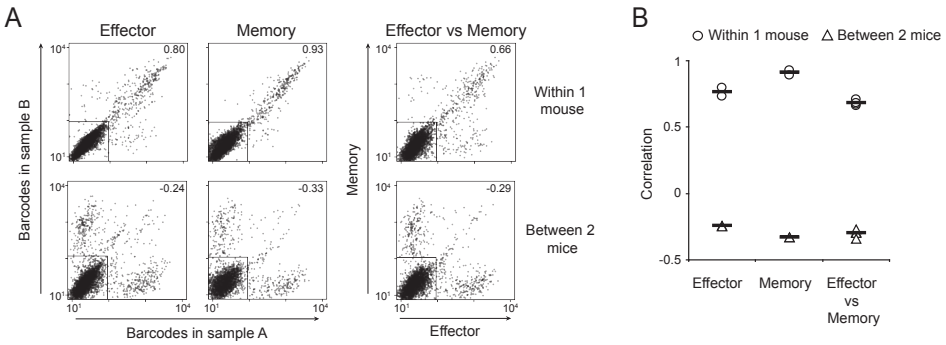

Figure 2. Early daughters give rise to both primary effector and secondary expanding memory cells. (**A**) From infection-matched recipients, a quarter spleen sample was obtained at day 8 to determine barcodes present in the effector population. The same mice were re-challenged with LM-OVA at day 28 and five days later the remaining three-quarter spleen was isolated to determine barcode content of the secondary expanding memory population. Representative barcode dot plots are shown. Values indicate the correlation between barcode signals of sample A and B. (**B**) Correlation analysis of barcodes present in effector and memory cells of either the same or different mice.

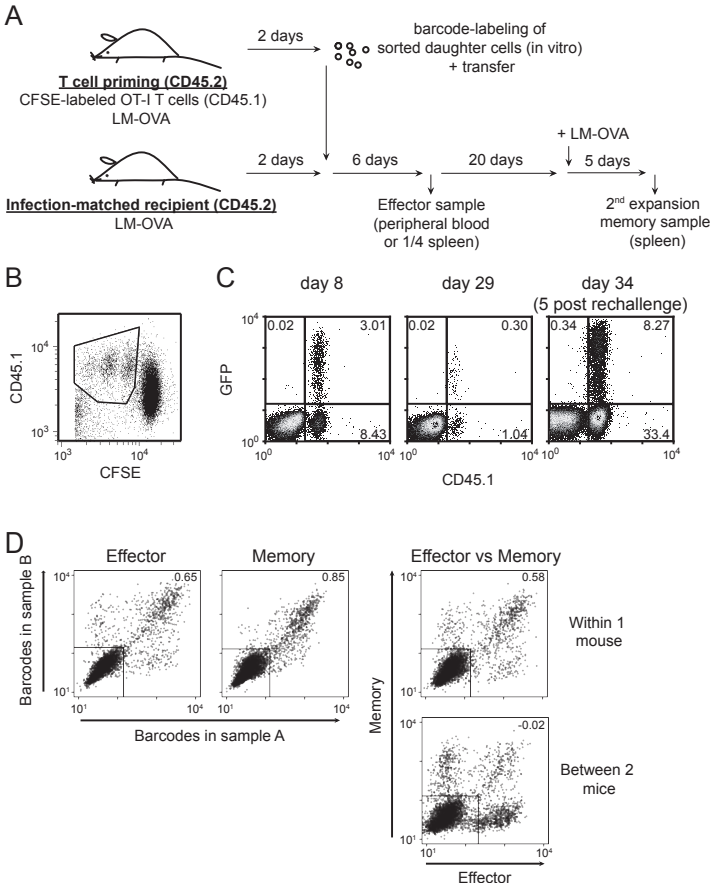

Figure 3. Effector and memory potential of sorted early daughter cells. (**A**) General set-up of the adoptive transfer experiments. CD45.2 mice received 10^6 CFSE-labeled CD45.1$^+$ OT-I T cells and were infected with LM-OVA (T cell priming group). Concomitantly, CD45.2 mice were infected with LM-OVA, however without receiving any OT-I T cells (infection-matched recipient group). At day 2 post infection, spleen cells from T cell priming mice were isolated and OT-I T cells that had divided at least once were sorted by flow cytometry. Then, sorted cells were labeled with barcode retrovirus and transferred into infection-matched recipient mice. At day 8 and 34 (5 days post rechallenge at day 29), blood and spleen samples were obtained for barcode analysis of effector and memory populations. (**B**) Flow cytometric sorting plot, gated on live CD8$^+$ T cells. Sorting gate is indicated. (**C**) Following transfer of sorted barcode-labeled daughters into infection-matched recipient mice, peripheral blood responses were tracked in time. Flow cytometry plots are gated on live CD8$^+$ T cells. (**D**) From infection-matched recipients, a large (~300 µl) blood sample was collected at day 8 to determine barcodes present in the effector population. The same mice were re-challenged with LM-OVA at day 29 and five days later a spleen sample was obtained to determine barcode content of the secondary expanding memory population. Barcode dot plots are shown. Values indicate the correlation between barcode signals of sample A and B. Note that only from one re-challenged mouse an expanding secondary memory population could be recovered and as a result no correlation plot could be generated.

interpretation of D1 cells. To address this issue we made use of CFSE dilution, to label only T cells with barcodes that have divided at least once (Fig. 3A). To this end, mice received CFSE-labeled OT-I T cells and were challenged by LM-OVA. Then, at day 2 post infection, the first 3 daughter cell generations (D1-D3) were sorted and labeled with barcodes in vitro (Fig. 3B). Four hours later, barcode-labeled daughters were transferred into infection-matched recipients to allow further differentiation into effector and memory cells. Monitoring the barcode-labeled daughters in peripheral blood indicated that these responses followed expected kinetics; i.e. the labeled cells expanded, peaked in numbers around day 8, contracted to ~10% of peak numbers around day 28 and showed enhanced expansion upon secondary antigen encounter (Fig. 3C).

From the infection-matched recipients, a large blood sample was obtained at day 8 to analyze barcodes present in the effector population. In addition, a spleen sample was obtained at day 5 post re-challenge to analyze the secondary expanding memory cells. Barcode analysis revealed that both effector and memory populations were quite efficiently sampled, with a barcode correlation of 0.65 and 0.85, respectively (Fig. 3D). Importantly, barcode comparison between the effector and memory populations demonstrated that also in this experimental setup the majority of barcodes was shared, which was reflected by a correlation of 0.58 (Fig. 3D). These data indicate that T cells, of which it was established that they had divided at least once, still retained the capacity to give rise to both effector and memory progeny. Although this behavior might be characteristic for the majority of early daughter cells, these data cannot rule out commitment of a minority of T cell clones at this early time point.

DISCUSSION

In response to infection, activated naïve T cells give rise to both short-lived effector and long-lived memory progeny. In this study, we have addressed the question at which point the progeny of activated T cells commit to the effector or memory lineage, and specifically whether an asymmetry in the first cell division could underlie this lineage decision. By labeling the first four daughter cell generations (D1-D4) that arise after infection with unique genetic tags and transferring these labeled daughters into infection-matched recipients, we were able to assess their developmental potential. These experiments revealed that the vast majority of early daughter cells were still able to yield both effector and memory progeny. A similar outcome was found, both when early daughters were labeled as a bulk activated population as well as when early daughters were labeled after CFSE-based sorting. These results indicate that the decision between short- and long-lived fate is regulated by successive stimulation of downstream progeny, suggesting that lineage commitment is a relatively late event following antigen encounter.

How can the choice between short-lived effector and long-lived memory fate then become established? A general picture that is emerging from most literature is that

continued or stronger stimulation drives cells into terminal effector differentiation, whereas more limited signaling favors the generation of memory cells (referred to as the decreasing potential model[19,20]). This stimulation typically involves to the combined effects of antigen, costimulation and cytokine signaling. Several lines of evidence indicate that when inflammation increases, this favors the generation of effector cells. For instance, sustained exposure to the pro-inflammatory cytokine IL-12 drives responding CD8 T cells into an effector phenotype[26], whereas IL-12 deficiency markedly increases memory cell generation[27,28]. Along the same note, IFN-γ is critically involved in driving successful clonal expansion and up-regulation of effector functions[29,30].

In contrast, when inflammation is restrained, this favors the generation of memory cells. For instance, when pathogen infection is terminated at a very early time point, the total number of memory cells generated remains unaltered, while effector cell numbers decrease dramatically[26,31]. Similarly, when mice are immunized by peptide-loaded dendritic cells in the absence of overt inflammation, responding CD8 T cells rapidly adopt a memory phenotype[26,32]. Further support for the notion that minimal stimulation favors memory development comes from studies on T cell homeostasis, which reported that as naïve T cells respond to lymphopenic environments, they undergo a slow homeostatic proliferation during which they progressively acquire phenotypic and functional characteristics of antigen-induced memory cells[33-35]. Interestingly, these homeostatic proliferation-induced memory cells can be equally effective at mediating protective immunity as antigen-induced "true" memory cells[36].

Another remarkable feature of memory T cell differentiation in response to antigen encounter is that it never seems to fail[10]. Both in settings with very high antigen loads and strong inflammatory signals (such as present during infection with highly virulent pathogens) as well as in settings with a relatively low degree of inflammation (such as during protein or dendritic cell immunizations), memory cells are generated[26,31]. In other words, memory cells might be generated according to a default developmental pathway that is entered as soon as a naïve T cells get activated and start to divide[37]. This observation points out a key conflict in the decreasing potential model, namely its stochastic nature. If continued stimulation selectively drives effector differentiation, how could it then be avoided that under high stimulatory conditions not all cells develop into short-lived effector cells and leave no memory cells behind? One potential explanation could be that the required level of stimulation to convert all memory precursors into short-lived effector cells is simply never reached during an immune response, because of intrinsic limitations in the availability of cytokines or APCs[12,13,38]. However, it remains difficult to reconcile a model based solely on stochastic mechanisms with the observation that the fraction of memory precursors at the peak of the primary response is more or less constant (~10%).

Intuitively, any faithful model that explains decisions between short-lived effector and long-lived memory fate should accompany a deterministic component that on one hand preserves the memory lineage, while on the other hand maintains the proper

flexibility to adjust effector cell numbers to the severity of infection. Even though a potential asymmetric division of the activated naïve T cell does not appear to lead to an immediate separation in T cell fate, it remains possible that unequal segregation of certain proteins or genetic factors renders the two daughter cells with varying susceptibility for additional stimuli at later time points. Alternatively, it could be that initial T cell divisions are symmetric, but asymmetry occurs as soon as downstream progeny have accumulated sufficient additional signaling. In fact, one might speculate that all divisions at which lineage commitment occurs are asymmetric, followed again by symmetric divisions of committed progeny to yield sufficient effector cells. For now, such models that combine features of bifurcative differentiation and decreasing potential are based on theoretical reasoning, and it remains to be experimentally determined at what point the progeny of activated T cells ultimately lose their long-lived potential as well as what factors might contribute to determining the underlying susceptibility for this event.

MATERIALS AND METHODS

Mice. C57BL/6 (B6), B6 CD45.1, OT-I T cell receptor transgenic and OT-I CD45.1 mice were bred in the animal facility of the Netherlands Cancer Institute. Mice were maintained under specific pathogen-free conditions. All experiments were performed according to institutional and national guidelines, and were approved by the Experimental Animal Committee of the Netherlands Cancer Institute.

Retroviral transduction. Retroviral supernatants were generated using Phoenix-E packaging cells as described[39] and stored at -80°C. To generate barcode-labeled daughter cells by retroviral transduction, recipients of either unmanipulated or CFSE-labeled OT-I T cells were infected with LM-OVA. After 48 hours, spleens were harvested and CD8 T cells were enriched either by magnetic bead separation (BD IMag CD8 enrichment kit), or by flow cytometric sorting based on CFSE-dilution. In case of sorting, cells were labeled by anti-CD8α-PE-Cy7 (BD, clone 53.6-7) and anti-CD45.1-APC (Southern Biotech, clone A20), and sorted on a FACSAria (BD). Purified or sorted cells were transduced with retroviral supernatant by spin infection as described[39]. Following spin infection, cells were cultured for an additional 2.5 h in retroviral supernatant. Then, cells were washed in HBSS (Invitrogen) and injected intravenously into infection-matched recipients. In some experiments, cells were cultured for two days to determine the transduction efficiency in IMDM medium (Invitrogen) supplemented with 8% heat-inactivated fetal calf serum and 100 U/ml penicillin + 100 μg/ml streptomycin (Roche), in the presence of 20 U/ml IL-2 (Chiron) and 10 ng/ml IL-7 (Preprotech). Cells were stained with anti-Vα2-PE (BD, clone B20.1), anti-CD8α-PerCP-Cy5.5 (BD, clone 53.6-7) and anti-CD45.2-APC (eBioscience, clone 104), and analyzed by flow cytometry on a CyAnADP (Beckman Coulter). Analysis was performed using Summit V4.3 software (Beckman Coulter).

Bacterial infections. Wild-type *Listeria monocytogenes* (LM) and *Listeria monocytogenes* that expresses a secreted form of OVA (LM-OVA)[40] were grown in

brain heart infusion broth (BD) to an OD_{600} of 0.1. For infections, mice were injected intravenously with 10^4 colony-forming units (CFU) LM or $2.5x10^4$ CFU LM-OVA for primary challenge and $2.5x10^5$ CFU LM-OVA for secondary challenge in HBSS. *Listeria* doses were confirmed by plating dilutions on brain heart infusion agar (BD).

Quantification and purification of barcode-labeled T cells. To quantify barcode-labeled T cells in peripheral blood samples, erythrocytes were lysed by ammonium chloride treatment and cells were stained with anti-CD8α-PE (BD, clone 53-6.7) and anti-CD45.1-APC, and analyzed by flow cytometry on a FACSCalibur (BD). To purify barcode-labeled T cells from spleen samples, spleens were homogenized through cell strainers (BD Falcon) and cells were stained with anti-Vα2-PE, labeled with anti-PE Microbeads (Miltenyi Biotec) and separated by MACS enrichment (Miltenyi Biotec).

Barcode recovery, microarray hybridizations and data analysis. Genomic DNA was isolated using a DNeasy tissue kit (Qiagen). To determine barcode sampling efficiency, barcode-containing gDNA samples were split into two equal parts (A and B) that were independently amplified by nested PCR[21]. PCR products were purified by MinElute columns (Qiagen), labeled with Cyanine-3 (Cy3) or Cyanine-5 (Cy5) fluorescent dyes (Kreatech) and hybridized to a barcode-microarray[21]. Fluorescence intensities, as quantified using ImaGene 6.0 software (BioDiscovery, Inc.) were normalized, corrected for background noise, and duplicates were averaged. Barcode dot plots depict fluorescence intensities of the hybridized A and B samples, in which each dot represents one of the 4,743 barcodes present on the barcode-microarray. Barcodes with a signal above background with $P<0.05$ were determined by one-sided *t*-test. The cut-off used for this quantification is indicated by the rectangular divider in the dot plots. The Pearson correlation between fluorescent signals of barcodes present within two samples was calculated. Calculations included a randomly drawn fraction of barcodes that were not present in a given sample (reference population), as described previously[21]. Note that the use of such a reference population within the calculations restricts correlation values to a range of -0.5 (lack of kinship) to 1 (full kinship).

CFSE labeling. Cell suspensions were washed in PBS/0.1% BSA and resuspended at $5x10^6$ cells/ml. CFSE (Molecular Probes) was added to a final concentration of 5 μM, and cells were incubated for 10 min at 37°C. Following quenching by addition of ice-cold culture medium, cells were washed in fresh medium, resuspended in HBSS, and injected intravenously into mice.

Partial splenectomy. Mice were anesthetized with isoflurane and the skin overlying the spleen was shaved and disinfected. A <1 cm incision was made in the skin and peritoneum. ¼ of the spleen was resected and the wound on the spleen was closed with Histoacryl ® Topical Skin Adhesive (TissueSeal). Thereafter, peritoneum and skin were closed with ~3 stitches and buprenorphine (0.1 μg/g body weight; Schering-Plough) was given as pain relief.

ACKNOWLEDGMENTS

We thank F. van Diepen and A. Pfauth for cell sorting; W. Brugman and R. Kerkhoven for microarray production; D. Sie for help with microarray analysis; S. Greven for animal bleeding; D. Busch (Munich, Germany) for providing LM-OVA; and D. van Heijst-Kal for theoretical discussions.

REFERENCE LIST

1. van Heijst, J. W. *et al.* Recruitment of antigen-specific CD8+ T cells in response to infection is markedly efficient. *Science* 325, 1265-1269 (2009).
2. Mercado, R. *et al.* Early programming of T cell populations responding to bacterial infection. *J. Immunol.* 165, 6833-6839 (2000).
3. Kaech, S. M. & Ahmed, R. Memory CD8+ T cell differentiation: initial antigen encounter triggers a developmental program in naive cells. *Nat. Immunol.* 2, 415-422 (2001).
4. van Stipdonk, M. J., Lemmens, E. E. & Schoenberger, S. P. Naive CTLs require a single brief period of antigenic stimulation for clonal expansion and differentiation. *Nat. Immunol.* 2, 423-429 (2001).
5. Chang, J. T. & Reiner, S. L. Protection one cell thick. *Immunity* 27, 832-834 (2007).
6. Masopust, D., Kaech, S. M., Wherry, E. J. & Ahmed, R. The role of programming in memory T-cell development. *Curr Opin Immunol* 16, 217-225 (2004).
7. Williams, M. A. & Bevan, M. J. Effector and memory CTL differentiation. *Annu Rev Immunol* 25, 171-192 (2007).
8. Reiner, S. L., Sallusto, F. & Lanzavecchia, A. Division of labor with a workforce of one: challenges in specifying effector and memory T cell fate. *Science* 317, 622-625 (2007).
9. Harty, J. T. & Badovinac, V. P. Shaping and reshaping CD8+ T-cell memory. *Nat Rev Immunol* 8, 107-119 (2008).
10. Ahmed, R., Bevan, M. J., Reiner, S. L. & Fearon, D. T. The precursors of memory: models and controversies. *Nat. Rev. Immunol.* 9, 662-668 (2009).
11. Jameson, S. C. & Masopust, D. Diversity in T cell memory: an embarrassment of riches. *Immunity* 31, 859-871 (2009).
12. van Faassen, H. *et al.* Reducing the stimulation of CD8+ T cells during infection with intracellular bacteria promotes differentiation primarily into a central (CD62LhighCD44high) subset. *J. Immunol.* 174, 5341-5350 (2005).
13. Catron, D. M., Rusch, L. K., Hataye, J., Itano, A. A. & Jenkins, M. K. CD4+ T cells that enter the draining lymph nodes after antigen injection participate in the primary response and become central-memory cells. *J. Exp. Med.* 203, 1045-1054 (2006).
14. D'Souza, W. N. & Hedrick, S. M. Cutting edge: latecomer CD8 T cells are imprinted with a unique differentiation program. *J. Immunol.* 177, 777-781 (2006).
15. Quigley, M., Huang, X. & Yang, Y. Extent of stimulation controls the formation of memory CD8 T cells. *J. Immunol.* 179, 5768-5777 (2007).
16. Stemberger, C. *et al.* A single naive CD8+ T cell precursor can develop into diverse effector and memory subsets. *Immunity* 27, 985-997 (2007).
17. Gerlach, C. *et al.* One naïve T cell, multiple fates in CD8+ T cell differentiation. *J. Exp. Med.* In press (2010).
18. Chang, J. T. *et al.* Asymmetric T lymphocyte division in the initiation of adaptive immune responses. *Science* 315, 1687-1691 (2007).
19. Ahmed, R. & Gray, D. Immunological memory and protective immunity: understanding their relation. *Science* 272, 54-60 (1996).
20. Kaech, S. M. & Wherry, E. J. Heterogeneity and cell-fate decisions in effector and memory CD8+ T cell differentiation during viral infection. *Immunity* 27, 393-405 (2007).
21. Schepers, K. *et al.* Dissecting T cell lineage relationships by cellular barcoding. *J. Exp. Med.* 205, 2309-2318 (2008).
22. Roe, T., Reynolds, T. C., Yu, G. & Brown, P. O. Integration of murine leukemia virus DNA depends on mitosis. *EMBO J.* 12, 2099-2108 (1993).

23. Panganiban, A. T. & Fiore, D. Ordered interstrand and intrastrand DNA transfer during reverse transcription. *Science* 241, 1064-1069 (1988).
24. Hu, W. S. & Temin, H. M. Genetic consequences of packaging two RNA genomes in one retroviral particle: pseudodiploidy and high rate of genetic recombination. *Proc. Natl. Acad. Sci. U S A* 87, 1556-1560 (1990).
25. Hajihosseini, M., Iavachev, L. & Price, J. Evidence that retroviruses integrate into post-replication host DNA. *EMBO J.* 12, 4969-4974 (1993).
26. Joshi, N. S. *et al.* Inflammation directs memory precursor and short-lived effector CD8(+) T cell fates via the graded expression of T-bet transcription factor. *Immunity* 27, 281-295 (2007).
27. Pearce, E. L. & Shen, H. Generation of CD8 T cell memory is regulated by IL-12. *J Immunol* 179, 2074-2081 (2007).
28. Takemoto, N., Intlekofer, A. M., Northrup, J. T., Wherry, E. J. & Reiner, S. L. Cutting Edge: IL-12 inversely regulates T-bet and eomesodermin expression during pathogen-induced CD8+ T cell differentiation. *J. Immunol.* 177, 7515-7519 (2006).
29. Curtsinger, J. M., Valenzuela, J. O., Agarwal, P., Lins, D. & Mescher, M. F. Type I IFNs provide a third signal to CD8 T cells to stimulate clonal expansion and differentiation. *J. Immunol.* 174, 4465-4469 (2005).
30. Kolumam, G. A., Thomas, S., Thompson, L. J., Sprent, J. & Murali-Krishna, K. Type I interferons act directly on CD8 T cells to allow clonal expansion and memory formation in response to viral infection. *J. Exp. Med.* 202, 637-650 (2005).
31. Badovinac, V. P., Porter, B. B. & Harty, J. T. CD8+ T cell contraction is controlled by early inflammation. *Nat Immunol* 5, 809-817 (2004).
32. Badovinac, V. P., Messingham, K. A., Jabbari, A., Haring, J. S. & Harty, J. T. Accelerated CD8+ T-cell memory and prime-boost response after dendritic-cell vaccination. *Nat Med* 11, 748-756 (2005).
33. Cho, B. K., Rao, V. P., Ge, Q., Eisen, H. N. & Chen, J. Homeostasis-stimulated proliferation drives naive T cells to differentiate directly into memory T cells. *J Exp Med* 192, 549-556 (2000).
34. Goldrath, A. W., Bogatzki, L. Y. & Bevan, M. J. Naive T cells transiently acquire a memory-like phenotype during homeostasis-driven proliferation. *J Exp Med* 192, 557-564 (2000).
35. Murali-Krishna, K. & Ahmed, R. Cutting edge: naive T cells masquerading as memory cells. *J Immunol* 165, 1733-1737 (2000).
36. Hamilton, S. E., Wolkers, M. C., Schoenberger, S. P. & Jameson, S. C. The generation of protective memory-like CD8+ T cells during homeostatic proliferation requires CD4+ T cells. *Nat Immunol* 7, 475-481 (2006).
37. Pham, N. L., Badovinac, V. P. & Harty, J. T. A default pathway of memory CD8 T cell differentiation after dendritic cell immunization is deflected by encounter with inflammatory cytokines during antigen-driven proliferation. *J Immunol* 183, 2337-2348 (2009).
38. Wong, P. & Pamer, E. G. Feedback regulation of pathogen-specific T cell priming. *Immunity* 18, 499-511 (2003).
39. Kessels, H. W., Wolkers, M. C., van den Boom, M. D., van der Valk, M. A. & Schumacher, T. N. Immunotherapy through TCR gene transfer. *Nat. Immunol.* 2, 957-961 (2001).
40. Pope, C. *et al.* Organ-specific regulation of the CD8 T cell response to Listeria monocytogenes infection. *J. Immunol.* 166, 3402-3409 (2001).

7

RECRUITMENT OF ANTIGEN-SPECIFIC CD8+ T CELLS IN RESPONSE TO INFECTION IS MARKEDLY EFFICIENT

Jeroen W.J. van Heijst[1], Carmen Gerlach[1], Erwin Swart[1], Daoud Sie[2], Cláudio Nunes-Alves[3], Ron M. Kerkhoven[2], Ramon Arens[1], Margarida Correia-Neves[3], Koen Schepers[1] and Ton N.M. Schumacher[1]

[1]Division of Immunology and [2]Central Microarray Facility, the Netherlands Cancer Institute, Amsterdam, the Netherlands; [3]Life and Health Sciences Research Institute (ICVS), School of Health Sciences, University of Minho, Braga, Portugal

Science. 325:1265-9 (2009)

The magnitude of antigen-specific $CD8^+$ T cell responses is not fixed, but correlates with the severity of infection. Although by definition T cell response size is the product of both the capacity to recruit naïve T cells (clonal selection) and their subsequent proliferation (clonal expansion), it remains undefined how these two factors regulate antigen-specific T cell responses. Here we determined the relative contribution of recruitment and expansion by labeling naïve T cells with unique genetic tags and transferring them into mice. Under disparate infection conditions with different pathogens and doses, recruitment of antigen-specific T cells was near constant and close to complete. Thus, naïve T cell recruitment is highly efficient and the magnitude of antigen-specific $CD8^+$ T cell responses is primarily controlled by clonal expansion.

7

INTRODUCTION, RESULTS & DISCUSSION

A key feature of adaptive immunity is its ability to recognize a wide range of pathogens by specific antigen receptors expressed on lymphocytes. Because the diversity of antigen receptors is large[1], the frequency of cells specific for any single antigen is extremely low (<1 in 10^5 cells)[2,3]. This leaves the immune system with the remarkable challenge of selecting those few pathogen-specific cells amongst the millions of cells that do not recognize a given pathogen at the moment infection occurs. This process of 'clonal selection' is followed by massive expansion of those selected cells to give rise to sufficient progeny to combat the invading pathogen. Thus, the magnitude of adaptive immune responses is regulated by two processes. First, the number of participating clones is set by the efficiency with which antigen-specific cells are recruited from the naïve repertoire. Second, the burst size of these participating clones - defined as the net sum of all proliferation and cell death - determines the total number of antigen-specific progeny that is generated per recruited cell.

The magnitude of T cell responses generated upon infection is not fixed, but is shaped according to the severity of infection[4,5]. Although this correlation is well established, it remains undefined to what extent changes in the magnitude of response are the result of an effect on naïve T cell recruitment or clonal burst size. To quantify the number of recruited T cell clones in live infection models we have labeled individual naïve antigen-specific $CD8^+$ T cells with unique DNA sequences (barcodes)[6]. Because these barcodes are passed on to all daughter cells, this labeling strategy allowed us to distinguish the progeny of different recruited T cells within the total antigen-specific T cell pool that emerges during infection. Thus, the number of different barcodes detected within an antigen-specific T cell population directly correlates with the number of naïve T cells that have been recruited.

To first investigate the impact of pathogen dose on $CD8^+$ T cell recruitment, we labeled OT-I T cell receptor (TCR) transgenic T cells, which are specific for a peptide fragment of chicken ovalbumin presented by major histocompatibility class I, with a library of barcodes by retroviral transduction. We then transferred 10^3 or 10^4 barcode-labeled GFP^+ OT-I T cells into C57Bl/6 (B6) mice. One day later, we infected mice with different doses of recombinant *Listeria monocytogenes* bacteria expressing the chicken ovalbumin-derived $OVA_{257-264}$ epitope (LM-OVA) recognized by the OT-I TCR. At the peak of the $CD8^+$ T cell response (fig. S1), the total number of barcode-labeled $CD8^+$ T cells in spleens was determined. We observed a ten-fold increase in the magnitude of the $CD8^+$ T cell response between the lowest and the highest LM-OVA dose (Fig. 1A). In addition, a 10-fold increase in the number of antigen-specific precursors (10^4 OT-I T cells) at a fixed high pathogen dose resulted in a further (four-fold) increased T cell response.

To compare the efficiency of T cell recruitment under varying pathogen doses, we determined the number of different barcodes present within the OVA-specific GFP^+ T cell population. Barcodes were recovered by PCR and hybridized to

a barcode-microarray[6]. Analysis of microarray data showed that barcode content obtained from duplicate samples of a single mouse was highly reproducible, indicating that repertoire sampling was reliable (Fig. 1B). Furthermore, use of barcodes between different mice did not overlap. All barcode signals detected were derived from CD8⁺ T cells that had been recruited into the immune response, as the signal from non-primed barcode-labeled cells was readily out-competed (fig. S2).

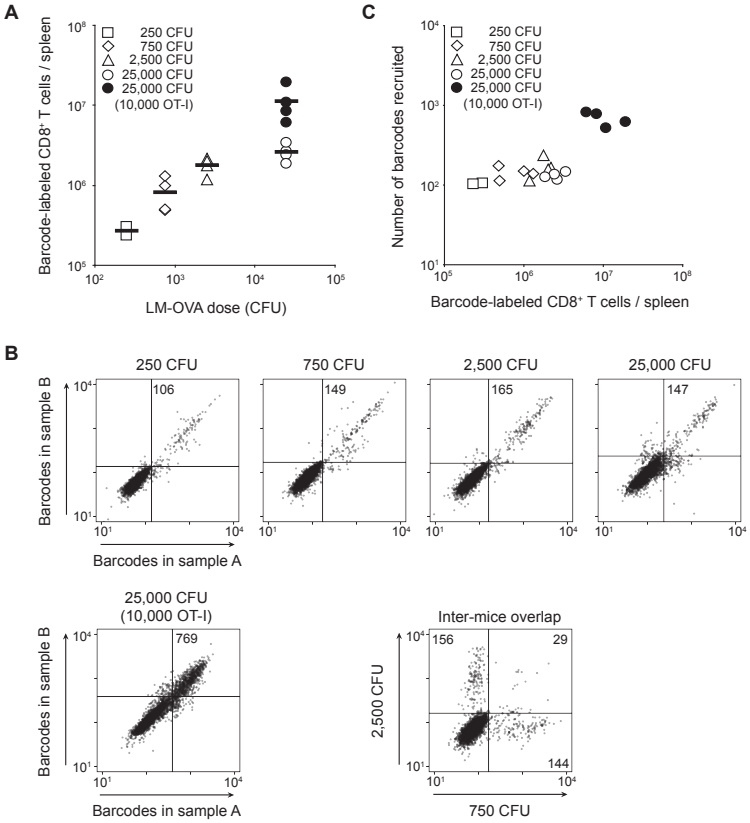

Figure 1. Effect of pathogen dose and precursor frequency on CD8⁺ T cell recruitment. (**A**) Magnitude of the barcode-labeled CD8⁺ T cell response. Recipients of 10^3, or where indicated 10^4, conA-activated GFP⁺ barcode-labeled OT-I T cells were challenged with the indicated doses of LM-OVA. At the peak of the CD8⁺ T cell response (day 8), the number of splenic barcode-labeled CD8⁺ T cells was determined. Diamonds represent individual mice, bars represent group mean. (**B**) Barcode analysis of samples described in (A), showing representative barcode dot plots. In these plots each dot represents the fluorescent intensity of one barcode of the library. Values indicate the number of barcodes detected above background. Inter-mice comparison demonstrates that each mouse contains a unique set of barcodes. (**C**) Comparison of the magnitude of the CD8⁺ T cell response to the number of antigen-specific precursors recruited for all individual mice. Data are representative of three independent experiments.

Interestingly, the number of different barcodes recovered from individual mice across the entire range of pathogen doses was highly comparable, with only a 1.5-fold difference in barcode numbers between the lowest and the highest LM-OVA dose (Fig. 1B). This indicates that the profoundly increased magnitude of the $CD8^+$ T cell response at higher pathogen dose occurs without a substantial increase in T cell recruitment. As the magnitude of a T cell response is the product of the number of T cell clones recruited and the burst size of each recruited clone, these data furthermore imply that clonal burst size was changed by seven-fold and thus forms the prime factor regulating T cell responses at varying pathogen dose (Fig. 1C). In contrast, when the available antigen-specific T cell repertoire was raised due to infusion of a larger number of T cell precursors, the observed increase in T cell response size (four-fold) was paralleled by an essentially proportional (five-fold) increase in the number of recruited barcodes (Fig. 1, B and C). Notably, near-constant recruitment of T cells at varying pathogen dose was also observed when naïve barcode-labeled OT-I T cells were generated in vivo, through injection of barcode-labeled OT-I thymocytes into the thymus of B6 recipients (fig. S3).

To determine whether near-constant recruitment also applies to other factors known to influence the magnitude of T cell responses, we addressed to what extent recruitment is affected by the duration of infection, or by pathogen type and route of infection. CFSE-dilution of OT-I T cells responding to LM-OVA infection revealed that Ampicillin antibiotic (Amp) treatment limits T cell priming to the first 72 hours post infection (fig. S4)[7]. To study how recruitment is affected by such a reduced duration of infection, recipients of naïve barcode-labeled OT-I T cells were challenged with LM-OVA with or without Amp treatment. Shortening the duration of infection reduced $CD8^+$ T cell responses by >ten-fold (Fig. 2A). However, the number of precursors recruited was only slightly lowered (~1.5-fold) (Fig. 2, B and C), indicating a change in clonal burst size by >seven-fold. Adoptive transfer of CFSE-labeled OT-I T cells from Amp-treated mice into either LM-OVA or wild-type LM-infected mice revealed that the enhanced clonal burst size observed upon prolonged infection is primarily due to increased T cell proliferation driven by sustained antigen exposure (fig. S5).

To examine whether near-constant recruitment occurs regardless of pathogen type or route of infection, recipients of naïve barcode-labeled OT-I T cells were challenged by either 1) systemic intravenous LM-OVA infection, 2) systemic intraperitoneal vaccinia virus-OVA infection, or 3) local intranasal influenza virus-OVA infection. A strong difference in the magnitude of $CD8^+$ T cell responses was observed, with the response to LM-OVA being >15-fold higher than the response to either vaccinia-OVA or influenza-OVA (Fig. 2D). Despite this major difference in T cell response, the number of recruited naïve T cells in response to these different pathogens was highly comparable (Fig. 2, E and F).

The above data indicate that T cell recruitment is highly constant, but do not reveal its efficiency. To directly enumerate recruitment efficiency, we quantified the number of antigen-specific T cells that do not undergo clonal expansion following infection. To

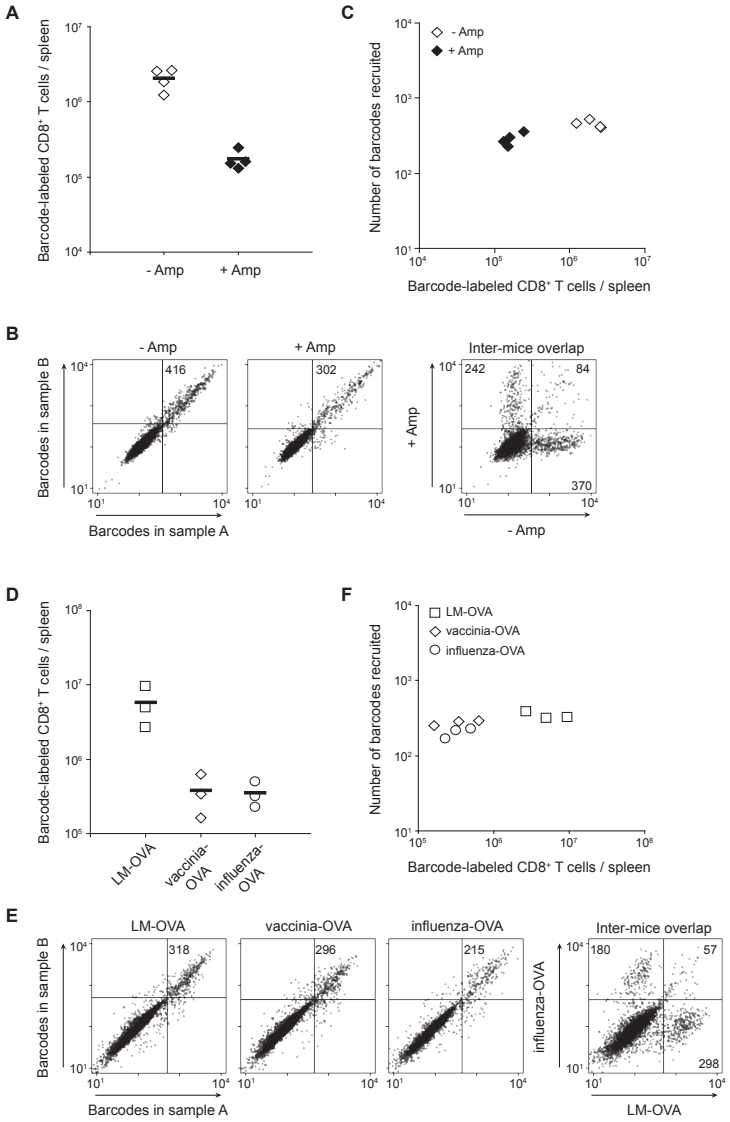

Figure 2. Effect of duration of infection and pathogen type on CD8⁺ T cell recruitment. (**A**) Magnitude of the barcode-labeled CD8⁺ T cell response of recipients of ~10^3 naïve barcode-labeled OT-I T cells that were infected with LM-OVA with or without Amp treatment. (**B**) Representative barcode dot plots of samples described in (A). (**C**) Comparison of the magnitude of the CD8⁺ T cell response to the number of antigen-specific precursors recruited for all individual mice. (**D**) Magnitude of the barcode-labeled CD8⁺ T cell response of recipients of ~10^3 naïve barcode-labeled OT-I T cells that were infected with LM-OVA, vaccinia-OVA, or influenza-OVA. (**E**) Representative barcode dot plots of samples described in (D). (**F**) Comparison of the magnitude of the CD8⁺ T cell response to the number of antigen-specific precursors recruited for all individual mice. Data are representative of two independent experiments.

this purpose, CD45.2 recipient mice received 5x10^3 CFSE-labeled congenic CD45.1$^+$ OT-I T cells and were challenged with either LM-OVA, wild-type LM, or left uninfected. Within the approximately 2x10^7 CD8$^+$ T cells recovered from pooled secondary lymphoid organs of wild-type LM-infected or uninfected mice at day 8 post infection, we detected on average 228 ± 24 and 288 ± 29 CFSE^{hi} (non-recruited) OT-I T cells, respectively (Fig. 3). Importantly, in mice infected with LM-OVA only a very low number (8 ± 7) of remaining CFSE^{hi} cells could be detected. This indicates that >95% of the OT-I T cell pool was selected to undergo clonal expansion when the OVA antigen was present and thus recruitment was close to complete.

Although the dissociation constant of the OT-I - K^b-OVA interaction (K_d = 6μ M)[8] is representative of the interactions observed for T cells that recognize foreign antigens (0.1-20 μM)[9,10], it was important to establish whether polyclonal T cell populations expressing a range of TCR affinities follow similar patterns of recruitment. To address this issue, we made use of "Limited" (Ltd) mice that express the OT-I TCRα chain transgene together with a Vα2 TCRα chain minilocus[11]. Rearrangement of this minilocus has been shown to result in the formation of a restricted repertoire of CDR3α variants (~40 different TCRs were described in lymph node CD8$^+$ T cells). Consistent with the hypothesis that CD8$^+$ T cells of Ltd mice display variable affinities for the OVA antigen, Ltd CD8$^+$ T cells showed a range of K^b-OVA tetramer binding (Fig. 4A). Furthermore, similar to what was observed for OT-I cells (Fig. 1, fig. S3) and endogenous OVA$_{257-264}$-specific CD8$^+$ T cells (fig. S6), an increased magnitude of the Ltd CD8$^+$ T cell response was observed at increasing LM-OVA doses, with

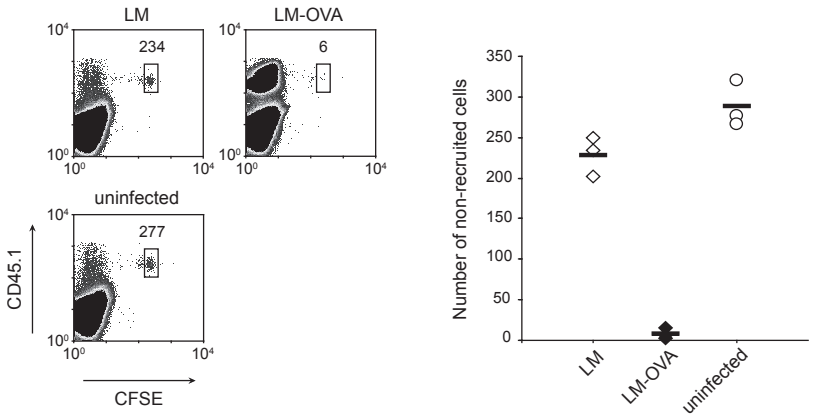

Figure 3. Antigen-specific CD8$^+$ T cell recruitment upon infection is close to complete. CD45.2 recipients of 5x10^3 CFSE-labeled CD45.1$^+$ OT-I T cells were infected with wild-type LM, LM-OVA, or left uninfected. At the peak of the CD8$^+$ T cell response, total spleen and lymph node CD8$^+$ T cells were analyzed by flow cytometry. Left: representative flow cytometry plots gated on live CD8$^+$ T cells; values indicate the number of non-recruited (CFSE^{hi}) OT-I T cells. Right: cumulative data for each group. Data are representative of six independent experiments.

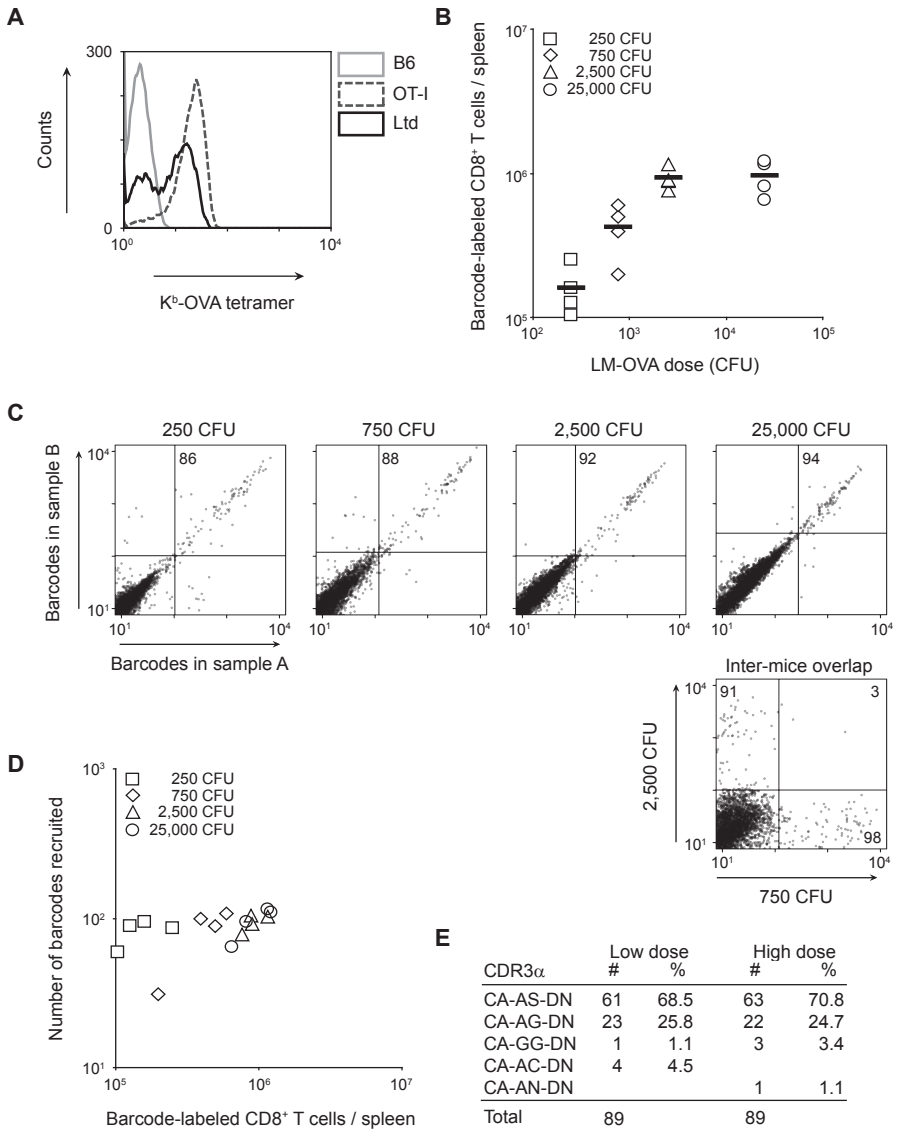

E

CDR3α	Low dose #	Low dose %	High dose #	High dose %
CA-AS-DN	61	68.5	63	70.8
CA-AG-DN	23	25.8	22	24.7
CA-GG-DN	1	1.1	3	3.4
CA-AC-DN	4	4.5		
CA-AN-DN			1	1.1
Total	89		89	

Figure 4. Efficiency of T cell recruitment of polyclonal T cell populations. (**A**) K^b-OVA tetramer binding of B6, OT-I and Ltd $CD8^+$ T cells. Representative histogram gated on live $CD8^+$ T cells is shown (two mice/group). (**B**) Magnitude of the barcode-labeled $CD8^+$ T cell response of recipients of 10^3 barcode-labeled Ltd $CD8^+$ T cells that were challenged with indicated LM-OVA doses. (**C**) Representative barcode dot plots of samples described in (B). (**D**) Comparison of the magnitude of the $CD8^+$ T cell response to the number of antigen-specific precursors recruited for all individual mice. (**E**) CDR3α TCR sequences of Ltd $CD8^+$ T cells responding to infection. Data represent pooled sequences of two low (250 CFU) and two high dose (25,000 CFU)-infected mice. Note that the dominance of the CDR3α amino acid sequences CA-AS-DN and CA-AG-DN TCR (which comprise 35% and 19% of the naïve Ltd repertoire, respectively)[11], increases to a combined 95% upon antigen-driven selection.

a six-fold difference between the lowest and the highest dose (Fig. 4B). Nevertheless, recruitment of Ltd $CD8^+$ T cells was only minimally altered (<1.5 fold; Fig. 4, C and D). Importantly, both at low and high antigen dose, the vast majority of recruited Ltd cells was characterized by two TCRα protein sequences (94.3% and 95.5% of sequences, respectively) (Fig. 4E). Furthermore, the relative proportion of these two TCRα protein sequences in the responding T cell population was identical between low and high dose-challenged mice. Notably, these two TCRs, which have near-identical affinity for the OVA antigen (fig. S7), were both encoded by a high number of different CDR3α DNA sequences (table S1), indicating that these Ltd responses are highly polyclonal at the DNA level and selected for "fitness" at the protein level.

Under highly disparate conditions of infection, naïve $CD8^+$ T cell recruitment is near constant and close to complete. This indicates that control of the magnitude of antigen-specific $CD8^+$ T cell responses primarily occurs through regulation of clonal burst size. The observed efficiency of recruitment also indicates that the process through which naïve T cells scan antigen-presenting dendritic cells (DCs) must be sufficiently robust to allow the vast majority of antigen-specific T cells to encounter a DC carrying cognate antigen within the first 72 hours of infection. Assuming that naïve antigen-specific $CD8^+$ T cells are present at a frequency of ~1:100,000 within a $CD8^+$ T cell pool of ~$20x10^6$ cells, it would require around $59x10^6$ T-DC interactions to achieve 95% recruitment, a number that is largely independent of variations in precursor frequency within the physiological range (see Materials and methods). It has been estimated that DCs are able to interact with at least 500 different T cells/hour[12,13], thus a pool of <2,000 antigen-presenting DCs could suffice to achieve this near-complete recruitment.

How can participation of high affinity clones be highly efficient even at low pathogen dose, with little evidence for participation of additional clones at greatly increased pathogen levels? Previous studies of the $CD4^+$ T cell response to injected soluble antigens have shown that a high proportion of the TCR diversity found in the naïve repertoire was also preserved during the early stages of antigen-induced proliferation[2,14]. Notably, one of these studies showed that whereas early during the response TCR diversity was still highly reflective of the naïve repertoire, at the peak of the immune response TCR diversity was skewed towards higher affinity clones[14]. In line with this, recent data have shown that lower affinity interactions do result in T cell activation in vivo, but these responses undergo premature contraction[15]. Together with our data, these studies support a model in which the immune system maximizes its potential to react towards invading pathogens by allowing a near-complete recruitment of high affinity T cells, independent of the conditions of infection (fig. S8). Although this may lead to concomitant activation of lower affinity cells, the abortive expansion of these clones forms a filter against their further participation[14,15].

MATERIALS AND METHODS

Mice. C57BL/6 (B6), OT-I T cell receptor (TCR) transgenic[16] and OT-I CD45.1 mice were bred in the animal facility of the Netherlands Cancer Institute. "Limited" (Ltd) mice[11] were bred in the animal facility of the ICVS, Portugal. Mice were maintained under specific pathogen-free conditions. All experiments were performed according to institutional and national guidelines, and were approved by the Experimental Animal Committee of the Netherlands Cancer Institute.

Barcode library and microarray generation. Generation of the barcode library and microarray has been described previously[6]. Briefly, the semi-random DNA stretch $(N_8\text{-}(SW)_5)_5\text{-}N_8$ was inserted 3' of the GFP sequence in the pLentilox3.4 vector. Following transformation, 4,743 *E. coli* cell clones were picked and individually expanded. The *E. coli* cell clones were pooled and subcloned into the pMX retroviral vector, to generate a Moloney-based retroviral barcode library. Next to this, barcodes from the individual *E. coli* cell clones were amplified by PCR and spotted in duplicate onto poly-L-lysine-coated glass slides to generate a barcode-microarray.

Retroviral transduction. Retroviral supernatants were generated using Phoenix-E packaging cells as described[17], and stored at -80°C. To generate barcode-labeled cells by *in vitro* retroviral transduction, OT-I or Ltd splenocytes were activated in IMDM (Invitrogen) supplemented with 8% heat-inactivated fetal calf serum, 100 U/ml penicillin plus 100 µg/ml streptomycin (Roche) and 0.5×10^{-5} M β-Mercaptoethanol (culture medium) in the presence of 2 µg/ml Concanavalin A (conA, Calbiochem) and 1 ng/ml IL-7 (Preprotech). After two days of culture, activated splenocytes were transduced with diluted retroviral supernatant by spin infection as described[17]. Retroviral supernatants were used at dilutions resulting in transduction efficiencies of 1-2%, at which the mean number of barcodes/cell is ~1.1 [6]. After O/N culture, cells were purified using Ficoll Paque Plus (Amersham Biosciences), stained with anti-CD8α-APC (BD, clone 53.6-7), and $GFP^+CD8\alpha^+$ cells were sorted on a FACSAria (BD) or MoFlo (Beckman Coulter). Sorted cells were washed in HBSS (Invitrogen) and injected intravenously (10^3 barcode-labeled T cells/mouse, unless indicated otherwise).

To generate naïve barcode-labeled OT-I T cells, OT-I thymocytes were transduced by spin infection in the presence of DOTAP transfection reagent (Roche) and 10 ng/ml IL-7 [18]. Four hours after transduction, cells were washed and incubated in DOTAP-free culture medium O/N. The next day, thymocytes were purified using Lympholyte-M (Cedarlane), and GFP^+ cells were sorted on a FACSAria or MoFlo. Sorted cells were washed in HBSS and injected intrathymically into anesthetized primary recipients (~5×10^5 barcode-labeled OT-I thymocytes/mouse). Three weeks later, spleen and lymph nodes of primary recipients containing mature naïve barcode-labeled OT-I T cells were pooled and enriched for $CD8^+$ T cells (BD IMag CD8 enrichment kit). Cells were washed in HBSS and injected intravenously into secondary recipients (~10^3 naïve barcode-labeled OT-I T cells/mouse).

Note that while we always aim to transfer 10^3 thymocyte-derived naïve barcode-labeled OT-I T cells, this number is based on the analysis of the very low frequency of GFP^+ T cells within the primary recipients (~0.01% of $CD8^+$ cells), and therefore the actual number of transferred cells may show some variation. To ensure that all mice within a single experiment receive the same number of barcode-labeled cells, each mouse is reconstituted with an equal volume of donor cells from a single pool.

Bacterial and viral infections. Wild-type *Listeria monocytogenes* (LM) and *Listeria monocytogenes* that expresses a secreted form of OVA (LM-OVA)[19] were grown in brain heart infusion broth (BD) to an OD_{600} of 0.1. For infections, mice were injected intravenously with 10^3 colony-forming units (CFU) LM or $2.5x10^3$ CFU LM-OVA in HBSS, unless specified otherwise. *Listeria* doses were confirmed by plating dilutions on brain heart infusion agar (BD). Ampicillin (Amp) sodium salt treatment (Sigma) consisted of 1 mg Amp injected intraperitoneally at the start of infection, plus 2 mg/ml in the drinking water for 3-5 consecutive days. The recombinant vaccinia virus strain that expresses the full length OVA protein (vaccinia-OVA) has been described[20]. For infections, mice were injected intraperitoneally with 10^6 plaque forming units (PFU) in HBSS. The recombinant influenza virus A/WSN/33 strain that expresses the H-$2K^b$-restricted $OVA_{257-264}$ epitope (influenza-OVA) has been described[21]. For infections, ether-anesthetized mice received an intranasal administration of 10^3 PFU in HBSS.

Quantification and purification of barcode-labeled T cells. Spleens were isolated and homogenized by mincing through cell strainers (BD Falcon). The total number of barcode-labeled T cells was determined by counting spleen samples, staining with anti-Vα2-PE (BD, clone B20.1), and analysis of the percentage of $GFP^+V\alpha2^+$ T cells by flow cytometry. Live cells were selected based on propidium iodide exclusion. To purify barcode-labeled T cells from spleen samples, cells were stained with anti-Vα2-PE, labeled with anti-PE Microbeads (Miltenyi Biotec) and separated by MACS enrichment (Miltenyi Biotec).

Barcode recovery, microarray hybridizations and data analysis. Genomic DNA was isolated using a DNeasy tissue kit (Qiagen). To determine barcode sampling efficiency, barcode-containing gDNA samples were split into two equal parts (A and B) that were independently amplified by nested PCR[6]. PCR products were purified by MinElute columns (Qiagen), labeled with Cyanine-3 (Cy3) or Cyanine-5 (Cy5) fluorescent dyes (Kreatech) and hybridized to the barcode-microarray. Fluorescence intensities, as quantified using ImaGene 6.0 software (BioDiscovery, Inc.), were normalized, corrected for background noise, and duplicates were averaged. Barcode dot plots depict fluorescence intensities of the hybridized A and B samples, in which each dot represents one of the 4,743 barcodes present on the barcode-microarray. To quantify T cell recruitment, the number of barcodes with a signal above background with $P<0.05$ was determined by a one-sided *t*-test. The cut-offs used for this quantification are indicated by the dividers in the dot plots.

CFSE-labeling. Cell suspensions were washed in PBS/0.1% BSA and resuspended at $5x10^6$ cells/ml. CFSE (Molecular Probes) was added to a final concentration of 0.5-5 μM, and cells were incubated for 10 min at 37°C. Following quenching by addition of ice-cold culture medium, cells were washed in fresh medium, resuspended in HBSS, and injected intravenously into mice. For analysis, the indicated lymphoid organs were homogenized and erythrocytes were removed by ammonium chloride treatment. Cells were stained with anti-CD8α-PE-Cy7 (BD, clone 53.6-7) and anti-CD45.1-APC (Southern Biotech, clone A20), and analyzed by flow cytometry on a CyAnADP (Beckman Coulter). Analysis was performed using Summit V4.3 software (Beckman Coulter).

TCR cloning and sequence analysis. OT-Iα chain variants encoding the CDR3α amino acids sequences CA-AS-DN, CA-AG-DN and CA-ARE-DN were ordered at GeneArt (Regensburg, Germany) and cloned into the pMX retroviral vector in front of an IRES-OT-Iα chain cassette. Retroviral supernatants were used to transduce conA-activated B6 splenocytes with the indicated TCRs. Transduction efficiency was determined by staining with anti-Vβ5-FITC (BD, clone MR9-4) and anti-Vα2-PE antibodies. Intracellular IFN-γ staining to determine functionality was performed using a Cytofix/Cytoperm with GolgiPlug kit (BD). To analyze the TCR repertoire of recruited Ltd $CD8^+$ T cells, responding cells were sorted based on anti-Vβ5-FITC, anti-CD45.2-PE (eBioscience, clone 104) and anti-CD8α-APC staining. gDNA from sorted cells was isolated and CDR3α regions were amplified by nested PCR using the following primers (5' to 3'): top –CAGCAGCAGGTGAGACAAAGT– and bottom –ATCGGCTGAGTGCATTGTCT– in the first round; top –TCCATACGTTCAGTGTCCGATAAA– and bottom –GGCTTTATAATTAGCTTGGTCCCAGAG– in the second round, with a 50°C annealing temperature. PCR products were cloned using TOPO TA cloning (Invitrogen) and individual colonies were analyzed by BigDye Terminator sequencing (Applied Biosystems).

Calculating T-DC interaction requirements for efficient recruitment. The number of T-DC interactions required to recruit 95% of antigen-specific T cells was calculated as follows. If X = the total number of $CD8^+$ T cells and Y = the number of antigen-specific $CD8^+$ T cells, then X/Y defines the average number of interactions required to recruit a first antigen-specific T cell. As this cell is now depleted from both the total T cell pool as well as from the antigen-specific T cell pool, the second recruitment event requires on average X-1/Y-1 interactions. These calculations can be continued until 95% of Y has been recruited. The sum of the interaction events required for each subsequent recruitment event provides the total number of T-DC interactions required to recruit 95% of antigen-specific T cells present at a precursor frequency of Y/X. As exemplified in the main text, assuming $X = 20x10^6$ and Y = 200, then ~$59x10^6$ T-DC interactions are required to achieve 95% recruitment. Interestingly, this number is largely independent of variations in precursor frequency within the physiological range, as 95% recruitment at a frequency of 1:200,000 (100 antigen-specific cells/mouse) or 1:20,000 (1,000 antigen-specific cells/mouse) would require ~$58x10^6$ and ~$60x10^6$ T-DC interactions, respectively.

ACKNOWLEDGMENTS

We thank F. van Diepen and A. Pfauth for cell sorting, D. Busch for LM-OVA, W. Brugman for microarray production and N. Armstrong for statistical help. We thank S. Naik and V. Ganusov for discussions and H. Jacobs, G. Bendle, J. Shu, M. Wolkers and S. Ariotti for reading the manuscript. GenBank accession numbers are FI903161 to FI903338.

REFERENCE LIST

1. Casrouge, A. *et al.* Size estimate of the alpha beta TCR repertoire of naive mouse splenocytes. *J. Immunol.* 164, 5782-5787 (2000).
2. Moon, J. J. *et al.* Naive CD4(+) T cell frequency varies for different epitopes and predicts repertoire diversity and response magnitude. *Immunity* 27, 203-213 (2007).
3. Obar, J. J., Khanna, K. M. & Lefrancois, L. Endogenous naive CD8+ T cell precursor frequency regulates primary and memory responses to infection. *Immunity* 28, 859-869 (2008).
4. Badovinac, V. P., Porter, B. B. & Harty, J. T. Programmed contraction of CD8(+) T cells after infection. *Nat. Immunol.* 3, 619-626 (2002).
5. Prlic, M., Hernandez-Hoyos, G. & Bevan, M. J. Duration of the initial TCR stimulus controls the magnitude but not functionality of the CD8+ T cell response. *J. Exp. Med.* 203, 2135-2143 (2006).
6. Schepers, K. *et al.* Dissecting T cell lineage relationships by cellular barcoding. *J. Exp. Med.* 205, 2309-2318 (2008).
7. Mercado, R. *et al.* Early programming of T cell populations responding to bacterial infection. *J. Immunol.* 165, 6833-6839 (2000).
8. Alam, S. M. *et al.* Qualitative and quantitative differences in T cell receptor binding of agonist and antagonist ligands 50. *Immunity* 10, 227-237 (1999).
9. Davis, M. M. *et al.* Ligand recognition by alpha beta T cell receptors 51. *Annu. Rev. Immunol.* 16, 523-544 (1998).
10. Cole, D. K. *et al.* Human TCR-binding affinity is governed by MHC class restriction 67. *J. Immunol.* 178, 5727-5734 (2007).
11. Correia-Neves, M., Waltzinger, C., Mathis, D. & Benoist, C. The shaping of the T cell repertoire 59. *Immunity* 14, 21-32 (2001).
12. Bousso, P. & Robey, E. Dynamics of CD8+ T cell priming by dendritic cells in intact lymph nodes. *Nat. Immunol.* 4, 579-585 (2003).
13. Beltman, J. B., Maree, A. F., Lynch, J. N., Miller, M. J. & de Boer, R. J. Lymph node topology dictates T cell migration behavior. *J. Exp. Med.* 204, 771-780 (2007).
14. Malherbe, L., Hausl, C., Teyton, L. & McHeyzer-Williams, M. G. Clonal selection of helper T cells is determined by an affinity threshold with no further skewing of TCR binding properties. *Immunity* 21, 669-679 (2004).
15. Zehn, D., Lee, S. Y. & Bevan, M. J. Complete but curtailed T-cell response to very low-affinity antigen. *Nature* 458, 211-214 (2009).
16. Hogquist, K. A. *et al.* T cell receptor antagonist peptides induce positive selection. *Cell* 76, 17-27 (1994).
17. Kessels, H. W., Wolkers, M. C., van den Boom, M. D., van der Valk, M. A. & Schumacher, T. N. Immunotherapy through TCR gene transfer. *Nat. Immunol.* 2, 957-961 (2001).
18. Gerlach, C. *et al.* One naïve T cell, multiple fates in $CD8^+$ T cell differentiation. *J. Exp. Med.* 207, 1235-1246 (2010).
19. Pope, C. *et al.* Organ-specific regulation of the CD8 T cell response to Listeria monocytogenes infection. *J. Immunol.* 166, 3402-3409 (2001).
20. Restifo, N. P. *et al.* Antigen processing in vivo and the elicitation of primary CTL responses 66. *J. Immunol.* 154, 4414-4422 (1995).
21. Topham, D. J., Castrucci, M. R., Wingo, F. S., Belz, G. T. & Doherty, P. C. The role of antigen in the localization of naive, acutely activated, and memory CD8(+) T cells to the lung during influenza pneumonia. *J Immunol* 167, 6983-6990 (2001).

SUPPLEMENTARY MATERIAL

Table S1. CDR3α DNA sequences of recruited Ltd CD8⁺ T cells.

CDR3α AS encoded by		Low dose		High dose		CDR3α AG encoded by		Low dose		High dose	
		#	%	#	%			#	%	#	%
GCA	AGT	51	83.6	52	82.5	GCA	GGT	14	60.9	11	50.0
GCC	TCT	3	4.9	4	6.3	GCG	GGG	2	8.7	3	13.6
GCA	AGC	3	4.9	3	4.8	GCG	GGT	2	8.7	1	4.5
GCA	TCC	4	6.6			GCA	GGG	1	4.3	2	9.1
GCA	TCT			2	3.2	GCA	GGC	3	13.0		
GCT	TCT			1	1.6	GCA	GGA	1	4.3		
GCG	TCC			1	1.6	GCT	GGT			2	9.1
						GCT	GGG			1	4.5
						GCC	GGT			1	4.5
						GCC	GGG			1	4.5
Total		**61**		**63**				**23**		**22**	

CDR3α DNA sequences of Ltd CD8⁺ T cells recruited into the response upon either low or high dose LM-OVA infection. Data represent pooled sequences from two low and two high dose-infected mice.

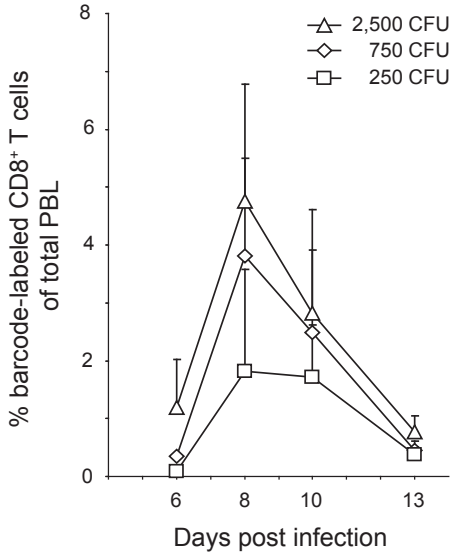

Figure S1. Kinetics of peripheral blood CD8⁺ T cell responses upon challenge with different LM-OVA doses. Mice received 10^3 conA-activated barcode-labeled OT-I T cells and were infected with the specified doses of LM-OVA. On the indicated days post infection, the percentage of barcode-labeled CD8⁺ T cells in peripheral blood was determined. Symbols indicate group averages + s.d. of three mice/group.

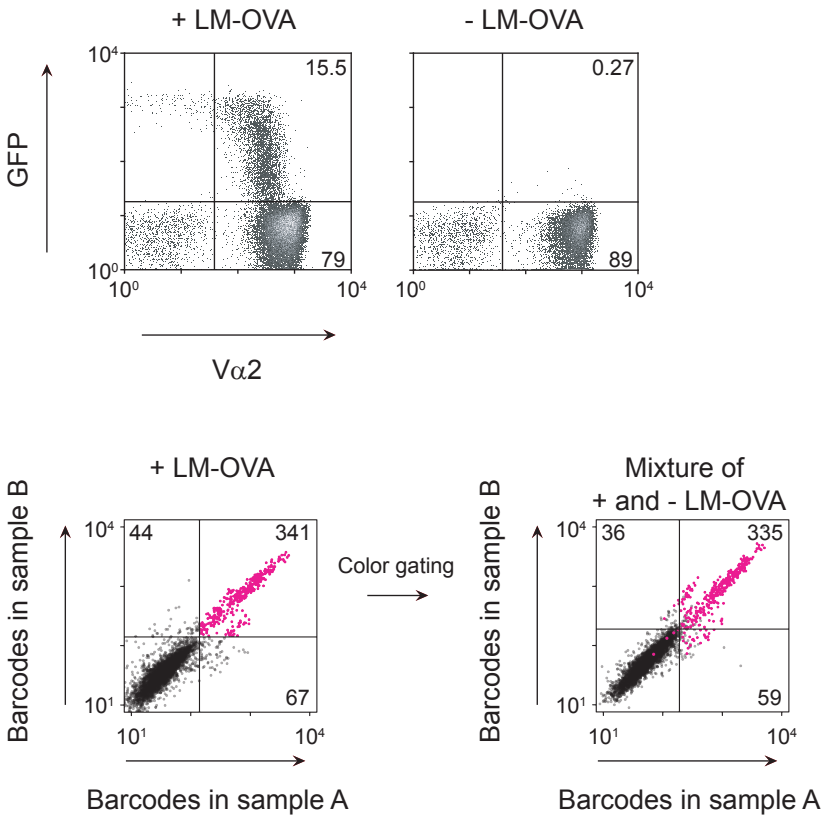

Figure S2. Detection by barcode-microarray is restricted to barcodes of T cells that have been recruited into the immune response. Mice received 10^3 conA-activated barcode-labeled OT-I T cells and were either infected with LM-OVA (+ LM-OVA) or not infected (- LM-OVA). At the peak of the $CD8^+$ T cell response, splenic $V\alpha2^+$ T cells (i.e. barcode-labeled OT-I T cells plus endogenous $V\alpha2^+$ T cells) were enriched by magnetic separation and used for flow cytometry and barcode analysis. Top panel: flow cytometry plots indicating the percentage of barcode-labeled (GFP^+) cells vs. non-barcode-labeled cells after Vα2 enrichment. Bottom panel: gDNA was isolated and barcode PCR amplifications were performed on either the + LM-OVA gDNA sample, or on a 1:1 mixture of the + LM-OVA and – LM-OVA gDNA sample. Resulting PCR products were hybridized to the barcode-microarray. Barcodes present above background in the + LM-OVA dot plot were color-labeled and gated to the + and – LM-OVA dot plot to determine to what extent the barcodes from the + LM-OVA sample dominated the combined sample. Values indicate the number of barcodes detected above background. Note that essentially all barcodes recovered from the mixed sample are derived from the + LM-OVA sample.

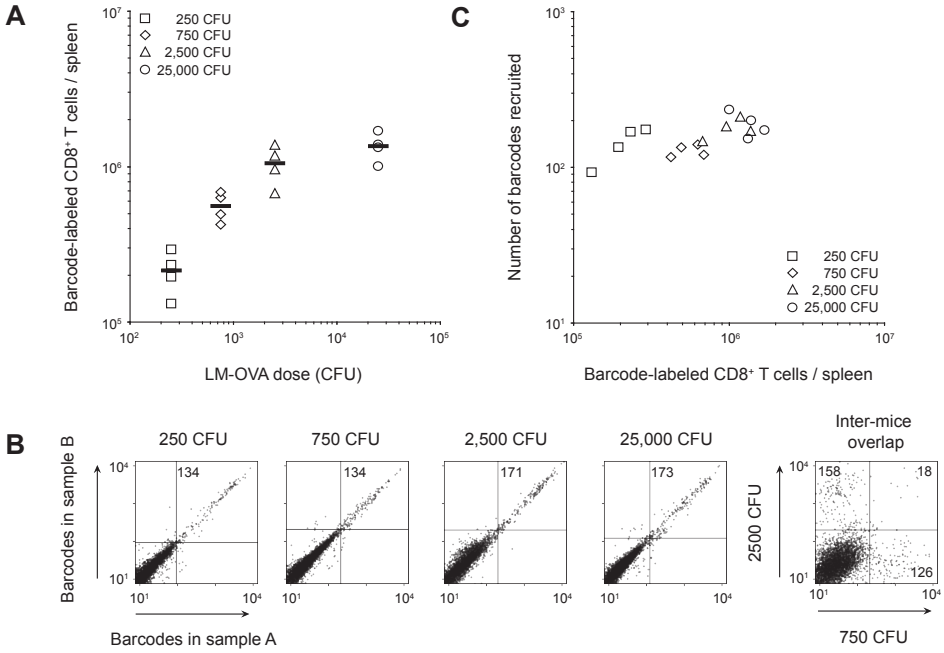

Figure S3. Effect of pathogen dose on naïve CD8⁺ T cell recruitment. (**A**) Magnitude of the barcode-labeled CD8⁺ T cell response of mice that received ~10^3 naïve barcode-labeled OT-I T cells and were challenged with the indicated doses of LM-OVA. (**B**) Barcode analysis of samples described under (A), showing representative barcode dot plots for each pathogen dose. Inter-mice comparison demonstrates that each mouse contains a unique set of barcodes. (**C**) Comparison of the magnitude of the CD8⁺ T cell response to the number of antigen-specific precursors recruited for all individual mice.

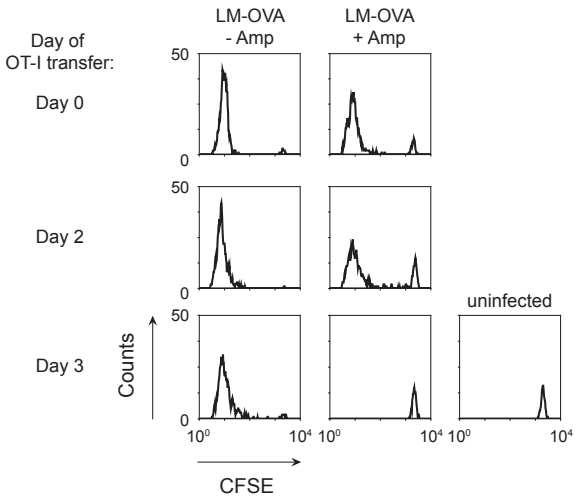

Figure S4. Kinetics of $OVA_{257-264}$ antigen presentation after LM-OVA infection and antibiotic treatment. 10^6 CFSE-labeled CD45.1⁺ OT-I T cells were transferred into CD45.2 recipients at various time points post LM-OVA infection with or without Amp treatment. Four days after transfer, T cell proliferation was measured by analysis of CFSE dilution of recovered spleen cells. Representative histograms gated on donor CD8⁺ CD45.1⁺ OT-I T cells are depicted (two mice/group).

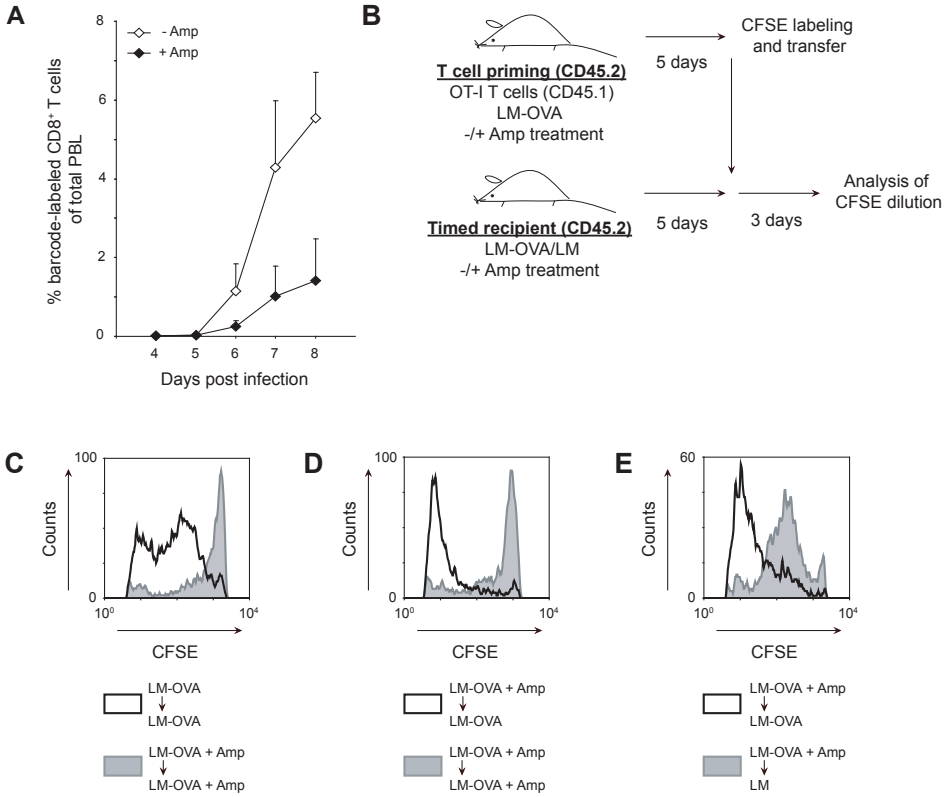

Figure S5. Enhanced CD8⁺ T cell burst size is driven by sustained antigen exposure. (**A**) Kinetics of peripheral blood CD8⁺ T cell responses after LM-OVA infection with or without antibiotic treatment. Mice received ~10^3 naïve barcode-labeled OT-I T cells, were infected with LM-OVA and were treated with or without Amp. Data depict the percentage of barcode-labeled CD8⁺ T cells in peripheral blood at the indicated time points. Diamonds indicate group averages + s.d. of four mice/group. (**B**) General set-up of the adoptive transfer experiments depicted in (C-E). CD45.2 mice received 10^3 CD45.1⁺ OT-I T cells, were infected with LM-OVA, and were either left untreated (- Amp) or treated with Amp (+ Amp; T cell priming group). Concomitantly, CD45.2 mice were infected with the indicated LM strain with or without Amp treatment, however without receiving any OT-I T cells (timed recipient group). At day 5 post infection, spleen cells from T cell priming mice were isolated, labeled with CFSE, and transferred into timed recipient mice. Three days later, CD45.1⁺ OT-I T cells in spleens of timed recipient mice were analyzed for CFSE dilution. (**C**) Cells from LM-OVA 'primed' mice without Amp treatment and cells from LM-OVA 'primed' mice with Amp treatment were each transferred into matched timed recipient mice. (**D**) Cells from LM-OVA 'primed' mice with Amp treatment were transferred into either untreated or Amp-treated timed recipient mice. (**E**) Cells from LM-OVA 'primed' mice with Amp treatment were transferred into either LM-OVA or LM-infected timed recipient mice. (**C**-**E**) Representative histograms gated on donor CD8⁺ CD45.1⁺ OT-I T cells are shown (two mice/group). Note that primed T cells transferred into LM-infected mice proliferate more than cells transferred into LM-OVA Amp-treated mice (compare gray histograms of C and D to E), indicating that inflammation in the absence of cognate antigen also does sustain T cell proliferation to some extent.

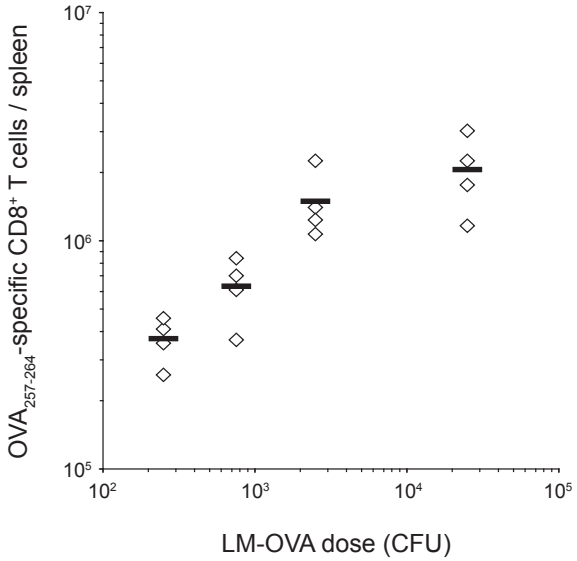

Figure S6. Effect of pathogen dose on endogenous OVA-specific CD8⁺ T cell responses. Mice were challenged with the indicated doses of LM-OVA. At the peak of the CD8⁺ T cell response, the magnitude of the splenic $OVA_{257-264}$-specific CD8⁺ T cell response was determined by K^b-OVA tetramer staining. Diamonds represent individual mice, bars represent group averages.

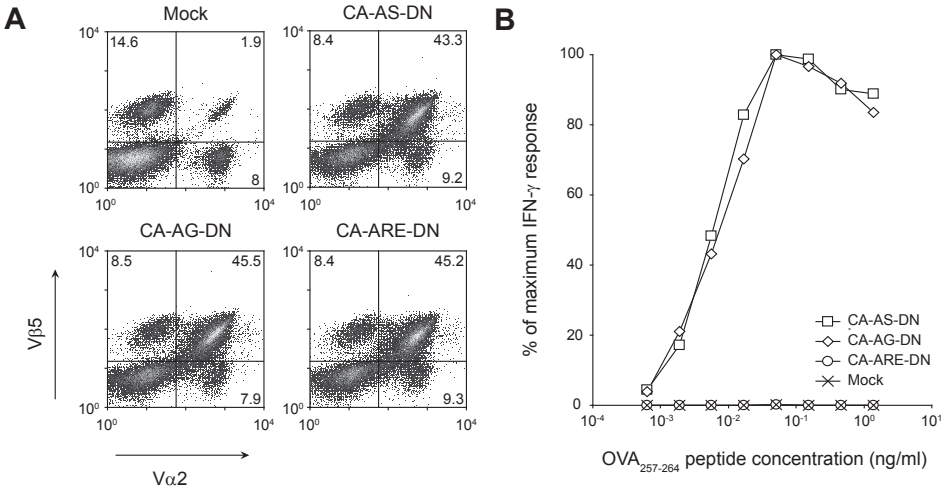

Figure S7. Antigen sensitivity of T cells expressing Ltd CDR3α variants. (**A**) B6 splenocytes were transduced with TCR constructs expressing the indicated Ltd CDR3α variants. FACS plots depicting the transduction efficiency of gated live CD8⁺ T cells are shown. (**B**) Intracellular IFN-γ staining of indicated TCR-transduced cell populations after stimulation with $OVA_{257-264}$ peptide. Data represents the dose-response curve normalized to the maximum percentage of IFN-γ producing cells for each cell population. Note that for the CA-ARE-DN TCR (the third most prevalent TCR in the Ltd naïve repertoire)[11] and mock-transduced cells no specific IFN-γ production above background was detected.

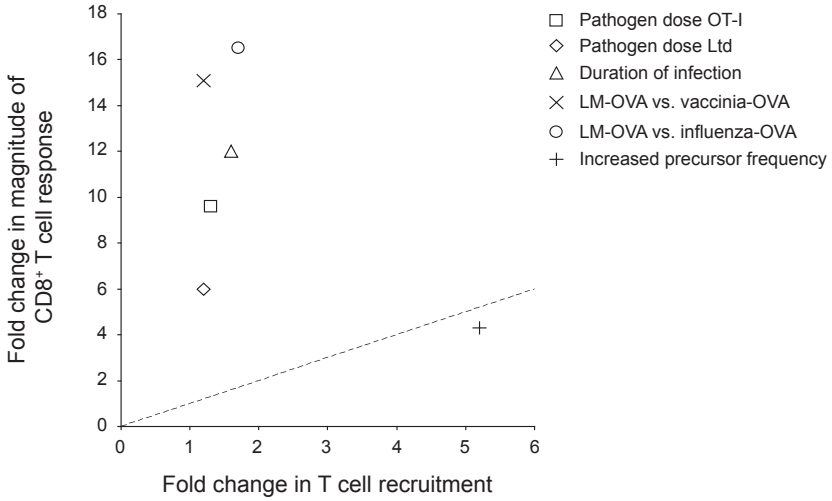

Figure S8. Variations in pathogen dose, duration of infection and pathogen type strongly affect the magnitude of the CD8$^+$ T cell response, while naïve T cell recruitment remains near constant. Data from Fig. 1 (lowest versus highest pathogen dose), Fig. 2 and Fig. 4 (lowest versus highest pathogen dose) were converted to plot the average fold change in T cell recruitment against the average fold change in the magnitude of the T cell response. The trend line indicates the predicted correlation in case variation in T cell response size would be fully explained by changes in T cell recruitment. Note that of all parameters tested, the magnitude of the T cell response only correlates with T cell recruitment in case T cell precursor frequency is altered.

8

THE CD8+ T CELL RESPONSE TO INFECTION IS DOMINATED BY THE PROGENY OF A FEW NAÏVE T CELLS

Carmen Gerlach[1], Jan Rohr[1], Nienke van Rooij[1], Arno Velds[2], Leïla Perié[1,3], Michael Hauptmann[4], Shalin H. Naik[1], Rob J. de Boer[3] and Ton N.M. Schumacher[1]

[1]Division of Immunology, [2]Deep sequencing Facility and [4]Bioinformatics and Statistics Group, Division of Molecular Biology, The Netherlands Cancer Institute, Department of Immunology, Amsterdam, the Netherlands; [3]Department of Theoretical Biology, Utrecht University, Utrecht, the Netherlands

unpublished

Following infection, antigen-specific $CD8^+$ T cell numbers increase dramatically. Analysis of antigen-specific T cell responses at the bulk cell level has provided insight into the average number of cell divisions that T cells undergo upon activation. However, it is unclear whether all naïve T cells of a given affinity for antigen produce equal numbers of progeny, or whether the total effector T cell pool is predominantly created by the output of few. To quantify how many daughter cells individual naïve T cells produce, we have generated naïve OT-I T cells harboring unique genetic tags (barcodes) and have measured the number of progeny per labeled cell by second-generation sequencing of barcode sequences after infection. Our data reveal that upon bacterial or viral infection, individual OT-I T cells that are recruited into the response produce highly variable numbers of daughter cells, and that this strong disparity in output is established during the first phase of infection. Importantly, the numerical dominance of the output of a small number of recruited cells becomes increasingly prominent when either CD80/CD86-mediated costimulation is disrupted, when T cell responses are induced by low affinity antigens or when pathogen load is low. These data indicate that in particular in situations in which T cell activation signals are limited, antigen-specific $CD8^+$ T cell responses are largely composed by the progeny of only a few cells.

INTRODUCTION

The CD8$^+$ T cell pool is shaped by pathogen encounter. The naïve CD8$^+$ T cell repertoire contains some ~80-1200 cells that recognize a given epitope[1,2]. Following infection, the majority of these antigen-specific CD8$^+$ T cells are recruited into the immune response[3] and collectively these cells produce up to 10^7 antigen-specific cells as progeny[2,4,5]. Based on this type of quantification of T cell responses at the bulk cell level, it has been estimated that CD8$^+$ T cells divide on average 14 times in response to LCMV infection[2,5]. An untested assumption in such quantifications is however that the clonal burst generated by each naïve T cell (i.e. the number of progeny) is roughly equal.

From CFSE dilution experiments it is apparent that naïve T cells - even when expressing the same T cell receptor – do not all complete their first division at the same time[6-8]. Likewise, asynchronous initiation of cell division by antigen specific T cells is suggested by imaging studies on explanted lymph nodes, in which generally only one of the antigen-specific T cells within the imaging field entered mitosis during a defined time frame[9,10]. However, whether asynchronous initiation of proliferation or other variables such as division and death rates would influence the progeny size of T cells with an identical antigen specificity remains unclear.

To reveal to what extent individual cells (in this case naïve antigen-specific T lymphocytes) differ in the number of progeny they produce it is essential to assign all the cells that are produced during an immune response to specific 'families', in which all the daughters from a single naïve T cell form a separate family. Over the past years, two fundamentally different technologies have been developed for such analysis of cellular descent[11]. First, cellular kinship can be revealed by the continuous tracing of cells by microscopy, and in recent work, the behavior of individual CpG-stimulated B cells and their progeny have been tracked *in vitro* by video microscopy[12]. These analyses have shown the existence of some degree of heritability in B cell division and death rates, with times to next division and times to death being more similar amongst siblings than between randomly picked cells within the population. The use of continuous tracing to reveal cellular kinship in vivo is presently limited to periods of hours and restricted to cases in which progeny stays local. However, T cell responses develop over periods of days and T cell progeny is not locally confined. Therefore, other technologies are required to map *in vivo* cell fate. Over the past years, two strategies have been developed towards this goal. Busch and colleagues have pioneered the transfer of individual T cells into recipient mice, thereby allowing fate mapping by allotype marking[13]. Alternatively, we have developed a technology to endow naïve T cells with unique genetic tags, which allows one to distinguish the progeny of individual cells on the basis of the genetic tag ('barcode') they carry. [3,11,14,15]. Specifically, through retroviral transduction of thymocytes[15] with a library of barcodes, a pool of naïve T cells, each carrying a unique genetic tag, can be created. As these barcodes are transferred to all progeny of the respective naïve T cell, all members of a given T cell family are marked with an identical barcode sequence.

Here we have combined this barcode labeling system with second-generation sequencing[16-19] to quantify the output of individual naïve T cells under different conditions of infection.

The data obtained reveal that within the population of responding T cells, individual T cell family sizes are highly variable, in spite of the fact that all tracked T cells possess the same antigen specificity. As a result of this, few T cell families dominate the overall response, with ~20% of the responding naïve T cells contributing to 90% of the total response magnitude. The dominance by a selected number of T cell families is established during the early phase of infection and becomes more pronounced in situations of weak T cell stimulation.

RESULTS

Quantification of T cell family size by second-generation sequencing

The development of the cellular barcoding technology[3,11,14,15] has made it possible to track the fate of several hundred individual naïve T cells and their daughters *in vivo*, as all progeny of the same naïve T cell precursor can be identified by an identical and unique genetic marker – the barcode. Previously, the representation of different T cell families within subpopulations of responding T cells (e.g. effector and memory T cell populations[15,20]) was determined by microarray hybridization. This readout system is well suited to detect the relative abundance of T cell families in two populations of interest by a ratiometric measurement. However, as the system is not calibrated, it is not possible to infer absolute T cell family sizes from the data obtained by this technology.

In order to accurately quantify the sizes of genetically tagged (T) cell families, we therefore developed a novel barcode-readout system that is based on second-generation sequencing. As second-generation sequencing (also referred to as next-generation or deep sequencing) yields millions of individual sequences within a single reaction[16-19], it has the potential to provide a highly quantitative measure of the abundance of individual DNA barcodes within a cell population, provided obviously that no significant bias is introduced during barcode recovery or amplification.

To first test to what extent barcode quantification by second-generation sequencing is able to accurately describe the frequency of cells with that specific tag within a cell population of interest, we transduced a human T cell line with the barcode library and generated 20 clones that each harbor a unique barcode. Subsequently, the clones were mixed in varying amounts and barcode frequencies within this mixed cell population were determined by second-generation sequencing. Comparison of these data with the input cell numbers per clone demonstrated that deviation from the expected ratio of 1 was small (max 1.87; min 0.33) for all clones constituting >0.2% of the total population (Fig. S1A). Thus, quantification of barcodes by deep sequencing can be used to describe the composition of cell populations over a large dynamic range (Fig. S1B).

OT-I T cell responses are dominated by the progeny of few naïve T cells

Having validated the use of deep sequencing for barcode quantification, we determined the extent to which the progeny of individual T cells that all share the same T cell receptor contribute to the overall ('bulk') response of these cells. To this purpose, naïve barcode-labeled (GFP^+) TCR-transgenic OT-I T cells were generated by thymocte transduction, and injected intra-thymically to allow for their differentiation into mature naïve T cells[15]. Approximately 800 barcode-labeled naïve OT-I T cells were transferred into B6 recipients, which were then infected with a recombinant *Listeria monocytogenes* strain expressing the SIINFEKL epitope (LM-OVA) that is recognized by the OT-I TCR. Seven days later, spleen and lymph nodes were harvested and the abundance of each barcode was quantified by second-generation sequencing. In addition, the overall OT-I T cell response magnitude was determined by flow cytometry.

To assess whether barcode quantification was reproducible, amplification and sequencing was performed in parallel on two independent half-samples taken from each recipient mouse, and read counts (reflecting sequence abundance) of all

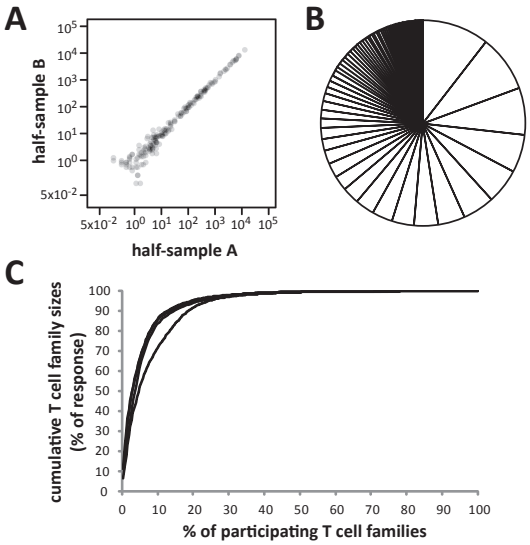

Figure 1: T cell responses are dominated by the progeny of few naïve T cells. ~800 naïve, barcode-labeled OT-I T cells were transferred into 4 B6 recipient mice that were infected with LM-OVA the next day. 7 days after infection, spleen and LNs were harvested and OT-I T cell family sizes were quantified. (**A**) Relative barcode abundances (# of reads out of 100'000) in two independent half-samples (sample A and B) of the same cell population of one representative mouse. Each dot corresponds to one barcode. A distribution control is provided in Fig. S2A. (**B**) Contribution of participating OT-I T cell families to the magnitude of the overall response. Each piece of the pie represents the average size of the first to n^{th} OT-I family for 4 mice. (**C**) Cumulative OT-I family sizes depicted as a function of the percentage of OT-I families participating in the response. Each line represents one mouse. Data are representative of 9 independent experiments.

barcodes were compared between the two half-samples (Fig. 1A). In all experiments, the prevalence of all barcodes identified within a given cell population was highly reproducible in these replicate measurements. Furthermore, overlap between barcodes recovered from different mice was low and for the low proportion of shared barcodes signal intensity was uncorrelated (Fig. S2A). This rules out sample contamination with barcodes originating from other samples as a confounding factor. Collectively, these data indicate that barcode deep sequencing forms a reproducible measure of barcode prevalence within a responding T cell population.

Interestingly, analysis of the relative abundance of the distinct barcode sequences detected within an antigen-specific T cell response indicated that the size of different OT-I families was highly diverse (Fig. 1A-C and S2B). Of the greater than 200 OT-I T cell families detected in each mouse of this experiment, the largest family constituted on average 10 percent of the total OT-I response (Fig. S2B, left plot; absolute family size >80,000 cells, right plot). In comparison, the median T cell family size was ~500-fold lower, at 0.015% of the overall response. Importantly, the smallest detected OT-I families were composed of ~4 cells, demonstrating that this assay system measured the progeny of OT-I T cells that had been recruited into the response. Thus, even though all tracked naïve T cells expressed the same TCR, there was a striking disparity in the amount of offspring they generated: On average, 50% of the total antigen-specific T cell response was formed by the progeny of just 3.5% of the activated OT-I cells, and 15% of the recruited T cells produced 90% of the effector T cell population (Fig. 1C).

Of the 2 display formats utilized to represent T cell family sizes (Fig. 1B+C), the first is expected to be sensitive to the amount of OT-I T cells that are recruited into the response, while the second is not. To formally test this, we transferred different numbers of naïve barcode-labeled OT-I cells into B6 recipients and quantified barcode abundance upon LM-OVA infection. As expected, the overall OT-I response magnitude was higher and a larger number of OT-I families participated in the response when a larger number of OT-I cells was transferred (Fig. S3B+C). Importantly, family sizes were highly variable in both groups (Fig. 2A-C and S3D). Plotting of the data demonstrated that - according to expectation - pie chart representations are influenced by the number of T cell families participating in the response, whereas saturation curves that plot the cumulative OT-I response magnitude as a function of the percentage of the total number of participating OT-I families are not. (Fig. 2B+C). Thus, the former type of data presentation is useful to reveal how the overall composition of a responding T cell population is influenced by variation in the conditions of infection (see below), while the latter specifically depicts the level of disparity in family sizes independent of the number of T cell families that participated.

Thus, the above data indicate that in response to LM-OVA infection, the progeny of a few T cells comprises the bulk of the overall OT-I T cell response. This numerical dominance by a minority of OT-I families was also observed in response to OVA-expressing influenza infection (Fig. 2D-F). Furthermore, this dominance was not

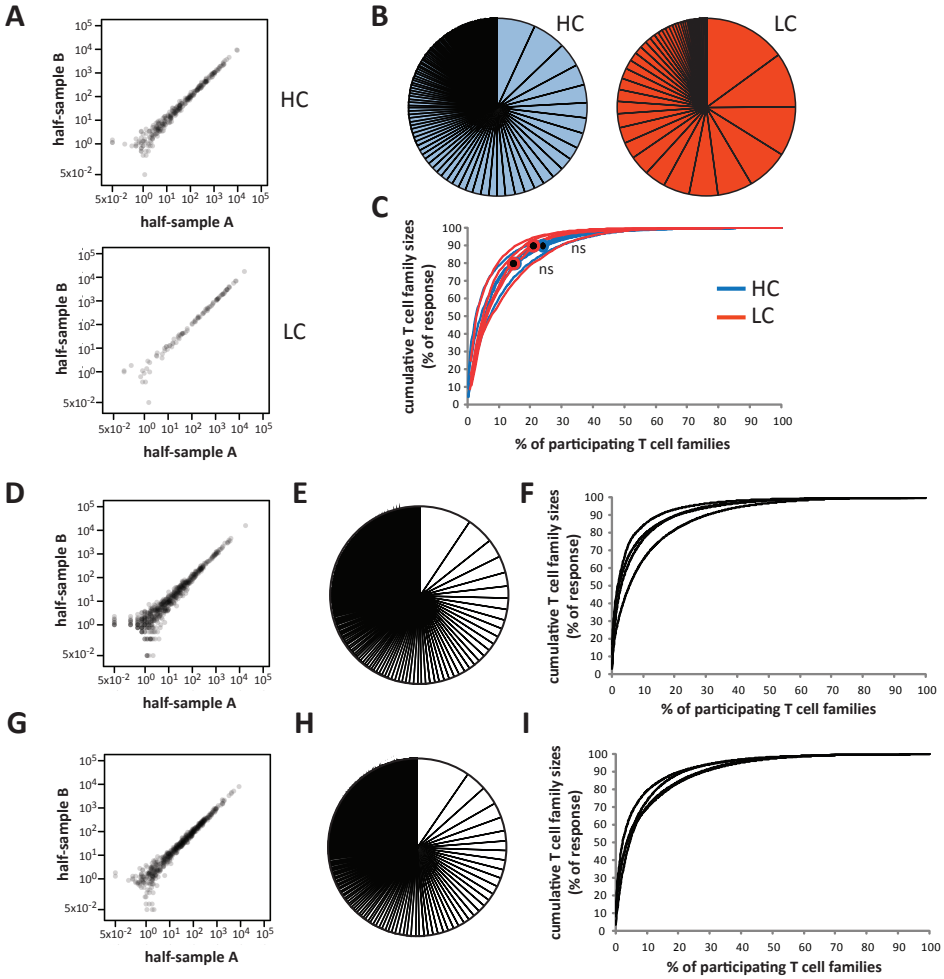

Figure 2: T cell family size disparity in OT-I rag2$^{-/-}$ T cell responses and as a function of naïve T cell frequency. (A-C) 760 (high cell numbers; HC) or 190 (low cell numbers; LC) naïve, barcode-labeled OT-I T cells were transferred into 5 B6 recipient mice that were infected with LM-OVA the next day. 7 days after infection, spleen and LNs were harvested and OT-I T cell family sizes were quantified. Representative distribution controls are provided in Fig. S3A. **(D-F)** ~400 naïve, barcode-labeled OT-I T cells were transferred into 4 B6 recipient mice that were infected with Influenza-OVA the next day. 9 days after infection OT-I T cell family sizes were quantified from spleen cells. A distribution control is provided in Fig. S3E. **(G-I)** ~1000 naïve, barcode-labeled OT-I, rag2$^{-/-}$ T cells were transferred into 4 B6 recipient mice that were infected with LM-OVA the next day. 7 days after infection, spleen and LNs were harvested and OT-I T cell family sizes were quantified. A distribution control is provided in Fig. S3F. (**A, D, G**) Relative barcode abundances (# of reads out of 100'000) in two independent half-samples (sample A and B) of the same cell population of one representative mouse. Each dot corresponds to one barcode. (**B, E, H**) Contribution of participating OT-I T cell families to the magnitude of the overall response. Each piece of the pie represents the average size of the first to nth OT-I family for 4 mice. (**C, F, I**) Cumulative OT-I family sizes depicted as a function of the percentage of OT-I families participating in the response. Each line represents one mouse. Circles represent the average % of participating T cell families per group to constitute 80% or 90% of the total response. (**C**) Differences in the fraction of participating T cell families constituting 80% (P=0.8413) and 90% (P=0.3095) are non-significant (ns).

related to rearrangement of the endogenous TCR loci in some of the OT-I T cells, as LM-OVA-induced responses of OT-I rag2$^{-/-}$ T cells were also largely composed by the output of a small number of cells (Fig 2G-I).

Once a large family – always a large family

To test at what time post infection the disparity in OT-I family sizes takes shape, we transferred barcode-labeled naïve OT-I T cells into B6 recipient mice and quantified family sizes in spleen and lymph nodes at day 5, 6, 7 or 8 after LM-OVA infection. As expected, the total number of OT-I T cells increased dramatically from day 5 to 8 (peak of response), with the largest (31-fold) expansion of the population occurring between day 5 and 6 (Fig S4B). Barcodes could be quantified reproducibly even from the small numbers of barcode-labeled cells obtained early after infection (Fig 3A) and the number of responding OT-I families was comparable at all days (Fig. S4C). Importantly, differences in family sizes were observed already at day 5, and the magnitude of these differences did not significantly change to day 8 (Fig 3B-C and S4D). This experiment demonstrates that a marked disparity in the clonal burst generated by individual T cells is already evident as early as day 5 post-infection, indicating that any factor influencing T cell family size must have acted before this time.

To address whether the T cell families that contributed most to the acute antigen-specific T cell response also remained dominant after the infection has waned, we harvested spleen cells from the same mice at two different time points after LM-OVA infection and compared OT-I T cell family sizes between these two samples. At both days, barcodes were reproducibly quantified (Fig. 4A). When the size of each OT-I family was compared between day 8 and 32, it was apparent that even though the exact order of dominance was not maintained, all families that were large at day 8 remained large 3 weeks later, intermediate families were still intermediate in size and small families remained small (Fig. 4B). Together, these kinetic data demonstrate that differences in OT-I T cell family sizes are present already early on during an antigen-specific T cell response and are maintained thereafter.

CD80/ CD86-mediated costimulation influences the disparity in T cell family sizes

The above data are consistent with a model in which the magnitude of the CD8^{+} T cell clonal burst is determined early after or during T cell activation. To determine whether the conditions under which T cell activation takes place could influence the observed disparity in T cell family sizes, we set out to create a setting in which T cell activating signals were reduced. For this purpose, disruption of CD80/86 mediated costimulation was selected, as the absence of CD80/86 is known to reduce T cell response magnitude substantially and signaling through CD28 is thought to function as a signal amplifier for weak signals received by the TCR[21]. Thus, in case T cell family size disparity would be influenced by the strength of the T cell activating signal, such a disparity may potentially be enhanced in a CD80/86 deficient setting.

To assess the effect of CD80/86 mediated costimulation on T cell family dominance, we transferred barcode-labeled naïve OT-I T cells into control B6 and

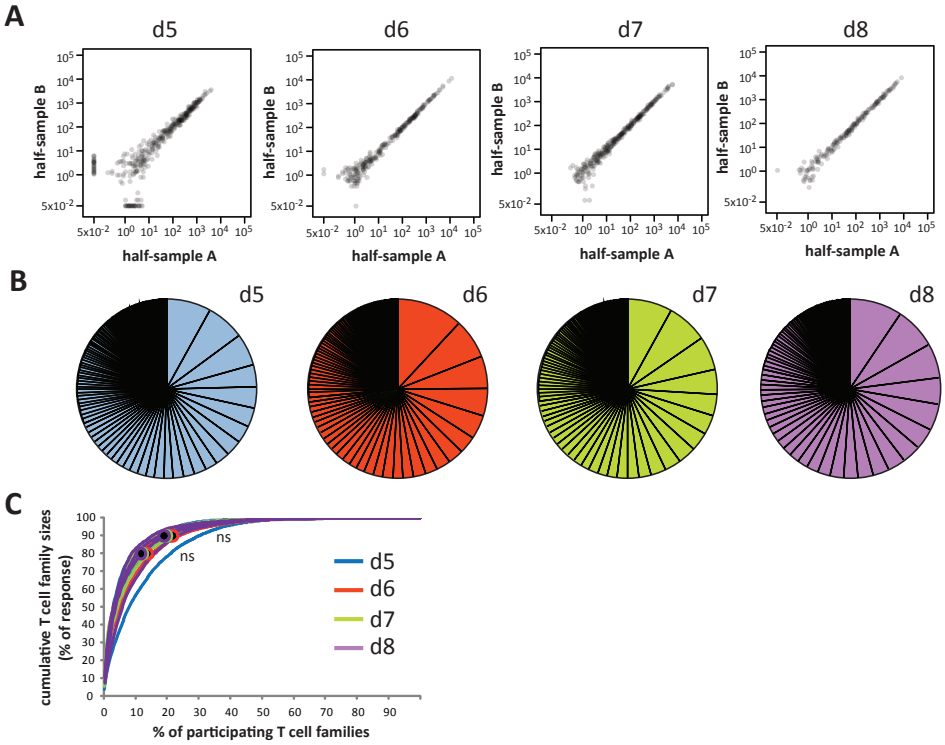

Figure 3: Differences in T cell family sizes are already observed early during the response. ~1600 naïve, barcode-labeled OT-I T cells were transferred into 16 B6 recipient mice that were infected with LM-OVA the next day. At day 5, 6, 7 and 8 after infection, spleen and LNs were harvested from 4 mice and OT-I T cell family sizes were quantified. (**A**) Relative barcode abundances (# of reads out of 100'000) in two independent half-samples (sample A and B) of the same cell population of one representative mouse. Each dot corresponds to one barcode. A distribution control is provided in Fig. S4A. (**B**) Contribution of participating OT-I T cell families to the magnitude of the overall response. Each piece of the pie represents the average size of the first to n^{th} OT-I family for 4 mice. (**C**) Cumulative OT-I family sizes depicted as a function of the percentage of OT-I families participating in the response. Each line represents one mouse. Circles represent the average % of participating T cell families per group to constitute 80% or 90% of the total response. Differences in the fraction of participating T cell families constituting 80% (P=0.5507) and 90% (P=0.4908) are non-significant (ns). Data are representative of 2 independent experiments.

$CD80^{-/-}CD86^{-/-}$ recipients and quantified both the overall response magnitude and individual OT-I family sizes at day 7 post LM-OVA infection.

The overall OT-I T cell response was markedly reduced in $CD80^{-/-}CD86^{-/-}$ mice (Fig. S5B) even though the number of participating OT-I families was only somewhat (~1.3-fold) reduced (Fig. S5C). Both in the absence and presence of CD80/CD86-mediated costimulation, individual OT-I family sizes were diverse (Fig. 5A-C and S5D), and as expected from the large difference in overall response magnitudes, the most dominant

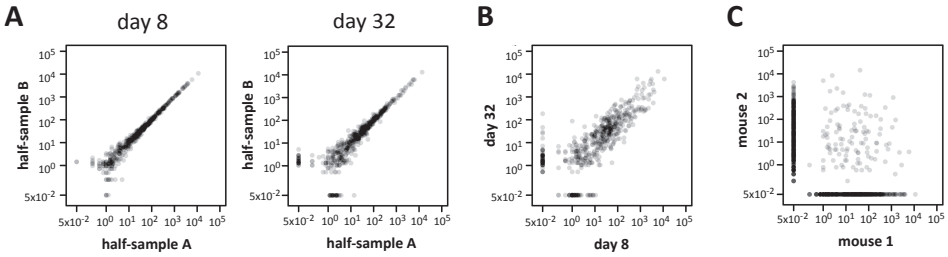

Figure 4: Differences in T cell family sizes are maintained during the response. ~640 naïve, barcode-labeled OT-I T cells were transferred into 4 B6 recipient mice that were infected with LM-OVA the next day. 8 days after infection ¼ of the spleen was isolated by partial splenectomy and the remainder of the spleen was isolated at day 32. OT-I T cell family sizes were quantified from both samples. (**A**) Read numbers per barcode in both half-samples obtained either at day 8 or 32. (**B**) Read numbers per barcode compared between two half-samples obtained at day 8 and day 32. (**C**) Representative distribution control.

OT-I families in the wild-type mice are larger in terms of absolute family members than in the CD80$^{-/-}$CD86$^{-/-}$ recipients (Fig. S5D, right graph). Interestingly, the largest OT-I family in the CD80$^{-/-}$CD86$^{-/-}$ recipients constituted a larger fraction of the total response than the most prevalent family in the wild-type mice (Fig. 5B and S5D, left graph). This is in part a reflection of the slight reduction in OT-I families participating in the response, but primarily the result of a significantly increased disparity in the clonal burst of the T cells that have been recruited: In order to constitute 90% of the total response, on average 33.5 out of 310 families (10.8%) in the knockout mice and 94 out of 387 families (24.3%) in the wildtype mice were required.

Taken together, this experiment shows that in the absence of CD80 and CD86-mediated costimulation, the overall response is dominated by even fewer OT-I T cell families. This occurs both because slightly fewer antigen-specific T cells are recruited into the response and in particular because amongst the families that do participate, the variation in family size is very pronounced.

The dominance of a few T cell families is more pronounced in response to lower affinity antigens and reduced antigen dose

To investigate if weaker T cell stimulation in general results in a more pronounced dominance of a few T cell families, we assessed whether disparity in T cell family sizes is shaped by antigen affinity.

To this purpose, OT-I family sizes were quantified 7 days after infection with *Listeria monocytogenes* strains harboring either the native OT-I ligand SII**N**FEKL (LM-OVA / LM-N4), or the altered peptide ligands SII**Q**FEKL (LM-Q4) or SII**T**FEKL (LM-T4). The latter two are recognized by OT-I T cells with ~18-fold and ~71-fold lower avidity, respectively[22].

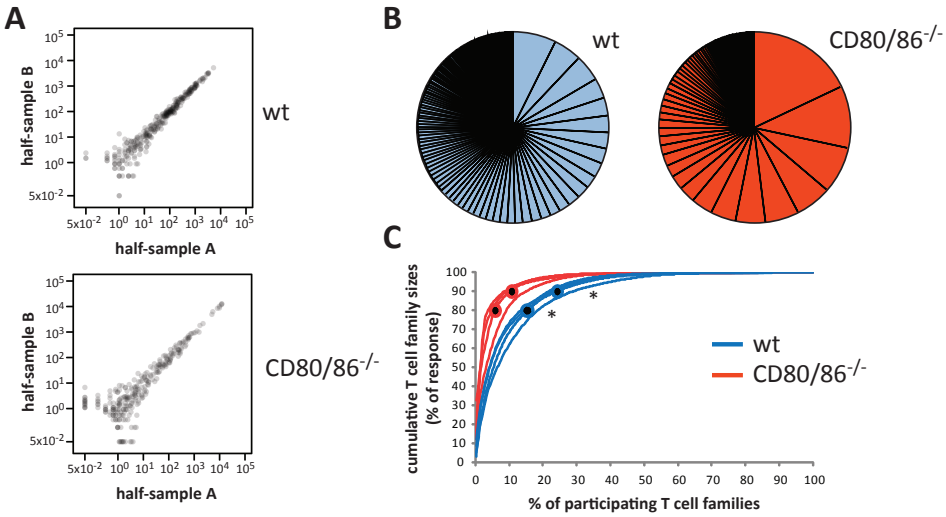

Figure 5: CD80/CD86-mediated costimulation influences the disparity in T cell family sizes. ~800 naïve, barcode-labeled OT-I T cells were transferred into 4 B6 or 4 CD80$^{-/-}$ CD86$^{-/-}$ recipient mice that were infected with LM-OVA the next day. At day 7 after infection OT-I family sizes were quantified from spleen and LN cells. (**A**) Relative barcode abundances (# of reads out of 100'000) in two independent half-samples (sample A and B) of the same cell population of one representative mouse. Each dot corresponds to one barcode. A distribution control is provided in Fig. S5A. (**B**) Contribution of participating OT-I T cell families to the magnitude of the overall response. Each piece of the pie represents the average size of the first to nth OT-I family for 4 mice. (**C**) Cumulative OT-I family sizes depicted as a function of the percentage of OT-I families participating in the response. Each line represents one mouse. Circles represent the average % of participating T cell families per group to constitute 80% or 90% of the total response. Differences in the fraction of participating T cell families constituting 80% (P=0.02857) and 90% (P=0.02857) are significant (*). Data are representative of 2 independent experiments.

Barcode quantification was reproducible (Fig. 6A) and as expected, the overall magnitude of the OT-I responses was markedly reduced in the lower affinity groups (Fig. S6B). Similar to T cell activation in the absence of CD80 and CD86, somewhat fewer OT-I families participated in the responses against the lower affinity antigens (Fig. S6C). In all groups T cell family sizes were diverse (Fig. 6B-C and S6D), however, in the groups stimulated by lower affinity antigens the dominant OT-I families contributed to a larger proportion of the overall response (Fig. 6B and S6D, left plot). Among the OT-I families participating in the response, the fraction of families required to constitute 80% or 90% of the overall response decreased significantly with reduced antigen affinity (Fig. 6C). Thus, the increased dominance of a small number of T cell families upon stimulation with low affinity antigen is due to two factors: a slight reduction (~1.4-fold) in the number of families participating in the response and a significantly larger disparity in family size among the families that do participate.

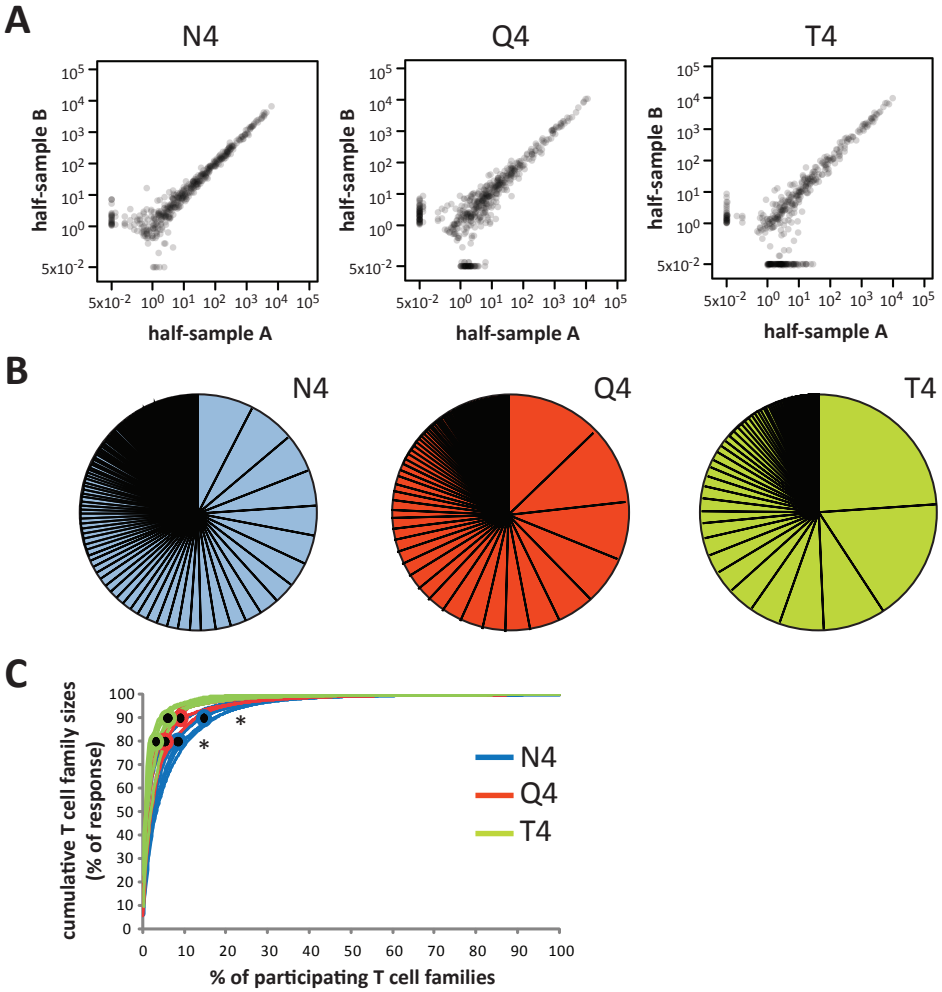

Figure 6: The dominance of a few T cell families is more pronounced in response to lower affinity antigens. ~640 naïve, barcode-labeled OT-I T cells were transferred into 16 B6 recipient mice, of which 5 were infected with LM-N4, 5 with LM-Q4 and 6 with LM-T4 the next day. At day 7 after infection OT-I family sizes were quantified from spleen and LN cells. (**A**) Relative barcode abundances (# of reads out of 100'000) in two independent half-samples (sample A and B) of the same cell population of one representative mouse. Each dot corresponds to one barcode. A distribution control is provided in Fig. S6A. (**B**) Contribution of participating OT-I T cell families to the magnitude of the overall response. Each piece of the pie represents the average size of the first to n^{th} OT-I family for 5-6 mice. (**C**) Cumulative OT-I family sizes depicted as a function of the percentage of OT-I families participating in the response. Each line represents one mouse. Circles represent the average % of participating T cell families per group to constitute 80% or 90% of the total response. The fraction of participating T cell families constituting 80% ($P=7.334\times10^{-5}$) and 90% ($P=3.766\times10^{-5}$) decreases significantly with decreasing antigen affinity (*). Data are representative of 2 independent experiments.

To further investigate the influence of T cell stimulation strength on the disparity of responding T cell family sizes, we quantified OT-I T cell family sizes after infection with different doses of LM-OVA bacteria. The magnitude of the bulk OT-I response was 6-fold lower after infection with the low bacterial dose (Fig. S7B) and in this experiment 2.6-fold fewer OT-I families participated in the response (Fig. S7C). From both groups, barcode quantification was reproducible (Fig. 7A) and family sizes were heterogeneous (Fig. 7B and S7D). Among the participating OT-I families, there was a trend towards a larger disparity in family sizes after low-dose infection. This observation did not reach statistical significance with the group sizes used. To increase the statistical power of the analysis, this experiment will be repeated with larger group sizes and an additional intermediate-dose group.

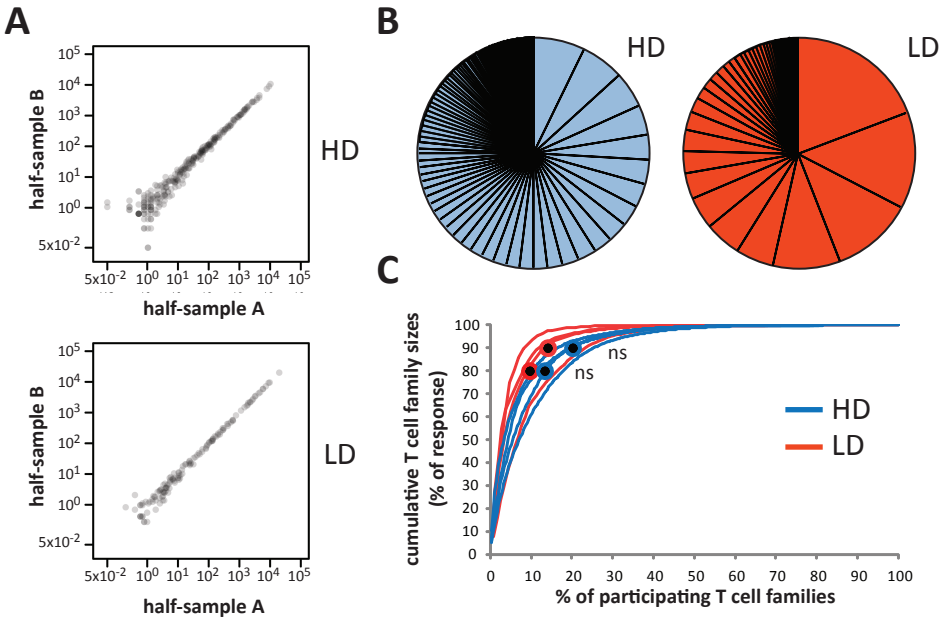

Figure 7: Influence of antigen dose on the disparity in T cell family sizes. ~880 naïve, barcode-labeled OT-I T cells were transferred into 8 B6 recipient mice, of which 4 were infected with 500 CFU LM-OVA (low dose; LD) and 4 with 25'000 CFU (high dose; HD) the next day. At day 7 after infection OT-I family sizes were quantified from spleen and LN cells. (**A**) Relative barcode abundances (# of reads out of 100'000) in two independent half-samples (sample A and B) of the same cell population of one representative mouse. Each dot corresponds to one barcode. A distribution control is provided in Fig. S7A. (**B**) Contribution of participating OT-I T cell families to the magnitude of the overall response. Each piece of the pie represents the average size of the first to n^{th} OT-I family for 4 mice. (**C**) Cumulative OT-I family sizes depicted as a function of the percentage of OT-I families participating in the response. Each line represents one mouse. Circles represent the average % of participating T cell families per group to constitute 80% or 90% of the total response. Differences between groups are non-significant (ns): 80% (P=0.2); 90% (P=0.2).

Together, these experiments demonstrate that OT-I T cell responses to lower affinity antigens are dominated by a smaller number of T cell families than T cell responses induced by high affinity antigen, and suggest that reduced antigen dose may lead to the same effect. Together with the data on the effect of CD80/86 costimulation, these results argue that the strength of the T cell activating signal determines the extent to which T cell responses are biased towards the output of a small number of cells.

DISCUSSION

While it is known that antigen-specific T cell populations expand dramatically upon infection, it is currently unclear whether all naïve T cells of a given affinity for antigen produce equal numbers of progeny. The aim of this study was therefore to quantify the output of individual naïve T cells in response to infection *in vivo*.

After developing a quantitative, second-generation sequencing-based readout system for use in conjuction with cellular barcoding, we demonstrated that individual OT-I T cells produce highly variable numbers of progeny upon OVA-expressing *Listeria monocytogenes* or influenza infection. As a result of this disparity, the total OT-I effector pool is dominated by only a few T cell families. It has previously been shown that T cell responses to infection are predominantly composed of T cells recognizing the antigen with high affinity[23-25]. Here we demonstrate that even within this high affinity repertoire, the progeny of only a minor fraction of the available cells dominates the response.

Two fundamentally different mechanisms could account for the observed disparity in T cell family sizes. First, individual T cell families could have distinct proliferation and/or death rates (collectively referred to as 'propagation rates' here). Second, individual antigen-specific naïve T cells could enter their first division at distinct moments in time and thus start to participate in the response asynchronously.

As we find that the extent of family size disparity does not significantly change after day 5 post infection, we consider it unlikely that stably distinct propagation rates for different T cell families underlie the observed disparity, as this would result in an increased disparity over time. Two more likely explanations for the observed dominance are therefore that I) not all antigen-specific T cells enter their first division at the same time and/or that II) propagation rates are variable between T cell families early after activation, but that this difference levels out before day 5. Using CFSE dilution, we are currently investigating the kinetics by which antigen-specific T cells complete their first division. We will subsequently use these data to mathematically model whether the measured differences in times to first division can explain the observed disparity in T cell family sizes, or whether additional early differences in propagation rates are required to obtain the pattern of T cell family dominance that is observed.

By inducing *in vivo* T cell activation in the absence or presence of CD80 and CD86-mediated costimulation, with antigens of different affinity, or with different antigen doses, we demonstrated that the extent of T cell family size disparity is not fixed, as

it was influenced by the environment in which the cells were stimulated. Conditions providing limited T cell stimulation intensified the disparity in output of the stimulated cells. These data suggest that the level of antigen affinity, antigen dose and CD80/CD86-mediated costimulation influence the variation in times to first division and/or propagation rates of the antigen-specific T cells.

What determines which of the antigen-specific T cells will form a large or a small family? In principle, these could be deterministic or stochastic processes. One could speculate that while all tracked T cells harbor the same TCR specificity, the level of TCR expression is variable. Those T cells with higher TCR density on their surface would recognize the antigen with higher avidity and could therefore initiate proliferation earlier or the stronger trigger they receive would speed up their expansion rate. Likewise, stochastic variation in signaling molecules may influence T cell behavior. As an alternative explanation, family dominance could simply be a matter of which T cell is at the right place at the right moment. As naïve T cell circulate between the secondary lymphoid organs, they are dispersed throughout the body and only a small fraction of the antigen-specific cell population will be close to the site of pathogen entry. It is conceivable that the conditions of antigen presentation and the inflammatory environment will be different for those cells that are already present at the infection site and those that arrive later. Whatever the underlying mechanism, in both cases an environment providing a weaker T cell activating signal can be expected to result in an increased diversity in times to first division and/or propagation rates of the antigen-specific T cells and thereby control T cell family size disparity.

MATERIALS AND METHODS

Mice. C57BL/6 (B6) mice were obtained from Charles River. CD80$^{-/-}$CD86$^{-/-}$ mice and TCR-transgenic OT-I and OT-I rag2$^{-/-}$ mice were bred and housed in the animal department of the Netherlands Cancer Institute (NKI). All animal experiments were performed in accordance with national guidelines and were approved by the Experimental Animal Committee of the NKI.

Generation and mixing of single-barcode clones. Retroviral supernatants were obtained by transfection of the barcode-library[14] DNA into Phoenix-A packaging cells using FuGENE™6 transfection reagent (Roche Diagnostics). Jurkat cells were transduced by spin-infection with diluted retroviral supernatants to reach a transduction efficiency of 1-2% (at this transduction efficiency, the mean number of barcodes per cell is close to one[14]). One day after transduction, GFP^{+} (transduced) cells were sorted as single-cells by FACS. From the clones that grew, genomic DNA was isolated and barcode sequences were amplified and sequenced by second-generation sequencing (as described below) to confirm the presence of one barcode per clone.

To assess how representative barcode quantification by second-generation sequencing is of the barcode abundance in a cell population, different cell numbers of twenty distinct single-barcode clones were mixed. The cell numbers ranged from 10

to 5'242'880 cells (2-fold steps), reaching a total of 10'485'750 cells. Genomic DNA was isolated from two of these mixtures and barcode sequences were amplified and sequenced as described below.

Generation and transfer of naïve, barcode-labeled T cells. Total thymocytes isolated from 4-8 weeks old OT-I or OT-I rag2$^{-/-}$ donor mice were transduced with the barcode-library by spin-infection (90min. 2000rpm) in culture medium (IMDM/ 8%FCS/ 100U/ml penicillin/ 100µg/ml streptomycin) supplemented with 10ng/ml recombinant murine IL-7 (Peprotech) and retroviral supernatant. Transductions were performed in non-tissue-culture treated 24-wells plates that had been pre-coated with retronectin (TaKaRa) for at least 2h and thereafter blocked with 2%BSA in MQ for ½ h. Retroviral supernatants containing the barcode-library were generated as described[14] and diluted prior to use to reach a transduction efficiency of approximately 10%. One day after transduction, thymocytes were purified using Lympholite (Cedarlane) and GFP^{+} cells were sorted by FACS. 0.5-1.3x10^{6} sorted cells were injected intra-thymically into 4-6 weeks old primary (1°) recipient B6 mice, as described previously[15]. Additional pain relief (carprofen; 5 µg/g body weight; Pfizer) was given s.c. 1 day after the operation. 2-3 weeks after intra-thymic injections, CD8^{+} T cells were isolated from spleen and LNs (cervical, axillary, brachial, mesenteric, inguinal, lumbar) of 1° recipient mice by negative selection (Mouse CD8 T Lymphocyte Enrichment Set; BD Biosciences). Enriched CD8^{+} cells, containing barcode-labeled naïve T cells[15] were pooled from several 1° recipients and then transferred i.v. into several 8-10 weeks old B6 secondary (2°) recipients (400-1600 barcode-labeled cells / 2° recipient). This pooling and distribution approach guarantees that each 2° recipient receives an equal number of barcode-labeled T cells. Before injection, the fraction of GFP^{+} cells (typically ~0.01%) was determined by FACS to obtain an approximation of the number of transferred barcode-labeled T cells.

Listeria and influenza A infections. One day after receiving barcode-labeled naïve OT-I cells, 2° recipient mice were infected i.v. with a *Listeria monocytogenes* strain expressing chicken ovalbumin containing either the native SIINFEKL sequence (LM-OVA / LM-N4) or the altered peptide ligands SIIQFEKL (LM-Q4) or SIITFEKL (LM-T4) that are recognized with respectively ~18 and 71-fold lower avidity by OT-I T cells[22]. Unless stated otherwise, 2.5x10^{3} CFU *Listeria* were administered.

Alternatively, mice were anesthetized with ether and infected intra-nasally (i.n.) with 10^{3} PFU of the recombinant influenza A/WSN/33 strain (Influenza-OVA) that expresses the H-2K^{b}-restricted OVA$_{257-264}$ epitope[26]. T cell responses to infection were monitored in blood by FACS.

Recovery of barcode-labeled cells from infected mice. Barcode-labeled OT-I or OT-I rag2$^{-/-}$ cells were recovered from spleen and LNs (cervical, axillary, brachial, mesenteric, inguinal, lumbar) of infected mice. To recover barcode-labeled spleen cells from living mice, partial splenectomy was performed as follows: Mice were anesthesized with isoflurane and the skin overlying the spleen was shaved and disinfected. A <1cm incision was made in the skin and peritoneum. ¼ of the spleen

was resected and the wound on the spleen was closed with Histoacryl® Topical Skin Adhesive (TissueSeal). Thereafter, peritoneum and skin were closed with ~3 stitches. Buprenorphine (0.1µg/g body weight; Schering-Plough) was given as pain relief 30 min. before and 6 h after the operation.

The isolated cells were subsequently enriched for Vα2$^+$ cells by MACS (Miltenyi Biotec; anti-PE Microbeads used after surface staining with Vα2-PE antibody) to facilitate efficient barcode recovery. To alleviate concerns that inter-group differences in total numbers and frequencies of barcode-labeled cells within the Vα2-enriched fraction might influence the efficiency of barcode amplification, the absolute number and percentage of GFP$^+$ cells being analyzed was adjusted between experimental groups. In practice, this meant that of the experimental group that induced a larger overall response, only a fraction of the isolated cells (harboring the same amount of GFP$^+$ cells as in the other group) was analyzed, after this sample had been topped with part of the previously removed Vα2$^-$ cells to adjust also the percentage of GFP$^+$ cells within the total cells being analyzed. In the experiment shown in Fig. 3, this adjustment occurred to the day 6 group, due to the small numbers of GFP$^+$ cells in the day 5 group. Of day 5 and 6, all GFP$^+$ cells were analyzed. All samples were stored as cell pellet at -80°C until barcode analysis.

The overall OT-I T cell response magnitude was determined by counting the number of GFP$^+$, Vα2$^+$ cells by flow cytometry within a small sample (1/100th) taken from the MACS-enriched fraction. This counting occurred directly after MACS enrichment and before the adjustment of GFP$^+$ cell numbers and percentages.

Flow cytometry. Cell surface stainings were performed with the following reagents: Vα2-PE (B20.1), CD8-PerCp-Cy5.5 (53-6.7), CD8-APC (53-6.7)(BD Biosciences). Analyses were performed on a FACS Calibur (BD Biosciences) and analyzed with Summit v4.3 (Beckman Coulter) software. Cell sorting was carried out on a FACSAria Cell Sorter (BD Biosciences) or MoFlo Highspeed Sorter (Beckman Coulter).

Barcode amplification and second-generation sequencing. Genomic DNA was isolated from the frozen cell pellets using the DNeasy tissue kit (QIAGEN). Each sample was subsequently divided in two halves (sample A and B) that were independently amplified and analyzed further. This sample splitting serves as sampling control to test if barcodes could be representatively detected in the sample[3,11,14,15] and if amplification would introduce a bias in relative barcode abundance.

Barcode sequences were amplified by nested PCR, using top-LIB (5'-TGCTGCC-GTCAACTAGAACA-3') and bot-LIB (5'-GATCTCGAATCAGGCGCTTA-3') primers[14] in the first round (30 cycles: 5'' 94°C; 5'' 57.2°C; 5'' 72°C). In the experiment shown in Fig. 2D-F, the first round primers described previously[14] were used. The second round served to attach the P5 (5'- AATGATACGGCGACCACCGAGATCT-3') and P7 (5'- CAAGCAGAAGACGGCATACGAGAT-3') adaptors required for deep sequencing on Illumina platforms, a sequencing primer annealing site ('seq_prim': 5'- ACACTCTTTCCCTACACGACGCTCTTCCGATCT-3') and a unique 6 bp index to the amplified barcode sequences. To enable multiplexing of several samples within

one sequencing lane, all 1st round PCR products of one sample were tagged with one of the 48 indices. All samples belonging to the same experiment were sequenced in the same lane. If the diversity of 48 index sequences and the number of samples per experiment allowed, multiple experiments were combined in one lane. Primers used in the second round PCR (30 cycles: 5'' 94°C; 5'' 57.2°C; 5'' 72°C) were according to the scheme: forward (5'-P7-seq_prim-index-CAGGCGCTTAGGATCC-3'), reverse (5'-P5-TGCTGCCGTCAACTAGAACA-3'). A list of the 48 index sequences is provided in Table S1. They were designed in a way that all indices differ by at least 2 bp, so that potential errors during amplification or sequencing leading to single-base changes within the index would not result in assignment of the read to a wrong sample.

After tagging all barcodes belonging to the same sample with a unique index, the second round PCR products of all samples meant for deep sequencing within the same lane were mixed at equal volumes. Subsequently, PCR products of the expected length (222bp) were purified from an e-gel (iBase, Invitrogen) and sequenced on GAIIx or HiSeq2000 platforms (Illumina). Total read lengths were 40 bp (GAIIx) or 50-60 bp (HiSeq2000), of which the first 22 bp consisted of the index and constant regions. The following 15 bp were used to distinguish between the different barcodes.

Controls in cellular barcoding experiments. To test whether the amount of template DNA per barcodes is large enough for reproducible barcode detection and quantification, in all experiments, each sample was divided in two half-samples that were independently amplified and sequenced (sampling controls[14]). A second essential control is the barcode distribution control[14], which tests the probability of two naïve T cells within the same mouse harboring the same barcode. If this would be the case, the progeny of these two founders could not be distinguished and would therefore faultily be analyzed as being one single family. The probability of such barcode sharing within the naïve T cell population can be estimated by determining the barcode overlap between two different mice[3,12-14].

Analysis of sequencing data. Sequence reads were first screened for quality by the software packages that are part of the Illumina pipeline and only high-quality reads were selected (~10-70x10^6 per run). Next, only reads showing a 100% match to the expected scheme: index-CAGGCGCTTAGGATCC-random_sequence were selected (typically >90% of reads), whereby a 100% match to one of the 48 index sequences was required. Of the random sequence (the barcode), only the first 15 bp were considered. To filter out reads that reflect PCR or sequencing errors within the 15 bp barcode region, all remaining reads were compared to a barcode reference list, and only sequences that showed a 100% match to one of the listed sequences were selected (typically 80-93%). Subsequently, total read numbers per (half-)sample were normalized (always downscaled) to 100,000 reads, which enables direct comparison of read numbers per (half-)sample. As an additional way to reduce noise, all barcodes of which the average of the two corresponding half-samples represented <0.0005% of the total reads (<0.5 reads out of 100'000) were excluded from further analysis. This filtering step removed on average 0.04% of the remaining reads.

OT-I T cell family sizes are depicted either as percentage of the total response size or as absolute number of GFP^+ (barcode-labeled) cells, obtained by multiplying the percentage of reads for a given barcode with the total number of GFP^+ cells isolated.

If barcode abundance is presented in dot-plots, half-samples are depicted separately (sample A and B) and read counts of '0' are set to '0.05' to allow their visualization in log-scale plots. Original '0' values are used in all calculations.

To calculate the # of expected cells harboring a particular barcode (as done in Fig. S1), the total read number of all samples was normalized to 10,485,750 (=the total number of cells in the input sample).

Statistical analyses were performed using the 2-sided exact Wilcoxon test when 2 groups were compared and the 2-sided exact Jonckheere-Terpstra test when 3 groups were compared. Probabilities were considered significant if <0.05. Analyses were performed with Cytel Studio StatXact software.

Generation of the barcode reference list. To distinguish between barcode sequences that are present within the library and sequences that are the result of PCR or deep-sequencing errors, we created a barcode reference list by deep-sequencing the barcode-library twice. After normalizing the total number of reads between both samples, all sequences that were detected in both samples were sorted by frequency. A dominant sequence that constituted approximately 15% of total reads and thereby presumably reflected a bias introduced in original library generation was discarded, as the likelihood of random sharing between mice would be high. Likewise, sequences that deviated only 2bp from this barcode (and could therefore be the result of errors created during the PCR of this sequence) were removed from the list. In this analysis >40'000 sequences were observed, of which >90% were very infrequent (Fig. S8A). As sequence/PCR errors are infrequent relative to the parental sequences, it should be possible to distinguish these by plotting the cumulative read number as a function of the number of sequences observed. As expected, we observed a steep change in the slope of the curve (indicating a substantial shift in the contribution subsequent barcodes made to the total pool of sequences), and only the highly prevalent sequences were present in both half samples at a ratio close to 1 (Fig. S8B). Sequences that cumulatively made up 92.5% of the reads (right of the vertical line in Fig. S8A+B) and those that were maximally 1.5-fold more prevalent in one of the two samples (two horizontal lines in Fig. S8B) were selected for the generation of the reference list. These cut-offs are chosen relatively stringent, so that library diversity might be slightly underestimated. In this way, a total of 2608 sequences were selected to constitute the barcode reference file. This is in line with the estimated size of the barcode-library, which was originally constructed from 4,743 clones[12] and is likely to have lost diversity during subsequent cloning steps.

ACKNOWLEDGEMENTS

We thank F. van Diepen and A. Pfauth for FACS sorting, E. Borg for technical assistance and Dr. D. Zehn for the provision of the LM-N4/Q4/T4-OVA strains.

REFERENCES

1. Obar, J. J., Khanna, K. M. & Lefrancois, L. Endogenous naive CD8+ T cell precursor frequency regulates primary and memory responses to infection. *Immunity* 28, 859-869 (2008).
2. Blattman, J. N. *et al.* Estimating the precursor frequency of naive antigen-specific CD8 T cells. *J. Exp. Med.* 195, 657-664 (2002).
3. van Heijst, J. W. *et al.* Recruitment of antigen-specific CD8+ T cells in response to infection is markedly efficient. *Science* 325, 1265-1269 (2009).
4. Murali-Krishna, K. *et al.* Counting antigen-specific CD8 T cells: a reevaluation of bystander activation during viral infection. *Immunity* 8, 177-187 (1998).
5. Butz, E. A. & Bevan, M. J. Massive expansion of antigen-specific CD8+ T cells during an acute virus infection. *Immunity* 8, 167-175 (1998).
6. Hasbold, J. *et al.* Quantitative analysis of lymphocyte differentiation and proliferation in vitro using carboxyfluorescein diacetate succinimidyl ester. *Immunol. Cell Biol.* 77, 516-522 (1999).
7. Gett, A. V. & Hodgkin, P. D. Cell division regulates the T cell cytokine repertoire, revealing a mechanism underlying immune class regulation. *Proc. Natl. Acad. Sci. U S A* 95, 9488-9493 (1998).
8. Veiga-Fernandes, H., Walter, U., Bourgeois, C., McLean, A. & Rocha, B. Response of naive and memory CD8+ T cells to antigen stimulation in vivo. *Nat. Immunol.* 1, 47-53 (2000).
9. Stoll, S., Delon, J., Brotz, T. M. & Germain, R. N. Dynamic imaging of T cell-dendritic cell interactions in lymph nodes. *Science* 296, 1873-1876 (2002).
10. Miller, M. J., Safrina, O., Parker, I. & Cahalan, M. D. Imaging the single cell dynamics of CD4+ T cell activation by dendritic cells in lymph nodes. *J. Exp. Med.* 200, 847-856 (2004).
11. Schumacher, T. N., Gerlach, C. & van Heijst, J. W. Mapping the life histories of T cells. *Nat. Rev. Immunol.* 10, 621-631 (2010).
12. Hawkins, E. D., Markham, J. F., McGuinness, L. P. & Hodgkin, P. D. A single-cell pedigree analysis of alternative stochastic lymphocyte fates. *Proc. Natl. Acad. Sci. U S A* 106, 13457-13462 (2009).
13. Stemberger, C. *et al.* A single naive CD8+ T cell precursor can develop into diverse effector and memory subsets. *Immunity* 27, 985-997 (2007).
14. Schepers, K. *et al.* Dissecting T cell lineage relationships by cellular barcoding. *J. Exp. Med.* 205, 2309-2318 (2008).
15. Gerlach, C. *et al.* One naive T cell, multiple fates in CD8+ T cell differentiation. *J. Exp. Med.* 207, 1235-1246 (2010).
16. Shendure, J. & Ji, H. Next-generation DNA sequencing. *Nat. Biotechnol.* 26, 1135-1145 (2008).
17. Voelkerding, K. V., Dames, S. A. & Durtschi, J. D. Next-generation sequencing: from basic research to diagnostics. *Clin. Chem.* 55, 641-658 (2009).
18. Kircher, M. & Kelso, J. High-throughput DNA sequencing--concepts and limitations. *Bioessays* 32, 524-536 (2010).
19. Zhou, X. *et al.* The next-generation sequencing technology and application. *Protein Cell* 1, 520-536 (2010).
20. Gerlach, C., van Heijst, J. W. & Schumacher, T. N. The descent of memory T cells. *Ann. N Y Acad. Sci.* 1217, 139-153 (2011).
21. Acuto, O. & Michel, F. CD28-mediated co-stimulation: a quantitative support for TCR signalling. *Nat. Rev. Immunol.* 3, 939-951 (2003).
22. Zehn, D., Lee, S. Y. & Bevan, M. J. Complete but curtailed T-cell response to very low-affinity antigen. *Nature* 458, 211-214 (2009).
23. Savage, P. A., Boniface, J. J. & Davis, M. M. A kinetic basis for T cell receptor repertoire selection during an immune response. *Immunity* 10, 485-492 (1999).
24. Trautmann, L. *et al.* Selection of T cell clones expressing high-affinity public TCRs within Human cytomegalovirus-specific CD8 T cell responses. *J. Immunol.* 175, 6123-6132 (2005).
25. Kedl, R. M., Kappler, J. W. & Marrack, P. Epitope dominance, competition and T cell affinity maturation. *Curr. Opin. Immunol.* 15, 120-127 (2003).
26. Topham, D. J., Castrucci, M. R., Wingo, F. S., Belz, G. T. & Doherty, P. C. The role of antigen in the localization of naive, acutely activated, and memory CD8(+) T cells to the lung during influenza pneumonia. *J. Immunol.* 167, 6983-6990 (2001).

SUPPLEMENTARY MATERIAL

Table S1: List of 48 index sequences.

index number	index sequence						
1	ACACAG	13	TGCTAC	25	GTCAGT	37	CACATC
2	TCACGA	14	TGCTCT	26	GTCATG	38	CACAGA
3	TCAGCT	15	AGTGCT	27	GTCTAC	39	AGTGTC
4	ACAGTG	16	CACACT	28	GTCTCA	40	AGTCGA
5	TCGACT	17	CAGAGT	29	CTGTGT	41	AGTCAC
6	TCGAGA	18	CAGATG	30	CTGACA	42	AGCTGA
7	TCGATC	19	GATCGA	31	CTACGA	43	AGCATC
8	ACGTAG	20	CATCTG	32	CATGTC	44	AGAGCA
9	ACTCTG	21	GATGCT	33	CATCAC	45	ACTGAC
10	TGACTG	22	GTACAC	34	CAGTGA	46	ATACGC
11	TGAGAC	23	GTACTG	35	CAGTAC	47	ATAGCG
12	AGCACT	24	GTAGCA	36	CACTCA	48	ATCACG

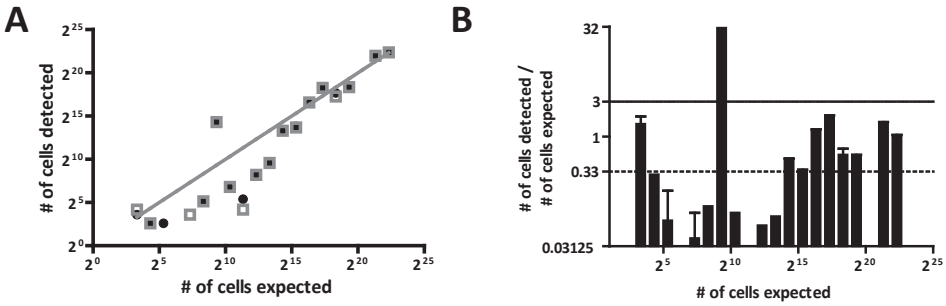

Figure S1: Representative quantification of barcode abundances by deep sequencing. Two identical mixes of different cell numbers of single-barcode clones were analyzed by deep sequencing. The detected barcode frequencies were compared to the expected frequencies, which are based on the input number of cells. (**A**) Each dot represents one barcode in the first measurement and each square the second measurement. The line marks the position where the # of cells detected equals the # of cells expected. (**B**) Ratio between the detected and expected cell numbers per barcode.

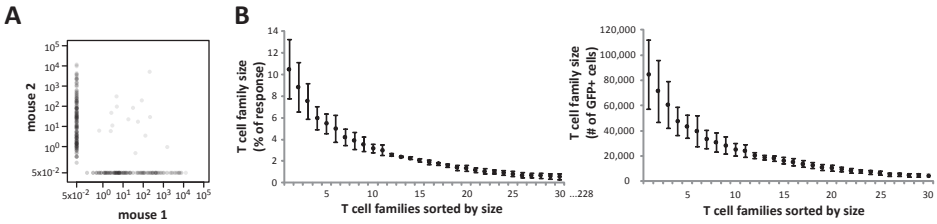

Figure S2: T cell responses are dominated by the progeny of few naïve T cells. Same experiment as depicted in Fig. 1. (**A**) Representative distribution control. The graph depicts the number of reads (out of 100'000) per detected barcode for 2 different mice. Each dot corresponds to one barcode. (**B**) Average OT-I T cell family sizes (+/- SD) of the largest 30 families out of an average total of 228 participating families.

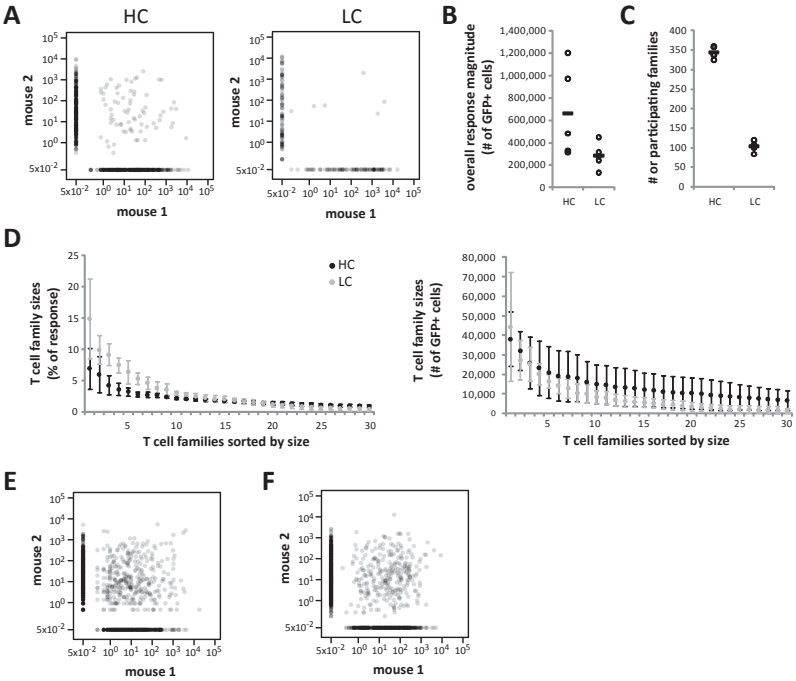

Figure S3: T cell family size disparity in OT-I rag2$^{-/-}$ T cell responses and as a function of naïve T cell frequency. (A-D) Same experiment as in Fig. 2A-C. HC: high cell numbers (760); LC: low cell numbers (190). (**A**) Representative distribution control. The graph depicts the number of reads (out of 100'000) per detected barcode for 2 different mice. Each dot corresponds to one barcode. (**B**) Overall response magnitude per group. Circles represent individual mice; bars averages. (**C**) Number of participating OT-I families per group. Circles represent individual mice; bars averages. (**D**) Average OT-I T cell family sizes (+/- SD) of the largest 30 families. **(E)** Same experiment as in Fig. 2D-F. Representative distribution control. On average 955 barcodes were detected. **(F)** Same experiment as in Fig. 2G-I. Representative distribution control. On average 804 barcodes were detected.

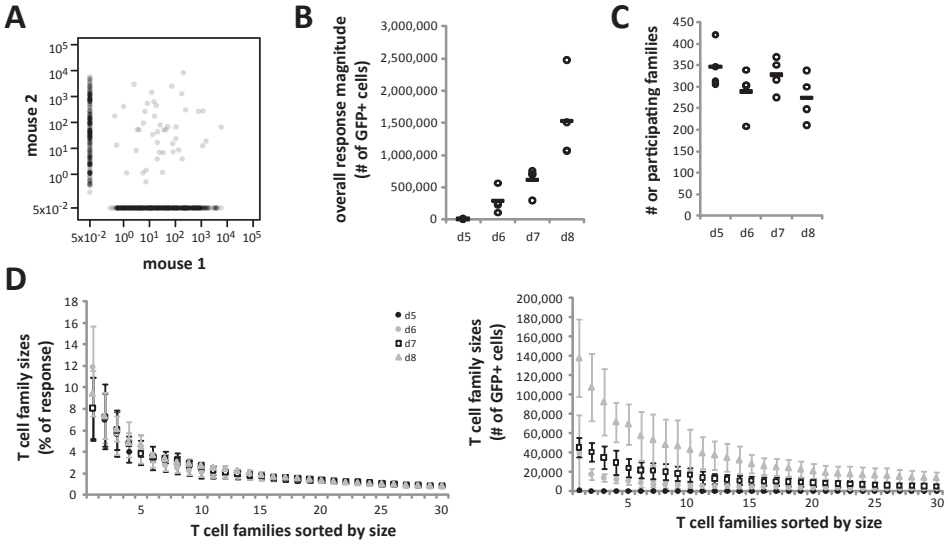

Figure S4: Differences in T cell family sizes are already observed early during the response. Same experiment as in Fig. 3. (**A**) Representative distribution control. The graph depicts the number of reads (out of 100'000) per detected barcode for 2 different mice. Each dot corresponds to one barcode. (**B**) Overall response magnitude per group. Circles represent individual mice; bars averages. (**C**) Number of participating OT-I families per group. Circles represent individual mice; bars averages. (**D**) Average OT-I T cell family sizes (+/- SD) of the largest 30 families.

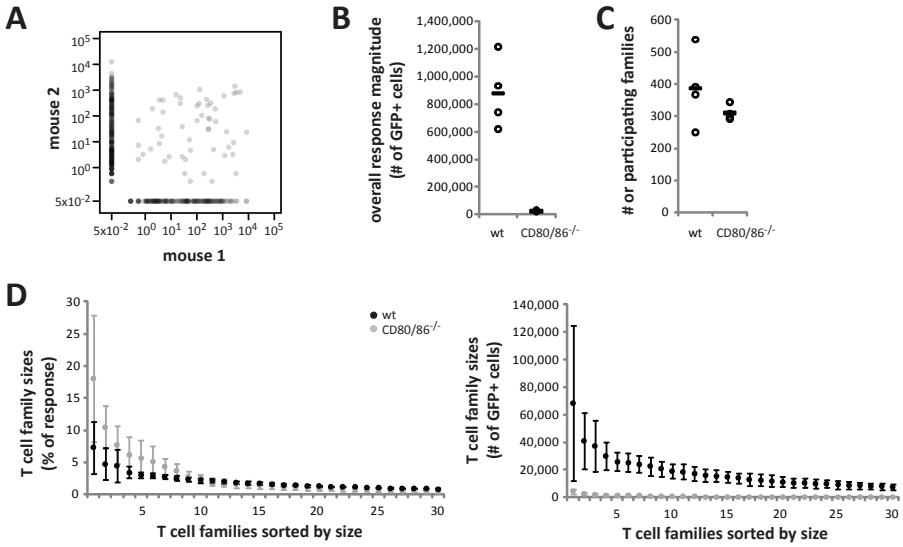

Figure S5: CD80/CD86-mediated costimulation influences the disparity in T cell family sizes. Same experiment as in Fig. 5. (**A**) Representative distribution control. The graph depicts the number of reads (out of 100'000) per detected barcode for 2 different mice. Each dot corresponds to one barcode. (**B**) Overall response magnitude per group. Circles represent individual mice; bars averages. (**C**) Number of participating OT-I families per group. Circles represent individual mice; bars averages. (**D**) Average OT-I T cell family sizes (+/- SD) of the largest 30 families.

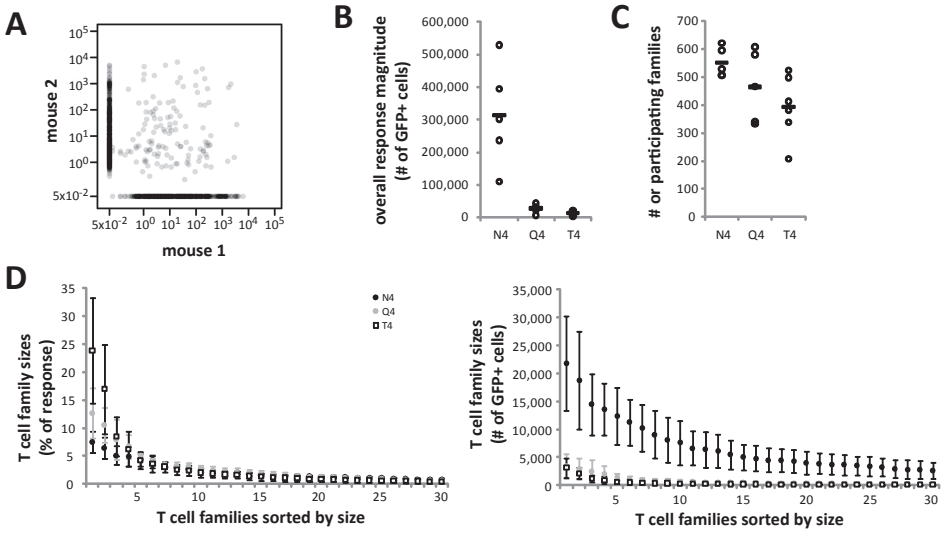

Figure S6: The dominance of a few T cell families is more pronounced in response to lower affinity antigens. Same experiment as in Fig. 5. (**A**) Representative distribution control. The graph depicts the number of reads (out of 100'000) per detected barcode for 2 different mice. Each dot corresponds to one barcode. (**B**) Overall response magnitude per group. Circles represent individual mice; bars averages. (**C**) Number of participating OT-I families per group. Circles represent individual mice; bars averages. (**D**) Average OT-I T cell family sizes (+/- SD) of the largest 30 families.

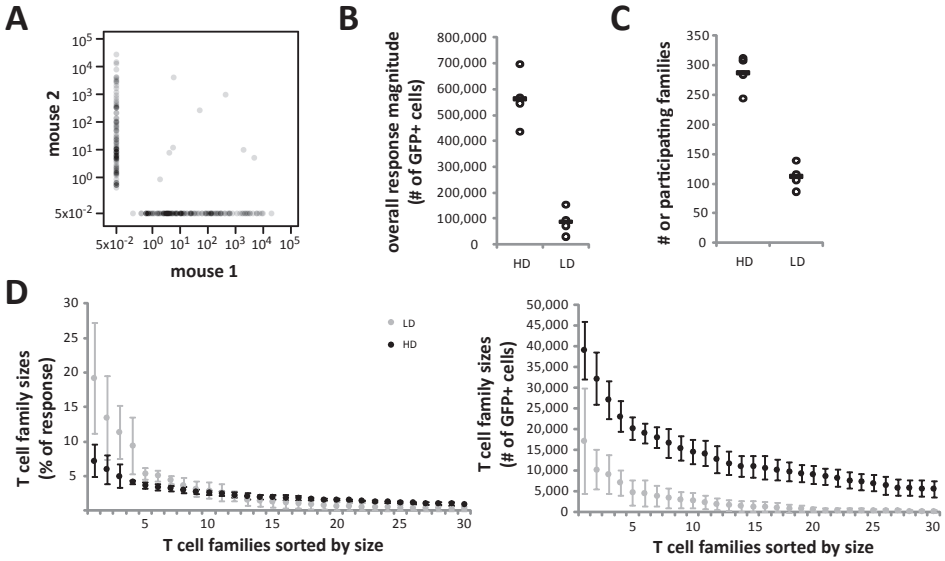

Figure S7: Lower antigen doses increase the inequality in T cell family sizes. Same experiment as in Fig. 5. HD: high dose (25'000 CFU); LD: low dose (500 CFU). (**A**) Representative distribution control. The graph depicts the number of reads (out of 100'000) per detected barcode for 2 different mice. Each dot corresponds to one barcode. (**B**) Overall response magnitude per group. Circles represent individual mice; bars averages. (**C**) Number of participating OT-I families per group. Circles represent individual mice; bars averages. (**D**) Average OT-I T cell family sizes (+/- SD) of the largest 30 families.

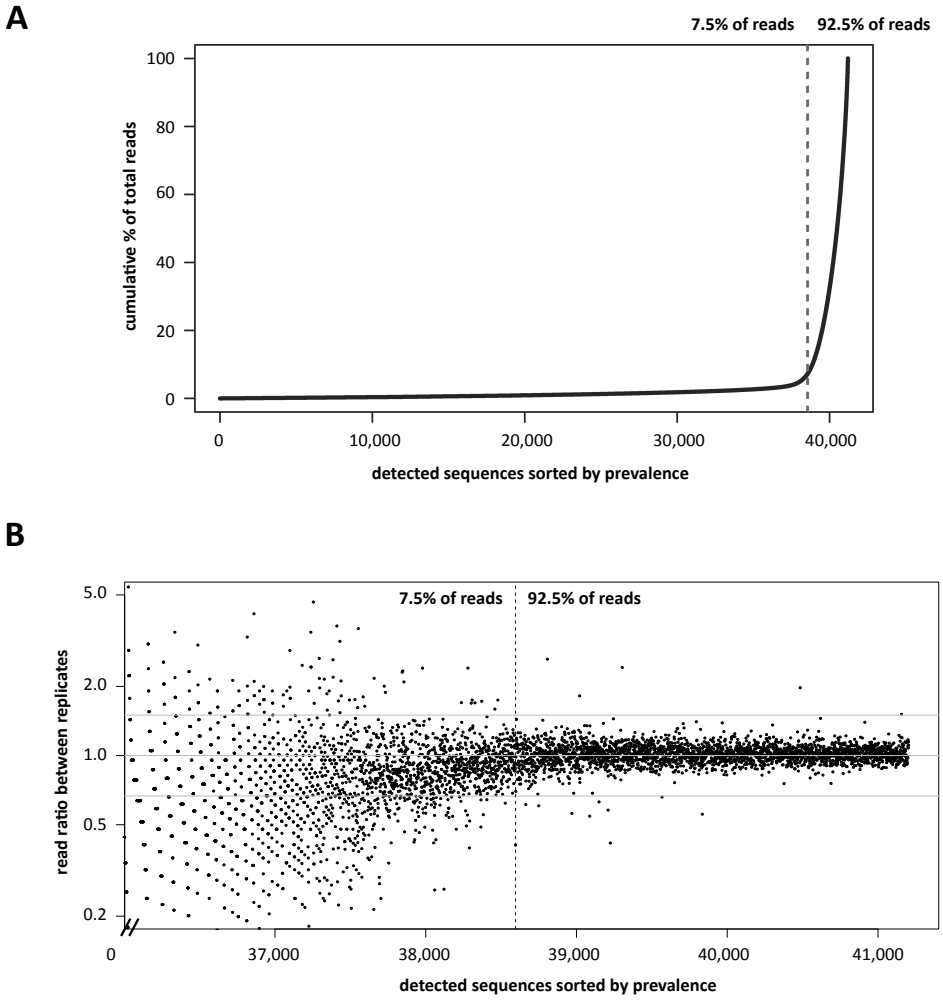

Figure S8: Generation of the barcode reference file. The barcode library was sequenced twice and the normalized reads of both samples are depicted. (**A**) Cumulative number of reads represented as a % of the total read count (100'000) per detected sequence. Vertical line represents the cut-off between 'noise' and 'real barcodes'. (**B**) Read ratio between both samples depicted per detected sequence. Each dot represents one detected sequence. Detected sequences are sorted by size and only the most prevalent ones are depicted (at least 36'000th position). The vertical line represents the cut-off between 'noise' and 'real barcodes'. The middle horizontal line indicates a read ratio of 1, the upper of 1.5 and the lower of 0.333. The outer two lines mark the second cut-off between 'noise' and 'real barcodes'.

9

SUMMARY AND GENERAL DISCUSSION

SUMMARY

This thesis describes the development and use of a novel technology for single-cell fate mapping, called cellular barcoding (**chapter 4**). The use of this technology allowed us to address multiple questions aimed at the acquisition of detailed knowledge on several aspects of T cell differentiation:

I) *Do individual T cell clones produce both effector and memory subsets?* By comparing the presence of unique genetic tags (barcodes) in antigen-specific effector and memory T cell populations in systemic and local infection models, at different anatomical sites and for TCR – pMHC interactions of different avidities, we revealed that under all conditions tested, individual naïve T cells yield both effector and memory $CD8^+$ T cell progeny (**chapter 5**). This indicates that naïve T cells are not yet committed to an effector or memory fate and thus that the decision to develop into either subset is not taken before the first cell division.

II) *Do T cells commit early in the response to a short-lived effector or a long-lived memory fate?* By providing the first three daughter generations with unique barcodes and subsequently analyzing their fate in infection-matched recipients, we found that under these experimental conditions the vast majority of the cells is not yet committed towards either a short- or long-lived fate (**chapter 6**). These data show that asymmetry of the first cell division, which was recently suggested to be the fate determining event[1], is unlikely to be responsible for imprinting effector and memory fates. Instead, the decision between longevity or death after antigen clearance appears to be a relatively late event after T cell activation and might require signals acquired by more downstream progeny.

III) *How is the magnitude of the T cell response regulated?* Using the cellular barcoding technology, we could measure whether the fraction of naïve T cells recruited into the response, and thereby the clonal composition of the response, changed depending on the severity of infection. We demonstrated that independent of the pathogen and its dose, recruitment of naive T cells into the response was near constant. Furthermore, recruitment was shown to be close to complete upon high-dose *Listeria monocytogenes* infection (**chapter 7**). This shows that in spite of their scarcity, antigen-specific T cells are recruited very efficiently, and that the magnitude of antigen-specific $CD8^+$ T cell responses is therefore primarily controlled by clonal expansion.

IV) *To what extent do individual naïve T cells contribute to the overall response?* Second-generation sequencing of barcodes demonstrated that individual naïve T cells produce highly variable numbers of daughter cells after *Listeria monocytogenes* infection, in spite of the fact that these T cells harbor the same TCR (**chapter 8**). The disparity in progeny sizes increased when T cells were activated by low affinity antigen.

Our data are consistent with a model in which the expansion of each individual antigen-specific T cell clone is influenced by signals received early during T cell activation.

GENERAL DISCUSSION

Fate mapping by cellular barcoding – strengths and limitations

Many aspects of T cell responses have been elucidated after following the behavior of transferred antigen-specific T cell populations that could be distinguished from the host by the expression of fluorescent or congenic markers. However, as with a group of humans, not necessarily all members of a group of cells behave in a uniform manner. Understanding T cell differentiation into divergent subsets therefore requires technologies to track the behavior of single cells rather than cell populations.

Since the advent of intra-vital microscopy, single cells have been tracked *in vivo*. The potential of this technology is however limited to a spatially confined area and a relatively short time frame, and motile cells are likely to migrate out of the imaging field. In 2007, the group of D. Busch described a single-cell transfer technology that allowed a single congenically marked antigen-specific T cell and its progeny to be followed over time *in vivo*[2]. Recently, this system has been refined to enable simultaneous tracking of up to 8 single cells that can be identified by a unique combination of congenic markers (D. Busch, personal communication). Development of the cellular barcoding technology has provided the means to perform *in vivo* single-cell fate mapping on a much larger scale. As this technology utilizes the introduction of unique DNA sequences (barcodes) to mark individual cells, the multitude of single-cell behaviors that can be assessed simultaneously is only limited by the diversity of barcode sequences available for cell labeling. Currently, hundreds of cells and their progeny can be distinguished within one mouse by cellular barcoding.

As a downside to the identification of T cells by DNA tags, each cell can only be analyzed once, as it has to be lysed to allow access to its DNA for barcode amplification. After single-cell transfer, individual T cells can theoretically be analyzed and sorted by flow cytometry and subsequently be re-injected for further tracking, although this is practically very challenging due to the small cell numbers. Clearly, intra-vital microscopy is the most suited technology to follow the exact same cell over time, although the time span during which this can be realized is relatively short. Also events occurring early after T cell activation can best be monitored by microscopy, as the two other technologies require some extent of clonal expansion before the progeny of the initially labeled cell can be detected either by flow cytometry or barcode analysis. The sensitivity of barcode detection has recently been improved by implementation of a new PCR protocol and second-generation sequencing as readout system. Nevertheless, efficient isolation of the transferred cells from the tissues remains a crucial step in both the single-cell transfer and the barcoding system.

Since barcode-labeling occurs by retroviral transduction, the barcoding technique brings with it the concern that the site of retroviral integration might influence

the behavior of the cell. This is something we cannot rule out, although it seems unlikely on the basis of theoretical arguments. Retroviral integrations occur at roughly random locations and as we are dealing with only ~400 integrations in each mouse (in each mouse ~400 uniquely labeled T cells are tracked), the chance is low that part of these barcodes would integrate in regions whose disruption would result in changes in T cell differentiation or proliferation. Furthermore, the observation that single naïve T cells give rise to both effector and memory cells and that the progeny sizes of different T cells are distinct was made both with our barcoding technology (chapter 5 and 8) and with the single-cell transfer system. If retroviral barcode integration would have substantially influenced T cell differentiation or proliferation, we would have obtained results distinct to those acquired after the transfer of single, untransduced T cells. To alleviate any concerns about the effect of retroviral integrations while maintaining the capacity for large-scale cell fate analysis, one could track the fate of cells that are marked by an endogenously generated barcode. Such barcoding without the need of retroviral transduction occurs in the BCM mouse that was recently developed in our lab by Jeroen van Heijst and Jos Urbanus. This mouse uses the Rag1, Rag2 and TdT enzymes to generate random barcodes at the junction of V, D and J gene segments that had been introduced into the Rosa 26 locus (unpublished).

The time of fate decisions

We (chapter 5) and others[2] have demonstrated that naïve T cells are not yet committed to a short-lived effector or long-lived memory fate, as individual antigen-specific naïve T cells produce both types of progeny *in vivo*. In my opinion, this one naïve cell – multiple fates mechanism makes a lot of sense in terms of host defense. It provides the host with both effector and memory cells of each activated clone and thereby ensures that those clones that are effective in the acute clearance of the pathogen will be preserved to provide protection upon renewed infection.

Our more recent experiments (chapter 6) furthermore provide evidence that short-lived and long-lived fates are not adopted until the 3rd cell division, as cells that had undergone 3 cell divisions produced both short-lived and long-lived progeny. This finding is in direct contrast with the claim that effector or memory commitment occurs during the 1st cell division through asymmetry of the division[1]. How can these seemingly opposed findings be explained? I consider the experimental data showing asymmetric partitioning of several molecules (including CD8) during the initial cell division to be strong[1,3,4] and they have been confirmed by an independent research group (E. Palmer, presentation at the NVVI Lunteren meeting 2011). Asymmetric inheritance of molecules does however not necessarily result in the acquisition of distinct fates.

The claim that asymmetric cell division produces one committed effector daughter and one committed memory daughter is based on an experiment in which 1x divided T cells were sorted into CD8^{hi} and CD8^{lo} populations (the putative effector and memory daughters respectively) that were then transferred into distinct recipient mice. Subsequently, the potential of both populations to reduce bacterial burden

after re-infection was assessed. When re-infection occurred 30 days after initial T cell activation, the CD8^{lo} (assumed memory) population was superior in reducing the amount of bacteria. Nevertheless, both populations provided significant protection relative to naïve mice. If all transferred CD8^{hi} cells would have been committed short-lived effector cells, they would have died by day 30 and thus been unable to provide protection at that time.

Other studies proposing short-lived and long-lived fates to be acquired early during the response relied on the transfer of sorted cell populations that expressed different levels of KLRG-1 or CD25 at ~4 days after infection[5-7]. The potential of these populations to survive long-term was shown to be different, but again the outcome was not absolute. Cell numbers of the putative short-lived cells were reduced 5 to 12-fold by 2 months after transfer, but clearly not all cells had died.

In my opinion, none of these studies therefore provides evidence for early fate commitment. Accordingly, I do not think that our data oppose those of Chang *et al.* or the other research groups. Instead of demonstrating fate commitment early during the response, these studies show that one of the two transferred cell populations gives rise to relatively larger numbers of long-lived memory cells. This could indicate the existence of two committed cell populations that are not accurately separated by CD8, KLRG-1 and CD25 expression profiles, but as we did not observe any fate commitment early during the response in our barcoding experiments, I consider this explanation unlikely. Probably, the observed difference in longevity reflects a 'bias' in the sorted populations to preferentially produce long-lived or short-lived progeny. A relatively minor bias is something we could not detect in our experiments, as the microarray-based barcode readout system only allowed us to visualize relatively large differences in barcode abundance between two populations of interest. It will be interesting to re-analyze these data with our new readout system that applies second-generation sequencing to quantify barcode sequences. Such analysis will reveal whether after a few cell divisions, some antigen-specific T cells produce relatively more long-lived progeny than others.

It can be argued that we did not observe any early fate commitment in our experiments, because an early imprinted fate could have been reset in (part of) the lymphocytes when they were isolated from their *in vivo* niche to introduce the barcode sequences. The same argument applies for the data of Chang *et al.* though, who isolated antigen-specific cells few days after activation for cell sorting. Formally, it therefore remains possible that effector and memory fates are imprinted into the different daughter cells during an asymmetric 1st cell division, but so far, this has not been shown unambiguously in experiments.

My interpretation of the currently available data is that antigen-reactive T cells accumulate a multitude of external signals throughout the course of the immune response – including those delivered during asymmetric cell division - and that the integration of these signals shapes the likelihood of the cells and their progeny to die or stay alive after pathogen clearance.

Recruitment of antigen-specific T cells into the response and the extent of their clonal expansion

In chapter 7 we conclude that 'Recruitment of antigen-specific CD8$^+$ T cells in response to infection is markedly efficient'[8]. One year later, La Gruta *et al.* state that: 'Primary CTL response magnitude in mice is determined by the extent of naïve T cell recruitment and subsequent clonal expansion'[9]. Unlike it might seem from these titles, both sets of data demonstrate that high-avidity CD8$^+$ T cells are efficiently recruited into the response to strong infections. This does not imply that recruitment into the response is equal under all conditions. Indeed, we found the efficiency of naïve T cell recruitment to be reduced by a factor of ~1.5, if T cells were stimulated by lower antigen doses, for shorter durations (chapter 7), by lower affinity antigens or in the absence of CD80 and CD86-mediated costimulation (chapter 8). La Gruta *et al.* found that for one of the two subdominant clones studied, only about one third of the MHC-tetramer-binding T cells had entered cell cycle by day 5. The capacity to bind MHC-tetramers and to proliferate upon antigen stimulation is however not the same. All antigen-responsive T cells usually bind tetramer, but the opposite is not necessarily true. T cells harboring TCRs of low antigen affinity might be able to bind tetramer, but not to proliferate after stimulation with a given antigen dose[10]. This means that in the study of La Gruta *et al.*, possibly not all of the tetramer-binding T cells could actually respond to the infection. In this case, the recruitment efficiency would have been underestimated.

If one nevertheless assumes that MHC-tetramer binding has accurately identified only antigen-reactive cells, these experiments would indicate a ~3-fold reduction in recruitment efficiency for one of the subdominant clones. The reduction in recruitment efficiency accounted in both studies however for only a minor part of the 10-30-fold reduction in overall response magnitude, demonstrating that the magnitude of the total antigen-specific response is primarily regulated by the average expansion that the antigen-specific clones undergo.

It has been estimated that CD8$^+$ T cells divide on average up to 14 times in response to LCMV infection[11,12], but the behavior of a group of cells does not imply that all members of the group display uniform behavior. While we demonstrated in chapter 5 that individual antigen-specific T cells behave similar in the sense that they produce both effector and memory progeny, we showed in chapter 8 that the amount of progeny per recruited cell is highly variable, even though the tracked cells possessed the same TCR. As a result of this, T cell responses were dominated by merely a fraction of the antigen-specific clones.

From this observation the question arises what the consequences of this dominance are for host defense. If all clones of similar TCR affinity for antigen were functionally comparable, one could argue that the exact clonal composition of the response (among cells with the same TCR) is irrelevant. Preliminary data of the group of D. Busch however indicate that clones harboring the same TCR differ in cytokine production and phenotype (D. Busch, personal communication). Therefore I consider it relevant to investigate whether there is a relation between clone size and cytotoxicity or cytokine

production. Experiments addressing this issue could be performed both by cellular barcoding and the single-cell transfer system. Using cellular barcoding, one could sort T cell populations producing different cytokines and subsequently assess whether the same order of clone sizes is found in both sorted populations. By performing this analysis on a large set of mice, one could establish whether particular functions are associated with clone size. Alternatively, donor T cell function and clone sizes could be compared in different recipients of single antigen-specific T cells.

So far, we have quantified T cell clone sizes only in secondary lymphoid organs. As it has been described that low-avidity T cells exit the priming lymph node prior to high-avidity clones[13], it would be appealing to assess whether in particular early after infection the distribution of clone sizes at a local effector site is different from the distribution in secondary lymphoid organs. If also some of the clones with TCRs of identical antigen affinity would leave the lymph node at an earlier time than others, these could dominate the early response at the effector site, while others could constitute the largest fraction in the lymph nodes. Knowing that functional and phenotypical differences exist between clones harboring the same TCR, it would furthermore be interesting to investigate whether potential differences in the preferential localization of the clones would be related to particular functional properties.

Our finding that the disparity in clone sizes is more pronounced in response to reduced T cell stimulation raises the question how vaccine-induced T responses are composed. Vaccines are usually less potent inducers of immune responses than infections with live bacteria, as used in our study in chapter 8. Does this mean that the dominance of a few clones is even more pronounced in vaccine-induced responses? Whether this is the case or not, the main remaining question is whether an increased clonal dominance correlates with a reduced potential to clear a pathogen. If so, I argue that in order to improve vaccine efficacy, one should aim to increase the expansion of the small clones. Obviously, this requires knowledge of the mechanisms underlying the unequal expansion of the antigen-specific clones, which should therefore be a focus of further research.

REFERENCES

1. Chang, J. T. *et al.* Asymmetric T lymphocyte division in the initiation of adaptive immune responses. *Science* 315, 1687-1691 (2007).
2. Stemberger, C. *et al.* A single naive CD8+ T cell precursor can develop into diverse effector and memory subsets. *Immunity* 27, 985-997 (2007).
3. Oliaro, J. *et al.* Asymmetric cell division of T cells upon antigen presentation uses multiple conserved mechanisms. *J. Immunol.* 185, 367-375 (2010).
4. Chang, J. T. *et al.* Asymmetric proteasome segregation as a mechanism for unequal partitioning of the transcription factor T-bet during T lymphocyte division. *Immunity* 34, 492-504 (2011).
5. Sarkar, S. *et al.* Functional and genomic profiling of effector CD8 T cell subsets with distinct memory fates. *J. Exp. Med.* 205, 625-640 (2008).
6. Kalia, V. *et al.* Prolonged interleukin-2Ralpha expression on virus-specific CD8+ T cells favors terminal-effector differentiation in vivo. *Immunity* 32, 91-103 (2010).
7. Joshi, N. S. *et al.* Inflammation directs memory precursor and short-lived effector CD8(+) T cell fates via the graded expres-

sion of T-bet transcription factor. *Immunity* 27, 281-295 (2007).

8. van Heijst, J. W. *et al.* Recruitment of antigen-specific CD8+ T cells in response to infection is markedly efficient. *Science* 325, 1265-1269 (2009).
9. La Gruta, N. L. *et al.* Primary CTL response magnitude in mice is determined by the extent of naive T cell recruitment and subsequent clonal expansion. *J. Clin. Invest.* 120, 1885-1894 (2010).
10. Bouneaud, C., Kourilsky, P. & Bousso, P. Impact of negative selection on the T cell repertoire reactive to a self-peptide: a large fraction of T cell clones escapes clonal deletion. *Immunity* 13, 829-840 (2000).
11. Blattman, J. N. *et al.* Estimating the precursor frequency of naive antigen-specific CD8 T cells. *J. Exp. Med.* 195, 657-664 (2002).
12. Butz, E. A. & Bevan, M. J. Massive expansion of antigen-specific CD8+ T cells during an acute virus infection. *Immunity* 8, 167-175 (1998).
13. Zehn, D., Lee, S. Y. & Bevan, M. J. Complete but curtailed T-cell response to very low-affinity antigen. *Nature* 458, 211-214 (2009).

&

NEDERLANDSE SAMENVATTING

CURRICULUM VITAE

LIST OF PUBLICATIONS

NEDERLANDSE SAMENVATTING

Deze samenvatting heeft tot doel om in niet-specialistische taal het onderwerp van dit proefschrift uit te leggen, hoe het onderzoek daarnaar gedaan is en wat de uitkomsten van het onderzoek zijn.

Kort samengevat heb ik in dit proefschrift onderzocht hoe individuele T-cellen (een bepaald type afweercellen) op een infectie reageren. In het verleden is veel kennis vergaard over de reactie van een grote groep T-cellen op infectie, maar aangezien niet noodzakelijkerwijs elk lid van een groep hetzelfde gedrag vertoont, wilde ik weten in welk opzicht de individuele groepsleden gelijk zijn of verschillen. Immers, de constatering dat Duitsers 'Bratwurst' eten betekent nog niet dat elke Duitser Bratwurst eet, of dat de Duitsers die Bratwurst eten dit tijdens elke maaltijd doen.

Inleiding

Ons lichaam wordt voortdurend blootgesteld aan ziekteverwekkers die meestal via ons voedsel, een ongewassen hand, of een hoest of nies afkomstig van een medemens in onze mond of neus terecht komen. Om te voorkomen dat deze ziekteverwekkers zich zo sterk in ons lichaam vermenigvuldigen dat het niet meer goed kan functioneren bezit het menselijke lichaam een afweersysteem tegen infecties. Dit afweersysteem wordt ook wel het immuunsysteem genoemd en bestaat grotendeels uit witte bloedcellen. Zodra ziekteverwekkers zoals bacteriën, virussen of parasieten ons lichaam binnen dringen komen de cellen van het afweersysteem in actie. B-cellen en T-cellen zijn de bekendste afweercellen, maar het immuunsysteem bestaat uit meer dan 10 verschillende celtypes die allemaal een specialistische rol vervullen en daarbij samenwerken in de afweer tegen infecties. T-cellen zijn onderverdeeld in $CD4^+$ T-cellen ('T-helpercellen') en $CD8^+$ T-cellen ('T-killercellen'). Dit proefschrift richt zich enkel op de reactie van $CD8^+$ T-cellen op een infectie. $CD8^+$ T-cellen staan ook bekend als 'killercellen' omdat ze de eigenschap bezitten om geïnfecteerde lichaamscellen op te sporen en deze vervolgens tot zelfmoord te dwingen. Aangezien virussen en sommige bacteriën zich vermenigvuldigen in geïnfecteerde lichaamscellen is het belangrijk dat deze geïnfecteerde cellen gedood worden, om verspreiding van het virus of de bacterie in ons lichaam te voorkomen.

T-cellen herkennen een geïnfecteerde lichaamscel met behulp van de zogenaamde T-celreceptor, die ook bepaalt welke infectie door deze T cel herkend kan worden (de 'specificiteit' van de T-cel). Niet alle T-cellen kunnen namelijk alle infecties herkennen, integendeel: er is voor elke infectie maar een kleine fractie (ongeveer 0.001%) van alle T-cellen die deze kan herkennen. Dit komt doordat T-cellen een vastgelegde specificiteit hebben, en doordat er talloze verschillende virussen, bacteriën en parasieten bestaan die het afweersysteem allemaal moet kunnen herkennen.

Voor een succesvolle T-cel reactie die tot bestrijding van een infectie leidt is een aantal processen van belang:

I. Eerst moeten de infectie-specifieke 'naïeve' T-cellen geactiveerd worden. Deze cellen moet als het ware verteld worden dat 'hun' infectie plaats heeft gevonden en dat ze daarom in actie moeten komen.
II. De geactiveerde T-cellen (ze zijn nu dus niet meer 'naïef') gaan vervolgens delen om grote aantallen T-cellen te genereren die de infectie kunnen bestrijden.
III. Ook verlaten de geactiveerde T-cellen de lymfeklier en/of de milt waar ze geactiveerd werden om naar de plek in het lichaam te migreren waar de infectie zich bevindt.
IV. Om geïnfecteerde lichaamscellen te kunnen doden moeten de geactiveerde en delende T-cellen nog een ontwikkeling ('differentiatie') tot 'effector'-T-cel doormaken. Alleen effectorcellen kunnen namelijk de moleculen produceren en uitscheiden die de geïnfecteerde lichaamscellen tot zelfmoord kunnen dwingen.
V. Ook maken sommige geactiveerde T-cellen een ontwikkeling door tot 'memory'-T-cel. Terwijl een groot aantal effector-T-cellen sterft nadat de infectie bestreden is blijven enkele geactiveerde T-cellen leven. Deze cellen worden memory-T-cellen of geheugencellen genoemd, aangezien zij de herinnering vormen van de infecties die het lichaam eerder heeft meegemaakt. Zodra er een nieuwe infectie met dezelfde bacterie of hetzelfde virus plaatsvindt, kunnen de memorycellen hier snel op reageren, vaak zonder dat de geïnfecteerde persoon zich ziek voelt. Dit is ook de basis van vaccinatie: vaccinatie creëert memory-T-cellen (en memory-B-cellen) die je beschermen tijdens een toekomstige infectie.

Hoewel we weten dat deze processen cruciaal zijn voor een effectieve afweerreactie, zijn een groot aantal aspecten van de ontwikkeling van T-cel reacties nog steeds onbekend.

Het doel en nut van dit onderzoek

We weten dat het aantal effectorcellen welke we hebben, bepaalt hoe goed we een infectie kunnen bestrijden, en dat het aantal memorycellen bepaalt hoe goed we beschermd zijn tegen herhaalde infecties. Echter het is nog grotendeels onbekend 1) hoe het lichaam de aantallen effector- en memorycellen reguleert en 2) wanneer en hoe memorycellen precies ontstaan.

Kunnen we meer effectorcellen krijgen door T-celactivatie efficiënter te maken? Of is het juist nuttiger om de deling van de effectorcellen te bevorderen om meer effectorcellen te verkrijgen?

Hebben sommige naïeve T-cellen na activatie alleen maar effectorcellen als nakomelingen en andere naïeve T-cellen alleen maar memory-nakomelingen, of ontstaan beide celtypes uit dezelfde naïeve T-cellen? Moeten we dus, als we memorycellen willen genereren, specifiek de naive T-cellen die memory-nakomelingen maken identificeren en daarna activeren, of maakt het niet uit welke naïeve T cellen we activeren aangezien ze toch allemaal memorycellen kunnen produceren?

Het doel van het onderzoek beschreven in dit proefschrift is om deze en andere fundamentele vragen te beantwoorden die betrekking hebben op de grootte van $CD8^+$ T-celreacties en het ontstaan van $CD8^+$ memory-T-cellen. Een gedetailleerde kennis van deze fundamentele processen zal helpen bij de ontwikkeling van nieuwe vaccins of therapieën die erop gericht zijn de T-celreactie te verbeteren. Daarnaast vind ik het ook simpelweg leuk om een complex systeem, zoals het afweersysteem te leren begrijpen.

De onderzoeksvragen

In hoofdstuk 7 stellen we de vraag hoe efficiënt de activatie van T-cellen verloopt. Hoe efficiënt worden de specifieke T-cellen tussen de grote aantallen aspecifieke cellen gevonden en vervolgens geactiveerd? Doet 100% van de specifieke T-cellen mee aan de T-celreactie, of misschien maar 1%? En is dit percentage hetzelfde bij verschillende infecties? Sommige infecties leiden namelijk tot een veel sterkere T-celreactie dan andere. Wij wilden bepalen of dit komt doordat een hoger percentage van de specifieke T-cellen meedoet aan de T-celreactie, of doordat de geactiveerde T-cellen meer nakomelingen hebben.

In hoofdstuk 8 onderzoeken we hoe vergelijkbaar de reacties van individuele T-cellen zijn. We weten dat er enkele honderden T-cellen op een willekeurige infectie kunnen reageren, maar reageren deze cellen allemaal op een uniforme manier? Krijgt iedere geactiveerde T-cel evenveel nakomelingen? Of bestaat het grootste gedeelte van de T-celreactie uit nakomelingen van een paar T-cellen, terwijl er veel meer geactiveerd werden?

De hoofdstukken 3, 5 en 6 gaan over de ontwikkeling van geactiveerde T-cellen tot effector- en memory-T-cellen. Eén van de kernvragen is wanneer een T-cel 'besluit' of hij zich gaat ontwikkelen tot een effectorcel die zeer efficiënt is in het doden van geïnfecteerde lichaamscellen (maar die ook sterft zodra de infectie opgeruimd is), of toch tot een langlevende memorycel die bescherming biedt zodra het lichaam opnieuw besmet raakt met dezelfde infectie? In hoofdstuk 5 onderzoeken we of dit besluit al plaatsvindt op het moment van T-celactivatie. Er bestaan namelijk verschillende theorieën over hoe en wanneer T-cellen in hun ontwikkeling vastleggen wanneer ze een effector- of memorycel worden. Hoofdstuk 3 beschrijft deze theorieën en bespreekt hoe sterk de bewijzen hiervoor zijn. Een van de theorieën stelt dat de sterkte waarmee een T-cel geactiveerd wordt, lotsbepalend is en dus vastlegt of alle nakomelingen van deze cel effector- of juist memory-T-cellen worden. Een andere theorie gaat ervan uit dat direct ná T-celactivatie, dus tijdens de eerste celdeling, bepaald wordt dat de ene dochtercel het effector-lot en de andere het memory-lot toebedeeld krijgt. Dit zou een mechanisme zijn waarmee gegarandeerd kan worden dat tijdens elke infectie effector- en memory-T-cellen gegenereerd worden. Deze theorie onderzoeken we in hoofdstuk 6.

De aanpak

De overeenkomst tussen deze onderzoeksvragen is dat we om een antwoord te vinden het lot van individuele T-cellen gedurende een infectie moeten kunnen volgen. Met de bestaande technieken was dit echter nog niet op grote schaal mogelijk.

Naïeve T-cellen met een unieke barcode

Om het lot van individuele T-cellen te kunnen volgen hebben we dus een nieuwe techniek moeten ontwikkelen, die we 'cellular barcoding' genoemd hebben (hoofdstuk 2+4). Net zoals in de supermarkt elk product een unieke streepjescode (barcode) heeft, krijgen individuele T-cellen met deze techniek een unieke 'barcode'. Deze barcodes zijn DNA-stukjes die we met behulp van een virus in de T-cellen aanbrengen. Sommige virussen kunnen namelijk hun eigen DNA in het DNA van een cel inbrengen. Van deze eigenschap maken we hier gebruik: we verwijderen een groot gedeelte van het virus-DNA en vervangen het door onze barcode-DNA-stukjes. Elk virusdeeltje draagt hierdoor een uniek barcode-DNA-stukje. Als we vervolgens de T-cellen met het barcodevirus in contact brengen, zorgt het virusdeeltje ervoor dat het barcode-DNA in het DNA van de T-cel wordt ingebouwd.

Helaas kunnen de barcode-virusdeeltjes het barcode-DNA alleen inbrengen in delende cellen. Dit vormde initieel een probleem, omdat wij het barcode-DNA in naïeve (dus nog ongeactiveerde) T-cellen wilden inbrengen en naïeve cellen niet delen. Daarom hebben we eerst nog een andere techniek moeten ontwikkelen die het mogelijk maakt om naïeve T-cellen te genereren die wel het barcode-DNA bevatten (hoofdstuk 5). Deze techniek werkt als volgt: we introduceren het barcode-DNA niet direct in T-cellen, maar in de voorlopercellen van naïeve T-cellen, omdat deze voorlopers wel delen. De voorlopercellen bevinden zich in de thymus, een klier boven het hart die ook wel zwezerik genoemd wordt. Om ervoor te zorgen dat elke voorlopercel een unieke barcode meekrijgt, brengen we de voorlopercellen in contact met zo weinig virusdeeltjes dat elke voorlopercel gemiddelt door slechts één virusdeeltje geinfecteerd wordt. Vervolgens moeten de voorlopercellen met barcodes zich verder ontwikkelden tot naïeve T-cel. Dit proces vindt normaalgesproken in de thymus plaats en daarom spuiten we de barcode-bevattende voorlopercellen in de thymus van een muis, zodat ze zich daar in de natuurlijke omgeving kunnen ontwikkelen tot naïeve T-cellen. Zodra de barcode-bevattende voorlopercellen de ontwikkeling tot naïeve T-cel hebben volbracht, isoleren we deze uit de milt en de lymfeklieren van de muis. Zo hebben we wat we wilden – een aantal uniek gelabelde naïeve T-cellen – en kunnen we het lot van individuele T-cellen volgen.

Uit dit laatste stuk wordt duidelijk dat we dit onderzoek niet met menselijke cellen hebben uitgevoerd, omdat we anders barcode-bevattende voorlopercellen in de thymus van een mens hadden moeten spuiten. Aangezien het afweersysteem van gewervelde dieren (inclusieve de mens) sterk op elkaar lijkt, hebben we dit onderzoek uitgevoerd in muizen en met muizencellen.

Barcodes tellen en vergelijken

Om de reactie van individuele T-cellen op een infectie te bestuderen hebben we de barcode-bevattende naïeve T-cellen in het bloed van muizen gespoten, die vervolgens een Listeria- of griepinfectie kregen. Voor deze infecties is gekozen omdat ze door de door ons gebruikte barcode-bevattende T-cellen herkend kunnen worden. Als gevolg van de infectie raken de naïeve T-cellen geactiveerd en gaan ze delen, waarbij de barcode van de naïeve T-cel doorgegeven wordt aan alle dochtercellen. Zodoende dragen alle nakomelingen van een enkele naïeve T-cel (een hele 'T-celfamilie') exact dezelfde barcode.

Deze barcodetechniek heeft het mogelijk gemaakt om een aantal nieuwe aspecten van de T-cel reactie te bestuderen.

Ten eerste kunnen we nu de diversiteit binnen een familie bestuderen: kan een enkele naïeve T-cel zowel nakomelingen hebben die zich ontwikkelen tot effectorcellen als nakomelingen die zich ontwikkelen tot memorycellen, of ontwikkelen alle nakomelingen van een naïeve T-cel zich slechts tot één van beide celtypes (hoofdstuk 5)? Dit hebben we getest door per barcode te vergelijken of deze in beide celtypes of slechts in één van beide voorkwam. Als een barcode in beide celtypes voorkomt, dan heeft deze naïeve T-cel zowel effector- als memory-nakomelingen; komt een barcode maar in één van beide types voor, dan bestaat er geen diversiteit binnen deze T-cel familie.

Ten tweede kunnen we de vergelijking van barcodes in effector- en memorycellen ook gebruiken om te testen of het effector- of memory-lot tijdens de eerste paar celdelingen vastgelegd wordt (hoofdstuk 6). Hiervoor hebben we niet de naïeve cellen, maar de 1-3 keer gedeelde cellen van een unieke barcode voorzien en vervolgens de barcodes in de effector- en memorycellen vergeleken. Als effector- en memorycellen verschillende barcodes bevatten, is het lot van de cel al vastgelegd op het moment van barcode-labeling. Als we daarentegen dezelfde barcodes in beide celtypes vinden, dan kunnen we daaruit afleiden dat het lot later wordt vastgelegd.

Ten derde kunnen we ook tellen hoeveel verschillende barcodes er tijdens een T-celreactie aanwezig zijn. Dit vertelt ons hoeveel T-celfamilies aan de reactie deelnemen en dat is van belang voor de vraag die we in hoofdstuk 7 stellen. Hier willen we bepalen of er tijdens een sterke T-celreactie (waarbij veel infectie-specifieke T-cellen gevormd worden) meer T-celfamilies aan de reactie meedoen, of dat de hoeveelheid T-celfamilies gelijk blijft en alleen het aantal nakomelingen per naïeve T-cel (dus de familiegrootte) toeneemt. Hiervoor hebben we tijdens sterke en minder sterke T-celreacties geteld hoeveel T-celfamilies aan de reactie deelnamen.

Ten slotte willen we in hoofdstuk 8 bepalen of alle T-celfamilies die deelnemen aan een reactie even groot zijn. Hiervoor was het niet alleen van belang om het aantal verschillende families dat aan een T-celreactie meedoet te kunnen bepalen, maar ook om het aantal familieleden per familie te tellen. Oftewel, hoeveel cellen in een reactie bevatten dezelfde barcode? Hiervoor konden we geen gebruik maken van de tot nu toe gebruikte 'microarray'-techniek, aangezien deze wel vast kan stellen welke barcodes in een groep cellen aanwezig zijn, maar niet exact hoe vaak de verschillende barcodes

aanwezig zijn. Daarom zijn we overgestapt op een 'deep-sequencing'-techniek die het mogelijk maakt om exact te tellen hoe vaak iedere barcode aanwezig is.

De antwoorden op de onderzoeksvragen

Zorgt een sterke infectie ervoor dat er meer T-celfamilies deelnemen aan de reactie?
We hebben tijdens sterke infecties (grote T-celreacties) en zwakke infecties (kleine T-celreacties) geteld hoeveel verschillende barcodes in de geactiveerde T-cellen aanwezig waren. Daarbij hebben we gevonden dat het aantal T-celfamilies dat deelneemt aan een grote T-celreactie maar marginaal (≈1.5x) groter is dan tijdens een kleine reactie. Een grote T-cel reactie kan echter tot 10 keer groter zijn dan een kleine reactie. Dit betekent dat de grootte van de T-celreactie primair bepaald wordt door het aantal nakomelingen dat elke geactiveerde T-cel produceert.

Zijn alle T-celfamilies even groot?
De combinatie van onze barcode techniek en de deep-sequencing-techniek heeft het mogelijk gemaakt om te bepalen hoe groot alle T-celfamilies op een bepaald tijdstip tijdens de T-celreactie zijn. Deze analyse liet zien dat de T-celreactie gedomineerd wordt door een kleine fractie van de deelnemende T-celfamilies: ongeveer 20% van de T-celfamilies maakt samen 90% uit van de totale T-celreactie. Deze scheve verhouding blijft gedurende de gehele T-celreactie grofweg behouden. We hebben ook laten zien dat dit verschil in familiegrootte toeneemt als de T cellen minder sterk gestimuleerd worden.

Maakt elke T-celfamilie zowel effector- als memory-T-cellen?
Door naïeve T-cellen van een unieke barcode te voorzien en na infectie te vergelijken welke barcodes in de effector- en de memoryceltypes aanwezig waren hebben we vastgesteld dat elke T-celfamilie effector- én memorycellen voortbrengt. Dit betekent dat het lot van een T-cel (of het een effector- of memorycel wordt) niet al tijdens de activatie van naïeve T-cellen vastgelegd wordt. Daarmee worden eerdere theorieën verworpen die stelden dat de sterkte van T-celactivatie lotsbepalend is.

Wordt het lot van een T-cel vroeg tijdens de reactie vastgelegd?
Als het effector- of memory-lot niet al tijdens T-celactivatie vastgelegd wordt, wordt het dan misschien tijdens de eerste celdeling vastgelegd? Volgens een theorie gebeurt dit door middel van een proces dat asymmetrische celdeling genoemd wordt. Asymmetrische celdeling betekent dat tijdens de celdeling beide dochtercellen een ander lot toebedeeld krijgen.

Door cellen die al 1-3 delingen hebben ondergaan met een unieke barcode te labelen en vervolgens per barcode te kijken of deze in effector- én memorycellen of maar in één van beide celtypes terecht kwam, hebben we vastgesteld dat T-cellen die 1-3 keer gedeeld hebben nog geen vastgelegd lot hebben. Het overgrote deel

van deze cellen had namelijk zowel effector- als memory-nakomelingen. Wij tonen hiermee aan dat het 'besluit' of een T-cel een effectorcel of een memorycel wordt, relatief laat in de T-celreactie plaatsvindt.

Conclusie

Het onderzoek beschreven in dit proefschrift toont aan dat de grootte van de $CD8^+$ T-celreactie hoofdzakelijk bepaald wordt door het gemiddelde aantal nakomelingen dat elke geactiveerde T-cel produceert. Hierbij is het opmerkelijk dat de hoeveelheid nakomelingen per geactiveerde T-cel sterk verschilt. Dit betekent, dat als wij door middel van b.v. vaccinatie de grootte van de T-celreactie willen verhogen (en dus meer effectorcellen genereren), het nuttig zal zijn om de T-cellen die nu weinig nakomelingen hebben zodanig te stimuleren dat ze meer nakomelingen krijgen.

Verder laat dit onderzoek zien dat elke naïeve $CD8^+$ T-cel na activatie effector- en memory-nakomelingen produceert, en dat het effector- en memory-lot nog niet is vastgelegd na 3 celdelingen. Dit betekent dat $CD8^+$ T-cellen pas op latere momenten in de T-celreactie 'besluiten' of ze sterven nadat de infectie bestreden is of ontwikkelen tot een langlevende memorycel. Als wij willen begrijpen hoe memorycellen ontstaan is het daarom zinvol om op de latere fases van de T-celreactie te focussen.

CURRICULUM VITAE

Carmen Gerlach werd geboren op 4 December 1980 te Hamburg in Duitsland en verhuisde op zesjarige leeftijd naar Nederland. In 2000 behaalde zij het Zeugnis der Allgemeinen Hochschulreife aan het Gymnasium van de Deutsche Schule Den Haag. In hetzelfde jaar begon zij aan de studie Biomedische Wetenschappen aan de Universiteit Leiden, waarvoor zij in 2003 cum laude het Bachelordiploma en in 2005 het Masterdiploma behaalde. Tijdens de Bachelorfase bracht zij zes maanden door als uitwisselingsstudente aan het Karolinska Institutet in Stockholm, Zweden en werd zij geselecteerd voor het Excellente Studenten Traject van het Leids Universitair Medisch Centrum (LUMC), in het kader waarvan zij gedurende 6 maanden naast haar studie onderzoek verrichte onder begeleiding van Dr. Marianne van Stipdonk op de afdeling Immunohematologie en Bloedtransfusie, sectie Tumorimmunologie van het LUMC. Tijdens het Masterprogramma liep zij twee wetenschappelijke stages. Het eerste onderzoek vond plaats in de groep van Dr. Anton Polderman op de afdeling Parasitologie van het LUMC en bevatte 3 maanden veldonderzoek in de regio Garu, Ghana. Hierop volgde de afstudeerstage onder begeleiding van Dr. Marianne van Stipdonk in de groep van Dr. Rienk Offringa en Prof. Kees Melief op de afdeling Immunohematologie en Bloedtransfusie, sectie Tumorimmunologie van het LUMC. Na het behalen van haar Masterdiploma begon zij in oktober 2005 aan haar promotieonderzoek onder begeleiding van Prof. Ton Schumacher op de afdeling Immunologie van het Nederlands Kanker Instituut in Amsterdam, waarvan het in dit proefschrift beschreven onderzoek het resultaat is. Vanaf eind 2011 zet zij haar wetenschappelijke loopbaan voort als post-doc in de onderzoeksgroep van Prof. Ulrich von Andrian aan de Harvard Medical School in Boston, USA. Ze heeft hiervoor een Rubicon beurs van de Nederlandse Organisatie voor Wetenschappelijk Onderzoek ontvangen.

LIST OF PUBLICATIONS

C. Gerlach, J.W. van Heijst and T.N. Schumacher. The descent of memory T cells. ***Ann N Y Acad Sci***. 1217 *(2011) 139-53*

T.N. Schumacher, C. Gerlach and J.W. van Heijst. Mapping the life histories of T cells. ***Nat Rev Immunol***. *10 (2010) 621-631*

C. Gerlach, J.W. van Heijst, E. Swart, D. Sie, N. Armstrong, R.M. Kerkhoven, D. Zehn, M.J. Bevan, K. Schepers and T.N. Schumacher. One naïve T cell, multiple fates in $CD8^+$ T cell differentiation. ***J Exp Med***. *207 (2010) 1235-46*

F.M Wensveen, K.P. van Gisbergen, I.A. Derks, C. Gerlach, T.N. Schumacher, R.A. van Lier, E. Eldering. Apoptosis threshold set by Noxa and Mcl-1 after T cell activation regulates competitive selection of high-affinity clones. ***Immunity***. *32 (2010) 754-65*

J.W. van Heijst, C. Gerlach, E. Swart, D. Sie, C. Nunes-Alves, R.M. Kerkhoven, R. Arens, M. Correia-Neves, K. Schepers and T.N. Schumacher. Recruitment of antigen-specific $CD8^+$ T cells in response to infection is markedly efficient. ***Science***. *325 (2009) 1265-9*.

K. Schepers, E. Swart, J.W. van Heijst, C. Gerlach, M. Castrucci, D. Sie, M. Heimerikx, A. Velds, R.M. Kerkhoven, R. Arens, and T.N. Schumacher. Dissecting T cell lineage relationships by cellular barcoding. ***J Exp Med***. *205 (2008) 2309-18.*

&